



**NTNU – Trondheim**  
Norwegian University of  
Science and Technology

# Modeling, Simulation and Control of Hydraulic Winch System

**Stian Skjong**

Marine Technology

Submission date: June 2014

Supervisor: Eilif Pedersen, IMT

Norwegian University of Science and Technology  
Department of Marine Technology





**NTNU – Trondheim**  
Norwegian University of  
Science and Technology

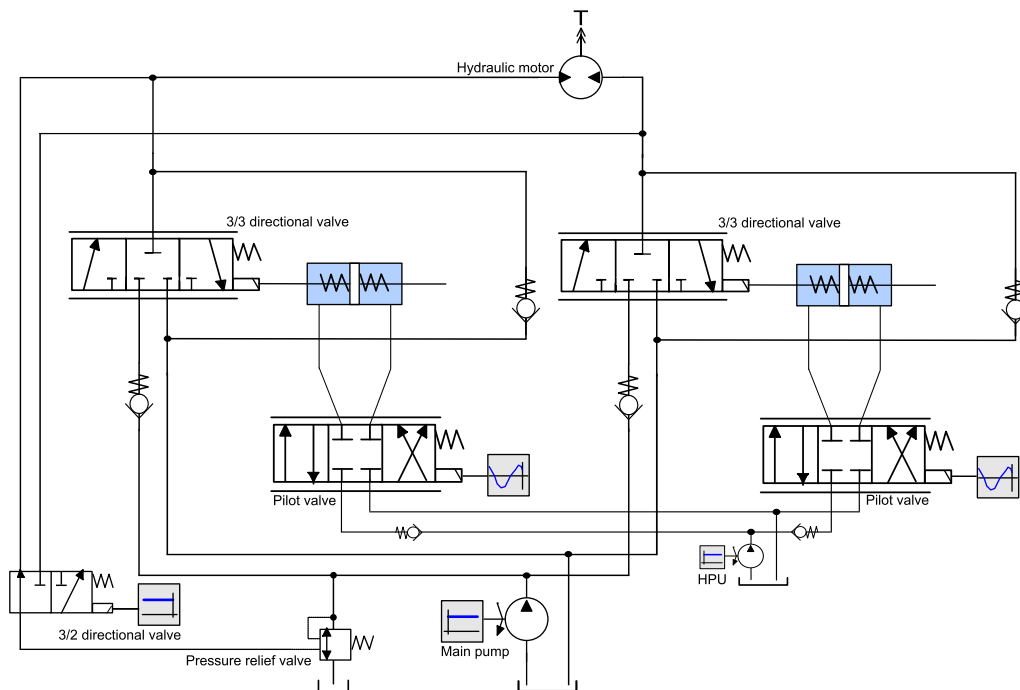
Department of Marine Technology

---

MASTER THESIS

Modeling, Simulation and Control  
of Hydraulic Winch System

---



June 2, 2014

**Author:**  
Stian Skjong

**Supervisor, NTNU:**  
Eilif Pedersen

**Co-supervisor, NTNU:**  
Asgeir Sørensen

**Supervisor, Rolls-Royce:**  
Jo-Einar Emblemsvåg



# Preface

This report contains the work done in my master thesis at the department of Marine Technology at NTNU. The thesis contains modeling and control theory, applied on a hydraulic winch system, which has been my direction of specialization in my master degree. This thesis is paper based which means that the work in this thesis is built around the two first papers given in Appendix B. The last paper is only partly written during this thesis and is submitted for International Conference on Bond Graph Modeling and Simulation 2014, ICBGM'2014. The work description regarding this thesis is found in Appendix A.

I would like to thank especially Jo-Einar Emblemsvåg in Rolls-Royce Marine for his support, good discussions, having the ability to remain critical, for believing in me and to see the benefits of investing time and resources in me.

A huge thanks to Eilif Pedersen, my mentor and good role model here at NTNU is also appropriate. His way to push me not to take shortcuts, but to keep going strong and doing a thorough job has a huge influence on the results in this thesis. He has a perpetual source of knowledge that I have benefited.

Last but not least, a huge thanks to my sparring partner I share office with, Børge Rokseth, for sharing experience and ideas with. His good humour and presence have made it easier to spend the huge amount of office hours this thesis has required.

Stian Skjong  
Trondheim, June 2, 2014



# Abstract

In this thesis a hydraulic low pressure winch system has been modeled using bond graph theory. The hydraulic winch system is assumed to be installed on an offshore vessel affected by environmental forces and disturbances such as waves and currents. The hydraulic system powering the winch consists mainly of two pilot operated 3/3-directional valves controlled by two 4/3-directional valves and a hydraulic motor. The system also includes a pressure relief valve, check valves, pump systems, piping and filters, see figure 1.4. The 3/3-directional valves are the main focus in the model and are therefore modeled with less simplifications compared to the other subsystems.

A thorough model study has been initiated to figure out the model limitations, sensitivity of model parameters and the ability to simplify the derived model without losing essential dynamics and characteristics. The effects of variable bulk modulus and fluid inertia in the 3/3-directional valves have been studied by comparing different step responses and motor load characteristics. The observations and results from this model analysis laid the groundwork for control of the hydraulic motor. A clear relation between the main valve displacements and the motor velocity and torque in 4/3 valve configuration gave reasons to believe that manual motor control done by the winch operator through control of the valve displacements was possible. Adaptive PID controllers were used as inner controllers to control the control slides in the main valves. These controllers were later on replaced with PD-controllers when outer control was derived because the adaptive controllers tended to be a bit slow.

Simplified state equations describing the motor dynamics were derived for control design purposes. The state equations extracted from the bond graph model showed high complexity, containing logic and discrete quantities, and were not suitable for control design. Model based speed- and torque controllers, based on sliding mode and backstepping control theory, were derived based on the simplified equations and implemented in the model. Different load cases were initiated to test the two controllers. A lumped wire-load model containing hydrodynamics, wire- and reel dynamics and environmental disturbances such as current and heave motions of the vessel were added in the total winch model to test the controllers in different operations with varying conditions and environments. The results from these controller tests gave reason to believe that a combination of these two controllers would be favourable in certain operations and would give increased safety in extreme cases such as stuck load and loss of load.

The derived speed and torque controller were put into a hybrid controller framework and a switching algorithm was designed with focus on switching stability and wanted functionalities for the winch system. It was observed that switching stability and winch functionality were closely connected and different winch operations were essential in the design of the switching algorithm. *Dwell time* and tracking error switching were used as the main controller switching restrictions together with functionality based switching conditions. Different simulations were initiated to test the hybrid controller such as stuck load, loss of load and landing of a load at the sea floor. A Luenberger observer was derived to estimate the motor load and the motor velocity by using the simplified state equations and the differential pressure across the hydraulic motor as measurement in order to ensure redundancy in the control system and be able to control the hydraulic winch even though the decoder measuring the hydraulic motor velocity fails.

**Keywords:** Hydraulic winch system, bond graph theory, sensitivity analysis, sliding mode, backstepping, lumped wire-load model, Luenberger observer, winch operations, load landing, stuck load, loss of load, hybrid controller, switching algorithm, dwell time, Bessel filter.

---

## Structure of the Thesis

A short description of each chapter is given below together with additional notes and references in order to help the reader navigate through this document.

**Chapter 1.** Introduction to the thesis and includes a system description, a section with related work done by other authors and a short introduction to bond graph theory. For more information about bond graph theory see Karnopp et al. (2006).

**Chapter 2.** Modeling of the hydraulic system driving the winch. This chapter is based on Skjong (2013) and includes all equations necessary to model the hydraulic system using bond graph theory. Model simplifications are argued for and verified in later chapters. Implementation issues are not discussed, but relates to the complexity and magnitude of the model and since the tolerances are set high in the solver, some logic must be implemented to ensure that the system is solvable. This is done mainly in C-elements and if the results from the integrator get below a predefined limit it is set to zero.

**Chapter 3.** Model study of the bond graph model derived for the hydraulic system in chapter 2. Includes comparisons of different step responses of the two 3/3-directional valve models with different complexity for various load cases. The chapter also includes two model parameter sensitivity analysis and more are given in Appendix D. A summary of all sensitivity cases are given in table 3.4.

**Chapter 4.** First hand control of the hydraulic motor. Contains studies of the relations between the main valve displacements and the motor velocity and motor torque. The operator is assumed to do the outer control job, setting the reference positions for the main valves based on velocity and torque measurements. For inner controller, controlling the control slide positions in the main valves, adaptive controllers are used (Iwai et al., 2006).

**Chapter 5.** Precise control of the hydraulic motor. Includes a summary of the simplified state equations and the resulting control laws derived in Skjong and Pedersen (2014a), see Appendix B.1. Both the speed controller and the torque controller are tested in two different simulations, one with constant load and one with varying load.

**Chapter 6.** Controller testing with lumped wire-load model. The speed- and torque controller are tested with a more realistic load model. This load model is a lumped wire-load model containing hydrodynamics, wire dynamics, reel dynamics and environmental disturbances, and is given in Skjong and Pedersen (2014c) in Appendix B.3. In addition to the given controller tests, two more are given in Skjong and Pedersen (2014a), see Appendix B.1.

**Chapter 7.** Hybrid control design. A short introduction to the hybrid controller design given in Skjong and Pedersen (2014b), see Appendix B.2, is given and one simple controller test is initiated in addition to the ones already given in the paper. Cases such as landing of load, stuck load and loss of load are discussed. A Luenberger observer is designed to estimate the motor velocity and load (Chen, 1998).

**Chapter 8.** Conclusion and proposed further work. The main results in the thesis are summarized and discussed and suggestions for further studies and work are given.

**Appendix A.** Work description.

**Appendix B.** Includes two papers made in this thesis and a paper regarding wire-load model.

**Appendix C.** Table of parameters used in this thesis.

**Appendix D.** Additional model parameter sensitivity studies.

**Appendix E.** Additional plots and case studies.



# Contents

<b>List of Figures</b>	<b>vii</b>
<b>List of Tables</b>	<b>xi</b>
<b>List of Symbols</b>	<b>xv</b>
<b>1 Introduction</b>	<b>1</b>
1.1 Introduction to the Hydraulic System . . . . .	2
1.2 Related Work . . . . .	4
1.3 Introduction to Bond Graph Theory . . . . .	5
<b>2 Modeling Hydraulic System</b>	<b>9</b>
2.1 Pilot Valve . . . . .	9
2.2 3/3-Directional Valve . . . . .	11
2.2.1 Valve Dynamics . . . . .	11
2.2.2 Flow Model . . . . .	13
2.2.3 Bond Graph Model . . . . .	13
2.3 Hydraulic Motor Model . . . . .	15
2.4 Pressure Compensator . . . . .	17
2.5 3/2-Directional Valve . . . . .	19
2.6 Finishing Total Model . . . . .	20
<b>3 Model Study</b>	<b>23</b>
3.1 Main Valve Study . . . . .	23
3.1.1 Simple Step Response . . . . .	23
3.1.2 Sine Reference . . . . .	29
3.1.3 Conclusion . . . . .	33
3.2 Model Parameter Sensitivity . . . . .	34
3.2.1 Flow Force Coefficient in Pressure Compensator . . . . .	35
3.2.2 Inertia of Hydraulic Motor . . . . .	36
3.2.3 Results from Parameter Sensitivity Study . . . . .	37
3.3 Chapter Summary and Conclusion . . . . .	38
<b>4 First Hand Control</b>	<b>39</b>
4.1 Manual Speed Control . . . . .	39
4.1.1 Control Slide Position and Motor Velocity . . . . .	39
4.1.2 First Hand Manual Speed Controller . . . . .	43
4.2 Manual Torque Control . . . . .	45
4.3 Chapter Summary and Conclusion . . . . .	50
<b>5 Precise Control</b>	<b>53</b>
5.1 State Equations . . . . .	53
5.2 Model Based Speed Controller . . . . .	54
5.2.1 Controller Test using Constant Load . . . . .	55
5.2.2 Controller Test using Random Motor Loading . . . . .	58
5.3 Model Based Torque Controller . . . . .	60
5.3.1 Controller Test using Constant load and Reference . . . . .	62

5.3.2	Varying Load, Varying Reference . . . . .	66
5.4	Chapter Summary and Conclusion . . . . .	69
<b>6</b>	<b>Controller Testing with Wire Model</b>	<b>71</b>
6.1	Speed Controller . . . . .	71
6.1.1	Load Case 1 . . . . .	72
6.1.2	Load Case 2 . . . . .	75
6.2	Torque Controller . . . . .	77
6.2.1	Load Case 1 . . . . .	78
6.2.2	Load Case 2 . . . . .	81
6.3	Additional Controller Tests . . . . .	83
6.4	Chapter Summary and Conclusion . . . . .	83
<b>7</b>	<b>Hybrid Control</b>	<b>85</b>
7.1	Hybrid Control Design . . . . .	85
7.2	Hybrid Controller Testing . . . . .	86
7.2.1	AHC with Changing Load . . . . .	86
7.2.2	Controller Tests given in Skjong and Pedersen (2014b) . . . . .	88
7.3	Observer Design . . . . .	89
7.4	Simulations using Observer . . . . .	90
7.4.1	Observer out of the Loop . . . . .	90
7.4.2	$T_{load}$ in Feed Forward . . . . .	92
7.4.3	Closed Loop with Observed Motor Velocity in Feedback . . . . .	92
7.5	Chapter Summary and Conclusion . . . . .	93
<b>8</b>	<b>Conclusion and Further Work</b>	<b>95</b>
	<b>Bibliography</b>	<b>I</b>
	<b>A Work Description</b>	<b>V</b>
	<b>B Papers</b>	<b>IX</b>
B.1	Control of Hydraulic Winch System (1/2) Model Based Control Designs . . . . .	IX
B.2	Control of Hydraulic Winch System (2/2) Hybrid Control Design . . . . .	XXI
B.3	Modeling Hydraulic Winch System . . . . .	XXXV
	<b>C Parameters</b>	<b>XLIII</b>
	<b>D Additional Sensitivity Studies</b>	<b>XLVII</b>
D.1	Volume Ratio in Bulk Modulus . . . . .	XLVII
D.2	Pressure Compensator . . . . .	XLVII
D.2.1	Nozzle Area in Pressure Compensator . . . . .	XLVII
D.2.2	Nozzle Flow Coefficient . . . . .	XLVIII
D.2.3	Plunger Diameter . . . . .	XLVIII
D.2.4	Flow Coefficient . . . . .	XLVIII
D.2.5	Inertia . . . . .	XLIX
D.2.6	Spring Stiffness . . . . .	L
D.2.7	Slope in Friction Function . . . . .	LI
D.2.8	Static Friction . . . . .	LII
D.2.9	Volume in Pressure Compensator . . . . .	LII

D.3	3/2-Directional Valve . . . . .	LIII
D.3.1	Gain in 3/2-Directional Valve Dynamics . . . . .	LIII
D.3.2	Natural Frequency . . . . .	LIV
D.3.3	Damping Ratio . . . . .	LIV
D.3.4	Flow Coefficient . . . . .	LIV
D.3.5	Initial Volume in 3/2-Directional Valve . . . . .	LV
D.4	Hydraulic Motor . . . . .	LVI
D.4.1	Internal Leakage in Hydraulic Motor . . . . .	LVI
D.4.2	Static Friction in Hydraulic Motor . . . . .	LVII
D.4.3	Friction Slope in Hydraulic Motor . . . . .	LVII
D.5	Outer System . . . . .	LVIII
D.5.1	Loss Factor in Pressure Line . . . . .	LVIII
D.5.2	Initial Volume in Volume P . . . . .	LIX
D.6	3/3-Directional Valve . . . . .	LIX
D.6.1	Control Slide Inertia . . . . .	LIX
D.6.2	Initial Volume, Volume 1 and 2 . . . . .	LIX
D.6.3	Natural Frequency in 4/3-Directional Valve Dynamics . . . . .	LX
D.6.4	Gain in 4/3-Directional Valve Dynamics . . . . .	LXI
D.6.5	Damping Ratio in 4/3-Directional Valve Dynamics . . . . .	LXII
<b>E</b>	<b>Additional Plots and Case Studies</b>	<b>LXIII</b>
E.1	Adaptive Controller . . . . .	LXIII
E.1.1	Adaptive Controller Gains . . . . .	LXIII
E.1.2	Random Reference Response . . . . .	LXIII
E.2	Additional Plots from 6.2 . . . . .	LXVI
E.2.1	Control Slide Positions and References, 6.2.1 . . . . .	LXVI
E.2.2	Differential Pressure and Variable Bulk Modulus, 6.2.1 . . . . .	LXVI
E.2.3	Hydraulic Motor Velocity, 6.2.2 . . . . .	LXVII
E.2.4	Control Slide Positions and References, 6.2.2 . . . . .	LXVII
E.2.5	Differential Pressure and Variable Bulk Modulus, 6.2.2 . . . . .	LXVII



# List of Figures

1.1	Ship in a marine operation affected by waves. . . . .	1
1.2	3/3 directional valve. . . . .	2
1.3	4/3 directional valve. . . . .	3
1.4	Model overview. . . . .	3
1.5	Power bond connecting subsystem A and B. . . . .	5
1.6	Mass-damper-spring system. . . . .	7
2.1	Bond graph model of pilot valve. . . . .	10
2.2	Symbol for pilot valve in bond graph model. . . . .	10
2.3	Bond graph model of 3/3-directional valve. . . . .	14
2.4	Main valve icon. . . . .	15
2.5	Bond graph model of hydraulic motor. . . . .	17
2.6	Icon for the hydraulic motor submodel. . . . .	17
2.7	Sketch of pressure compensator. . . . .	18
2.8	Bond graph model of pressure compensator. . . . .	19
2.9	Icon for pressure compensator model. . . . .	19
2.10	Bond graph model of 3/2-directional valve. . . . .	19
2.11	Icon for 3/2-directional valve model. . . . .	19
2.12	Total bond graph model of the system presented in figure 1.4. . . . .	21
3.1	Reference, velocity limitation and control slide positions for the advanced model. . . . .	25
3.2	Motor velocity, flow through pressure compensator and variable bulk modulus. . . . .	25
3.3	Difference between control slide positions $x_A$ , $x_A - x_{A,simp}$ . . . . .	26
3.4	Difference between motor velocities $v$ , $v - v_{simp}$ . . . . .	27
3.5	Difference in control slide position, load sweep. . . . .	28
3.6	Difference in motor velocity, load sweep. . . . .	28
3.7	Reference, velocity limitation and control slide positions for the advanced model. . . . .	30
3.8	Motor velocity, flow through pressure compensator and variable bulk modulus. . . . .	31
3.9	Difference between control slide positions $x_A$ , $x_A - x_{A,simp}$ , and motor velocities $v$ , $v - v_{simp}$ . . . . .	31
3.10	Hydraulic motor velocities. . . . .	32
3.11	Differences between motor velocities. . . . .	33
3.12	Difference in control slide position, load sweep. . . . .	33
3.13	Difference in hydraulic motor velocities, load sweep. . . . .	34
3.14	Sensitivity of flow force coefficient in pressure compensator. . . . .	36
3.15	Sensitivity of inertia in the hydraulic motor. . . . .	36
4.1	Relation between motor velocity and control slide position, main valve A. $T_{ms}=2000$ Nm. . . . .	39
4.2	Results from the motor velocity mapping, $T_{ms}=2000$ Nm. . . . .	41
4.3	Relation between motor velocity and control slide position, main valve A. $T_{ms}=20000$ Nm. . . . .	41
4.4	Results from the motor velocity mapping, $T_{ms}=20000$ Nm. . . . .	42
4.5	Control slide position and motor velocity with P-controller. . . . .	42
4.6	$r_s$ v.s. $r_o$ . . . . .	44
4.7	Reference and actual position of control slide A. . . . .	44
4.8	Motor velocity. . . . .	45

4.9	Relation between differential pressure and control slide position, main valve A. $T_{ms} = 2000 \text{ Nm}$ .	46
4.10	Relation between differential pressure and control slide position, main valve A. $T_{ms} = 2000 \text{ Nm}$ , low pass filtered differential pressure.	47
4.11	Control slide position, $x_A$ , and differential pressure, $\Delta p$ .	47
4.12	Control slide position, $x_A$ , and differential pressure, $\Delta p$ .	48
4.13	Relation between differential pressure and control slide position, main valve A. $T_{ms} = 2000 \text{ Nm}$ , low pass filtered differential pressure.	49
4.14	Control slide position, $x_A$ , and differential pressure, $\Delta p$ .	49
4.15	Control slide position, $x_A$ , and differential pressure, $\Delta p$ .	50
4.16	Control slide position, $x_A$ , motor velocity, $v$ and motor load, $T_m$ .	51
4.17	Control slide position, $x_A$ , differential pressure, $\Delta p$ and motor load, $T_m$ .	52
5.1	Hydraulic motor velocity and reference.	57
5.2	Difference between velocity reference and actual motor velocity.	57
5.3	Control slide positions and speed controller output.	58
5.4	Differential pressure across the hydraulic motor and variable bulk modulus in volume A, B, P and R.	59
5.5	Motor loading characteristics.	59
5.6	Hydraulic motor velocity and reference.	60
5.7	Difference between velocity reference and actual motor velocity.	60
5.8	Control slide positions and speed controller output.	61
5.9	Differential pressure across the motor and variable bulk modulus in volume A, B, P and R.	61
5.10	Torque and reference.	63
5.11	Tracking error.	64
5.12	Control slide positions and references.	64
5.13	Hydraulic motor velocity.	65
5.14	Differential pressure across the motor, $\Delta p$ , and variable bulk modulus.	65
5.15	Torque and reference.	67
5.16	Tracking error.	67
5.17	Control slide positions and references.	68
5.18	Hydraulic motor velocity.	68
5.19	Differential pressure across the motor, $\Delta p$ , and variable bulk modulus.	69
6.1	Hydraulic motor velocity and reference.	73
6.2	Difference between velocity reference and actual motor velocity.	73
6.3	Control slide positions and speed controller output.	74
6.4	Differential pressure across the motor and variable bulk modulus in volume A, B, P and R.	74
6.5	Hydraulic motor velocity and reference.	75
6.6	Difference between velocity reference and actual motor velocity.	76
6.7	Control slide positions and speed controller output.	76
6.8	Differential pressure across the motor and variable bulk modulus in volume A, B, P and R.	77
6.9	Torque and reference.	79
6.10	Tracking error.	79
6.11	Hydraulic motor velocity.	80
6.12	Top and bottom vertical wire position.	80
6.13	Torque and reference.	81
6.14	Tracking error.	82
6.15	Top and bottom vertical wire position.	82

7.1	Hydraulic motor velocity, reference, magnified areas around controller switching and active controller. . . . .	87
7.2	Torque, reference, magnified areas around controller switching and active controller. . . . .	87
7.3	Observed motor velocity compared to the measured motor velocity. . . . .	91
7.4	Observed motor velocity compared to the measured motor velocity. . . . .	91
7.5	Comparison of simulations with and without $T_{load}$ in feed forward. . . . .	92
7.6	Comparison of vertical load positions between simulations with measured velocity and estimated velocity. . . . .	93
D.1	Sensitivity of volume rate in bulk modulus. . . . .	XLVII
D.2	Sensitivity of nozzle area in pressure compensator. . . . .	XLVIII
D.3	Sensitivity of nozzle flow coefficient in pressure compensator. . . . .	XLIX
D.4	Sensitivity of plunger diameter in pressure compensator. . . . .	XLIX
D.5	Sensitivity of flow coefficient, $\alpha$ in pressure compensator. . . . .	L
D.6	Sensitivity of inertia in pressure compensator. . . . .	L
D.7	Sensitivity of spring stiffness in pressure compensator. . . . .	LI
D.8	Sensitivity of slope in friction function in pressure compensator. . . . .	LI
D.9	Sensitivity of static friction in pressure compensator. . . . .	LII
D.10	Sensitivity of initial volume in pressure compensator. . . . .	LIII
D.11	Sensitivity of gain in the 3/2-directional valve dynamics. . . . .	LIII
D.12	Sensitivity of natural frequency in the 3/2-directional valve dynamics. . . . .	LIV
D.13	Sensitivity of damping ratio, $\zeta$ , in the 3/2-directional valve dynamics. . . . .	LV
D.14	Sensitivity of the flow coefficient in the 3/2-directional valve. . . . .	LV
D.15	Sensitivity of initial volume in the 3/2-directional valve dynamics. . . . .	LVI
D.16	Sensitivity of internal leakage in the hydraulic motor. . . . .	LVI
D.17	Sensitivity of static friction for the hydraulic motor. . . . .	LVII
D.18	Sensitivity of slope in friction function for the hydraulic motor. . . . .	LVIII
D.19	Sensitivity of loss factor in pressure line. . . . .	LVIII
D.20	Sensitivity of initial volume in volume P. . . . .	LIX
D.21	Sensitivity of inertia in control slide, main valves. . . . .	LX
D.22	Sensitivity of initial volumes 1 and 2 in control slide, main valves. . . . .	LX
D.23	Sensitivity of natural frequency in pilot valve dynamics. . . . .	LXI
D.24	Sensitivity of gain in the pilot valve dynamics. . . . .	LXI
D.25	Sensitivity of damping ratio, $\zeta$ , in the pilot valve dynamics. . . . .	LXII
E.1	Adaptive gains for controller given in section 4.1.2. $T_{ms} = 20000$ Nm, control slide references as given in figure 4.7. . . . .	LXIII
E.2	Slide position, reference signal and velocity limitation. . . . .	LXIV
E.3	Adaptive gains. . . . .	LXIV
E.4	Controller output and its components before saturation. . . . .	LXV
E.5	Volume states. . . . .	LXV
E.6	Control slide positions and references. . . . .	LXVI
E.7	Differential pressure across the motor, $\Delta p$ , and variable bulk modulus. . . . .	LXVI
E.8	Hydraulic Motor Velocity. . . . .	LXVII
E.9	Control slide positions and references. . . . .	LXVII
E.10	Differential pressure across the motor, $\Delta p$ , and variable bulk modulus. . . . .	LXVIII





# List of Tables

1.1	Some basic bond graph elements used. . . . .	6
3.1	Reference signals in simple step response simulation. . . . .	23
3.2	Reference signals and motor load for the sine response simulation . . . . .	29
3.3	Reference signals for parameter sensitivity analysis. . . . .	35
3.4	Results from parameter sensitivity studies . . . . .	37
4.1	Reference signals in relation study. . . . .	40
4.2	Adaptive control law parameters. . . . .	44
5.1	States, variables and parameters for hydraulic motor. . . . .	54
5.2	Reference signals for test of speed controller . . . . .	56
5.3	Reference signals for test of speed controller. . . . .	62
5.4	Reference signals for test of speed controller. . . . .	66
6.1	Reference signals for testing of speed controller . . . . .	71
6.2	Reference signals for test of torque controller . . . . .	77
C.1	Parameters and coefficients used in the bond graph model. . . . .	XLIII



# List of Symbols

<b>Abbreviations</b>	<b>Description</b>
<i>GES</i>	Global Exponentially Stability, page 62
<i>p</i>	Momentum state in bond graph theory , first used in eq. (1.3), page 6
<i>p.e</i>	Effort in bond graph theory , first used in eq. (1.3), page 6
<i>p.f</i>	Flow in bond graph theory , first used in eq. (1.3), page 6
<i>q</i>	Displacement state in bond graph theory , first used in eq. (1.3), page 6
AHC	Active Heave Compensation, page 62
Dp	Dynamic Positioning , page 1
EKF	Extended Kalman Filter, page 96
GAS	Globally Asymptotically Stability, page 55
HPU	Hydraulic Power Unit , page 4
MRU	Motion Reference Unit, page 71
PMS	Power Management System , page 1
ZOH	Zero-Order-Hold, digital to analogue converter , page 14

<b>Constants</b>	<b>Description</b>	<b>Unit</b>
$\beta_h$	Bulk modulus of pipeline , first used in eq. (2.7), page 11	<i>Pa</i>
$\beta_f$	Bulk modulus hydraulic fluid , first used in eq. (2.7), page 11	<i>Pa</i>
$\mathbf{K}$ ,	Observer gain vector, first used in eq. (7.6), page 90	—
$\Delta p_{set}$	Opening pressure for check valve , first used in eq. (2.19), page 13	<i>Pa</i>
$\gamma_1$	Proportional gain parameter for adaptive law , first used in eq. (4.3), page 43	$\frac{V}{m^3 s}$
$\gamma_2$	Derivative gain parameter for adaptive law , first used in eq. (4.3), page 43	$\frac{Vs}{m^3}$
$\gamma_3$	Integral gain parameter for adaptive law , first used in eq. (4.3), page 43	$\frac{V}{m^3 s^3}$
$\mathcal{O}$	Observability matrix, first used in eq. (7.6), page 90	—
$\mu_c$	Coulomb friction coefficient , first used in eq. (2.22), page 15	—
$\mu_s$	Static friction coefficient , first used in eq. (2.22), page 15	—
$\mu_v$	Viscous friction coefficient , first used in eq. (2.22), page 15	—
$\omega$	Natural frequency , first used in eq. (2.2), page 9	$\frac{rad}{s}$
$\rho$	Fluid density , first used in eq. (2.4), page 10	$\frac{kg}{m^3}$
$\sigma$	Modification term in adaptive law , first used in eq. (4.3), page 43	$\frac{1}{s}$
$\tau$	Time constant , first used in eq. (2.19), page 13	<i>s</i>
$\zeta$	Damping ratio , first used in eq. (2.2), page 9	—
<i>a</i>	Sign parameter , first used in eq. (2.4), page 10	—
$A_{cp}$	Area of piston in pressure compensator - piston rod, page 18	$m^2$
$A_{max}$	Maximal area , first used in eq. (2.4), page 10	$m^2$
$A_s$	Area of control slide , first used in eq. (2.6), page 11	$m^2$
<i>b</i>	Damping coefficient , first used in eq. (1.5), page 7	$\frac{Ns}{m}$
$b_{cstop}$	Damping parameter of stopping element in pressure compensator , page 18	$\frac{Ns}{m}$
<i>c</i>	Coulomb coefficient, first used in eq. (5.1), page 54	—

$C_d$	Flow coefficient , first used in eq. (2.26), page 18	—
$D_m$	Displacement, hydraulic motor , first used in eq. (2.25), page 15	$\frac{m^3}{rev}$
$D_s$	Control slide diameter , first used in eq. (2.14), page 12	$m$
$D_2$	Controller gain, first used in eq. (5.10), page 55	$\frac{1}{s}$
$D_3$	Controller gain, first used in eq. (5.10), page 55	$\frac{N}{m^2 rad}$
$D_h$	Hydraulic diameter , first used in eq. (2.30), page 20	$m$
$D_m$	Displacement hydraulic motor, first used in eq. (5.1), page 54	$m^3$
$D_{pi}$	Interior pipe diameter , first used in eq. (2.6), page 11	$m$
$f$	Natural frequency , first used in eq. (2.2), page 9	$Hz$
$f_{pl}$	Loss factor for viscous losses in pipes , first used in eq. (2.6), page 11	—
$F_s$	Static friction , first used in eq. (2.22), page 15	$N$
$G$	Conductance of laminar resistance , first used in eq. (2.23), page 15	$\frac{m^5}{Ns}$
$g$	Gravitational acceleration , first used in eq. (1.5), page 7	$\frac{m}{s^2}$
$h$	Height of rectangular valve opening , first used in eq. (1.1), page 2	$m$
$I_f$	Fluid inertia , first used in eq. (2.8), page 12	$\frac{kg}{m^4}$
$I_m$	Inertia, hydraulic motor, first used in eq. (5.1), page 54	$kgm^2$
$K$	Gain , first used in eq. (2.2), page 9	$\frac{m}{N}$
$k$	Spring stiffness , first used in eq. (1.5), page 7	$\frac{N}{m}$
$k_1$	Gain in sliding surface 1, first used in eq. (5.10), page 55	$\frac{1}{s}$
$k_2$	Controller gain, first used in eq. (5.10), page 55	$\frac{rad}{s^2}$
$k_3$	Controller gain, first used in eq. (5.10), page 55	$\frac{N}{m^2 s}$
$k_{cstop}$	Spring stiffness of stopping element in pressure compensator , page 18	$\frac{N}{m}$
$k_{cs}$	Spring stiffness in pressure compensator , page 18	$\frac{N}{m}$
$k_c$	Design parameter for check valve , first used in eq. (2.18), page 13	$\frac{m^6}{Pas^2}$
$K_i$	General symbol for integral gain , first used in eq. (2.21), page 14	
$K_p$	General symbol for proportional gain , first used in eq. (2.21), page 14	
$L_p$	Length of pipe , first used in eq. (2.6), page 11	$m$
$m$	Mass , first used in eq. (1.5), page 7	$kg$
$m_c$	Weight of moving parts in pressure compensator , page 18	$kg$
$n$	Volume ratio of gas and air , first used in eq. (2.7), page 11	—
$p_0$	Initial pressure , first used in eq. (2.6), page 11	$Pa$
$p_{L1}$	Loss constant , first used in eq. (2.11), page 12	$\frac{Ns^2}{m}$
$p_{L2}$	Loss constant , first used in eq. (2.11), page 12	$\frac{Ns}{m}$
$p_{vap}$	Vapour pressure of hydraulic fluid , page 16	$Pa$
$s$	Slope coefficient , first used in eq. (2.11), page 12	—
$T_d$	Sampling delay , first used in eq. (2.21), page 14	$s$
$T_{ms}$	Constant motor load , first used in eq. (3.0), page 24	$Nm$
$T_s$	Sampling time , first used in eq. (2.21), page 14	$s$
$V_0$	Initial volume at each side of the control cylinder , first used in eq. (2.6), page 11	$m^3$
$V_A$	Volume, first used in eq. (5.1), page 54	$m^3$
$V_B$	Volume, first used in eq. (5.1), page 54	$m^3$
$V_{max}$	Maximal slope of reference signal allowed , first used in eq. (2.20), page 14	$\frac{m}{s}$
$x_{c0}$	Pre-compression in pressure compensator , page 18	$m$

$x_{clim}$	Maximal stroke of piston in pressure compensator , page 18	$m$
$x_{max}$	Maximal displacement of control slide, first used in eq. (5.10), page 55	$m$
$x_{olap}$	Overlap in main valve , first used in eq. (2.16), page 13	$m$
<b>Variables</b>	<b>Description</b>	<b>Unit</b>
$\alpha_c(x_c)$	Variable flow coefficient in pressure compensator , first used in eq. (2.28), page 18	–
$\alpha_p$	Flow parameter, pressure side, first used in eq. (5.1), page 54	–
$\alpha_r$	Flow parameter, return side, first used in eq. (5.1), page 54	–
$\alpha_{x_s}$	Flow coefficient, main valve , first used in eq. (2.16), page 13	$\frac{m}{s} \sqrt{\frac{kg}{Nm}}$
$\beta_v$	Variable bulk modulus , first used in eq. (2.6), page 11	$Pa$
$\hat{x}$	Observer states, first used in eq. (7.6), page 90	
$\Delta p$	Differential pressure , first used in eq. (2.3), page 10	$Pa$
$\dot{Q}$	Flow , first used in eq. (1.2), page 5	$\frac{m^3}{s}$
$\omega_m$	Hydraulic motor velocity , first used in eq. (2.22), page 15	$\frac{rad}{s}$
$\tilde{y}$	Measurements in observer, first used in eq. (7.6), page 90	$Pa$
$A_i(r)$	Pilot valve opening area , first used in eq. (2.4), page 10	$m^2$
$A_n(x_c)$	Variable nozzle area in pressure compensator , first used in eq. (2.26), page 18	$m^2$
$A_{co}(x_c)$	Opening area in pressure compensator , first used in eq. (2.28), page 18	$m^2$
$C_d(r)$	Variable flow coefficient , first used in eq. (2.4), page 10	–
$e_i$	Integral error , first used in eq. (2.21), page 14	$ms$
$e_p$	Proportional error , first used in eq. (2.21), page 14	$m$
$e_T$	Error variable for torque control, first used in eq. (5.13), page 62	$Nm$
$F$	Force , first used in eq. (1.2), page 5	$N$
$f_m$	Hydraulic motor factor describing the fluid characteristics , first used in eq. (2.25), page 15	–
$H_p$	Transfer function describing the pilot valve dynamics , first used in eq. (2.2), page 9	
$i$	Transformer modulus for hydraulic motor , first used in eq. (2.24), page 15	–
$k_{cf}(x_c)$	Flow force parameter in pressure compensator , first used in eq. (2.28), page 18	$m^4$
$k_f$	Flow force coefficient , first used in eq. (2.14), page 12	–
$P$	Power , first used in eq. (1.2), page 5	$N\frac{m}{s}$
$p$	Pressure , first used in eq. (1.2), page 5	$Pa$
$p_{A,s}, p_{B,s}$	Coefficients used in calculating $f_m$ , first used in eq. (2.25), page 16	–
$p_{loss}$	Viscous losses in pipes , first used in eq. (2.6), page 11	$Pa$
$p_m$	Angular momentum, hydraulic motor, first used in eq. (5.1), page 54	$Nms$
$P_{pump}$	Pump pressure, first used in eq. (5.1), page 54	$Pa$
$Q$	Fluid flow , first used in eq. (2.4), page 10	$\frac{m^3}{s}$
$Q_F$	Filtered flow , first used in eq. (2.19), page 13	$\frac{m^3}{s}$
$r$	Control input with dynamics , first used in eq. (2.4), page 10	–
$r_s$	Control slide reference , first used in eq. (4.3), page 43	$m$
$s_1$	Sliding surface 1, first used in eq. (5.10), page 55	
$s_2$	Sliding surface 2, first used in eq. (5.10), page 55	
$T_m$	Hydraulic motor torque , first used in eq. (2.24), page 15	$Nm$
$T_{dm}$	Reference torque, first used in eq. (5.13), page 62	$Nm$
$T_{load}$	Torque, hydraulic motor, first used in eq. (5.1), page 54	$Nm$

$T_{pump}$	Return pressure, first used in eq. (5.1), page 54	$Pa$
$u$	General controller output , first used in eq. (2.2), page 9	—
$v$	Velocity , first used in eq. (1.2), page 5	$\frac{m}{s}$
$v_1$	Virtual control, first used in eq. (5.10), page 55	$Pa$
$x_1$	Displacement state in mass-damper-spring example , first used in eq. (1.5), page 7	$m$
$x_2$	Velocity state in mass-damper-spring example , first used in eq. (1.5), page 7	$\frac{m}{s}$
$x_c$	Stroke of pressure compensator , first used in eq. (2.26), page 18	$m$
$x_s$	Valve displacement , first used in eq. (1.1), page 2	$m$
$x_A$	Volume state, hydraulic motor, first used in eq. (5.1), page 54	$m^3$
$x_B$	Volume state, hydraulic motor, first used in eq. (5.1), page 54	$m^3$
$x_{d2}$	Reference motor velocity, first used in eq. (5.10), page 55	$\frac{rad}{s}$
$x_H$	Control slide position, hoisting side, main valve A, first used in eq. (5.1), page 54	$m$
$x_L$	Control slide position, lowering side, main valve B, first used in eq. (5.1), page 54	$m$
$x_{m1}$	Hydraulic motor angle, first used in eq. (5.2), page 54	$rad$
$x_{m2}$	Hydraulic motor velocity, first used in eq. (5.2), page 54	$\frac{rad}{s}$
$y$	General symbol for output signal , first used in eq. (2.20), page 14	—
$y_s$	Valve opening , first used in eq. (1.1), page 2	$m^2$
$y_{heave}$	Heave position relative to surface , first used in eq. (6.0), page 78	$m$
$z_{s1}$	Virtual control, first used in eq. (5.10), page 55	$\frac{rad}{s}$
$z_{s2}$	Virtual control, first used in eq. (5.10), page 55	$Pa$
$\hat{x}_1$	Observed motor velocity , first used in eq. (7.6), page 90	$\frac{rad}{s}$
$\hat{x}_2$	Observed differential pressure , first used in eq. (7.6), page 90	$Pa$
$\hat{x}_3$	Observed motor load , first used in eq. (7.6), page 90	$Nm$
$K_d^A$	Derivative gain in adaptive law , first used in eq. (4.3), page 43	$\frac{Vs}{m}$
$K_i^A$	Derivative gain in adaptive law , first used in eq. (4.3), page 43	$\frac{V}{ms}$
$K_p^A$	Proportional gain in adaptive law , first used in eq. (4.3), page 43	$\frac{V}{m}$

# 1 | Introduction

In many offshore operations executed from ships highly advanced equipment are used. One example of such an operation is a ship performing subsea operations. The oil industry offshore has many examples of such operations. When the offshore oil rush started in earnest in Norway in 1969, by the finding of the oil reservoir "Ekofisk", the marine technological development accelerated. Maybe too fast, which the offshore divers got to experience first hand. In the summer in 1971 the oil production from Ekofisk started, which was a bummer for some of the politicians in Norway who stated that they would drink all oil ever produced in the North Sea.

In addition to drilling technology, subsea operations executed from ships became a money machine for third parties. Pipelines were to be installed on the sea floor, welded together by divers who were submerged from ships in diving bells, and high precision installations of "christmas trees" at the top side of the oil wells, preventing blow-outs and oil pollutions. The hard competition for the contracts drove the technological development even further. Now, the technological development has lead to perfection of systems such as dynamic positioning, DP, and heave compensated systems.

In every subsea operations performed by surface vessels, a winch system is more or less used. The

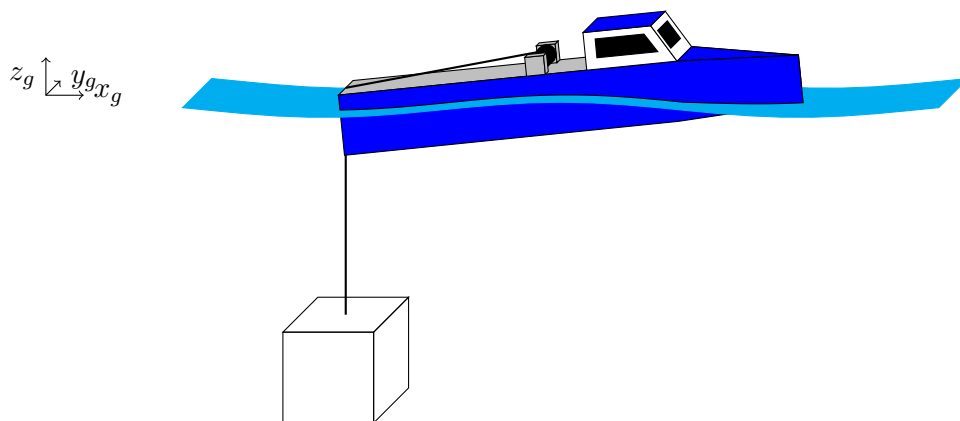


Figure 1.1: Ship in a marine operation affected by waves.

leading winch designs are either electrical driven or hydraulic powered systems. Electric driven winches are compact designs where an electrical motor, such as a permanent magnet motor, drives the reel where the wire is stored. The electrical motor is directly connected to the reel, which is placed on deck, and must be well designed in order to withstand the harsh environment such as sea water and large changes in temperature. The electrical motor is powered through the power management system in the vessel, PMS, and is controlled through a transformer to enable different hoisting or lowering velocities and tensions. The PMS must be well designed in order to handle large power peaks. It is also often necessary to have large gear ratios between the motor and the reel which would lead to large inertia forces that gives challenges in fast and precise winch control.

The hydraulic powered winch design is larger since pipelines, pumps and valves are part of the design. The pumping system is often placed below deck and connected to a hydraulic motor on deck which drives the reel with the stored wire. The reel velocity and torque are controlled trough valves which enables the usage of constant speed hydraulic pumps powered by the PMS. The hydraulic winch system is easier to control in lowering winch operations than the electrical

winch system, which has to have separate brakes or an electrical system consisting of resistors that can dissipate the power generated in such operations.

The hydraulic system is often either a high pressure system or a low pressure system. In a high pressure system less flow is required compared to the low pressure system, but the pressure is larger compared to a low pressure system. In this thesis a low pressure hydraulic winch system is to be studied. The work description regarding this thesis is given in Appendix A.

## 1.1 Introduction to the Hydraulic System

The low pressure hydraulic system that is to be studied in this thesis is a classical and well known hydraulic system where a hydraulic motor is controlled by one or more valves. Low pressure is relative, but here it is meant to be below 100 bars. Usually a 4/3-directional valve is used in such systems but here two 3/3-directional valves are used instead. The reason for this is that it enables more control settings and by controlling the two valves opposite of each other they will together act as one 4/3-directional valve, which will be in focus in this study. The 3/3- and 4/3-directional valve get their names from the number of inputs and outputs, the number of valve settings and the opening or flow characteristics. A 3/3 valve has together 3 inputs and outputs and has 3 valve settings, a 4/3 valve has in total 4 inputs and outputs and 3 valve settings. The word "directional" may be a little vague but it refers to the ability to direct flows in different directions. Often "proportional" is used wrongly as a synonym for this type of valves. The word proportional says something about the valve opening characteristics. By moving the valve a given distance, lets say  $x_s$ , the valve opening area is  $y_s$  and there is a proportional relationship between  $x_s$  and  $y_s$ . If the valve opening is rectangular the relationship is given as

$$y_s = hx_s \quad (1.1)$$

where  $h$  is the height of the rectangular opening.

Figure 1.2 shows a sketch of a 3/3-directional valve (1.2a) and a simplified 3/3-directional valve symbol (1.2b).

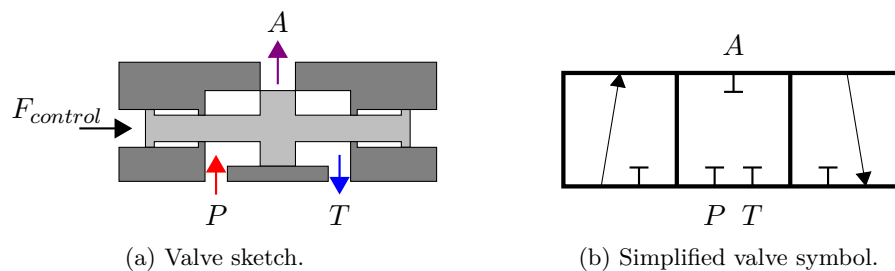


Figure 1.2: 3/3 directional valve.

Often the valve symbol has a spring and an extra arrow at one of the short sides to indicate that it has a centring spring and is controllable respectively. For comparison figure 1.3 shows a 4/3 directional valve.

As can be seen from figure 1.3a there is five inputs and outputs in total, but since two of them are equal, the T ports, the valve is still a 4/3-directional valve. This means that the number of inputs and outputs must be unique in the naming convention. The port  $F_{control}$  in the figures is the control force applied to the valve in order to control the valve displacements and thereby the valve opening. For small valves this force can be generated through a magnetic field with voltage as control actuation. This is referred to as a solenoid operated valve where the moving



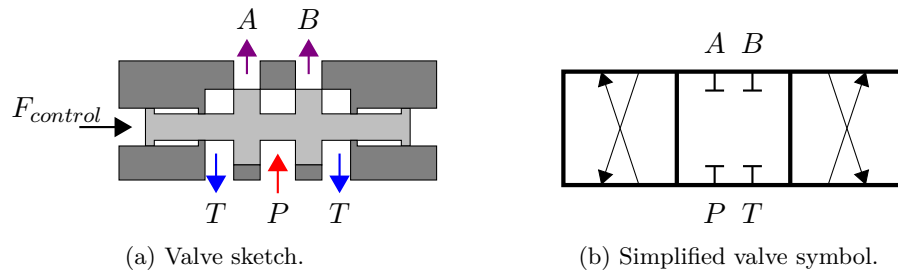


Figure 1.3: 4/3 directional valve.

part in the valve is the plunger with wire windings wrapped around generating the magnetic field. For larger valves the strength of the magnetic field must be large in order to generate enough force to control the valve opening with a fast enough response. Thus large valves is often controlled mechanically or hydraulically. For hydraulic controlled valves another valve is required to direct the *pilot* flow to each side of the main valve. This pilot valve is smaller and can therefore be solenoid operated. This also means that the main valve is controlled through a pilot valve. The 3/3-directional valves that are studied here are of the pilot operated type and figure 1.4 shows a schematic overview of the total system.

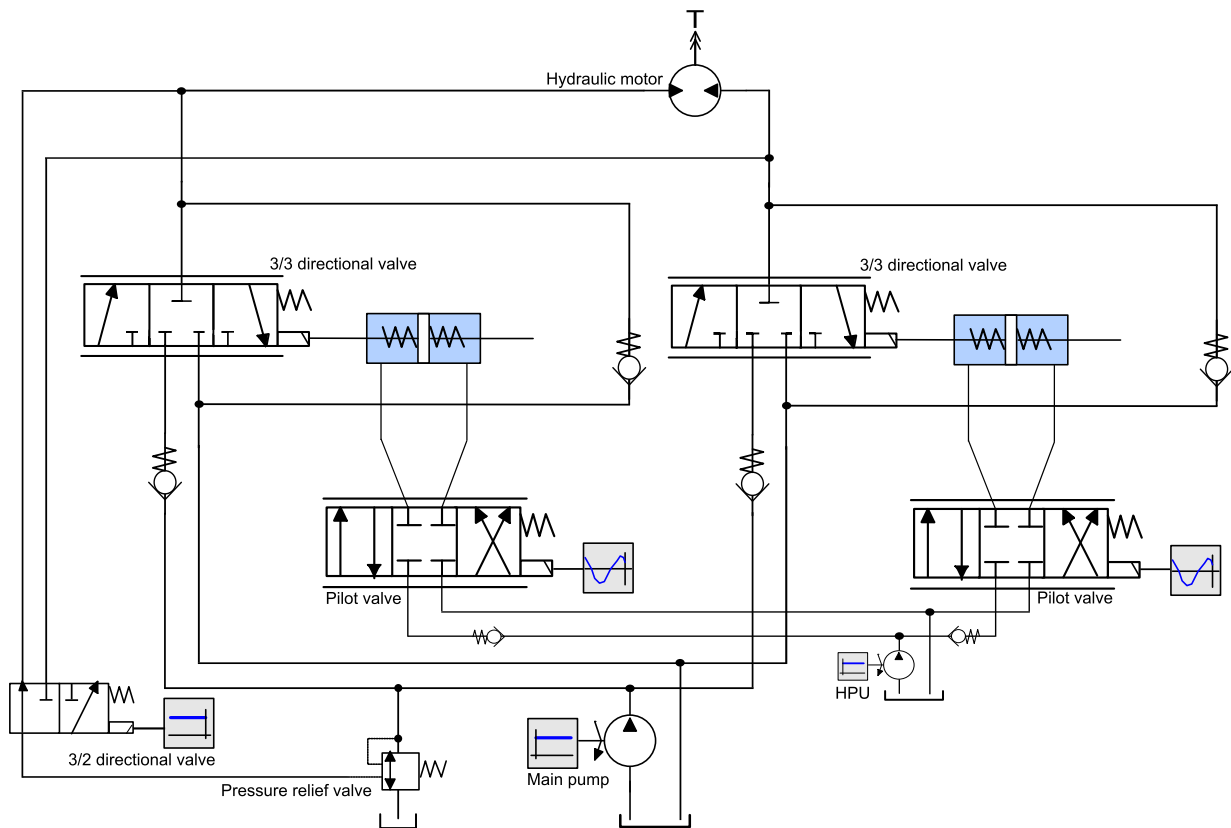


Figure 1.4: Model overview.

The 3/3-directional valves are given in the figure as 3/3 directional valve symbol and double rodded pistons. These pistons, the moving parts in the valves, are often referred to as the *control slides*. As the figure shows there are springs inside control slides. These symbolizes centring springs that centres the control slides if the pilot pressure is lost. There are also two check-valves for each main valve, one connected to the pressure line to prevent fluid flow from the motor to the main pump if the load is large, and the other connected to the return line to prevent the delivered pressure to be lower than the tank pressure.

The pilot valve directs the pilot flow from the HPU, Hydraulic Power Unit, to control the main valve. There are also check-valves on these pressure pipelines.

In the lower left corner in the figure there is a 3/2-directional valve and a pressure relief valve. The 3/2-directional valve directs the highest pressure of the two motor sides to the pressure relief valve. The relief valve makes sure that the pressure in the main system doesn't get too large, only a few bars higher than the motor loading pressure.

## 1.2 Related Work

Hydraulic systems have been studied in academia since its origin and there exist many references for related work containing directional valves. Hydraulic systems for controlling a winch is only one area of usage, but all systems including valves are based on the same dynamics and the goal is often to control the system through these valves. However the main focus is often either modeling for control purposes or precise modeling for benchmarking.

In Yang et al. (2012) a solenoid operated directional valve is modeled using bond graph theory and includes a thoroughly model parameter sensitivity analysis using simple voltage step responses. The results show that the valve response is really fast and is expected to be much faster than the main valve responses in the hydraulic winch power system given in figure 1.4. This gives reason to believe that the solenoid operated pilot valves in the hydraulic system can be assumed ideal and the dynamics may be modeled as a second order transfer function, as a simplification.

The flow and pressure through the valves are the main contributors for changing the valve dynamics. That is why it is important to model the losses in valves properly. In Borutzky et al. (2002) an orifice flow model for laminar and turbulent conditions are studied. This was also done in Skjong (2013) and in this thesis only turbulent flows are assumed since the error by excluding laminar flow from the model showed to be negligible. However CFD analysis should be performed in order to determine the flow coefficients and flow force coefficients as functions of valve displacement. In this thesis these coefficients included in the model are assumed constant. Later on it is easy to include variable coefficients if such data are available.

The directional valves are used in various systems. Many related studies show the use of a directional valve in positioning a piston, a servo, a load or in pressure compensation systems. In Kim et al. (2010) a high gain observer based nonlinear position control for electro-hydraulic servo systems are studied and in Lei et al. (2013) sliding mode control in piston control for asymmetrical hydraulic cylinder with connected chambers are studied. In these papers the models are derived for control purposes and show that linear control theory does not give satisfying performance. That is why model based control laws such as sliding mode control, observer based control and backstepping control often are used. This is also elaborated in Çetin and Akkaya (2010) and the conclusion is that the PID-controller used is working around its set-point, but the accuracy decreases outside this region and there is no guarantee that the system remains stable.

When it comes to control of hydraulic winches there are many related studies that look at specific winch operations such as lowering a load from air into water. In KÜchler and Sawodny (2010) a control algorithm for lowering or hoisting a load in the water entry phase is studied. Two controllers are used, one for trajectory tracking and stabilization and one for compensation of the environmental disturbance given from measurements. The measurements are affected by time delays and a feed forward is used to minimize this effect. In KÜchler et al. (2011) active control for an offshore crane using prediction of the vessel's motion is studied. The vessel's motion is measured and wave spectrum analysis including wave frequency peak detection is initiated to predict the vessels motion. These two studies are closely related to the scope of this

thesis. On the contrary, this thesis should focus more on the modeling of the winch system and how simple model based controllers can act together to minimize the environmental disturbances using only simple measurements.

As a summary, related work show that valve dynamics are complex and dependent on flows and pressures in the system. These dynamics are nonlinear and must be included in the model to get realistic responses. If the system is to be controlled through valves, nonlinear control theory should be considered to obtain a satisfying system performance.

### 1.3 Introduction to Bond Graph Theory

To model the hydraulic system bond graph theory is used. In Karnopp et al. (2006) a bond graph is said to simply consists of subsystems linked together by lines representing power bonds. Since power is the product of flow and effort in a system the power bonds relate subsystems to each other with efforts and flows. The definition of effort and flow may vary from system to system, but the product, the power, is always the same. In a hydraulic system the effort is given as pressure and the flow is given as the fluid flow. In a mechanical system however the effort is given as force and the flow is given as velocity. By multiplying the effort and the flow,

$$P = p\dot{Q} = [Pa] \cdot \left[ \frac{m^3}{s} \right] = \left[ N \frac{m}{s} \right] \quad (1.2a)$$

$$P = Fv = [N] \cdot \left[ \frac{m}{s} \right] = \left[ N \frac{m}{s} \right] \quad (1.2b)$$

we see that the power is the same. The effort and flow are shortened to  $e$  and  $f$  respectively. By describing the efforts and the flows between subsystems one can determine the interaction between the subsystems. Figure 1.5 shows a principal sketch of how subsystems are connected through power bonds. The direction of the half-arrow gives the direction for the effort, and

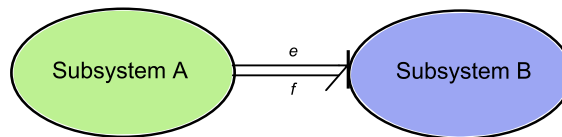


Figure 1.5: Power bond connecting subsystem A and B.

the flow goes in the opposite direction. If subsystem A and B were mechanical systems a force from subsystem A is applied to subsystem B and as a counteraction a velocity is given back to subsystem A from B. Or, subsystem B gives a velocity to subsystem A and gets a responsive force in return.

In bond graph theory different building blocks are used. These are summarized in table 1.1. Both the  $S_e$  and  $S_f$  elements are sources, effort and flow respectively. If hydraulics are modeled then  $S_e$  is a pressure source and  $S_f$  is a fluid flow source. The  $R$  element is describing energy dissipation like friction forces or viscous forces. It can also be used to model valves as seen later on. The  $C$  element describes the stored energy in the system, like a spring in a mechanical system or an accumulator in a hydraulic system. Inertia in a mechanical system or an inductor in an electrical circuit is given as a  $I$  element. Transformation of efforts and flows between subsystems is usually done by using a  $TF$  element. To sum different contributions of effort the  $1$ -junction is used and to sum different contributions of flow the  $0$ -junction is used. There is also one more basic element that is not included in the table. This is the gyrator element,  $GY$

that transforms flows to efforts and vice versa. This element can be associated with a generator that gets a rotational velocity, a flow, and transforms it to voltage, an effort.

Table 1.1: Some basic bond graph elements used.

Symbol	Relation
$S_e \dashrightarrow$	$e = e(t)$ , given
$S_f \dashrightarrow$	$f = f(t)$ , given
$\dashrightarrow R$	$e = \Phi_R(f)$
$\dashrightarrow R$	$f = \Phi_R^{-1}(e)$
$\dashrightarrow C$	$e = \Phi_C^{-1}(\int_0^t f dt)$
$\dashrightarrow C$	$f = \frac{d}{dt}[\Phi_C(e)]$
$\dashrightarrow I$	$f = \Phi_I^{-1}(\int_0^t e dt)$
$\dashrightarrow I$	$e = \frac{d}{dt}[\Phi_I(f)]$
$\xrightarrow{1} TF \xrightarrow{2}$	$e_1 = m e_2$ $f_2 = m f_1$
$\dashrightarrow TF \dashrightarrow$	$e_2 = \frac{1}{m} e_1$ $f_1 = \frac{1}{m} f_2$
$\begin{array}{c} e_2 \uparrow f_2 \\ \xrightarrow{f_1} \mathbf{1} \xrightarrow{f_3} \\ \downarrow f_1 \end{array}$	$e_1 - e_2 - e_3 = 0$ $f_1 = f_2 = f_3$
$\begin{array}{c} e_2 \uparrow f_2 \\ \xrightarrow{f_1} \mathbf{0} \xrightarrow{f_3} \\ \downarrow f_1 \end{array}$	$e_1 = e_2 = e_3$ $f_1 - f_2 - f_3 = 0$

In bond graph theory only two of the basic elements are candidates for state generation. A state is a variable that is unique and can describe the dynamics in a system. The states describe the dynamics in a system through differential equations. From physics we know that a one dimensional mass-damper-spring system has the position and the velocity as states if only first order differential equations are used. By modeling a mass-damper-spring system using bond graph theory a  $C$ ,  $I$  and a  $R$  element are used together with  $\mathbf{0}$ -junctions,  $\mathbf{1}$ -junctions,  $S_e$  and/or  $S_f$  elements. To get the same states from a bond graph we know that one of the elements must describe the position and one must describe the velocity. Since the  $R$ -element only describes dissipation of energy it can not contribute to any states. This means that the  $C$ -and  $I$ -elements must give the system states. Then it is not surprising that the  $C$  element gives the displacement and the  $I$ -element gives the momentum,

$$q = \int_0^t p \cdot f dt \tag{1.3a}$$

$$p = \int_0^t p \cdot e dt. \tag{1.3b}$$

A well known syntax in graph theory is that  $p.e$  is the effort,  $p.f$  is the flow,  $q$  is the state from

the  $C$  element and  $p$  is the state from the  $I$  element. To finish the mass-damper spring system, see figure 1.6, we may write the states as

$$\dot{q} = \frac{p}{m} \quad (1.4a)$$

$$\dot{p} = -kq - b\frac{p}{m} + mg \quad (1.4b)$$

By defining  $x_1 = q$  and  $x_2 = \frac{p}{m}$  we can rewrite the differential equations as

$$\dot{x}_1 = x_2 \quad (1.5a)$$

$$m\dot{x}_2 = -kx_1 - bx_2 + mg \quad (1.5b)$$

which is the well known one dimensional mass-damper-spring system of differential equations. The mass-damper-spring system is important in dynamics since almost every physical system can relate to it.

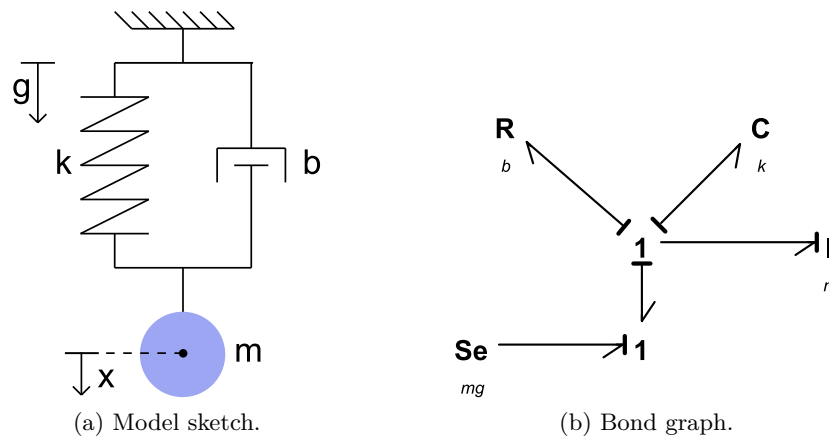


Figure 1.6: Mass-damper-spring system.

By taking a closer look at figure 1.6b small lines orthogonal to each power bond can be seen. This is the causality mark and gives the direction of the effort. The different causality mark and the associated equations are also given in table 1.1. For the  $S_e$ - and  $S_f$ -element the causality mark is located at the half arrow tip and the opposite end of the arrow tip respectively. In other words the causality of these elements is predetermined. For the  $C$ - and  $I$ -element the causality mark is important and is given as integral causality, as in figure 1.6b or differential causality which is opposite of the marks given in the figure. To get states from the  $C$ - and  $I$ -elements integral causality is required. This is also the mode physics appears in real life, but by using simplified models we may come in touch with differential causality. Since almost every model is simplified it is quite usual that differential causality appears. In practise some tricks can be applied to restore integral causality in the model. If not, the elements with differential causality are not unique and must be described by other states. Another phenomenon is algebraic loops. These appear when causality can't be assigned uniquely. The  $R$ -element can have the causality mark at both ends of the half arrow tip, only one at a time though. When an algebraic loop appears the two elements that causes the algebraic loop must be related to each other as a constraint.

When modeling using the software 20Sim both differential causalities and algebraic loops are solved by the program, but when abstracting the differential equations from the bond graph model, which is the beauty of using bond graph theory, one must solve these manually. For more information about bond graphs the book by Karnopp et al. (2006) is recommended. A

more thorough description of the hydraulic system is given in the following chapters. The next chapter takes the aim at modeling the presented hydraulic system in order to be able to design relevant control laws for controlling the hydraulic motor in various settings and environments later on.

## 2 | Modeling Hydraulic System

The hydraulic system that is to be modeled has been presented in figure 1.4 and a short description has been given in chapter 1. To model a system of this size it is important to have a clear understanding of the purpose and the limits of the model that is to be developed. This is important not only because of the workload but also the complexity and the time it takes to solve the model in simulations. A model developer usually wants the model to converge to the physical system with high accuracy, but also that the model is fast to solve. These wishes are often contradictions since an accurate model often has a high level of complexity and thus is slow in simulations and a fast model often has a low level of complexity and thus is not that accurate. To be able to develop a model that is *fast enough* and has an accuracy within a certain required limit, the purpose with the model must be reviewed. The purpose of the model for the hydraulic system is to be able to reproduce the main dynamics as fast as possible and be able to make control laws for controlling the system. This means that the model must at least catch the slower dynamics in the system with high accuracy. This gives room for assumptions and simplifications when modeling. These assumptions and simplifications will be stated and argued for as they come. The bond graph model is based on the results from previous work, see Skjong (2013).

As a modeling strategy the line of control is followed, starting with the pilot valve, then the main valve and so on.

### 2.1 Pilot Valve

The pilot valve is assumed to be solenoid operated and receives voltage as input. The dynamics of such a valve are relative fast compared to other dynamics in the system and therefore it is reasonable to do simplifications to save simulation time without losing too much accuracy. In Yang et al. (2012) a bond graph model of a solenoid operated 4/3 directional valve was developed where all reasonable effects were taken into account. As seen the response of such a valve is fast but also complex. For the system given in figure 1.4 it is assumed that the dynamics of the pilot valve can be given as a mass-damper-spring system, as given in (1.5), except that  $mg$  is changed to  $u$ , where  $u$  is a control input. This simplification is reasonable since the pilot valve has fast dynamics and the contribution to the total model error should be small. This set of first order differential equations can be written as a transfer function,

$$H_p(s) = \frac{x(s)}{u(s)} = \frac{1}{ms^2 + bs + k} \quad (2.1)$$

or

$$H_p(s) = \frac{K\omega^2}{s^2 + 2\zeta\omega s + \omega^2} \quad (2.2)$$

where  $\omega^2 = \frac{k}{m} = f^2 4\pi^2$ ,  $K = \frac{1}{k}$  and  $\zeta = \frac{b}{2} \sqrt{\frac{1}{mk}}$ . For a solenoid operated valve the input is transformed from voltage to magnetic force which moves the valve spool. In the simplified model we may assume that the valve input is limited between  $\pm 10$  V. This means that the pilot valve is fully open in positive direction when the input is 10 V and fully open in negative direction when the input is -10 V after a short period of time due to the pilot dynamics. In bond graphs the pilot valve is given as in figure 2.1. As the figure shows the pilot valve dynamics are added to the input signal to the valve. Port P and T is the HPU pressure, tank pressure or return

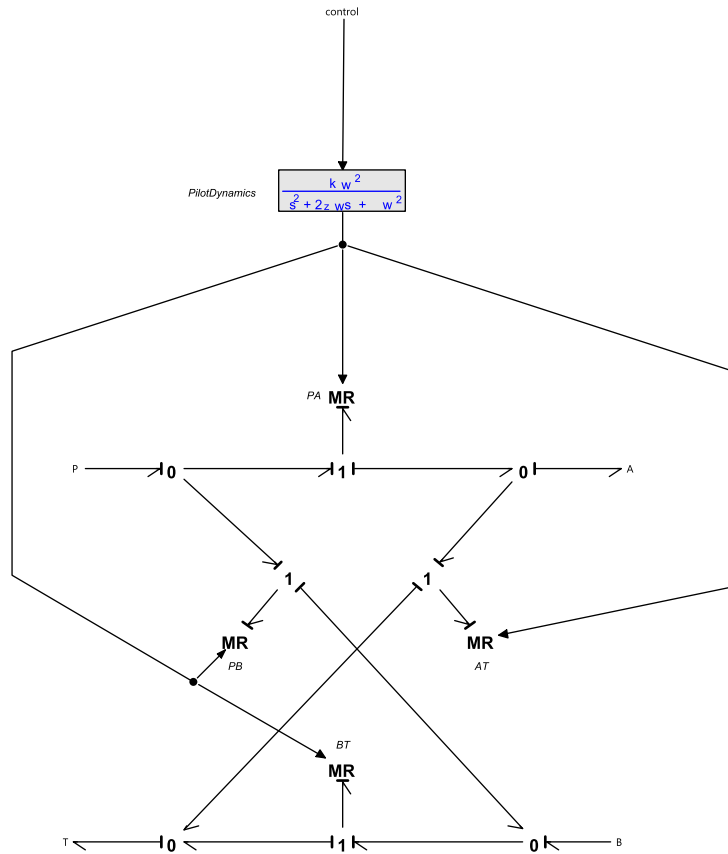


Figure 2.1: Bond graph model of pilot valve.

pressure respectively. Port A and B are the two outputs from the valve. The settings are the same as shown in figure 1.3. Each MR-element is programmed to open in a certain range within the input signal. The flow through each MR element is given as

$$Q = \text{sign}(\Delta p) C_d(r) A_i(r) \sqrt{\frac{2}{\rho} |\Delta p|} \quad (2.3)$$

where  $r$  is the output signal from the transfer function,  $C_d(r)$  is the flow coefficient that may be dependent on the valve position,  $A_i(r)$  is the opening area,  $\rho$  is the pilot fluid density,  $Q$  is the flow of hydraulic fluid and  $\Delta p$  is the differential pressure across the valve. This equation can be derived from Bernoulli's equation.  $A_i(r)$  is given as

$$A_i(r) = \text{limit}\left(\frac{ar}{10} A_{max}, 0, A_{max}\right) \quad (2.4)$$

where  $a = 1$  for the MR-elements PA and BT,  $a = -1$  for PB and AT and  $A_{max}$  is the maximal valve opening area. There are also flow forces acting on the valve, both static and transient flow forces. These are assumed small and negligible since the pilot valve dynamics are simplified. It is also assumed that there is no leakage, or at least that it is negligible. In 20Sim the pilot valve model is implemented as a submodel with its own symbol as given in figure 2.2.

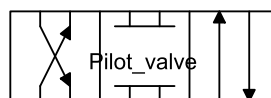


Figure 2.2: Symbol for pilot valve in bond graph model.



The next system to model is the main valve, the 3/3 directional valve.

## 2.2 3/3-Directional Valve

To model the 3/3-directional valve the same approach as used when modeling the pilot valve can be applied. However instead of using a transfer function to describe the valve dynamics bond graph elements should be used. The reason for this is because this gives more options and gives the ability to include more complexity in the model. As for the pilot valve the main valve can be divided into two submodels, one describing the valve dynamics and the other describing the flow through the valve. These two submodels are not connected by power bonds but by signals. To elaborate this, it is known that the control slide position determines the opening area in the valve and thus the flow through it can be determined if the pressures are known. This gives a signal from the submodel describing the valve dynamics to the submodel describing the flow. However there should also be signals from the flow model to the valve dynamics giving the flow forces acting on the control slide.

### 2.2.1 Valve Dynamics

Starting with the model describing the valve dynamics there should be a connection between the pilot valve and the main valve delivering the pilot flow through pipes. These pipes have some viscous losses that should be included in the model. These viscous losses are given as

$$p_{loss} = \frac{1}{2} f_{pl} \rho \frac{L_p}{D_{pi}} |Q|Q \quad (2.5)$$

where  $f_{pl}$  is the loss factor,  $L_p$  is the length of the pipes and  $D_{pi}$  is the inside diameter of the pipes. Also control cylinder accumulation and fluid inertia in the pipes could be included, but these contributions are also assumed small. For the sake of it, the fluid inertia in the pipes connecting the pilot valve and the main valve and the cylinder accumulation are included in the model to check the validity of the assumption to be able to exclude them. The cylinder accumulations are modeled as C-elements where

$$p = \frac{\beta_v Q}{V_0 \pm A_s x_s} + p_0 \quad (2.6)$$

and where  $p$  is the pressure in the volume,  $\beta_v$  is the pressure dependant bulk modulus of the hydraulic fluid,  $V_0$  is the initial volume,  $A_s$  is the area of the control slide and  $p_0$  is the initial pressure.

The variable bulk modulus (McCloy and Martin, 1980) used in the model is given as

$$\frac{1}{\beta_v} = \frac{1}{\beta_h} + \frac{1}{\beta_f} + \frac{n}{1.4p} \quad (2.7)$$

where  $\beta_h$  is the bulk modulus for the pipeline, or the valve housing,  $\beta_f$  is the constant bulk modulus for the hydraulic fluid and  $n = \frac{V_g}{V_f}$  is the volume ratio of gas (air) and fluid. As can be seen from (2.6) and (2.7) they are both dependent on each other, so iterations must take place which will cause the solving time in simulations to increase. The fluid inertia is modeled as an I-element,

$$Q = \frac{\int_0^t \Delta p}{I_f} dt \quad (2.8)$$

where  $I_f = \frac{4\rho L_p}{D^2 \pi}$ . Also some fluid volumes are necessary to include in the model to obtain integral causalities. These volumes are also modeled as C-elements,

$$p = \frac{\beta_v \int_0^t Q dt}{V_0} + p_0. \quad (2.9)$$

The pilot pressure gives forces on both sides of the control slide which means that the effort is changed from pressure to force before interacting with the main valve dynamics. This transformation is done by using a TF-element in bond graph theory with equations given as in table 1.1 where  $m = A_s$  and where  $A_s$  is the control slide Area. The main valve also has a centring spring, centring the control slide to the *zero* position if pilot pressure is lost. In the zero position there is no flow through the valve. The spring is also pre-compressed, which means that there is a discontinuity at zero position. This can be solved by modeling the spring forces as

$$F = k_s x_s + \frac{2k_s x_{s0}}{\pi} \arctan(x_s s) \quad (2.10)$$

where  $k_s$  is the spring stiffness,  $x_s$  is the control slide position, as before, and  $s$  is a parameter describing the slope in the  $\arctan(\cdot)$  function. Also some viscous and friction losses are present acting on the control slide. These are assumed to be given as a second order function and by using an R-element the dissipative force can be expressed as

$$F = p_{L1} |\dot{x}_s| \dot{x}_s + p_{L2} \dot{x}_s \quad (2.11)$$

where  $p_{L1}$  and  $p_{L2}$  are loss constants. Another phenomenon called hydraulic cylinder stiction can in some cases be relevant to include in the model. If the seals in the valve are tight and stiff and the hydraulic fluid is thick the stiction would be relevant and could be included as a coulomb friction. However this is not included in this model because the stiction contribution is assumed small and negligible. It is assumed that there always is an oil film between the control cylinder and the valve housing that never gets broken. To finish the valve model control slide inertia is included as an I-element and flow forces acting on the control slide as an MSe-element where a static flow force is given as

$$F = \frac{k_f(x_s) Q^2 \rho}{\pi D_s x_s} \quad (2.12)$$

where  $k_f(x_s)$  is a flow force coefficient, that could be dependent on the control slide displacement, describing the magnitude of the flow force and can be found from CFD analysis,  $D_s$  is the control slide diameter and is the height of the valve opening and  $Q$  is the flow through the valve. This equation can also be written as an ordinary equation describing the drag force,

$$F = \frac{1}{2} \rho \frac{Q^2}{\pi D_s x_s} C_d \quad (2.13)$$

where

$$k_f(x_s) = \frac{1}{2} C_d \quad (2.14)$$

and where  $C_d$  is a flow coefficient that may be dependent on the control slide position. There are also transient flow forces acting on the control slide but these are assumed small compared to the inertia forces and is therefore neglected.

### 2.2.2 Flow Model

The flow forces acting on the control cylinder have already been discussed but the flow through the valve has to be included in the model. When the flow opens from P to A, see figure 1.2, then  $x_s$  is positive. Since there is a check valve between the valve and the pump pressure line the flow can be assumed to only go from P to A and never from A to P. This simplifies the model because the check valve doesn't need to be included further when modeling. One important assumption when neglecting the check valve is that the dynamics are fast and the valve closes almost instantaneously if the pump pressure drops below the pressure at port A.

There can also be an overlap in the valve, a dead band. This means that the flow through the valve can be written as

$$Q = \begin{cases} Q(x_s) & \text{for } x_s > x_{olap} \\ 0 & \text{else} \end{cases} \quad (2.15)$$

where  $x_{olap} \geq 0$  is the overlap and

$$Q(x_s) = \begin{cases} \alpha(x_s)(x_s - x_{olap})\pi D_s \sqrt{\frac{2}{\rho} \Delta p} & \text{for } \Delta p > 0 \\ 0 & \text{else} \end{cases} \quad (2.16)$$

where  $\alpha(x_s)$  is a flow coefficient that may be dependent on the control slide position. For the flow between port A and port T there is no check valve so it may flow both ways. This gives

$$Q = \begin{cases} -\alpha(x_s)\text{sign}(\Delta p)(x_s + x_{olap})\pi D_s \sqrt{\frac{2}{\rho} |\Delta p|} & \text{for } x_s < -x_{olap} \\ 0 & \text{else.} \end{cases} \quad (2.17)$$

Also for the main valve it is assumed no leakage, both exterior and interior.

There are also two more check valves, one for the HPU pressure line and one to prevent the pressure at port A to be below the tank pressure. Since these check valves have fast dynamics they are only considered as open or closed. The flow through them are given as

$$Q = \begin{cases} \sqrt{\frac{\Delta p}{k_c}} & \text{for } \Delta p \geq \Delta p_{set} \\ 0 & \text{else} \end{cases} \quad (2.18)$$

where  $k_c$  is a design parameter. If the valve settings (closed/open) causes simulation problems then a first order transfer function can be used to give the valve some dynamics. Then

$$Q_F = \int_0^t \frac{Q - Q_F}{\tau} dt \quad (2.19)$$

where  $\tau$  is a time constant and  $Q_F$  is the flow after filtered through the first order transfer function and  $Q$  is as given in (2.18).

### 2.2.3 Bond Graph Model

The bond graph model of the pilot valve and the main valve is given in figure 2.3, both with and without cylinder accumulation and fluid inertia.

As an addition to what already mentioned, a position controller for the main valve, a velocity limitation function for the reference signal, sampling blocks and a ZOH-block (Zero-Order-Hold), are implemented. The velocity limitation function is just a first order transfer function,

$$y(s) = \frac{V_{max}}{s + V_{max}} r(s). \quad (2.20)$$

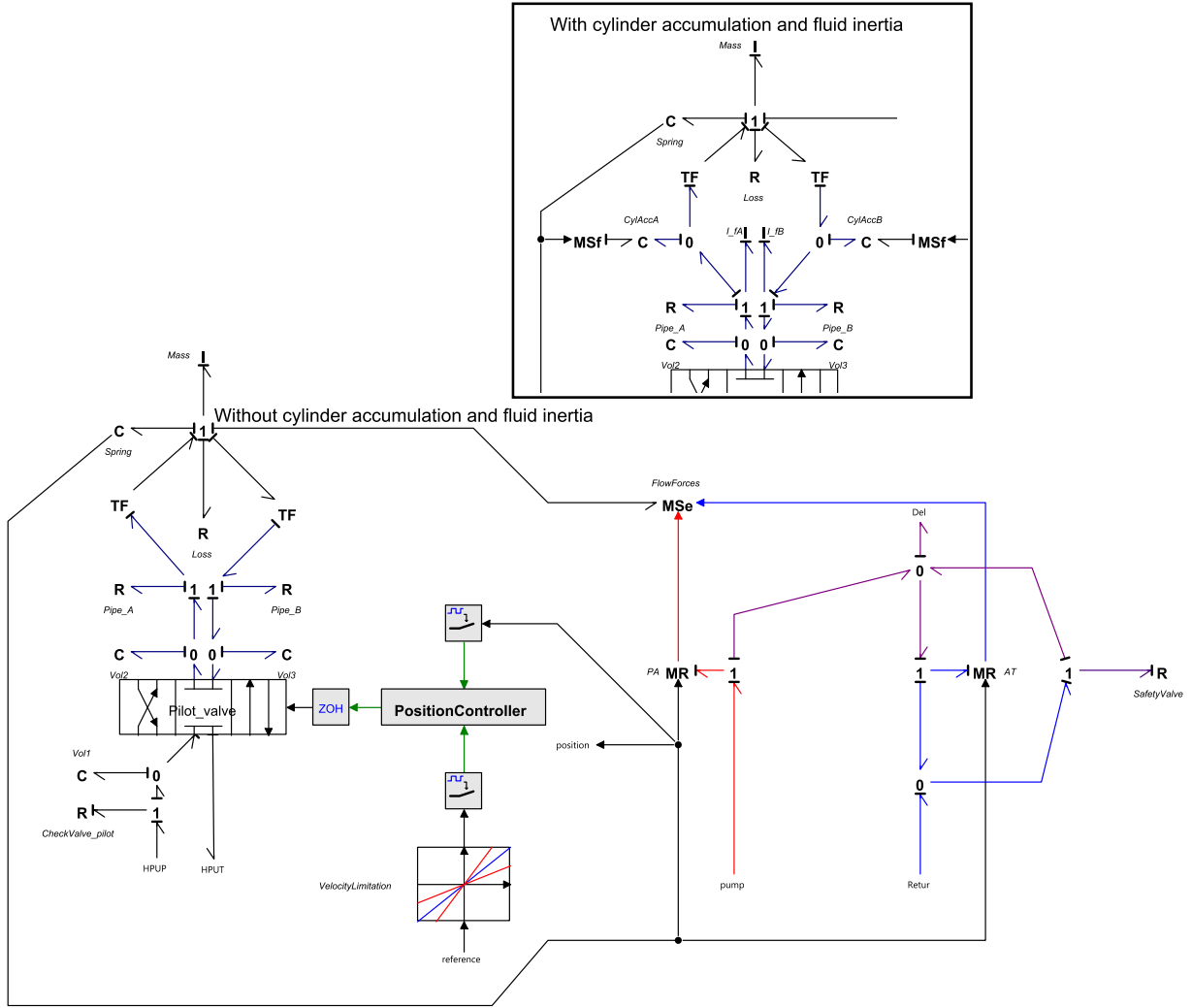


Figure 2.3: Bond graph model of 3/3-directional valve.

Since the transfer function may add a bias to the tracking error a PI-controller is implemented. This gives

$$e_p = r_{k-1} - y_{k-1} \quad (2.21a)$$

$$e_i = \int_0^t e_p dt \quad (2.21b)$$

$$y(k) = \int_0^t (K_p e_p + K_i e_i - y_{k-1}) V_{max} dt \quad (2.21c)$$

where  $e_p$  and  $e_i$  are errors,  $K_p$  is the proportional gain,  $K_i$  is the integral gain,  $r$  is the input and  $y$  is the output from the velocity limitation function respectively and  $V_{max}$  is the maximal slope of the reference signal allowed.

The sampling block turns analogue signals into digital signals with a sampling time  $T_s$ . The sampling boxes may also have a fixed sampling delay,  $T_d$ . The zero-order-hold block turns the digital signals into analogue signals.

The position controller controls the position of the control slide according to given reference signals. For simplicity this *inner controller* is set as a P-controller for now. To simplify the global bond graph model, the bond graph given in figure 2.3 is put into a submodel with its own icon given in figure 2.4.

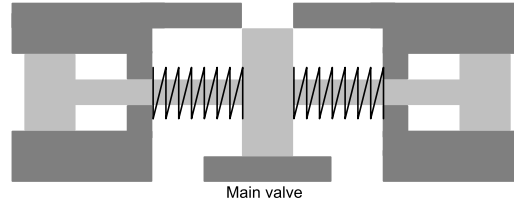


Figure 2.4: Main valve icon.

The next system to model is the hydraulic motor.

## 2.3 Hydraulic Motor Model

The hydraulic motor used here is a one cambered hydraulic motor with fixed displacement. The motor is driven by the differential pressure, the difference in pressure between the pressures delivered by the main valves. Such a motor almost always has an internal leakage that needs to be included in the model and a variable gear ratio given by the characteristics of the hydraulic fluid. Friction and viscous losses should also be included.

Starting with the inertia of the motor the rotating parts of the motor as well as the rotating fluid should be considered. Since the bulk modulus is variable the mass of the fluid inside the motor is varying, but this variation is considered small and negligible.

The friction losses include two parts, static friction and lubricated friction. The static friction is only present when the motor speed is zero and the lubricated friction is only present when the motor rotates. These effects is in Pedersen and Engja (2010) expressed as

$$F = F_s \left( \mu_s \tanh(\omega_m s) - \frac{1}{2}(\mu_s - \mu_c) \tanh \left( s \left( \omega_m - \frac{c}{s} \right) \right) + \frac{1}{2}(\mu_c - \mu_s) \tanh \left( s \left( \omega_m + \frac{c}{s} \right) \right) \right) + F_s \mu_v \omega_m \quad (2.22)$$

where  $\omega_m$  is the hydraulic motor velocity,  $F_s$  is the static friction,  $\mu_s$ ,  $\mu_c$  and  $\mu_v$  is the static, coulomb and viscous friction coefficient respectively and  $s$  is a slope parameter in the friction function. The internal leakage is proportional to the differential pressure,

$$Q = G \Delta p, \quad (2.23)$$

where  $G$  is the leakage parameter, also called conductance of laminar resistance, and  $\Delta p$  is the differential pressure.

To finish the hydraulic motor model transformations between pressure and torque and fluid flow and angular rate are needed. These transformations are given as

$$Q = i \cdot \omega_m \quad (2.24a)$$

$$T_m = i \cdot p \quad (2.24b)$$

where  $T_m$  is the hydraulic motor torque and  $i$  is the transformer modulus and is given as

$$i = f_m \frac{D_m}{2\pi} \quad (2.25)$$

where  $D_m$  is the displacement of the motor and  $f_m$  is a factor describing a simplified fluid

characteristic,  $0 \leq f_m \leq 1$ , and is given by algorithm 1 (Controllab, 2014).  $p_A$  is the pressure at side A of the motor (hoisting side),  $p_B$  is the pressure at side B of the motor (lowering side,  $\Delta p = p_A - p_B$ ),  $p_{vap}$  is the vapour pressure for the hydraulic fluid and  $p_{A,s}$  and  $p_{B,s}$  are variables used in the algorithm. This fluid characteristics describes the gear ratio which is dependent on the pressure. For pressures equal to or lower than the vapour pressure,  $p_{vap}$ , the motor will experience cavitation and will not generate any torque.

---

**Algorithm 1** Calculating  $f_m$  (Controllab, 2014)

---

```
 $p_{A,s} = 1 - \frac{p_A}{p_{vap}}$ 
 $p_{B,s} = 1 - \frac{p_B}{p_{vap}}$ 
if  $\omega_m > 0$  and  $p_{A,s} < 0$  then
     $f_m = 0$ 
else
    if  $\omega_m > 0$  and  $p_{A,s} < 1$  then
        if  $p_{A,s} < 0.5$  then
             $f_m = 2p_{A,s}^2$ 
        else
             $f_m = 4p_{A,s} - 2p_{A,s}^2 - 1$ 
        end if
    else
        if  $\omega_m < 0$  and  $p_{B,s} < 0$  then
             $f_m = 0$ 
        else
            if  $\omega_m < 0$  and  $p_{B,s} < 1$  then
                if  $p_{B,s} < 0.5$  then
                     $f_m = 2p_{B,s}^2$ 
                else
                     $f_m = 4p_{B,s} - 2p_{B,s}^2 - 1$ 
                end if
            else
                 $f_m = 1$ 
            end if
        end if
    end if
end if
```

---

The finished bond graph model for the hydraulic motor is given in figure 2.5. The port Load in the bond graph gives the motor loading. The bond graph model is put into a submodel with its own icon shown in figure 2.6. As the figure shows two volumes have been added, one on each side of the motor. The reason for adding these volumes is to obtain integral causality in the model. These volumes also have variable bulk modulus, which are given as before in (2.7) and (2.9). The figure also shows that an effort source has been added to the submodel describing the motor loading. For more thorough controller testing later on a more realistic model of the motor loading should be implemented than an effort source, describing the wire, reel and loading dynamics.

The next part to include in the model is the pressure compensator.

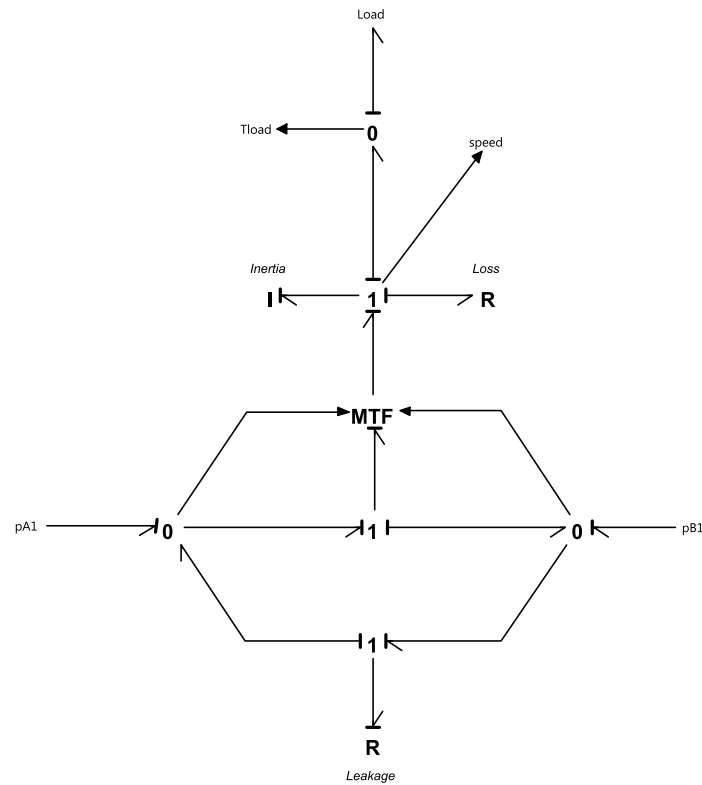


Figure 2.5: Bond graph model of hydraulic motor.

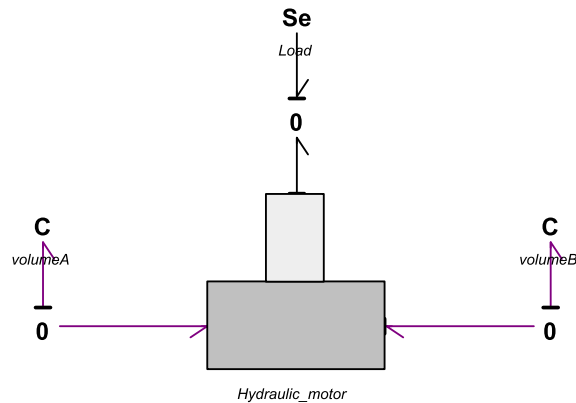


Figure 2.6: Icon for the hydraulic motor submodel.

## 2.4 Pressure Compensator

The pressure compensator, or the pressure relief valve which often called, has the purpose of limiting the pressure in the main system to only a few bars higher than needed. This is due to safety as well as minimizing wear and tear of the system. The pressure relief valve is assumed to be self controlled by the highest pressure in the hydraulic motor as pilot pressure. It should have a spring, so it closes itself and a nozzle to give extra damping to the pilot pressure. It is not that important for the total model that the pressure compensator is precisely modeled, but it should be able to restrict the pressure without causing problems for the main valve control. If the nozzle is not well-designed it can create oscillations in the pressure which causes problems for the controller.

As described, the pressure compensator has three ports, the pump pressure, the highest pressure

of  $p_A$  and  $p_B$  (the pressures on each side of the motor) and the return pressure. A sketch of the pressure compensator is given in figure 2.7.

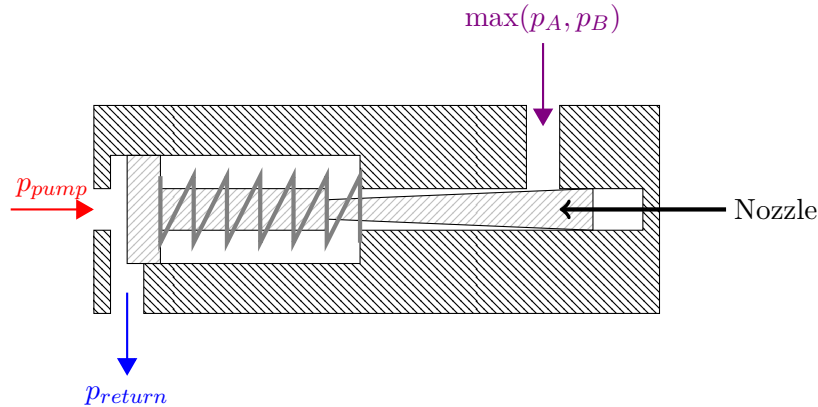


Figure 2.7: Sketch of pressure compensator.

To model the pressure compensator both mechanical and hydraulic dynamics and interactions in between must be taken care of. The pilot pressure flows through a nozzle, which dissipates energy, and is expressed as

$$Q = C_d \text{sign}(\Delta p) A_n(x_c) \sqrt{\frac{2}{\rho} |\Delta p|} \quad (2.26)$$

where  $C_d$  is a flow coefficient and  $A_n(x_c)$  is the opening area in the nozzle which may vary with the stroke  $x_c$ . The pilot pressure acts on the piston, giving a closing force. This is modeled with a TF-element with the transformer modulus given as the area of the piston,  $A_{cp}$ .

The moving piston has a mass given as  $m_c$  and a spring, which may be pre-compressed a distance  $x_{c0}$ , with a spring stiffness given by  $k_{cs}$ . The friction is given by (2.22). Also a stopping element should be implemented so that the piston displacement is restricted. This is done by implementing a stiff spring,  $k_{cstop}$ , and a powerful damper,  $b_{cstop}$ , that are initiated if the piston tries to go outside its limits,  $0 \leq x_c \leq x_{clim}$ . The last force acting on the piston is the flow force from the flow through the valve. This flow is given as

$$Q = \alpha_c(x_c) A_{co}(x_c) \text{sign}(\Delta p) \sqrt{\frac{2}{\rho} |\Delta p|} \quad (2.27)$$

where  $\alpha_c(x_c)$  is a flow coefficient that may be dependent on the piston displacement and  $A_{co}(x_c)$  is the opening area. The flow force is given as

$$F = \frac{k_{cf}(x_c) \rho Q^2}{A_{co}(x_c)} \quad (2.28)$$

where  $k_{cf}(x_c)$  is a flow force parameter that also may vary with the piston displacement.

The finished bond graph model of the pressure compensator is given in figure 2.8. In the model there is also added a volume, including the same equations for volume accumulation and variable bulk modulus as given in (2.7) and (2.9). The bond graph model is put into a submodel with its own icon given in figure 2.9.

The next part to model is the 3/2-directional valve feeding the pressure compensator with pilot pressure.



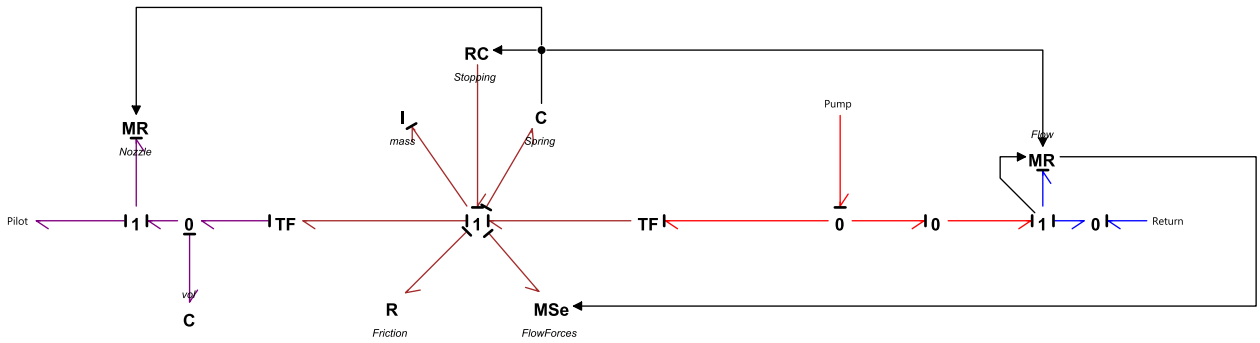


Figure 2.8: Bond graph model of pressure compensator.



Figure 2.9: Icon for pressure compensator model.

### 2.5 3/2-Directional Valve

The 3/2-directional valve can be modeled the same way as the pilot valve only with less valve options. By assuming the same dynamics as the pilot valve, the transfer function given in (2.2) can be used, the flow through the valve is given by (2.3) and the area is given as

$$A_i(r) = \text{limit}(ar A_{max}, 0, A_{max}) \tag{2.29}$$

where  $a = \pm 1$ ,  $r$  is the reference signal ( $\pm 1$ ) and  $A_{max}$  is the maximal opening area. Figure 2.10 shows the bond graph model of the valve.

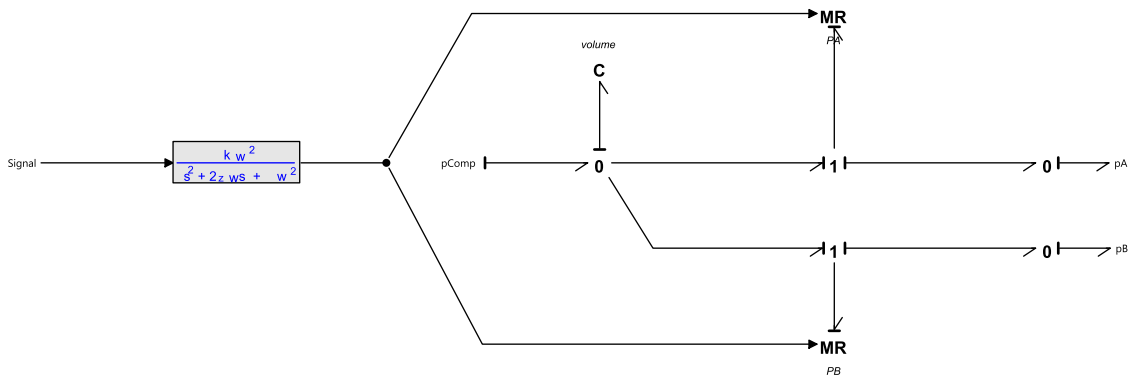


Figure 2.10: Bond graph model of 3/2-directional valve.

As seen in the figure there is also a volume, added to obtain integral causality, and is modeled the same way as before. This bond graph model is also implemented in a submodel with its own icon given in figure 2.11.

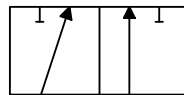


Figure 2.11: Icon for 3/2-directional valve model.

The next to model is the pipeline connecting all submodels together, filters, pump, HPU and other contributors to the total model.

## 2.6 Finishing Total Model

To finish the total bond graph model described in figure 1.4 the submodels need to be connected by power bonds. These power bonds represent all the piping connecting the system together. Also pipe resistance, volumes, pump, HPU and other resistances must be included.

The pump is modeled as a MSf-element where a signal gives the pump flow. Also internal leakage is included and is given as in (2.23). Pipe resistances are given as in (2.5) and the volumes are modeled as before, (2.7) and (2.9). It is also reasonable to assume that a filter and a cooler is present in the return line causing pressure drops. The contributions from such parts are gathered in one bond graph element and the flow through this element is given as

$$Q = \frac{1}{4} \text{sign}(\Delta p) D_h^2 \pi \sqrt{\frac{2|\Delta p|}{C_d \rho}} \quad (2.30)$$

where  $D_h$  is the hydraulic diameter. When it comes to the HPU, it is assumed that the pump in the HPU is pressure compensated and is able to deliver the amount of flow needed. This simplifies the HPU model to only a set of Se elements for each main valve, one for pilot pressure and the other for return pressure. A more realistic HPU model was tested in Skjong (2013) and the results showed that the simplified HPU model used here is good enough for the purpose of the model.

The total bond graph model is given in figure 2.12. As can be seen from the figure a box named LOGIC has been implemented between the 3/2-directional valve and the control signal. This is only a box that determines which of the pressures  $p_A$  and  $p_B$  is highest and feeds it to the directional valve if the given signal is  $|r| > 1$  (outside the limit). So if the user sets the control signal to 2, the LOGIC-box control the 3/2-directional valve on its own.

Now, when the bond graph model is finished, the model should be tested in order to find its limits, the effect of the fluid inertia and variable bulk modulus in the main valves, to find parameter and variable dependencies and the possibility to simplify the model even more.

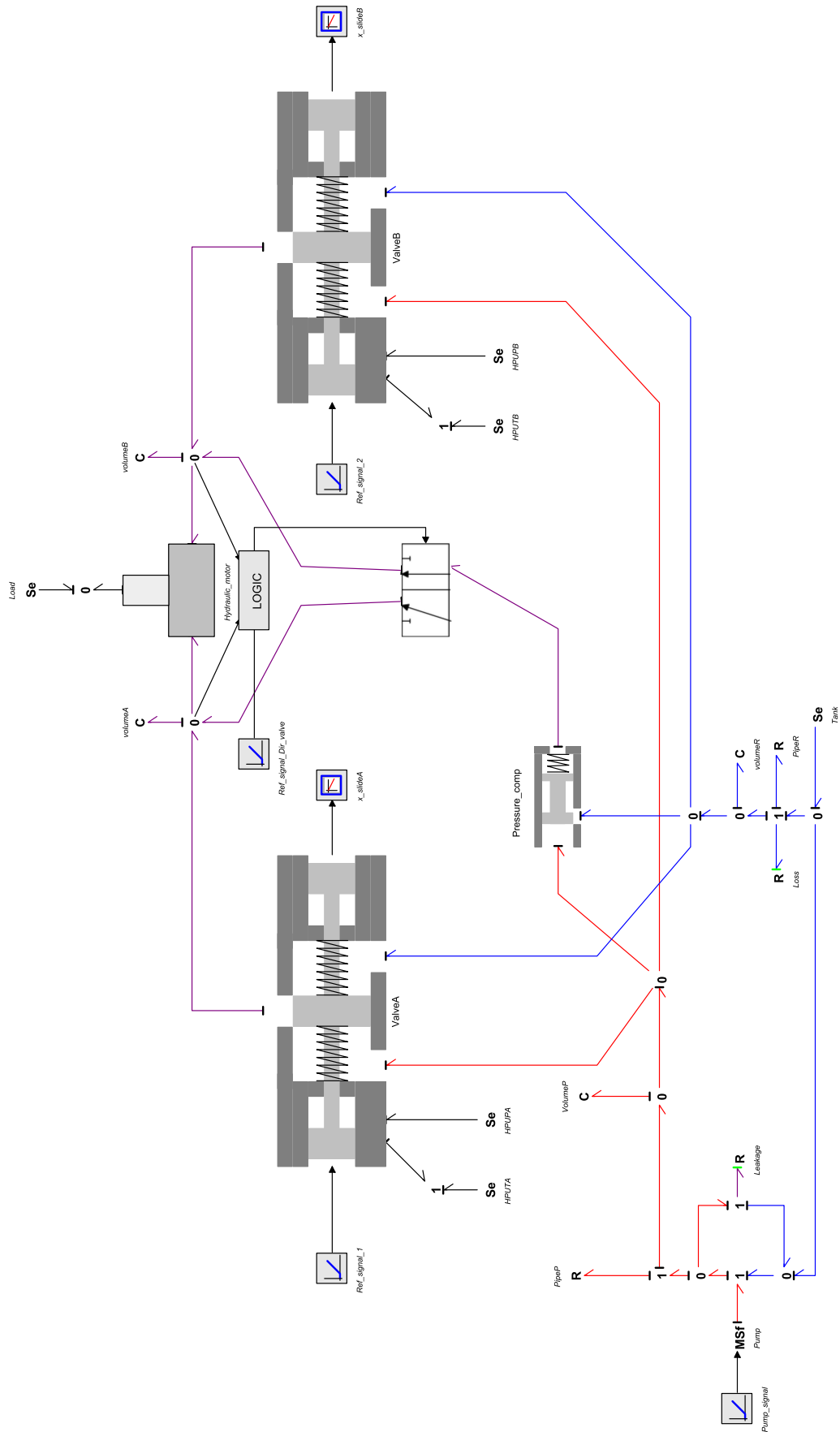


Figure 2.12: Total bond graph model of the system presented in figure 1.4.



## 3 | Model Study

To be able to design suitable control laws for controlling the hydraulic motor a model study is necessary in order to get an understanding of all connections, the model limits and weaknesses, and to find possibilities to simplify the model even more. This is important since there is a lot of logics implemented in the bond graph model. Logics are not that desirable in control laws since they may cause discontinuities, "jumps", in the output control signals. Also abstracting only the essential dynamics describing the main characteristics in the total system is desirable when designing control laws, and if the control laws based on simplified equations work in the process model, it will give reason to believe that the control laws are robust and will work if implemented in a real system.

Before the system is studied more thoroughly through simulations, all parameters and coefficients must be accounted for. The total parameter list is given in table C.1 in Appendix C. The pump flow, motor load and the reference signals are not given in the table but given in each simulation case.

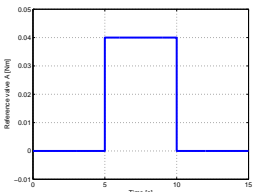
### 3.1 Main Valve Study

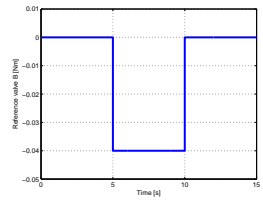
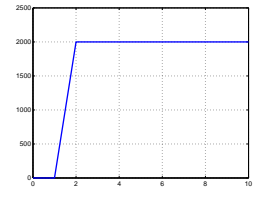
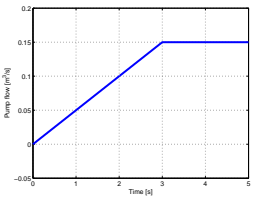
The main valves, the 3/3-directional valves, are the most important elements in the model since the motor is controlled through these. That is also why the bond graph models for the main valves contain less simplifications compared to all the other models. However it is of interest to study the effect of simplifying the model and to study the valve dynamics when parameters are changed.

#### 3.1.1 Simple Step Response

The first simulation that is to be performed is a simple valve step response. The model including fluid inertia effects, variable bulk modulus and cylinder accumulations used. The P-controller, controlling the control slides through the pilot valve has a proportional gain set to 6000 V/m. The reference signals used in this simulation is given in table 3.1.

Table 3.1: Reference signals in simple step response simulation.

Description	Value
$r_{ValveA}$ , Reference signal for main valve A (a step starting at t=5s with a magnitude of 0.04 m and a step back to zero at t=10s)	$r_{ValveA} = 0.04\text{step}(5) - 0.04\text{step}(10)$ 

<p><math>r_{ValveB}</math>, Reference signal for main valve B (a step starting at <math>t=5</math>s with a magnitude of <math>-0.04</math> m and a step back to zero at <math>t=10</math>s)</p>	<p><math>r_{ValveB} = -0.04\text{step}(5) + 0.04\text{step}(10)</math></p> 
<p><math>T_m</math>, Hydraulic motor load (a ramp starting at <math>t=1</math>s with a magnitude of <math>2000</math> Nm and stopping at <math>t=2</math>s)</p>	<p><math>T_m = 2000\text{ramp}(1) - 2000\text{ramp}(2)</math></p> 
<p><math>\dot{Q}_p</math>, Pump flow (a ramp starting at <math>t=0</math>s with a slope of <math>0.05</math> <math>m^3/s^2</math> and stopping at <math>t=3</math>s)</p>	<p><math>\dot{Q}_p = 0.05\text{ramp}(0) - 0.05\text{ramp}(3)</math></p> 
<p><math>r_{3/2}</math>, Reference signal for 3/2-directional valve (<math>r_{3/2} = 2-</math> means that the LOGIC-box controls the valve)</p>	<p><math>r_{3/2} = 2-</math></p>

The simulation time is set to 15 s and it is expected that the calculation time is high. The slide positions are shown in figure 3.1. As can be seen in the figure, there is a small delay between the signals. A part of this delay has to do with the sampling delay that was set to  $T_d = 0.002$  s. Other contributions come from the velocity limitation transfer function, which adds an extra phase to the signal. Small oscillations can also be seen which is expected since the controller used has no damping. What can not be seen in the figure is a small bias between the references and the positions. This comes from the velocity limitation and means that also an integral effect should be included in the process model controller design when the velocity limitation function is present. The simulation results shown in the figure only shows a small part of the whole model and say nothing about variable bulk modulus, flow through the pressure compensator or the motor velocity. These are shown in figure 3.2.

The motor velocity seems to be almost proportional to the control slide that opens for pressure. This means that for a manual motor control the operator can set the reference position to the control slides to obtain wanted motor velocity. This is however not a precise motor velocity control. Also the internal leakage in the motor gives a small negative velocity when the slide positions are zero and the load is positive, but this can not be seen in the figure. The small oscillations shown in the lower right corner in figure 3.1 is almost invisible at the hydraulic motor velocity. This means that later on when a motor speed controller is to be designed the inner main valve control can be fast and allowed some oscillation as long as it is stable.

The flow through the pressure compensator is negative, which from the sign convention used when modeling means that hydraulic fluid flows from the pressurized pipeline to the return

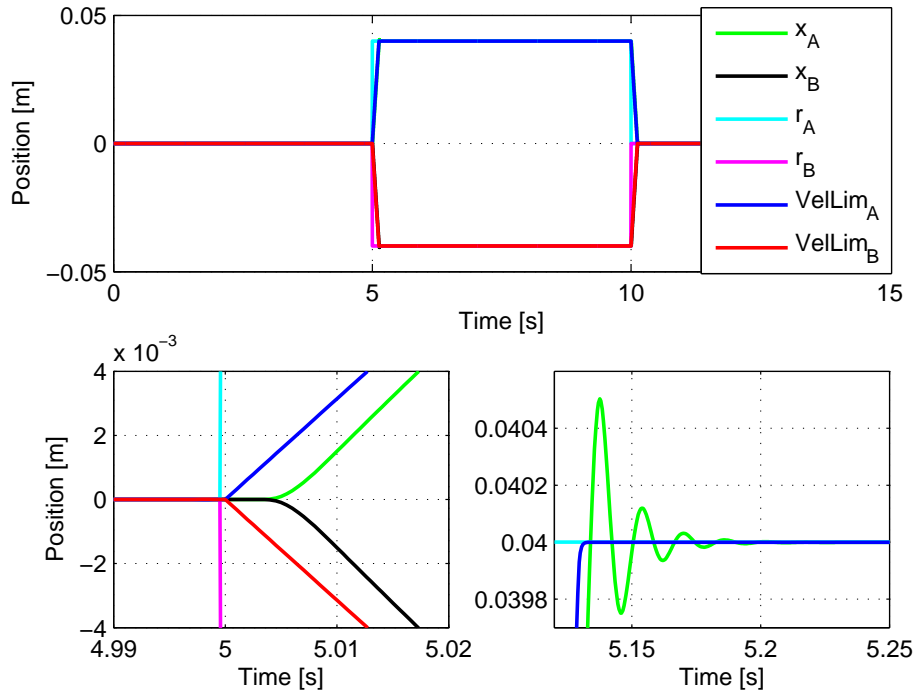


Figure 3.1: Reference, velocity limitation and control slide positions for the advanced model.

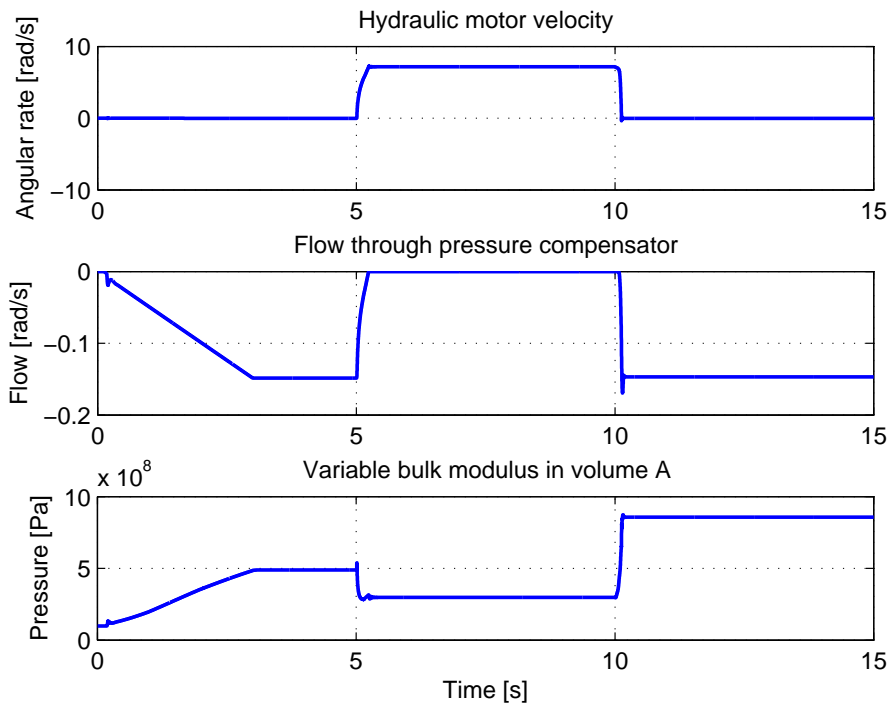


Figure 3.2: Motor velocity, flow through pressure compensator and variable bulk modulus.

tank. The pressure compensator opens when the pump starts and the control slide positions are zero, but closes when the control slides start moving. In general the flow through the pressure compensator should never be zero because this means that the main pumps are not able to deliver the pressure needed in the system.

The last plot shows the variable bulk modulus in volume A (see figure 2.12). The bulk modulus drops when the motor starts rotating and increases again when the motor stops. This is as expected since the bulk modulus is proportional to the fluid volume pressure.

From this simulation it looks like everything in the model works fine. However this simple simulation of 15 seconds took almost 130 seconds to be solved in 20Sim. Therefore it is important to study the effects that makes the simulation slow and simplify if possible. It is expected that the variable bulk modulus and the fluid inertia in the main valves slow down the solver. By removing the variable bulk modulus for the HPU system, the cylinder accumulation and the fluid inertia in the main valves the same simulation can be solved in 19 s. The results from this simulation seems to coincide with the previous simulation and it is almost impossible to see the difference when comparing them side by side. Thus the difference between control slide positions are calculated and shown in figure 3.3.

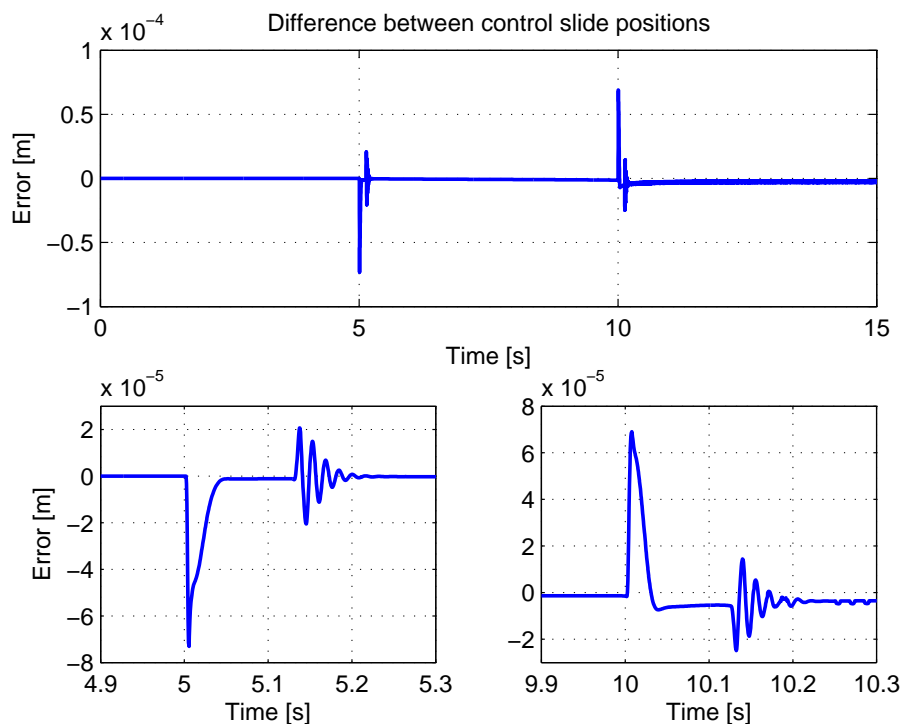


Figure 3.3: Difference between control slide positions  $x_A$ ,  $x_A - x_{A,simp}$ .

As seen in the figure the difference is not large and the largest deflections between the two simulations appear when the control slides are accelerated. This is expected since removing the fluid inertia, cylinder accumulations and variable bulk modulus the time constants for the main valves are changed. This affects the response time of the main valves. The largest difference is almost  $8 \times 10^{-5}$  m, 0.08 mm. This is not much and if the difference does not propagate much in the other systems, then the simplification done is argued for. At  $t = 5$  s the difference is negative. The difference was given as  $x_A - x_{A,simp}$  (advanced model - simplified model) and since the control slides have positive acceleration it means that the simplified control slide is faster than the advanced control slide. At  $t = 10$  s the difference is positive. The control slides have negative acceleration, which also means that the simplified control slide is faster than the advanced one. When designing control laws for controlling the hydraulic motor it is important that the controllers are faster than the system to be controlled. Since the simplified model has a faster response compared to the advanced model it is reasonable to assume that a controller that works in the simplified model also works in the advanced model. Figure 3.4 shows the



difference in motor velocity.

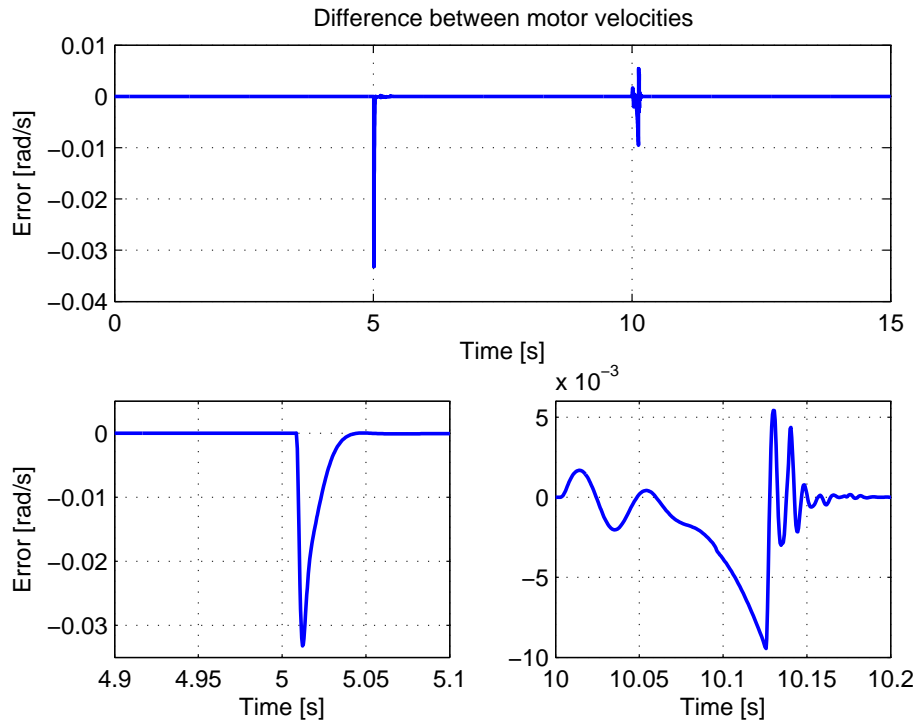


Figure 3.4: Difference between motor velocities  $v$ ,  $v - v_{simp}$ .

As seen in the figure the largest difference is the peak at  $t=5$  s with an absolute magnitude of  $0.033 \text{ rad/s} = 0.315 \text{ rpm}$ , which is relatively small. At  $t=5$  s the difference is also negative, which also here means that the simplified model is faster than the advanced one. At  $t=10$  s the peak is also negative but positive oscillations are present as seen in the plot in the lower right corner. The magnitude of this peak is really small and it is difficult to determine whether the difference comes from simulation errors or the difference between the models.

These differences given in figure 3.3 and 3.4 are calculated from simulations with a motor loading of  $T_m = 2000 \text{ Nm}$ . It is of great interest to see how these differences change when the motor load changes. A parameter sweep of the load is done in 10 steps, starting at  $T_m = 2000 \text{ Nm}$  and stops at  $T_m = 20000 \text{ Nm}$  with the same references and simulation settings as before. Figure 3.5 shows the differences between the control slide positions.

As seen in the figure the results from the first simulation with  $T_m = 2000 \text{ Nm}$  are almost reproduced. The characteristic peaks at  $t=5$  s and  $t=10$  s seem to be global results. It is important to mention the calculation errors since the absolute and relative error limits are set to 0.0001 in 20Sim (Controllab, 2014). The reason for such a high limit is because both models are calculated together and lack of computing power forces the tolerances to be high. However the results seem clear, the differences seem to be limited and small.

Figure 3.6 shows the difference in motor velocity between the two models. Also the difference between the two motor velocities seems to be limited and the results in figure 3.4 are almost reproduced globally as for the difference between the control slide positions. The difference also seems to decrease when the load gets higher. This is not surprising since a higher load gives higher inertia and the difference in control slide positions have less influence on the motor velocity.

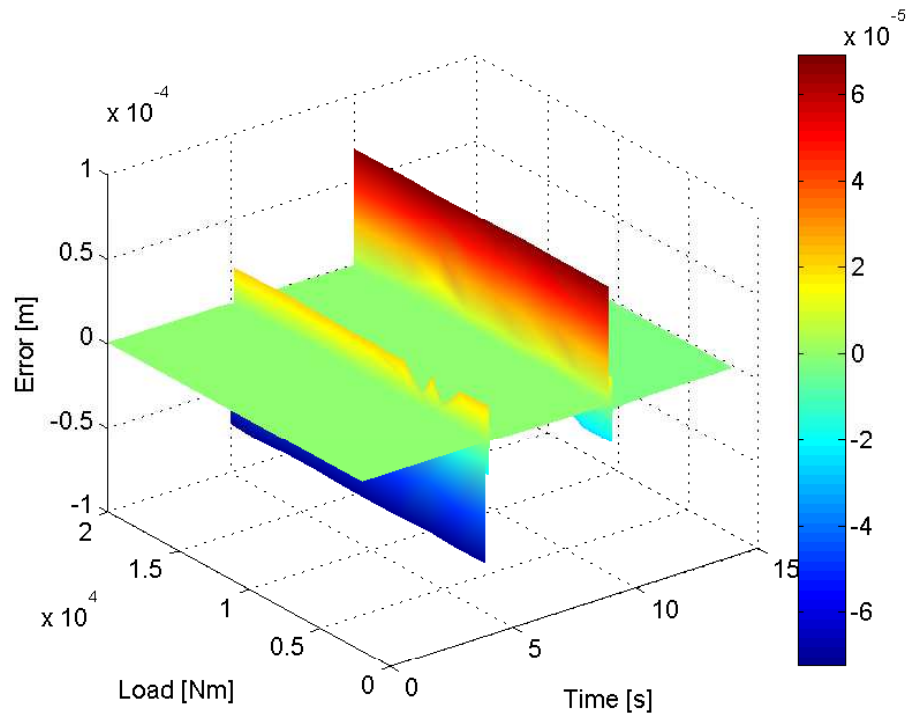


Figure 3.5: Difference in control slide position, load sweep.

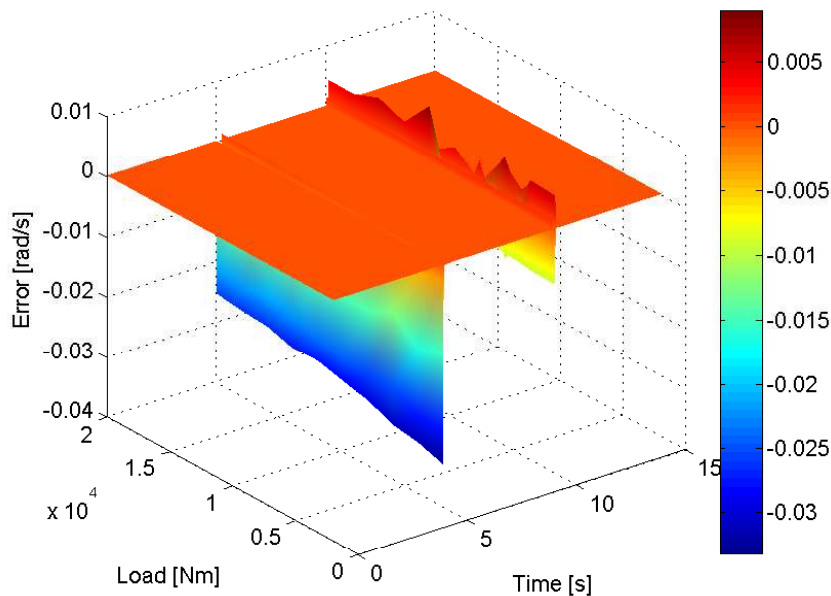


Figure 3.6: Difference in motor velocity, load sweep.

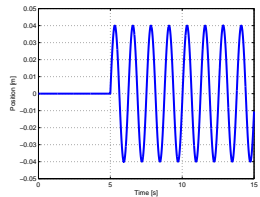
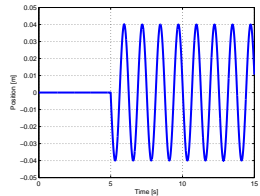
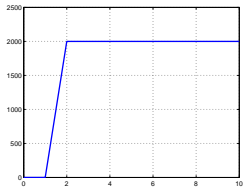
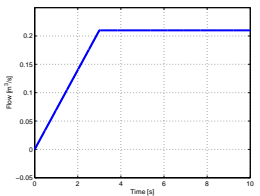
Until now only responses from positive control slide references for main valve A has been studied. The reason for this is because the load is set positive and the delivered pressure therefore works against the motor load. For negative references the motor would get a high negative velocity since the pressure and the load works together, accelerating the hydraulic motor. In the next simulation the responses from a sine reference is studied.

### 3.1.2 Sine Reference

When sine reference signals for the control slides are used it is expected that the differences studied in 3.1.1 would be different. Assuming that the motor loading is positive there would be situations where the load and the differential pressure, driving the motor, have the same direction. This will give the hydraulic motor a seriously acceleration and the velocity is expected to be high. When this happens small changes in control slide positions would contribute to changing the motor speed and thus the difference between the motor velocity in the advanced model and the simplified model is expected to increase.

Table 3.2 gives the reference signals and the motor load used in this simulation.

Table 3.2: Reference signals and motor load for the sine response simulation

Description	Value
$r_{ValveA}$ , Reference signal for main valve A (a sine function starting at $t=5$ s with an amplitude of 0.04 m and a frequency of $\omega = \frac{5}{2\pi}$ )	$r_{ValveA} = 0.04\text{step}(5)\sin(5(t - 5))$ 
$r_{ValveB}$ , Reference signal for main valve B (a sine function starting at $t=5$ s with an amplitude of -0.04 m and a frequency of $\omega = \frac{5}{2\pi}$ )	$r_{ValveB} = -0.04\text{step}(5)\sin(5(t - 5))$ 
$T_m$ , Hydraulic motor load (a ramp starting at $t=1$ s with a magnitude of $T_{ms}$ and stopping at $t=2$ s, $T_{ms}$ varies.)	$T_m = T_{ms}\text{ramp}(1) - T_{ms}\text{ramp}(2)$ 
$\dot{Q}_p$ , Pump flow (a ramp starting at $t=0$ s with a slope of $0.07 \text{ m}^3/\text{s}^2$ and stopping at $t=3$ s)	$\dot{Q}_p = 0.07\text{ramp}(0) - 0.07\text{ramp}(3)$ 
$r_{3/2}$ , Reference signal for 3/2-directional valve ( $r_{3/2} = 2$ - means that the LOGIC-box controls the valve)	$r_{3/2} = 2$ -

The simulation time is set to 15 s, the sampling delay is 0.002 s and  $T_{ms} = 2000$  Nm. The slide positions for the advanced model are shown in figure 3.7. As can be seen in the figure the

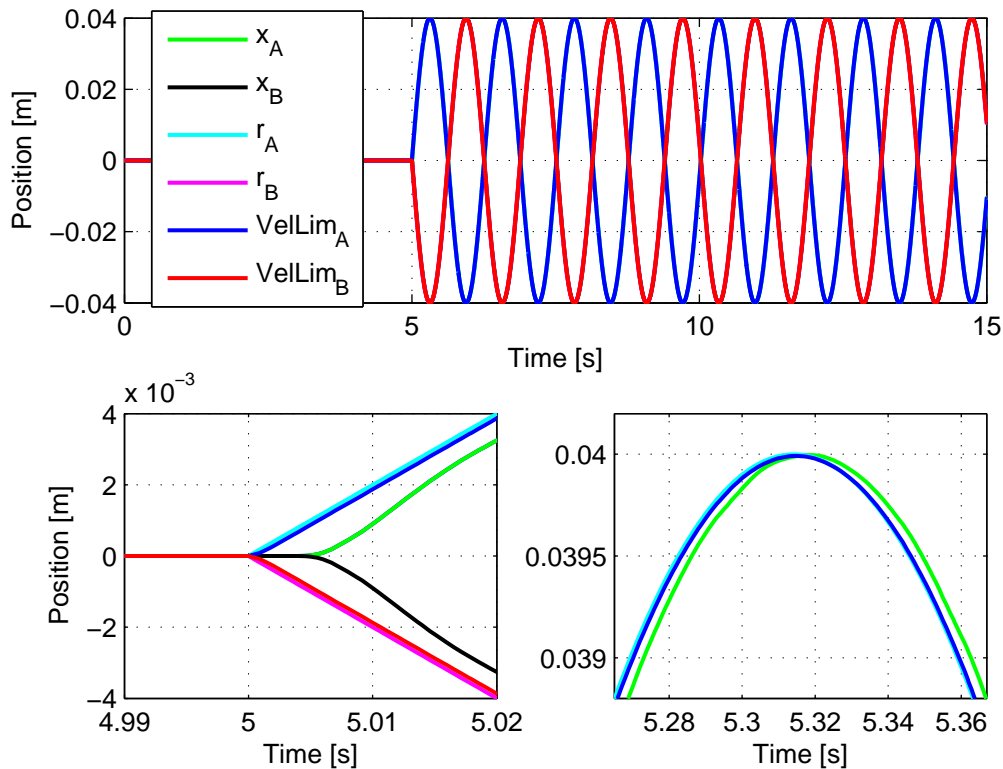


Figure 3.7: Reference, velocity limitation and control slide positions for the advanced model.

velocity limitation function coincide with the reference signal and the valve positions seems to follow the reference with great precision when neglecting the sampling delay and the transfer function phase. The plot in the lower left corner shows that the control slides use a small amount of time to get accelerated, as expected since the fluid inertia is present in the model. This effect is easier to see in this simulation compared to the previous one since the phase from the velocity limitation function is smaller. Figure 3.8 shows the hydraulic motor velocity, the flow through the pressure compensator and the variable bulk modulus in volume A.

The hydraulic motor velocity seems to oscillate around the zero line with a constant amplitude which means that the motor load is not large enough to make the hydraulic motor *speed*. The pressure compensator oscillates in phase with the motor velocity which means its dynamics are fast enough to follow the pressure changes in the main pressure line. The last plot shows the variable bulk modulus in volume A which also seems to oscillate in phase with the other dynamics.

Since the hydraulic motor does not speed it would be reasonable to assume that the difference in control slide positions and motor velocities between the advanced and the simplified model would be similar to the differences studied in 3.1.1. Figure 3.9 shows the differences.

Except for the peaks at  $t = 5$  s the figure shows that the differences are small. The peaks are caused by the acceleration of the control slides as discussed before. As can be seen the differences are comparable to the differences in section 3.1.1 due to the effects already discussed. However when setting  $T_{ms} = 20000$  Nm the results are quite changed. Figure 3.10 compares the hydraulic motor velocities for  $T_{ms} = 2000$  Nm and  $T_{ms} = 20000$  Nm by using the advanced model.

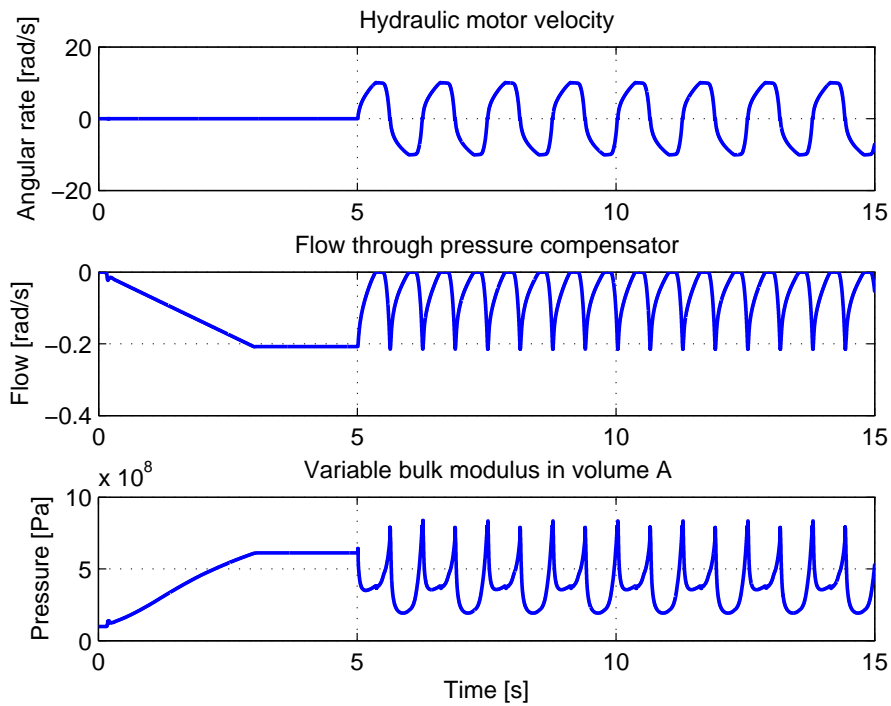


Figure 3.8: Motor velocity, flow through pressure compensator and variable bulk modulus.

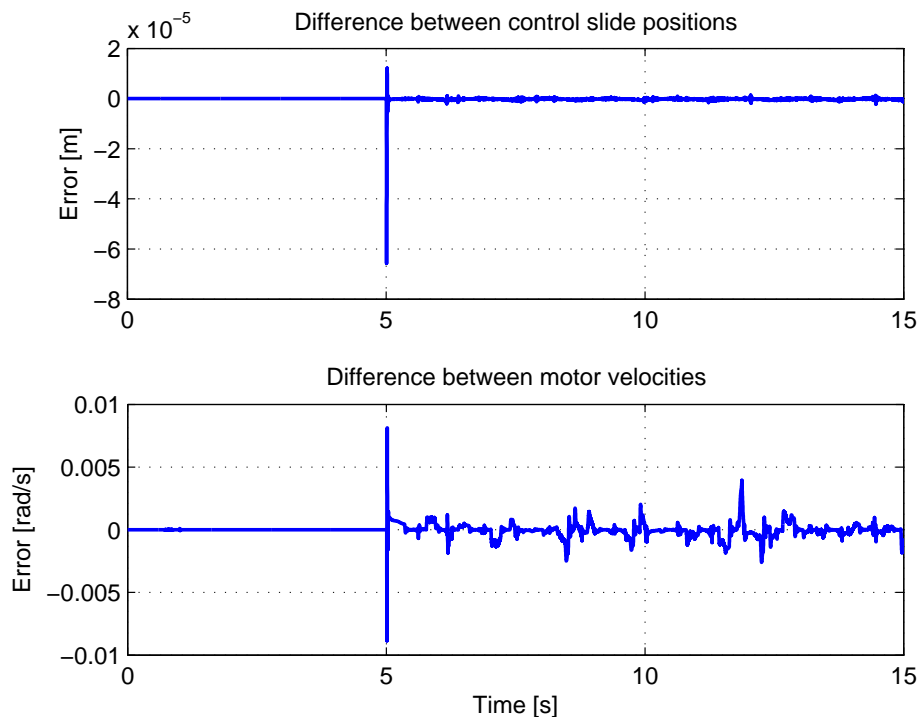


Figure 3.9: Difference between control slide positions  $x_A$ ,  $x_A - x_{A,simp}$ , and motor velocities  $v$ ,  $v - v_{simp}$ .

As seen in the figure the hydraulic motor starts speeding when the position of control slide A is negative. The plot in the lower left corner shows the difference between the two simulations when the hydraulic motor reaches the highest velocity. The simulation with higher motor loading has

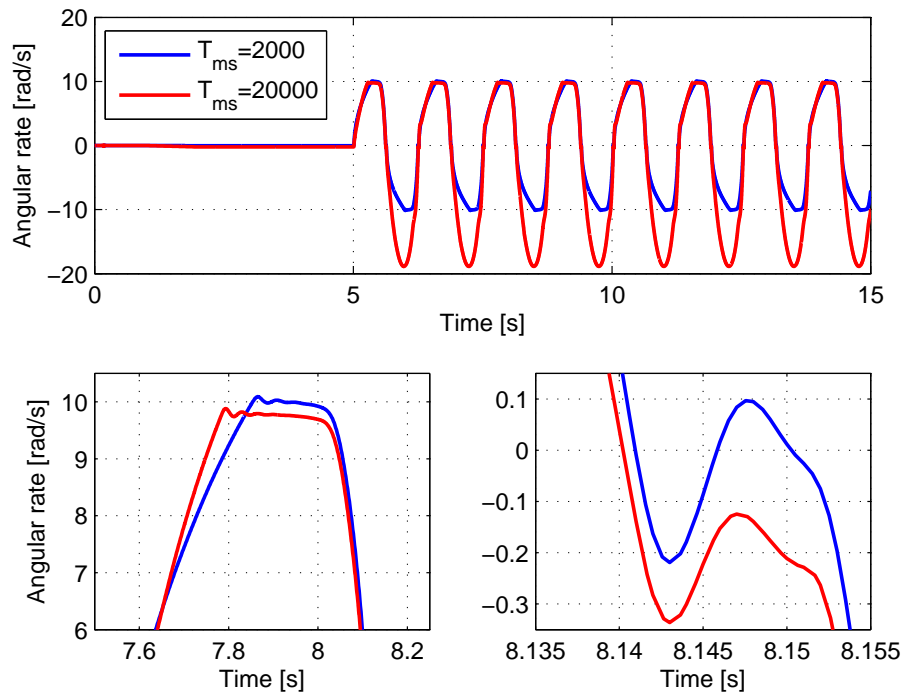


Figure 3.10: Hydraulic motor velocities.

a lower maximal velocity than the other, which is reasonable since the pressure is higher which gives larger losses in the main valves and larger internal leakage in the hydraulic motor. The plot in the lower right corner in the figure shows the motor velocity when the motor changes direction of rotation. The characteristics given in the plot come from the dead bands in the main valves and forces the safety valve to open to prevent cavitation. The flow through the safety valve is lower than through the main valves and the motor is forced to slow down. When the valves have passed the dead bands the motor is accelerated again. This effect must be included in motor controller designs later on. The plot also shows that the simulation with  $T_{ms} = 20000$  Nm is slower than the other. This may seem to be a contradiction when comparing with the plot in the lower left corner, but the simulation with the highest motor loading uses longer time to slow down than the other. This can also be seen when looking at the first crossing between the two lines, where the motor velocity with the lowest motor loading has a faster response in the beginning and is slowed down much quicker than the other simulation.

By comparing the difference between the control slide positions for the advanced and the simplified model for  $T_{ms} = 2000$  Nm and  $T_{ms} = 20000$  Nm there is not much of a difference. However by comparing the hydraulic motor velocities the differences are much larger than before. This is shown in figure 3.11.

The peaks are much larger in the speeding area and affects the rest of the simulations with larger peaks all over, as expected. The differences in the control slide positions affects the hydraulic motor much more when the motor is speeding. However the difference is not that large, the difference is only  $\frac{0.317 \text{ rad/s}}{18.874 \text{ rad/s}} 100\% = 1.68\%$  of the maximal velocity.

As for the single step analysis in section 3.1.1 a sweep of the motor loading is applied. Figure 3.12 shows the difference in control slide positions.

The figure shows that the difference between the control slide positions are limited and seem to be almost independent of the motor loading as for the single step response in section 3.1.1.

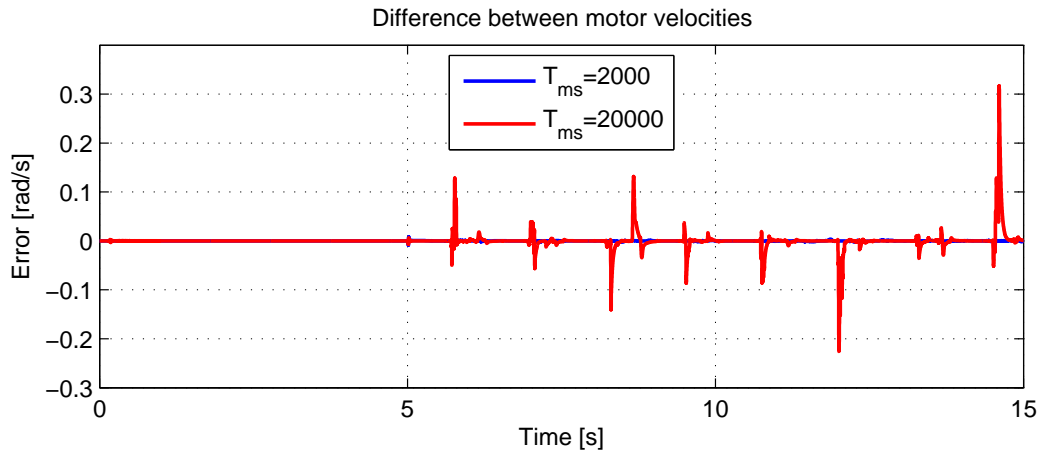


Figure 3.11: Differences between motor velocities.

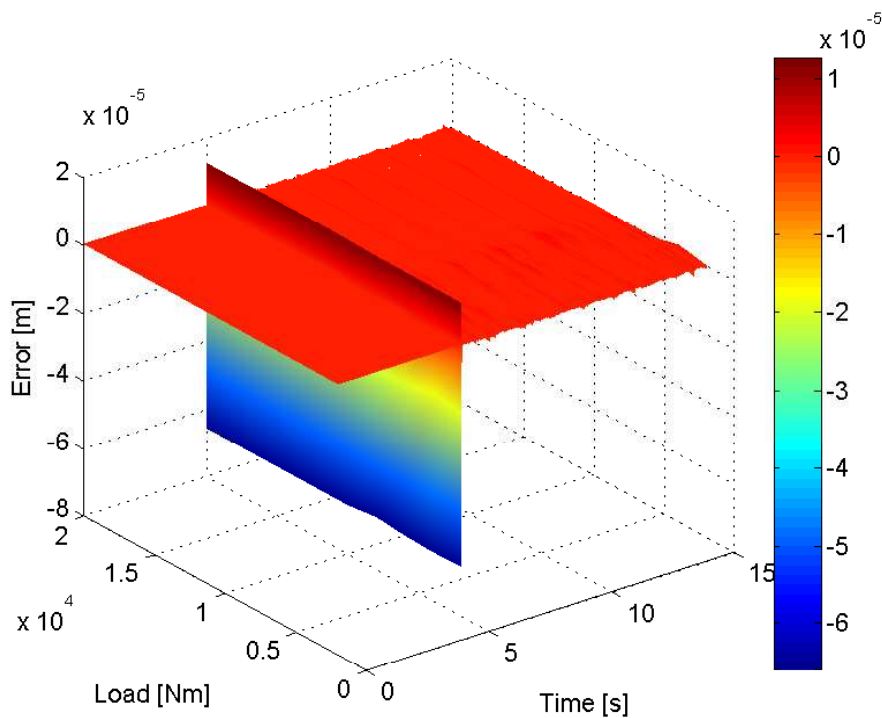


Figure 3.12: Difference in control slide position, load sweep.

There is a peak at  $t = 5$  s for all motor loading cases. This is due to the valve dynamics, the simplified main valve has faster dynamics than the advanced one and therefore it starts moving before the advanced main valve. Figure 3.13 shows the difference between the motor velocities.

As the figure shows the difference between the motor velocities increases with the loading and is expected since the difference between the control slide positions have a larger impact on the motor velocity when the motor speeds.

### 3.1.3 Conclusion

The simulations done show that the simplified model has faster dynamics than the advanced model. This means that when designing control laws for the hydraulic motor the simplified

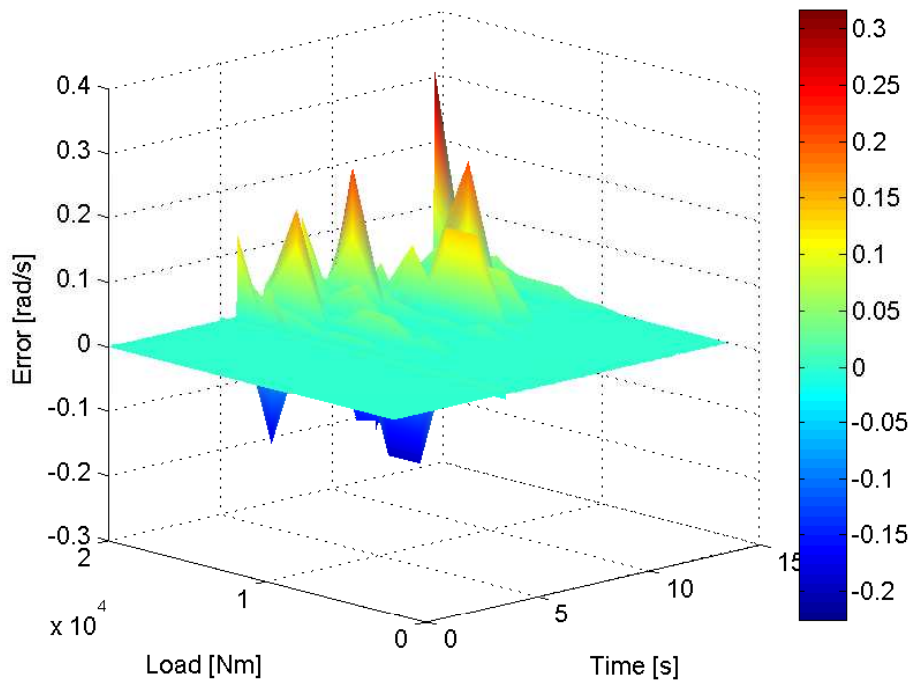


Figure 3.13: Difference in hydraulic motor velocities, load sweep.

model can be used without concerns because the control algorithm must be faster than the model dynamics. For the "sine-referenced" simulation it was shown that the difference in motor velocities was affected by the difference in control slide position mainly when the motor was speeding. However the difference was not alarming and since the motor is to be controlled we may neglect the differences between the advanced and the simplified model. This means that the simplified model is good enough for further studies and motor control designs. This also affects the solving time in simulations, which decreases.

## 3.2 Model Parameter Sensitivity

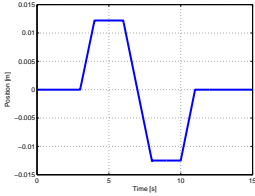
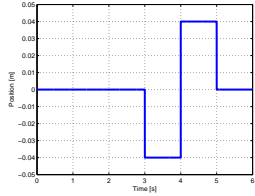
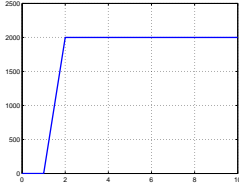
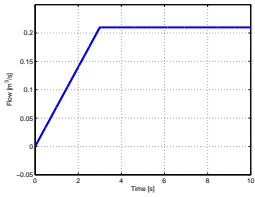
Some of the parameters in the model are hard to determine precisely in reality. Therefore a model parameter sensitivity analysis for some of the model parameters is initiated. In Appendix D more studies are given. The parameter sensitivities are studied by comparing the motor velocities when the simulation settings are held constant. The reason for choosing the motor velocity as the reference is because the hydraulic motor velocity is to be controlled later on. Some of the parameters may not give a large change in motor velocity but an increase in simulation solving time.

The reference signals for the model parameter sensitivity simulations are given in given in table 3.3.

$T_{ms}$  is set to 2000Nm and the simulation time is set to 6s. Only two parameter sensitivity studies are given in this section. See Appendix D for more cases.



Table 3.3: Reference signals for parameter sensitivity analysis.

Description	Value
$r_{ValveA}$ , Reference signal for main valve A (a step function starting at $t=3$ s with a magnitude of 0.04 m, a step of -0.08 m at $t=4$ s and a step back to zero at $t=5$ s)	$r_{ValveA} = 0.04\text{step}(3) - 0.08\text{step}(4) + 0.04\text{step}(5)$ 
$r_{ValveB}$ , Reference signal for main valve B (a step function starting at $t=3$ s with a magnitude of -0.04 m, a step of 0.08 m at $t=4$ s and a step back to zero at $t=5$ s)	$r_{ValveB} = -0.04\text{step}(3) + 0.08\text{step}(4) - 0.04\text{step}(5)$ 
$T_m$ , Hydraulic motor load (a ramp starting at $t=1$ s with a magnitude of $T_{ms}$ and stopping at $t=2$ s, $T_{ms}$ varies.)	$T_m = T_{ms}\text{ramp}(1) - T_{ms}\text{ramp}(2)$ 
$\dot{Q}_p$ , Pump flow (a ramp starting at $t=0$ s with a slope of $0.07 \text{ m}^3/\text{s}^2$ and stopping at $t=3$ s)	$\dot{Q}_p = 0.07\text{ramp}(0) - 0.07\text{ramp}(3)$ 
$r_{3/2}$ , Reference signal for 3/2-directional valve ( $r_{3/2}=2$ - means that the LOGIC-box controls the valve)	$r_{3/2} = 2-$

### 3.2.1 Flow Force Coefficient in Pressure Compensator

The flow force coefficient in the pressure compensator is in table C.1 given as 0.6-. The flow force coefficient is changed with  $\pm 50\%$  and the simulation results are shown in figure 3.14.

The figure shows that the oscillations in the start of the simulation are not affected by the changes in the flow force parameter. However the motor dynamics in the steps are changed significantly. For an increasing flow force coefficient the motor seems to respond faster than a decreased flow force coefficient. This, without affecting the damping of the hydraulic motor.

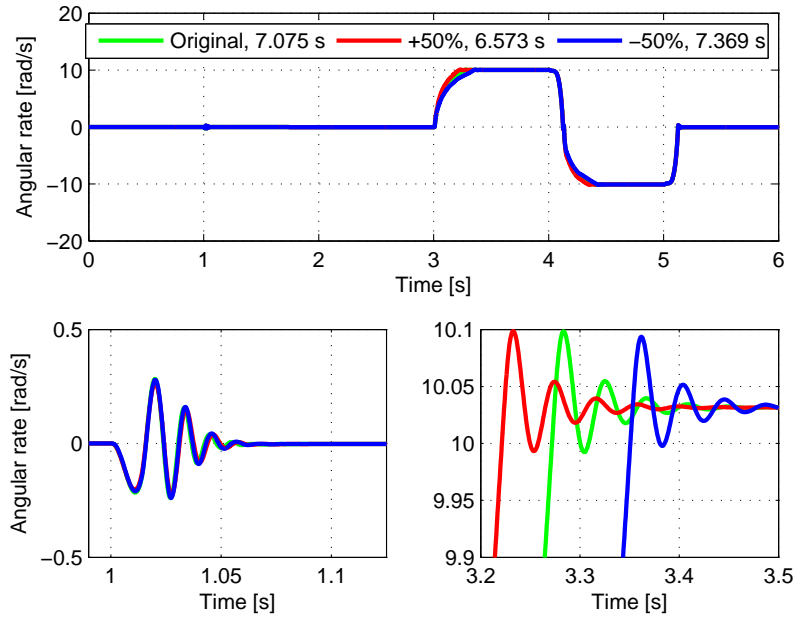


Figure 3.14: Sensitivity of flow force coefficient in pressure compensator.

Also the solving time is reduced by over 0.5 s for the increased flow force coefficient and increased by almost 0.3 s for the decreased flow force coefficient.

### 3.2.2 Inertia of Hydraulic Motor

The inertia of the hydraulic motor, including both hydraulic fluid in motion and the rotating parts is set to  $50 \text{ kgm}^2$  in table C.1. The inertia is changed with  $\pm 50\%$  and the results are given in figure 3.15.

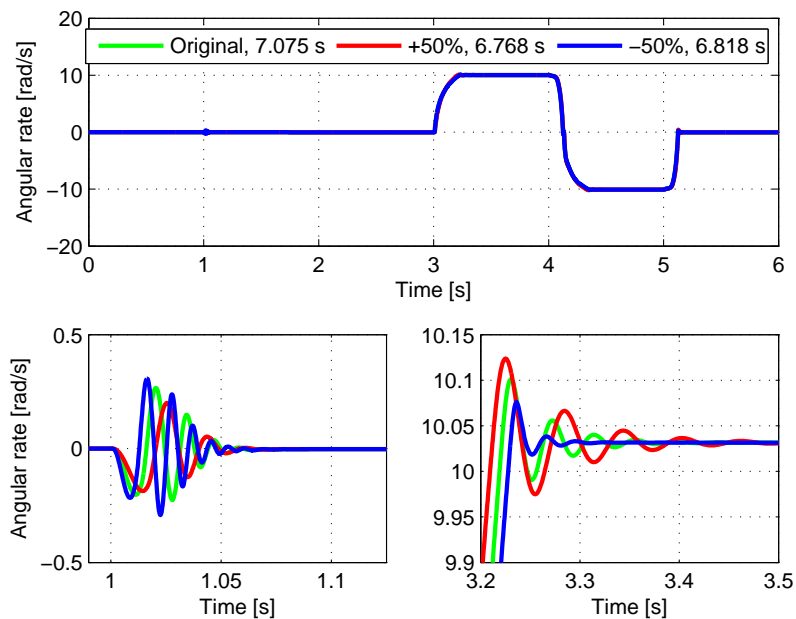


Figure 3.15: Sensitivity of inertia in the hydraulic motor.

The increase in hydraulic motor inertia gives a slower response of the hydraulic motor. This is the same effect as discussed earlier, the motor is slow to respond and uses some time to be accelerated. The increase also adds more oscillations to the motor velocity in the step. The decreased motor inertia gives a faster motor response and less oscillations in the step response, even though it seems to have less damping in the start of the simulation. This is due to the motor's ability to rotate much quicker and is affected more by the force applied at  $t = 1$  s. These results is comparable to increasing or decreasing the load of the hydraulic motor, which would give almost the same effect.

### 3.2.3 Results from Parameter Sensitivity Study

The results from the parameter sensitivity studies, including those given in Appendix D, are briefly summarized in table 3.15.

Table 3.4: Results from parameter sensitivity studies

Parameter	Increase	Decrease	Figure
Flow force coefficient in pressure compensator	Faster response	Slower response	3.14
Inertia of hydraulic motor	Faster response Higher overshoot in step	Slower response Lower overshoot in step	3.15
Volume ratio in bulk modulus	Slower response Lower overshoot in step	Faster response Higher overshoot in step	D.1
Nozzle area in pressure compensator	Faster response Higher overshoot in step	Slower response Lower overshoot in step	D.2
Nozzle flow coefficient in pressure compensator	Faster response Higher overshoot in step	Slower response Lower overshoot in step	D.3
Plunger diameter in pressure compensator	Faster total response Slower start response	Slower total response Faster start response	D.4
Flow coefficient in pressure compensator	Faster total response Slower start response	Slower total response Faster start response	D.5
Inertia in pressure compensator	Negligible changes	Negligible changes	D.6
Spring stiffness in pressure compensator	Negligible changes	Negligible changes	D.7
Slope in friction function in pressure compensator	Faster response Higher overshoot in step	Slower response Lower overshoot in step	D.8
Static friction in pressure compensator	Slower response Lower overshoot in step	Faster response Higher overshoot in step	D.9
Initial volume in pressure compensator	Faster response	Slower response	D.10
Gain in 3/2-directional valve dynamics	Faster response	Negligible changes	D.11
Natural frequency in 3/2-directional valve dynamics	Negligible changes	Negligible changes	D.12
Damping in 3/2-directional valve dynamics	Negligible changes	Negligible changes	D.13
Flow coefficient in 3/2-directional valve dynamics	Lower overshoot in step	Lower overshoot in step Slower response in step	D.14

Initial volume in 3/2-directional valve dynamics	Negligible changes	More damping in step	D.15
Internal leakage in hydraulic motor	Slower response in step Decreased max velocity	Faster response in step Increased max velocity	D.16
Static in hydraulic motor	Faster response in step Decreased max velocity	Slower response in step Increased max velocity	D.17
Slope in friction function in hydraulic motor	Negligible changes	negligible changes	D.18
Loss factor in pressure line	Negligible changes	negligible changes	D.19
Initial volume in volume P	Slower response in step Higher overshoot in step	Faster response in step Lower overshoot in step	D.20
Inertia in control slide, main valve	Negligible changes	Negligible changes	D.21
Initial volume 1 and 2 in main valve	Negligible changes	Negligible changes	D.22
Natural frequency in pilot valve	Negligible changes	Negligible changes	D.23
Gain in pilot valve dynamics	Negligible changes	Slower response in step Lower overshoot in step	D.24
Damping ratio in pilot valve dynamics	Slower response in step	Negligible changes	D.25

### 3.3 Chapter Summary and Conclusion

The proposed advanced and simplified main valve models have been simulated and compared with different reference signals and motor loads. The main results were that the simplified main valve model had a faster response than the advanced and the decrease in solving time in the simulations was significant. For negative motor velocities and higher loads the hydraulic motor started speeding and the difference between the two models increased. However since the simplified model is faster than the advanced one, the control algorithms that is to be designed are for controlling the motor and since the controller dynamics must be faster than the motor dynamics, the proposed simplifications for the main valve are argued for.

The parameter study shows that some of the parameters affect both the hydraulic motor response and the solving time for the simulations. From now on the same values presented in table C.1 are used as long as no conflicts in the simulations appear.

For fluid flows that give a low Reynolds number the flow coefficients tend to give linear contributions in reality. This effect was studied in (Skjong, 2013) and neglected here since the contributions were moderate.

# 4 | First Hand Control

In the previous chapters the presented hydraulic winch system in figure 1.4 has been modeled and studied thoroughly. Simplifications were done and argued for through simulations and the finished model is now ready to be controlled. In this chapter *first hand control* for motor velocity and torque are to be studied. With *first hand control* it is meant a general control that does not necessary needs to be that precise. Both motor velocity control and motor torque control, through an operator, are in the scope of this chapter.

## 4.1 Manual Speed Control

In chapter 3 an observation regarding the relation between the control slide position and motor velocity was made. By comparing the control slide position for main valve A and the motor velocity one might approximate the motor speed by commanding a reference for the control slide.

### 4.1.1 Control Slide Position and Motor Velocity

Figure 4.1 shows the control slide position together with the motor velocity for the same simulation that was done in section 3.1.2.

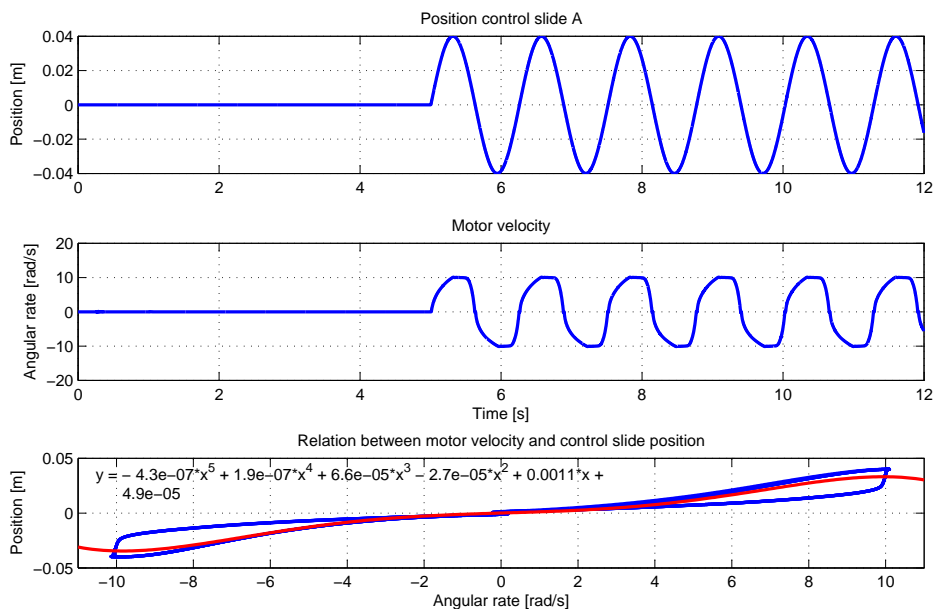


Figure 4.1: Relation between motor velocity and control slide position, main valve A.  $T_{ms} = 2000 \text{ Nm}$ .

As can be seen when comparing the two first plots the motor speed is not quite a symmetric graph, but has the characteristics of a geometric function. That is why the last plot looks like a

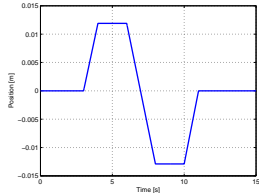
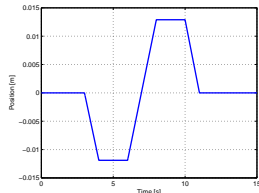
rotated bow tie. If the motor speed was symmetric then the last plot would only be in one line. Also a 5th order polynomial is drawn in the last plot, giving the relation

$$x_A = -4.3 \cdot 10^{-7} \omega_m^5 + 1.9 \cdot 10^{-7} \omega_m^4 + 6.6 \cdot 10^{-5} \omega_m^3 - 2.7 \cdot 10^{-5} \omega_m^2 + 0.0011 \omega_m + 4.9 \cdot 10^{-5} \quad (4.1)$$

where  $\omega_m$  is the motor velocity and  $x_A$  is the control slide position for main valve A. If the load shifted sign,  $x_A$  should be replaced with  $x_B$ . The motor velocity is also dependent on the pump flow and the motor load. By assuming the pump flow is held constant and the motor load is kept as  $T_{ms} = 2000 \text{ Nm}$ , a test of this relation can be done. Note that the relation only holds when the two main valves are in 4/3-operation mode since the data is collected from such a valve setting. If the preferred motor velocity is  $5 \text{ rad/s}$  then  $x_A$  is given by (4.1) as  $0.0119 \text{ m}$ . If the preferred motor velocity is  $-5 \text{ rad/s}$  then  $x_A = -0.0129 \text{ m}$ . Of course this would never give exactly the preferred motor velocity, but the error should not be that large.

The reference signals for the control slides are given in table 4.1.

Table 4.1: Reference signals in relation study.

Description	Value
$r_{ValveA}$ , Reference signal for main valve A	$r_{ValveA} = 0.0119\text{ramp}(3) - 0.0119\text{ramp}(4) - 0.0124\text{ramp}(6) + 0.0124\text{ramp}(8) + 0.0129\text{ramp}(10) - 0.0129\text{ramp}(11)$ 
$r_{ValveB}$ , Reference signal for main valve A	$r_{ValveB} = -0.0112\text{ramp}(3) + 0.0112\text{ramp}(4) + 0.0124\text{ramp}(6) - 0.0124\text{ramp}(8) - 0.0129\text{ramp}(10) + 0.0129\text{ramp}(11)$ 

The results from the simulation are shown in figure 4.2.

As the figure shows the maximal positive motor velocity obtained is  $5.283 \text{ rad/s}$  and the maximal negative motor velocity obtained is  $5.650 \text{ rad/s}$ . It is not surprising that the negative motor velocity is larger in absolute value than the positive due to the effects discussed earlier, containing motor speeding, internal motor leakages and due to the accuracy of the regression line and (4.1). The errors are given as  $\frac{-0.283}{5} 100\% = -5.66\%$  and  $\frac{-0.650}{5} 100\% = -13\%$  for the maximal positive and negative motor velocity respectively. Another source of error is that only two decimals in the regression is used. However such a mapping in full scale, containing different motor loads, pump flows and different valve operation settings would be tremendous and less accurate. Also notice the flat region in the motor velocity around  $t = 7 \text{ s}$ , which is due to the dead bands in the main valves.

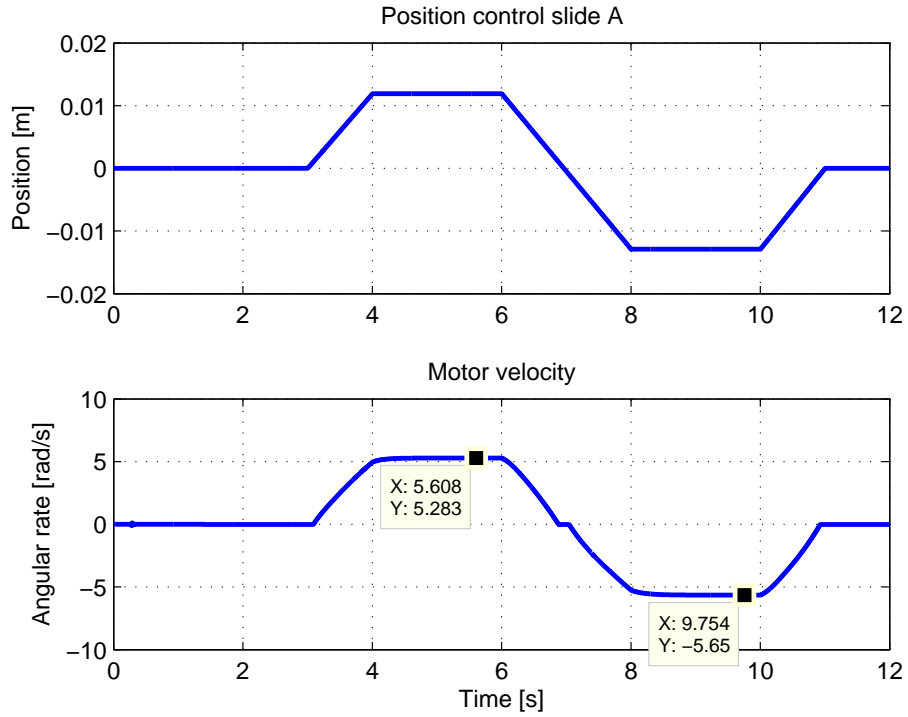


Figure 4.2: Results from the motor velocity mapping,  $T_{ms}=2000$  Nm.

For completeness the same simulations are done for  $T_{ms} = 20000$  Nm. Figure 4.3 shows the relation between the control slide position and the motor velocity.

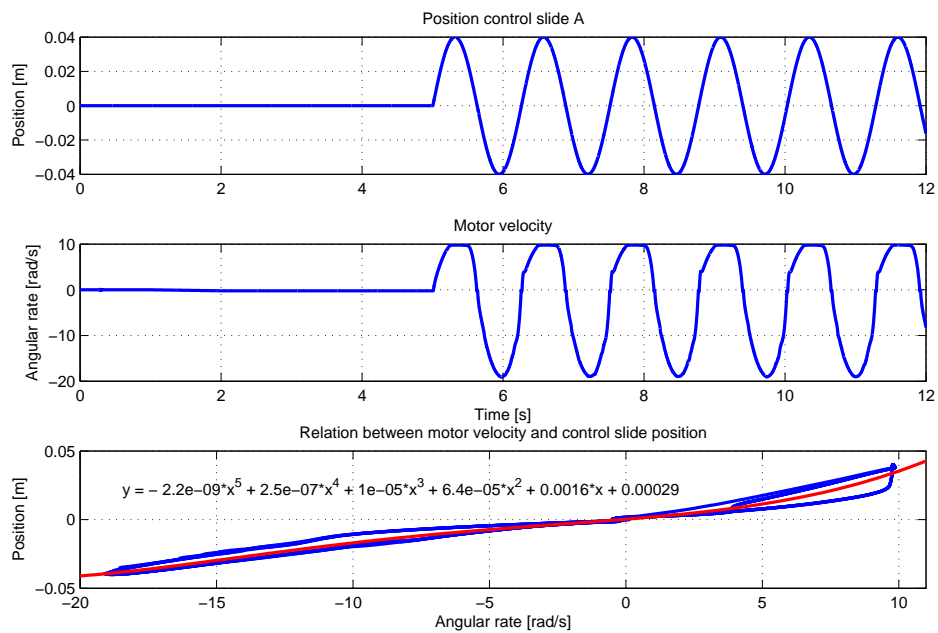


Figure 4.3: Relation between motor velocity and control slide position, main valve A.  $T_{ms} = 20000$  Nm.

The relation is expressed as

$$x_A = -2.2 \cdot 10^{-9} \omega_m^5 + 2.5 \cdot 10^{-7} \omega_m^4 + 1 \cdot 10^{-5} \omega_m^3 + 6.4 \cdot 10^{-5} \omega_m^2 + 0.0016 \omega_m + 0.00029 \quad (4.2)$$

and for  $\omega_m = 5 \text{ rad/s}$ ,  $x_A = 0.0112 \text{ m}$  and for  $\omega_m = -5 \text{ rad/s}$ ,  $x_A = -0.0071 \text{ m}$ . The reference signals for control slide A and B are changed respectively and have the same form as given in table 4.1. The results are given in figure 4.4.

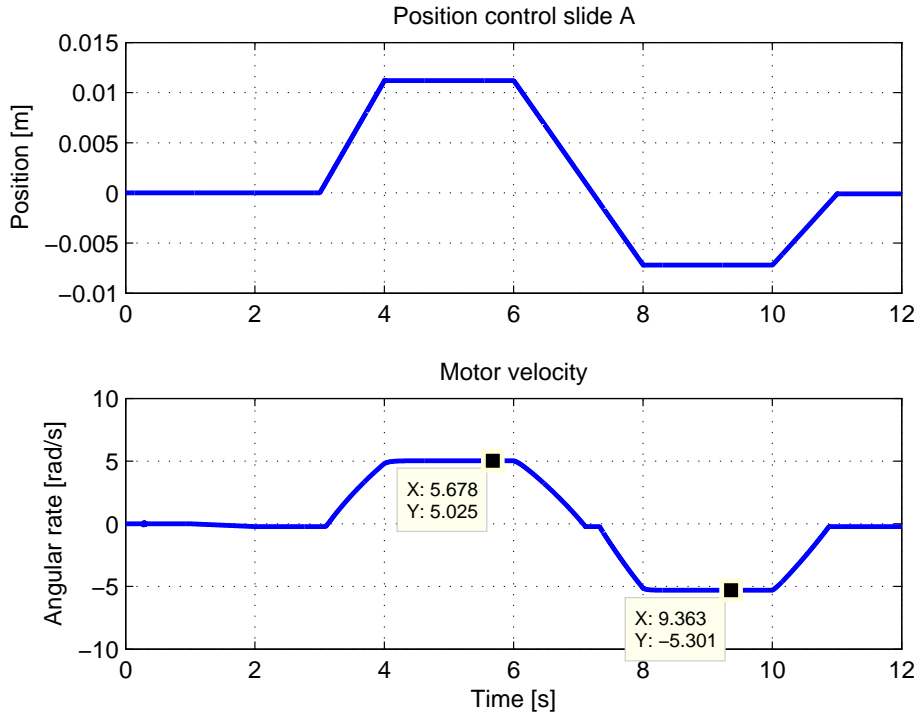


Figure 4.4: Results from the motor velocity mapping,  $T_{ms}=20000 \text{ Nm}$ .

As seen in the figure the results are better than in the first simulation, given in figure 4.2, where  $T_{ms} = 2000 \text{ Nm}$ . The errors are now  $\frac{-0.025}{5} 100\% = -0.5\%$  and  $\frac{-0.301}{5} 100\% = -6.02\%$  for the maximal positive and negative motor velocity respectively. This has to do with the regression line which seems to fit the data set better in this load case. Figure 4.5 shows a closer look at the control slide position for main valve A and the motor velocity at some interesting points.

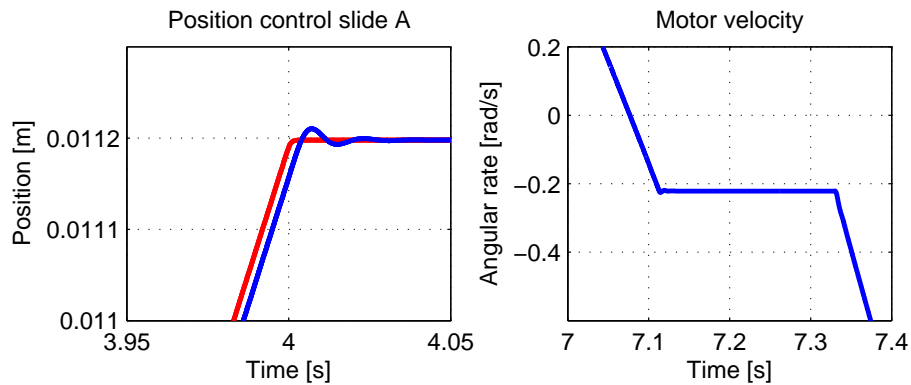


Figure 4.5: Control slide position and motor velocity with P-controller.

As can be seen there is a small delay between the reference and the control slide position, as expected, and the vertical line in the plot to the right shows the effect from the dead bands in



the main valves.

### 4.1.2 First Hand Manual Speed Controller

As seen in the previous subsection there is a relation between the control slide positions and motor velocity. However the first hand controller, or the *normal speed controller*, is intended manual motor control, where an operator manually sets the control slide references using a joystick to obtain the preferred motor velocity, assuming the motor velocity is observable for the operator. This would also give the operator the opportunity to change valve settings, not only do 4/3 valve control.

In such a control mode it is important that the *inner controller*, the control slide position controller, is stable, accurate and fast. The controller should also have the ability to adapt to the dynamics in such a way that the response of the control slide feels the same in different cases for the operator. The changes in the dynamics could come from unmodeled quantities, changes in system parameters or wear of the hydraulic system. In that way the winch operator would get a stronger feeling of proportionality between the control slide displacement and the motor velocity. Such a controller could be model based, in which it would require larger computing power compared to an ordinary PID-controller. The intermediate would be an adaptive PID-controller, which is used here.

The adaptive parameters in the adaptive PID controller are the controller gains and have their own dynamics. In Iwai et al. (2006) the adaptive controller gains are given as

$$\dot{K}_p^A(t) = \gamma_1 e_s(t)^2 - \sigma K_p^A(t) \quad (4.3a)$$

$$\dot{K}_d^A(t) = \gamma_2 e_s(t) \dot{e}_s(t) - \sigma K_d^A(t) \quad (4.3b)$$

$$\dot{K}_i^A(t) = \gamma_3 e_s(t) \int_0^T e_s(t) dt - \sigma K_i^A(t) \quad (4.3c)$$

where  $K_p^A$ ,  $K_d^A$  and  $K_i^A$  are the proportional gain, derivative gain and integral gain respectively,  $\gamma_1$ ,  $\gamma_2$  and  $\gamma_3$  are positive constants describing the magnitude of the gains,  $e_s$  is the control error given as  $e_s = x_s - r_s$  and  $\sigma$ ,  $0 < \sigma < 1$ , is a modification term making the gain tuning laws more robust for unmodeled dynamics.

Looking at the motor velocity in figure 4.2 and 4.4 a small flattening can be seen around  $t = 7$  s. This has to do with the overlap, the dead band, in the main valves as mentioned before. It would be desired for the operator that the controller would cross the dead band as fast as possible automatically by the controller. By assuming that the operator feeds the control algorithm with the actual length of valve opening, not the control slide displacement as before, the "jump" over the dead band can be expressed as

$$r_s = r_o + \frac{2x_{olap}}{\pi} \arctan(s \cdot r_o) \quad (4.4)$$

where  $r_o$  is the reference given by the operator and  $s$  is related to the slope of the jump and is a design parameter. By setting  $s = 1000$ , assuming  $r_o = 0.5 \sin(t)$  and  $x_{olap} = 0.1$  m then  $r_s$  is given as in figure 4.6.

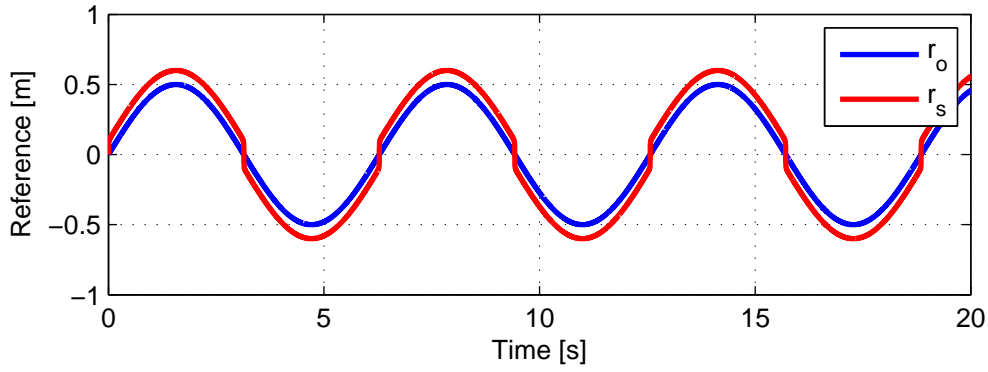


Figure 4.6:  $r_s$  v.s.  $r_o$

Table 4.2 shows the parameters that have been tuned for the inner controller.

Table 4.2: Adaptive control law parameters.

Part	Description	Value
Inner Controller	$\sigma$ , Modification term	0.5-
	$\gamma_1$ , Proportional gain parameter	1e11-
	$\gamma_2$ , Derivative gain parameter	1e5-
	$\gamma_3$ , Integral gain parameter	1-
	$s$ , Slope in arctan()-function	1e6-

The same simulation as given in figure 4.4, with  $T_{ms} = 20000$  Nm, is redone, but now with the new adaptive inner controller. The results are shown in figure 4.7.

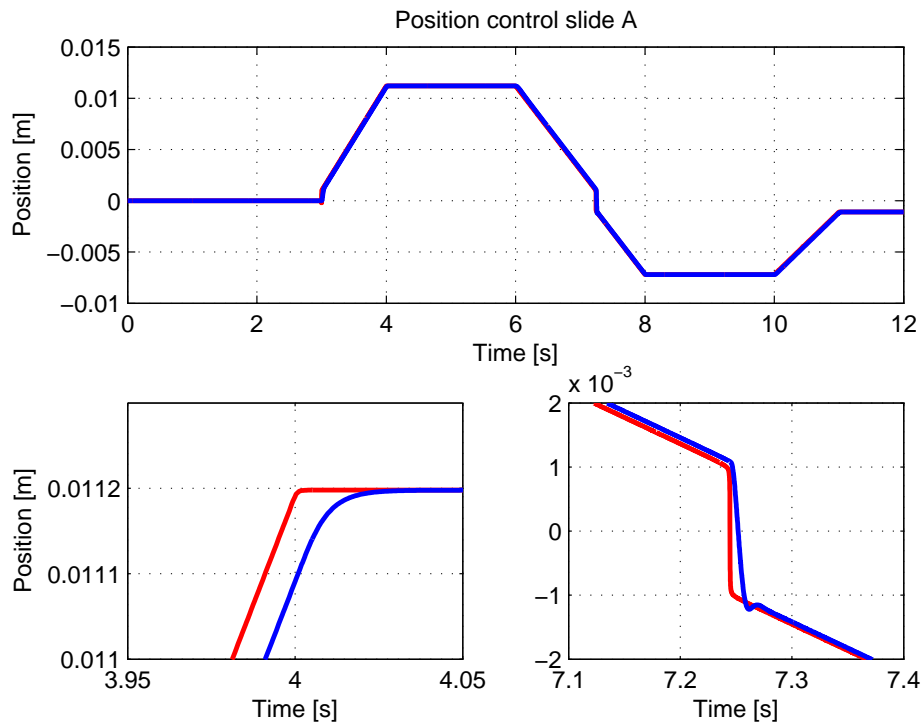


Figure 4.7: Reference and actual position of control slide A.

By comparing the plot given in the lower left corner with the first plot in figure 4.5 it can be seen that the oscillations are gone, but the delay between the reference and the actual control slide position seems to be increased. However this is not a big deal since the controller does not have to be extremely fast since the operator is controlling the motor velocity, but later on, when more precise controllers are to be studied, the adaptive law may be too slow. The plot in the lower right corner shows that the controller jumps over the dead band as fast as possible, generating a small overshoot after the jump. The motor velocity is shown in figure 4.8.

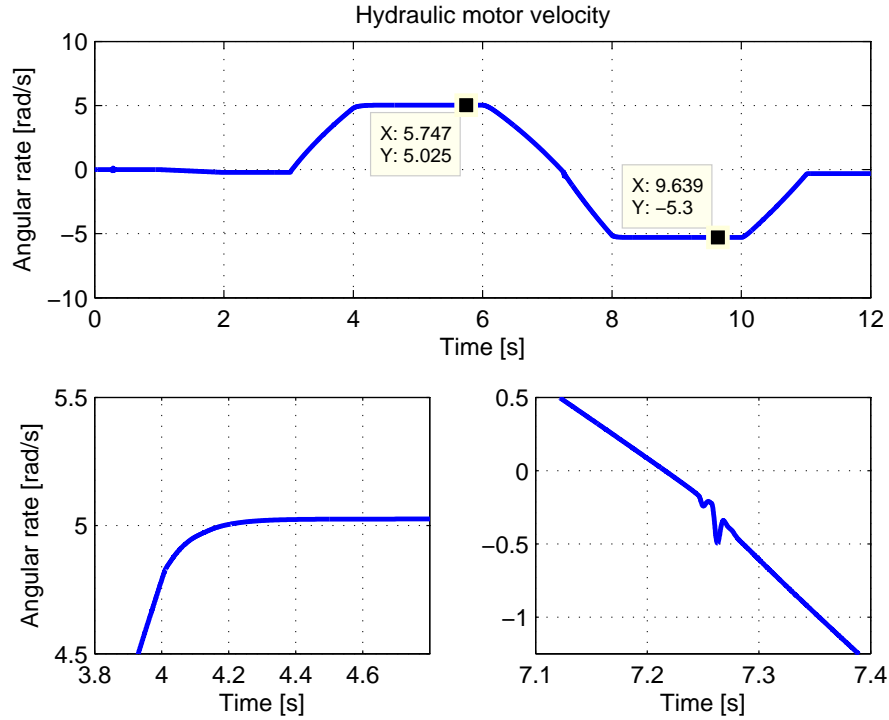


Figure 4.8: Motor velocity.

As seen in the figure the characteristic flattening in motor velocity shown in figure 4.4 at  $t \approx 7$  s seems to be gone. It is replaced by a small oscillation, which cannot be avoided due to the dead bands in the main valves. The adaptive control law also includes integral effect. This is not necessary for the simplified bond graph model, but may be appreciated in real life implementation, and if the velocity limitation function given in 2.20 is used which generated a small bias between the reference given by the operator and the limited reference.

The adaptive controller gains are shown in figure E.1 in Appendix E, together with a random reference simulation testing the adaptive controller.

## 4.2 Manual Torque Control

Hydraulic motor torque control can be done through controlling the differential pressure across the motor, since

$$T_m := \frac{D_m}{2\pi} \Delta p \quad (4.5)$$

where  $T_m$  is the motor torque,  $D_m$  is the volume of the motor per revolution, and  $\Delta p$  is the differential pressure. The differential pressure is controlled indirectly by control slide position control, just as the motor velocity, but is much more sensitive to other effects like the pressure

compensator, load disturbances and variable bulk modulus than the motor velocity. Figure 4.9 shows the control slide position, differential pressure and the relation between them for the same simulation as done in 3.1.2 with  $T_{ms} = 2000$  Nm and by using the P-controller as inner controller.

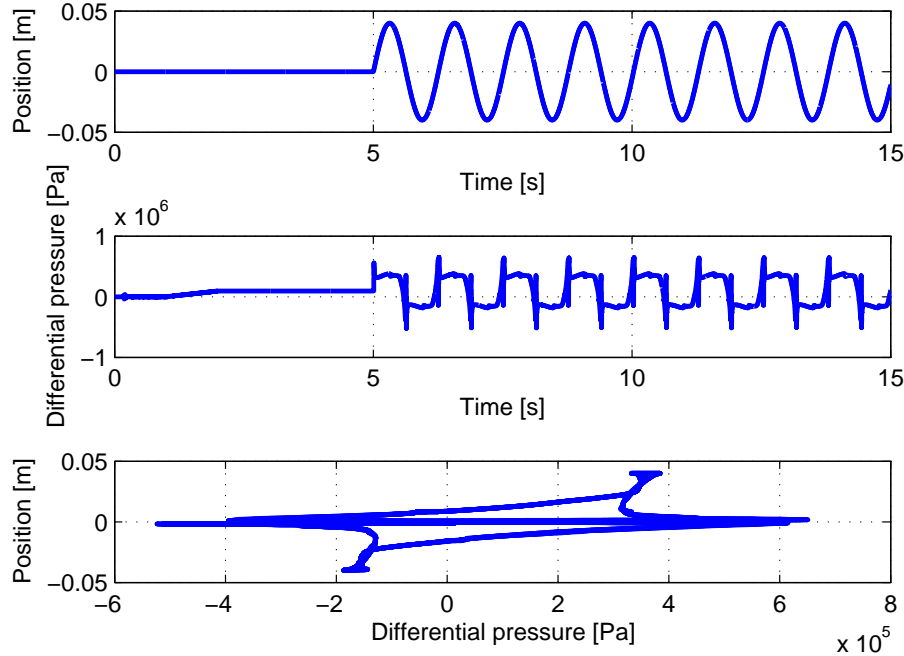


Figure 4.9: Relation between differential pressure and control slide position, main valve A.  $T_{ms} = 2000$  Nm.

As can be seen in the second plot the differential pressure is not clean, it has a lot of noise. This noise comes mainly from when the main valves cross the dead bands. As seen in the last plot the noise reduces the possibility to find a good relation between the two quantities. The differential pressure measurements must be filtered through a low pass filter in order to get a better understanding of the relation, because the differential pressure also seems to have the geometric characteristics as the control slide position.

using a first order transfer function,

$$H_{LPF}(s) = \frac{k}{\tau s + 1} \quad (4.6)$$

where  $k = 1$  - is the gain and  $\tau = 0.05$  s/rad is the time constant, as a low pass filter, the differential pressure measurements are cleaned up as figure 4.10 shows.

The danger with filtering is that one may loose important data. The figure shows that the differential pressure measurements are much nicer and cleaner, but looks rather edged at the maximal absolute values. This may imply loss of important data. However the last plot shows that it is now possible to find a mathematical expression relating the differential pressure to the control slide position,

$$x_A = -9.7 \cdot 10^{-31} \Delta p^5 - 6.2 \cdot 10^{-26} \Delta p^4 + 2.5 \cdot 10^{-18} \Delta p^3 - 6.9 \cdot 10^{-13} \Delta p^2 + 5 \cdot 10^{-8} \Delta p - 0.00035 \quad (4.7)$$

If the differential pressure was set to  $\Delta p = 3$  bar, giving a motor torque of about  $T_m = 6210$  Nm, the control slide position would be given as  $x_A = 0.0172$  m. For  $\Delta p = -1$  bar, giving a motor torque of about  $T_m = -2070$  Nm, the control slide position is given as  $x_A = -0.0147$  m. By using

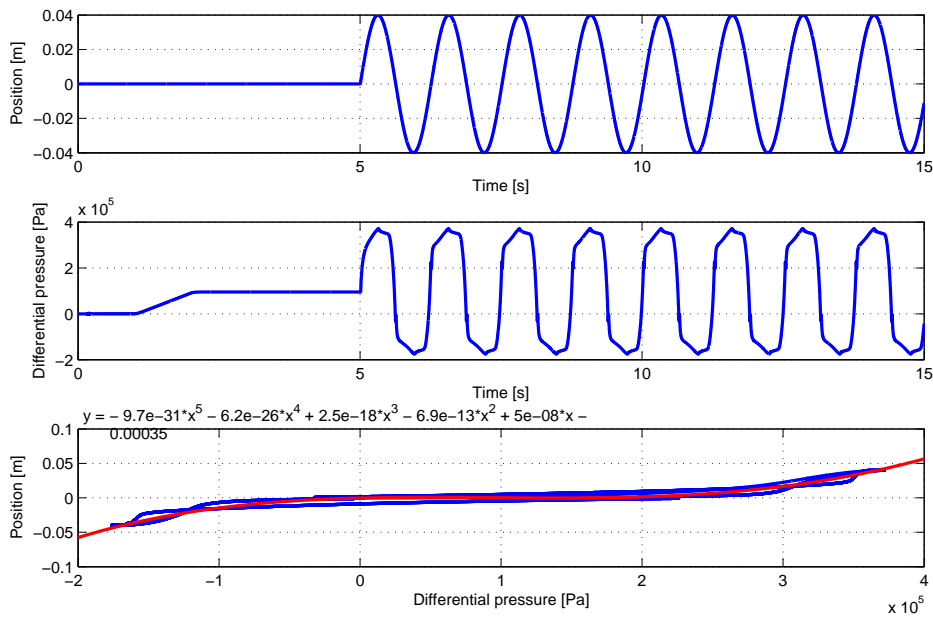


Figure 4.10: Relation between differential pressure and control slide position, main valve A.  $T_{ms} = 2000 \text{ Nm}$ , low pass filtered differential pressure.

the same control slide reference geometry as previous (see table 4.1), a test of the relation may be performed. The results from the simulation, using the P-controller, are shown in figure 4.11.

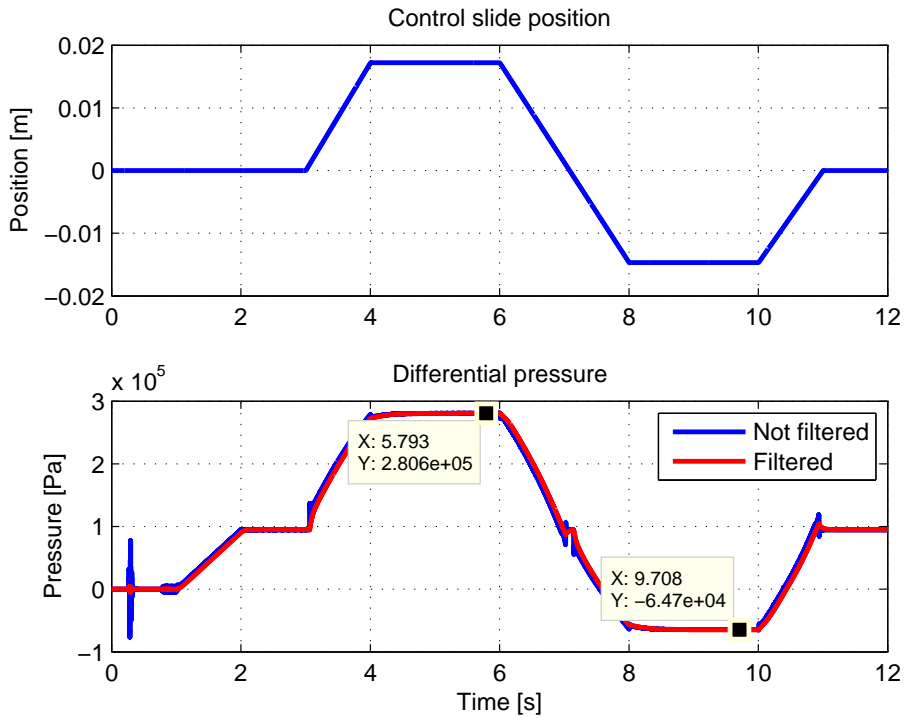


Figure 4.11: Control slide position,  $x_A$ , and differential pressure,  $\Delta p$ .

As seen in the figure the maximal differential pressure is 2.806 bar, giving an error of  $\frac{0.1940}{3} 100\% = 6.47\%$ . The lowest differential pressure is -0.647 bar, giving an error of  $\frac{0.353}{1} 100\% = 35.3\%$ . These

results are not that bad taking the filtering and the sensitivity into account.

The same simulation is done with the adaptive controller designed in section 4.1.2. The filtered relation is shown in figure 4.12.

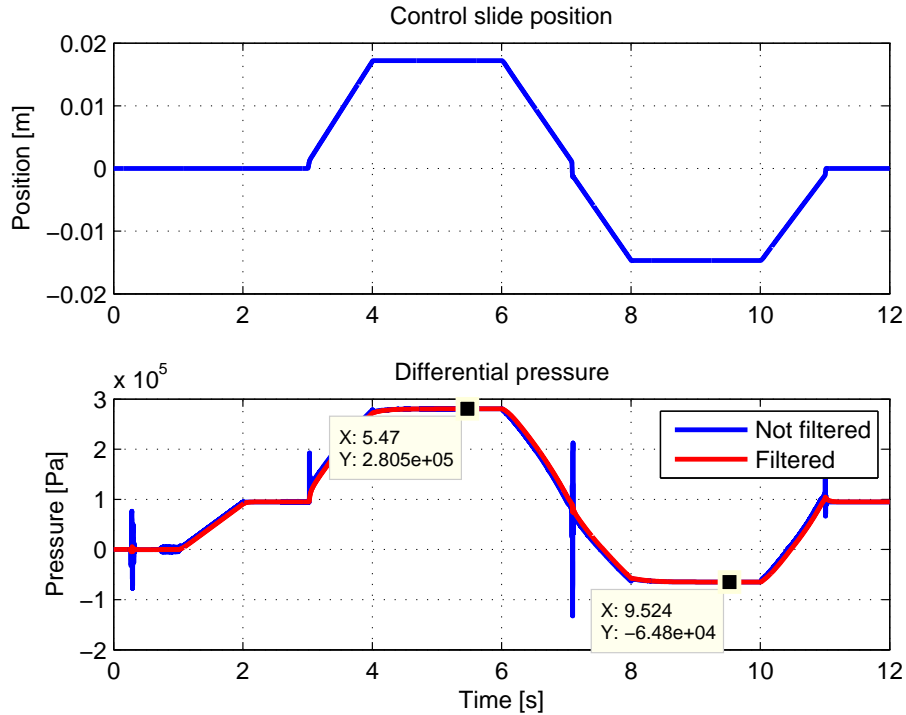


Figure 4.12: Control slide position,  $x_A$ , and differential pressure,  $\Delta p$ .

As seen in the figure the pressure peaks are larger when passing the dead band compared to figure 4.11, but the filtered signal is smoother. Since the operator observes the filtered signal, the simulation with adaptive control would give him better results. Also the motor speed would be cleaner as seen in section 4.1.2.

For completeness the same simulation is done for  $T_{ms} = 20000$  Nm. Figure 4.13 shows the relation between the control slide position and the differential pressure. The relation is expressed mathematically as

$$x_A = 2 \cdot 10^{-30} \Delta p^5 - 6.2 \cdot 10^{-24} \Delta p^4 + 6.8 \cdot 10^{-18} \Delta p^3 - 2.9 \cdot 10^{-12} \Delta p^2 + 3.5 \cdot 10^{-7} \Delta p - 0.001 \quad (4.8)$$

Since  $\Delta p = -1$  bar is not present in the figure, the pressure that is to be tested is  $\Delta p = 12$  bar, which gives approximately  $T_{ms} = 24840$  Nm and  $x_A = 0.0219$  m, and  $\Delta p = 5$  bar, which gives  $T_{ms} = 10350$  Nm and  $x_A = -0.0334$  m. Note that more than two decimals in the polynomial is used to find these numbers, since  $x_A = 0.1137$  m for  $\Delta p = 12$  bar when using only two decimals.

The simulation results using the P-controller are shown in figure 4.14. Using the numbers given by the figure the errors are given as  $\frac{0.15}{12} 100\% = 1.25\%$  and  $\frac{-0.321}{5} 100\% = -6.42\%$  respectively. It seems like the error decreases as the pressure increases. The results from the same simulation but with the adaptive controller are shown in figure 4.15.

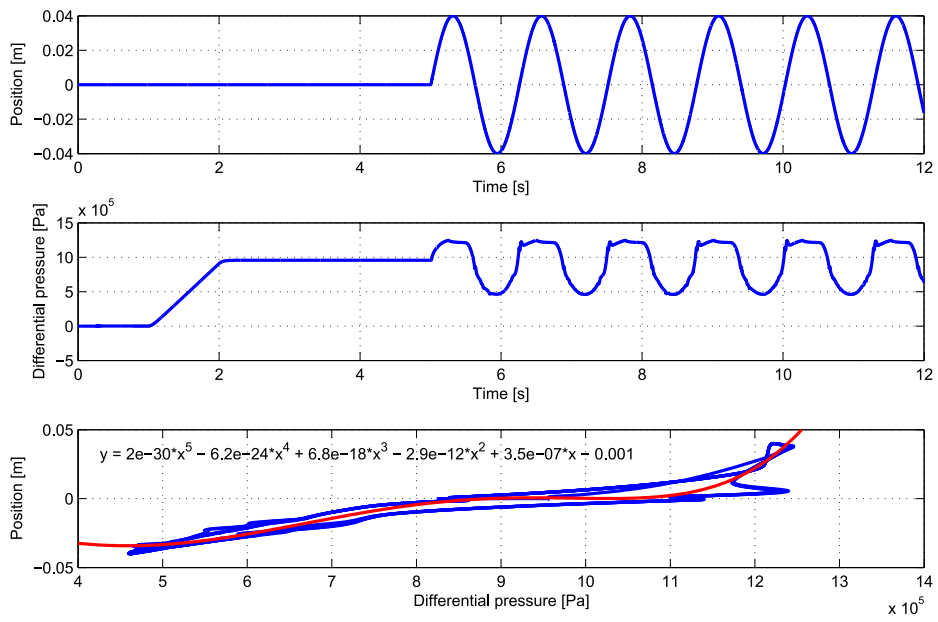


Figure 4.13: Relation between differential pressure and control slide position, main valve A.  $T_{ms} = 2000$  Nm, low pass filtered differential pressure.

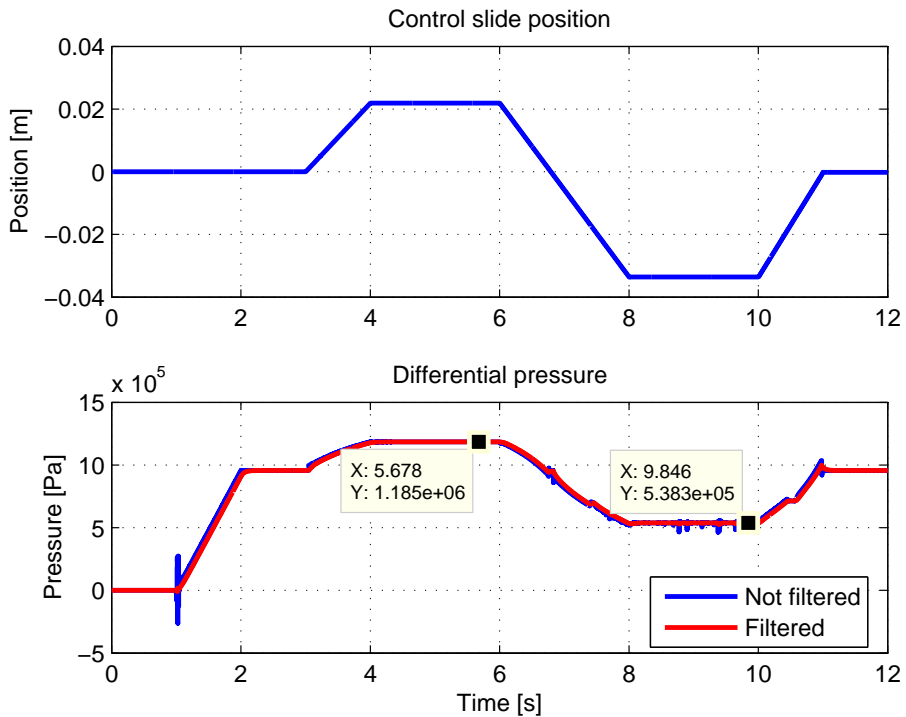


Figure 4.14: Control slide position,  $x_A$ , and differential pressure,  $\Delta p$ .

The error seems to be in the same range as when using the P-controller. The characteristic peak is present when the control slides pass the dead bands in the main valve. However the filtered differential pressure are smooth and clean.

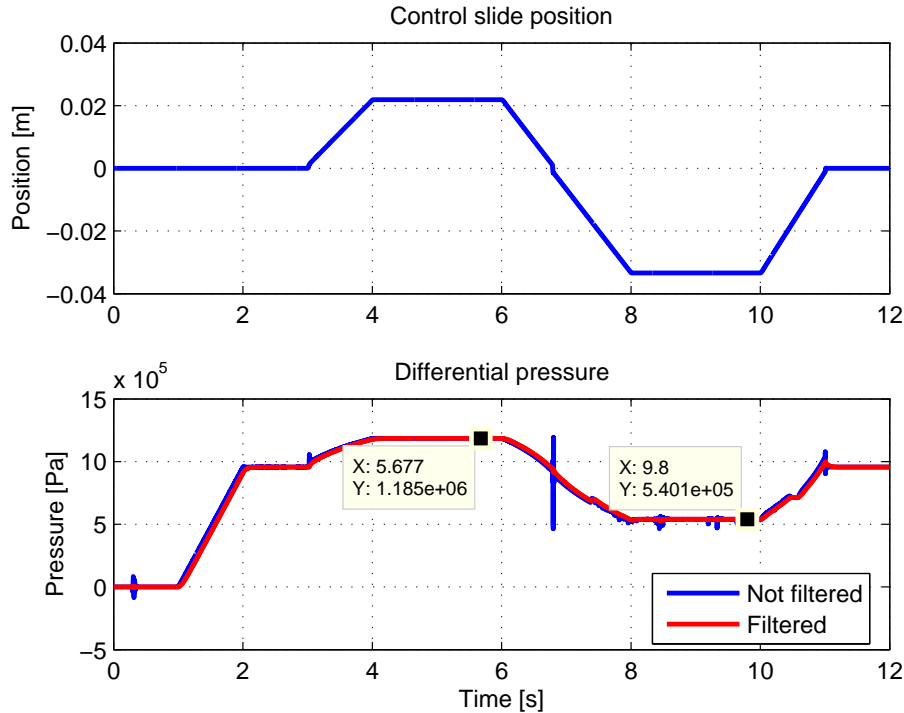


Figure 4.15: Control slide position,  $x_A$ , and differential pressure,  $\Delta p$ .

### 4.3 Chapter Summary and Conclusion

In this chapter manual speed- and torque control of the hydraulic motor have been studied under ideal conditions. An adaptive PID-controller for inner control was designed and tested, giving good results. The analysis relating the control slide positions to the motor velocity and the differential pressure could be extended to give more data. Figure 4.16 shows a parameter sweep of the motor load, from 2000 Nm to 20000 Nm through 10 steps.

As seen in the figure the relation between the motor velocity and the control slide position seems to flatten out when the motor load increases, giving a almost linear relation when  $T_m = 20000$  Nm. It also shows that the load has a large influence on negative motor velocity. This means that if a PID-controller was to be used as the outer controller, setting the reference for the inner controller, the gains would be dependent on the motor load. This would change the control problem to a hybrid control problem, since the gains would have to be updated with an update law through motor load measurements. When the update law is initiated a filter should be used to smooth out the transition of the gains. This gives a new problem; stability when switching gains. If the outer controller is fast and the load changes rapidly the update law would be initiated often, which again would affect the stability. In Hespanha (2002) these effects are discussed and switching restrictions are given to prevent instability like dwell-time switching and hysteresis switching. Another approach is to interpolate between the controller gains, but this would be quite a work, without knowing how good the results are going to be.

Since the relation is non-linear and seems to become more linear with the increase of motor load, a PID-controller is not ideal as outer control, especially since the relation changes that much. Note that if the controlled system was linear, a PID-controller would be the same as a model based controller, where the gains in the controller would be determined by the system parameters in a stability analysis. However if a PID-controller was to be used as an outer controller, different load cases should be studied in order to tune the gains in the controller for the different load



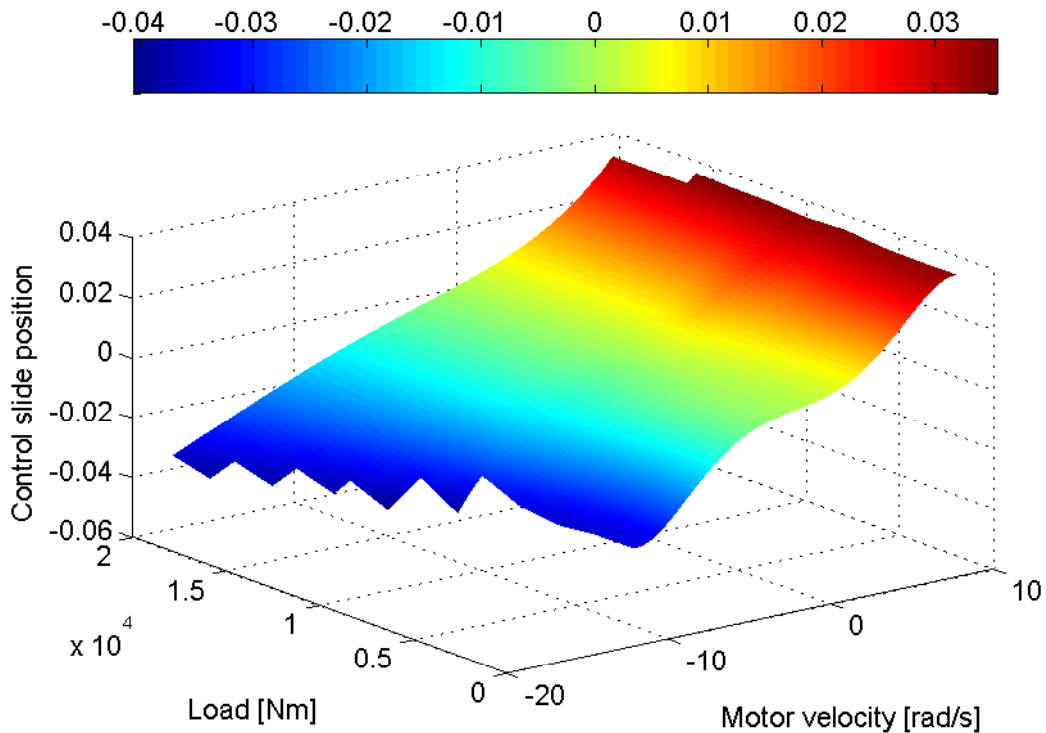


Figure 4.16: Control slide position,  $x_A$ , motor velocity,  $v$  and motor load,  $T_m$ .

cases. Then an update law, with restrictions to assure stability in the switching, or a algorithm interpolating the gains must be designed surrounded by a well-designed safety algorithm that assures safety in every conceivable cases.

Figure 4.17 shows the relation between the differential pressure, hydraulic motor load and control slide position for main valve A with parameter sweep of the motor loading. The figure shows different peaks for large control slide positions. This is due to the lack of data from the analysis. The steps in the sweep should be made smaller to get more data. It can also be seen that the non-linear relation between the differential pressure and the control slide position does not get linearised with the increase of motor load as the motor velocity relation in the previous figure. This supports the assumption about sensitivity of the differential pressure. If a table based controller, a PID-controller with varying controller gains, is to be used as an outer control even more load cases should be studied. And different main pump flows must also be included in the study.

However it is nearly impossible to account for all different cases and variations of variables that affect both the motor velocity and the differential pressure so the outer controller must be robust and most likely slow to assure stability. This will affect the precision of the controller.

Hybrid PID-based outer controllers, or table based controllers, are not studied further. The outer controllers are assumed to be highly dependent of system states and variables and therefore model based controllers should be in the scope of study.

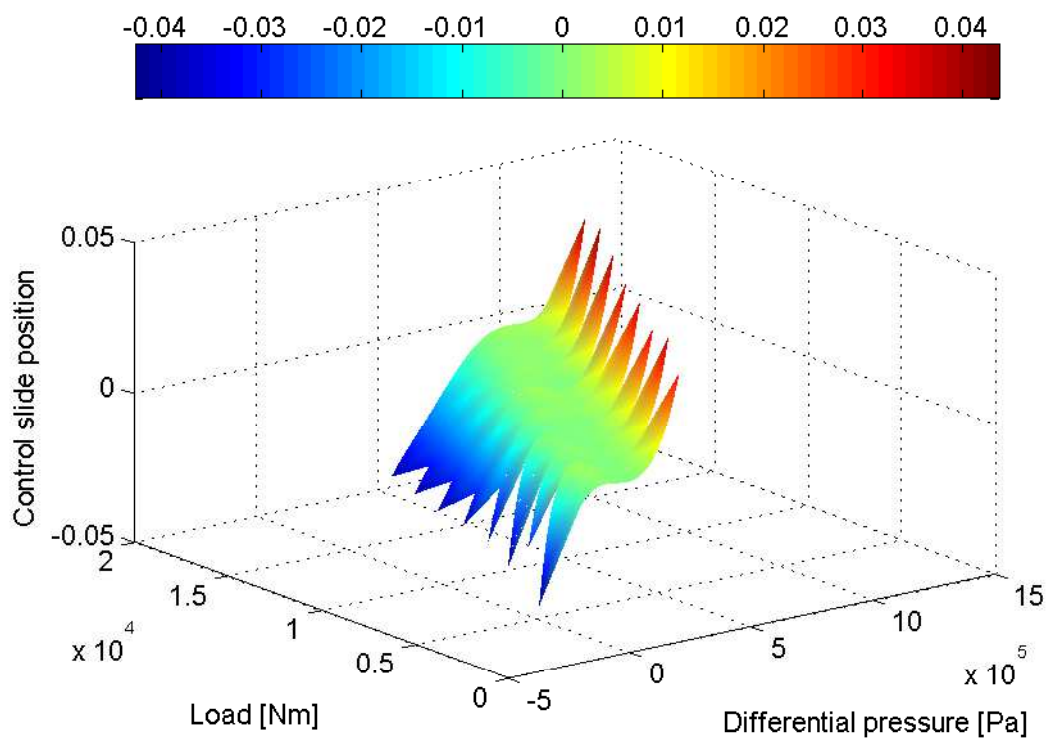


Figure 4.17: Control slide position,  $x_A$ , differential pressure,  $\Delta p$  and motor load,  $T_m$ .

# 5 | Precise Control

In chapter 4 first hand control of the hydraulic motor was studied. It was concluded that a model based speed controller and a model based torque controller should be derived and used as outer controllers, giving control slide references to the inner controllers. In this chapter precise model based outer controllers are presented and studied. The state equations describing the relevant dynamics used in the control designs are presented. The state equations abstracted from the bond graph model are complex, containing logics and discrete quantities, and are not suitable for control design. Therefore simplified state equations are derived and used.

## 5.1 State Equations

As mentioned in chapter 1, one of the many benefits with using bond graph models is that the state equations can easily be abstracted from the model. The state equations for the angular motor momentum and the accumulated volumes in volume A and B are given as

$$\dot{p}_m = \frac{D_m \beta}{2\pi} \left( \frac{x_A}{V_A} - \frac{x_B}{V_B} \right) - T_{load} - F_s \mu_v \frac{p_m}{I_m} \quad (5.1a)$$

$$- F_s \left( \mu_s \tanh\left(s \cdot \frac{p_m}{I_m}\right) - \frac{1}{2}(\mu_s - \mu_c) \tanh\left(s \left(\frac{p_m}{I_m} - \frac{c}{s}\right)\right) + \frac{1}{2}(\mu_c - \mu_s) \tanh\left(s \left(\frac{p_m}{I_m} + \frac{c}{s}\right)\right) \right)$$

$$\dot{x}_A = \left\{ \begin{array}{l} \alpha_p \pi D_s (x_H - x_{olap}) \sqrt{\frac{2(P_{pump} - \frac{\beta x_A}{V_A})}{\rho}} \quad \text{for } (x_H - x_{olap}) \geq 0 \text{ and } (P_{pump} - \frac{\beta x_A}{V_A}) \geq 0 \\ 0 \quad \text{else} \end{array} \right\} \quad (5.1b)$$

$$+ \left\{ \begin{array}{l} \alpha_r \pi D_s (x_{olap} - x_H) \text{sign}\left(\frac{\beta x_A}{V_A} - T_{pump}\right) \sqrt{\frac{2\left|\frac{\beta x_A}{V_A} - T_{pump}\right|}{\rho}} \quad \text{for } (x_{olap} - x_H) \geq 0 \\ 0 \quad \text{else} \end{array} \right\}$$

$$+ G\beta \left( \frac{x_B}{V_B} - \frac{x_A}{V_A} \right) - \frac{D_m p_m}{2\pi I_m}$$

$$\dot{x}_B = \left\{ \begin{array}{l} \alpha_p \pi D_s (x_L - x_{olap}) \sqrt{\frac{2(P_{pump} - \frac{\beta x_B}{V_B})}{\rho}} \quad \text{for } (x_L - x_{olap}) \geq 0 \text{ and } (P_{pump} - \frac{\beta x_B}{V_B}) \geq 0 \\ 0 \quad \text{else} \end{array} \right\} \quad (5.1c)$$

$$+ \left\{ \begin{array}{l} \alpha_r \pi D_s (x_{olap} - x_L) \text{sign}\left(\frac{\beta x_B}{V_B} - T_{pump}\right) \sqrt{\frac{2\left|\frac{\beta x_B}{V_B} - T_{pump}\right|}{\rho}} \quad \text{for } (x_{olap} - x_L) \geq 0 \\ 0 \quad \text{else} \end{array} \right\}$$

$$- G\beta \left( \frac{x_B}{V_B} - \frac{x_A}{V_A} \right) + \frac{D_m p_m}{2\pi I_m}.$$

In the equations above  $x_H$  and  $x_L$  are treated as control inputs where  $x_H$  is the control slide position for the main valve on the hoisting side of the motor (main valve A in this case) and  $x_L$  is the control slide position for the main valve on the lowering side of the motor (main valve B). The states, variables and parameters are explained in table 5.1. Note that the bulk modulus is

assumed constant in the control designs, even though it is highly variable.

Table 5.1: States, variables and parameters for hydraulic motor.

Variables	Description	Parameters	Description
$p_m$	– Angular momentum	$D_m$	– Motor displacement
$x_A$	– Volume state	$\beta$	– Bulk modulus
$x_B$	– Volume state	$V_A$	– Volume
$x_H$	– Control slide displacement	$V_B$	– Volume
$x_L$	– Control slide displacement	$F_s$	– Friction parameter
$T_{load}$	– Motor load	$c$	– Coulomb coefficient
$P_{pump}$	– Pump pressure	$s$	– Slope for coulomb friction
$T_{pump}$	– Return pressure	$I_m$	– Hydraulic motor inertia
$\alpha_p$	– Flow parameter, pump	$d$	– Angular friction
$\alpha_r$	– Flow parameter, return	$D_s$	– Hydraulic diameter
		$x_{olap}$	– Overlap in control slide
		$G$	– Leakage parameter

The equations given in (5.1) are complicated and should be simplified and transformed into motor velocity and differential pressure across the hydraulic motor. Some of the dynamics given in the equations can be neglected without losing the main characteristics of the system. In Skjong and Pedersen (2014a), which is given in Appendix B.1, simplified state equations are derived for 4/3 valve control and given as

$$\dot{x}_{m1} = x_{m2} \quad (5.2a)$$

$$\dot{x}_{m2} = \frac{1}{I_m} \left[ \frac{Dm}{2\pi} \Delta p - F_s \mu_v x_{m2} - T_{load} \right] \quad (5.2b)$$

$$\Delta \dot{p} = \frac{\beta \alpha \pi D_s}{V \sqrt{\rho}} u \sqrt{\Delta p_{pump} - \text{sign}(u) \Delta p} - \frac{\beta D_m}{2\pi V} x_{m2} - \frac{\beta G}{V} \Delta p. \quad (5.2c)$$

where  $x_{m1}$  is the hydraulic motor angle,  $x_{m2}$  is the angular rate,  $\Delta p$  is the differential pressure across the hydraulic motor and  $u$  is the controller output from the outer controller without dead band compensation. In addition to these simplified state equations, control laws for speed control and torque control are derived in Skjong and Pedersen (2014a).

## 5.2 Model Based Speed Controller

The model base speed controller is a sliding mode based backstepping controller and is elaborated in Skjong and Pedersen (2014a) in Appendix B.1. The resulting control law is given as

$$x_H = \text{limit} \left( u + \frac{2x_{olap}}{\pi} \arctan(s \cdot u), -x_{max}, x_{max} \right) \quad (5.3)$$

and is the dead band compensation where  $x_{olap}$  is the overlap, the dead band, in the main valves,  $s$  is a parameter related to the slope in the  $\arctan(\cdot)$ -function,  $x_{max}$  is the maximal control slide displacement and  $u$  is the ideal output from the speed controller for main valves without dead bands and is given as

$$\begin{aligned}
u = \frac{V\sqrt{\rho}}{\beta\alpha\pi D_s\sqrt{p_L(u_{pre})}} & \left( -k_1 z_{s1} + D_2 s_1 + k_2 \text{sign}(s_1) \right. \\
& - \frac{D_m}{2\pi I_m} s_1 + \dot{v}_1 + \frac{\beta D_m}{2\pi V} x_{m2} \\
& \left. - D_3 s_2 - k_3 \text{sign}(s_2) + \frac{\beta G}{V} \Delta p \right)
\end{aligned} \tag{5.4}$$

where

$$p_L(u_{pre}) := \Delta p_{pump} - \text{sign}(u_{pre})\Delta p \tag{5.5}$$

and  $u_{pre}$  is the previous value of  $u$ .  $k_1$ ,  $k_2$ ,  $k_3$ ,  $D_2$  and  $D_3$  are controller gains,  $z_{s1}$  is the tracking error defined as

$$z_{s1} := x_{m2} - x_{d2} \tag{5.6}$$

where  $x_{d2}$  is the reference motor velocity,  $s_1$  is the first sliding surface defined as

$$s_1 := z_{s1} + k_1 \int_0^t z_{s1} dt \tag{5.7}$$

$v_1$  is a virtual control variable given as

$$v_1 = \frac{2\pi I_m}{D_m} \left( \frac{F_s \mu_v}{I_m} x_{m2} + \frac{T_{load}}{I_m} + \dot{x}_{d2} - D_2 s_1 - k_2 \text{sign}(s_2) \right) \tag{5.8}$$

and  $s_2$  is the second sliding surface defined as

$$s_2 := s_1 + z_{s2} \tag{5.9}$$

where

$$z_{s2} := \Delta p - v_1 \tag{5.10}$$

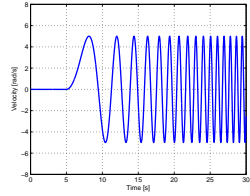
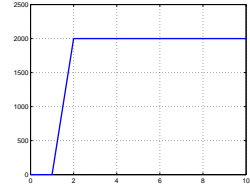
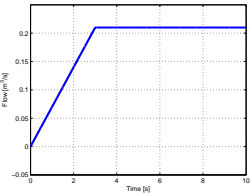
Note that  $T_{load}$  is the motor loading and must be estimated if used in the control law. For now  $T_{load}$  is assumed measurable.

The given control law ensures GAS, Globally Asymptotically Stability, of the system under the assumptions given in Skjong and Pedersen (2014a). The controller parameters are set to  $k_1 = 900 \text{ 1/s}$ ,  $k_2 = 0.01 \text{ rad/s}^2$ ,  $k_3 = 1000 \text{ Pa/s}$ ,  $D_2 = 200 \text{ 1/s}$ ,  $D_3 = 20 \text{ Pa/rad}$  and  $s = 200000$ -. Two tests of the controller with the model derived in chapter 2 are to be initiated, one with constant motor loading and one with random motor loading.

### 5.2.1 Controller Test using Constant Load

A frequency sweep of the motor velocity reference is to be tested. For inner controller the adaptive PID-controller derived in section 4.1.2 is used with the same parameters as before. The reference signals are given in table 5.2.

Table 5.2: Reference signals for test of speed controller

Description	Value
$x_{2d}$ , Reference signal for hydraulic motor velocity (a $\sin(\cdot)$ -sweep starting at $t=5$ s with a magnitude of $5 \text{ rad/s}$ and a frequency of $\omega = 0 \text{ rad/s}$ and ending at $t=30$ s with a frequency of $\omega = 8 \text{ rad/s}$ , $f = \frac{4}{\pi} \text{ Hz}$ )	
$T_m$ , Hydraulic motor load (a ramp starting at $t=1$ s with a magnitude of $T_{ms}$ and stopping at $t=2$ s, $T_{ms}$ is specified in the simulation.)	$T_m = T_{ms}\text{ramp}(1) - T_{ms}\text{ramp}(2)$ 
$\dot{Q}_p$ , Pump flow (a ramp starting at $t=0$ s with a slope of $0.07 \text{ m}^3/\text{s}^2$ and stopping at $t=3$ s)	$\dot{Q}_p = 0.07\text{ramp}(0) - 0.07\text{ramp}(3)$ 
$r_{3/2}$ , Reference signal for 3/2-directional valve ( $r_{3/2} = 2$ - means that the LOGIC-box controls the valve)	$r_{3/2} = 2$ -

$T_{ms}$  is set to 2000 Nm. Figure 5.1 shows the motor velocity and the reference velocity.

As seen in the figure the motor velocity seems to coincide with the reference. At the first maxima, seen in the plot in the lower left corner of the figure, the motor velocity is a bit higher than the reference. This is due to the inertia of the motor. However it is small and the tracking is low. When the frequency of the reference signal increases, this overshoot gets larger but it is so small that it cannot be seen in the first plot. Also it looks like the motor velocity is faster than the reference signal when looking at the plot in the lower left corner. This is however not the case, the motor reacts slower than the reference signal and uses little more time to slow down. The plot in the lower right corner shows the motor speed when the main valves cross the dead bands and shows that the dead band compensation removes the vertical line as seen in figure 4.5. Figure 5.2 shows the difference between the reference velocity and the actual motor velocity,  $x_{d2} - x_{m2}$ .

The error looks to increase with increasing frequency of the reference velocity, which is expected. By excluding the error peaks the error is small. The error peaks come from each crossing of the dead bands in the two main valves and can not be removed except trying to cross the dead bands as fast as possible, as already done. Another reason for this error is the dynamics of the pressure compensator. When the main valves cross the dead bands the pressure peaks acts

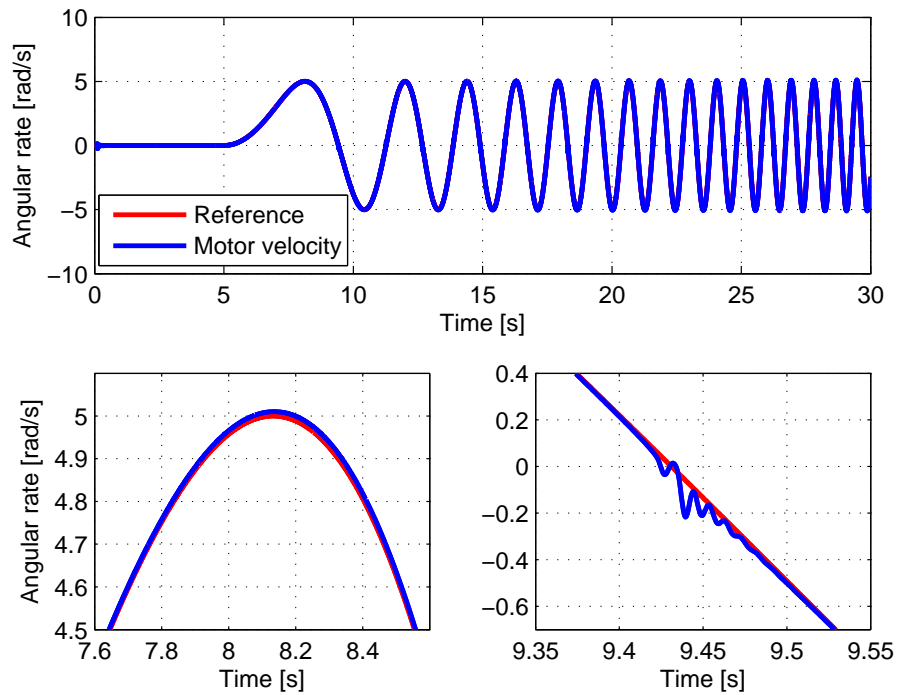


Figure 5.1: Hydraulic motor velocity and reference.

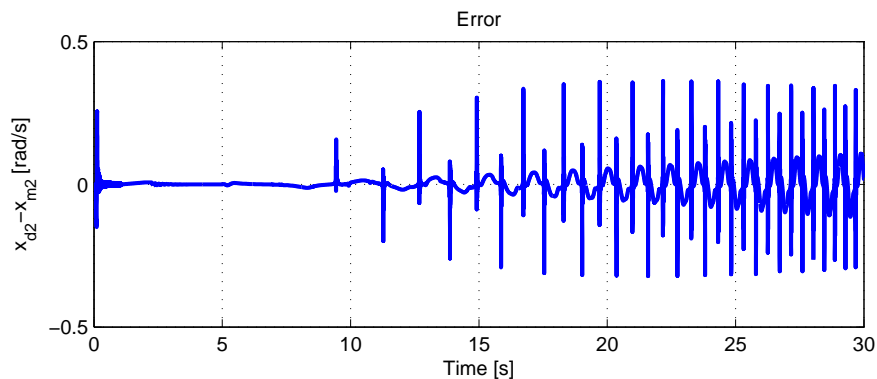


Figure 5.2: Difference between velocity reference and actual motor velocity.

on the pressure compensator and if the pressure compensator is not well-designed it will not damp out the peaks but regenerate them in the pump pressure making it harder for the speed controller to stabilize the motor velocity. The parameters for the pressure compensator given in C.1 are not optimal since crossings of the dead bands generate large pressure peaks in the pump pressure. This also sets a limit for how fast the speed controller can be tuned. These peaks in the differential pressure,  $\Delta p$ , can be seen in figure 5.4. This is also why the pump flow is set large so that the pressure compensator always is open, making it easier for the speed controller.

Figure 5.3 shows the control slide displacements and the reference positions generated by the speed controller.

As seen in the figure the control slide positions are good compared to the commanded reference except for a little delay. The delay seems to be larger than only the sample delay, meaning that the adaptive controller is littlebit slow. Note that the velocity limitation function is removed now when an outer controller is implemented. The delay generated by the adaptive controller

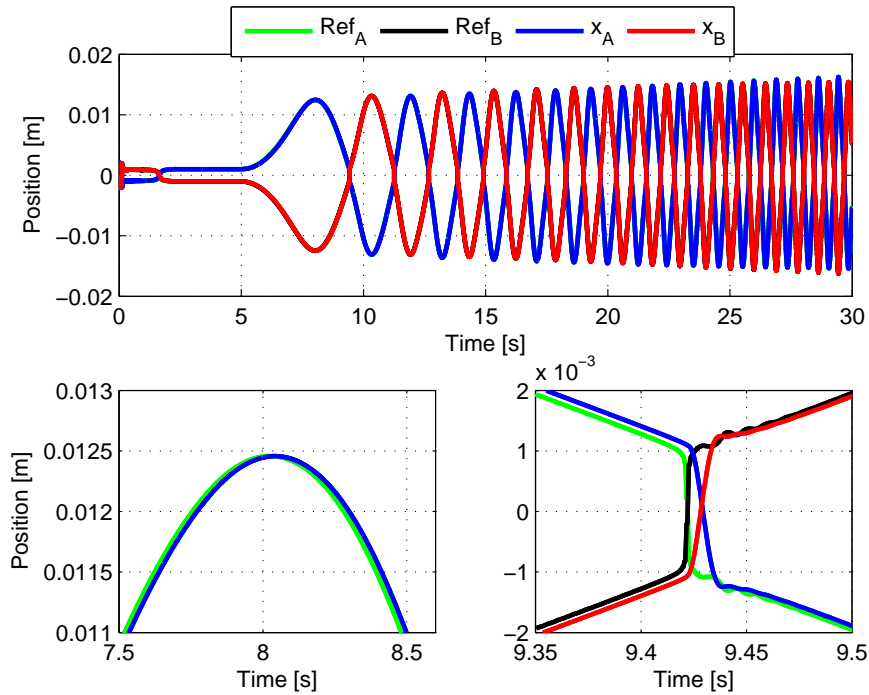


Figure 5.3: Control slide positions and speed controller output.

was also given as a comment in section 4.1.2, and most likely the error would be slightly lower if the simple P-controller was used as inner controller instead since it showed faster responses. However the adaptive PID-controller gets the job done and there is almost no oscillations in the control slide positions. The crossings of the dead bands are fast and the positions look stable. Figure 5.4 shows the differential pressure across the hydraulic motor and the variable bulk modulus in some of the many volumes in the system.

## 5.2.2 Controller Test using Random Motor Loading

To complete the controller testing for now, the same test is initiated but with different motor loading characteristics. Now  $T_{ms} = 10000$  Nm and a random load with amplitude 1000 Nm and a maximal frequency of  $f = 10$  Hz is added. The motor loading characteristics are shown in figure 5.5.

The maximal frequency of the variable load is much higher than what is to be expected in reality but is initiated to see how the controller operates under extreme conditions. Figure 5.6 shows the motor velocity compared to the reference.

As can be seen in the first plot the motor velocity seems to follow the reference with good precision. However the plot in the lower left corner in the figure shows that there are small oscillations around the reference. This is to be expected when a high frequency noise is added to the motor load. Because of the sampling delay it will be impossible to remove the tracking error completely. The plot in the lower left corner shows that the crossings of the dead bands are still good, generating only some small oscillations just as in the previous controller test. The difference between the reference and the actual motor velocity is shown in figure 5.7.

The error looks to be almost as in the previous controller test except some extra noise between  $t = 5$  s and  $t = 10$  s and some around  $t = 13$  s. It also looks like the effect of the noise is reduced when the frequency of the reference signal increases. This is expected since the motor acceler-



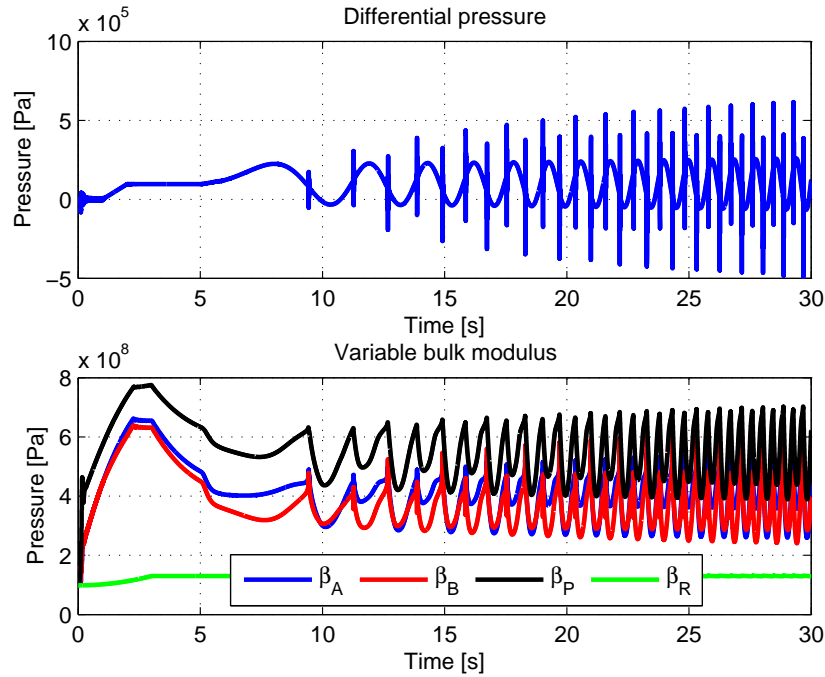


Figure 5.4: Differential pressure across the hydraulic motor and variable bulk modulus in volume A, B, P and R.

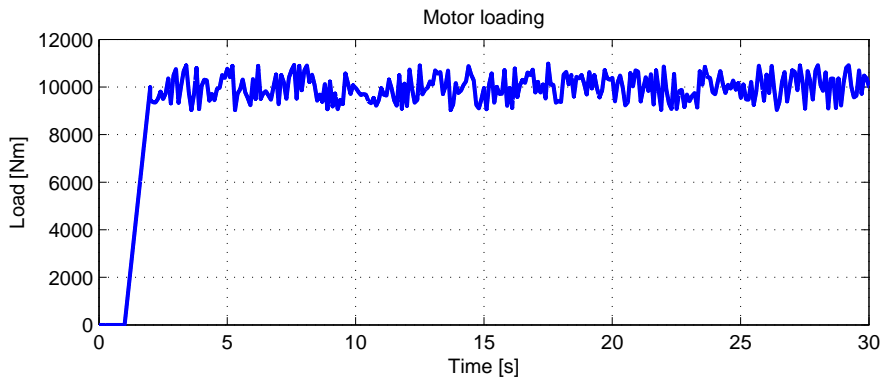


Figure 5.5: Motor loading characteristics.

ation is larger and more power in controlling the motor velocity is applied through the main valves. Figure 5.8 shows the control slide positions and the commanded reference from the speed controller.

The results are quite similar to the previous controller test, the inner controller works good and controls the control slides to the commanded position with the same delay as seen before. The plot in the lower left corner shows that there are some oscillations in the commanded control slide references which is expected because of the loading characteristics. The plot in the lower right corner shows that the crossings of the dead bands in the main valves seem to be as good as in the previous test. Figure 5.9 shows the differential pressure across the motor and the variable bulk modulus in some volumes in the model.

As can be seen in the figure the noise in the motor loading can also be found in the differential pressure across the motor and the variable bulk modulus.

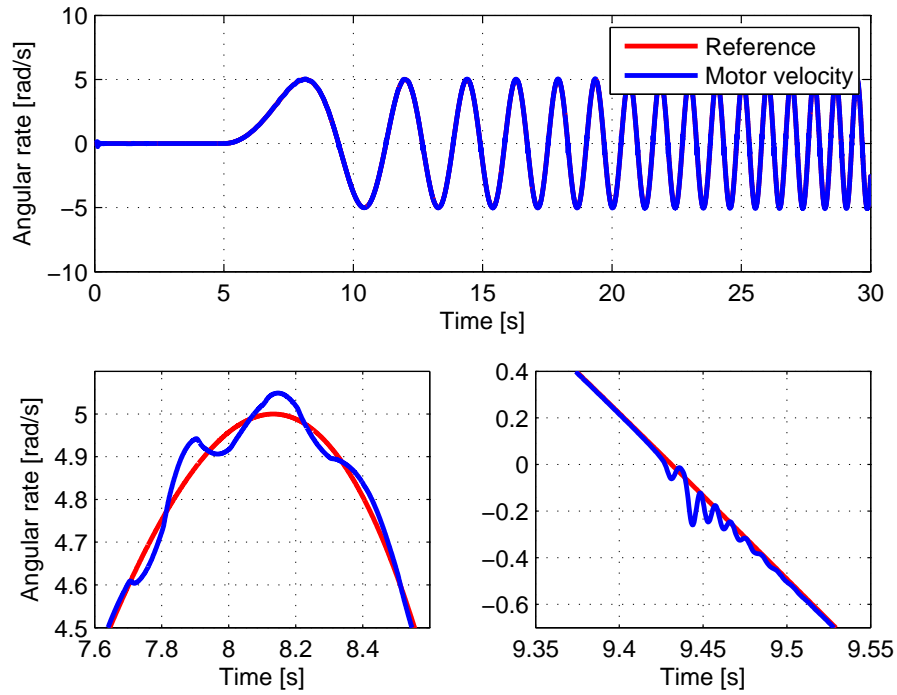


Figure 5.6: Hydraulic motor velocity and reference.

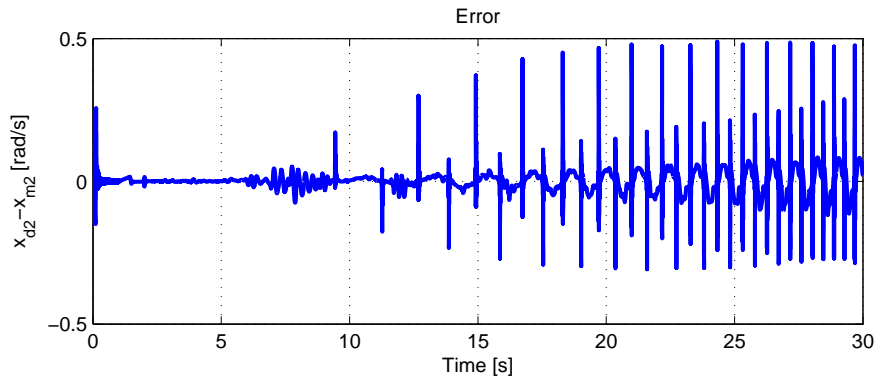


Figure 5.7: Difference between velocity reference and actual motor velocity.

### 5.3 Model Based Torque Controller

The model based torque controller is derived as a sliding mode controller and is also elaborated in Skjong and Pedersen (2014a), see Appendix B.1. To summary, the control law is given as

$$u := \frac{2V\sqrt{\rho}}{\beta\alpha D_s D_m \sqrt{p_L(u_{pre})}} \left( \frac{\beta D_m^2}{4\pi^2 V} x_{m2} + \frac{\beta G D_m}{2\pi V} \Delta p + \dot{T}_{dm} - k_1 e_T - D_2 s_1 - k_2 \text{sign}(s_1) \right) \quad (5.11)$$

where  $T_{dm}$  is the reference torque,  $k_1$ ,  $k_2$  and  $D_2$  are controller gains and  $e_T$  is the tracking error defined as

$$e_T := \frac{D_m}{2\pi} \Delta p - T_{dm} \quad (5.12)$$

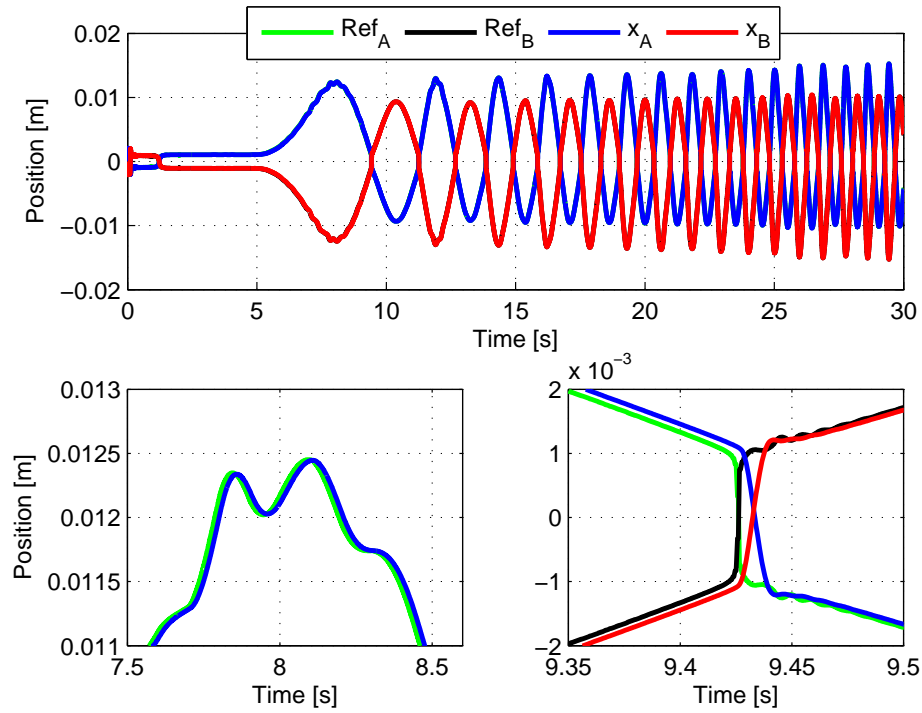


Figure 5.8: Control slide positions and speed controller output.

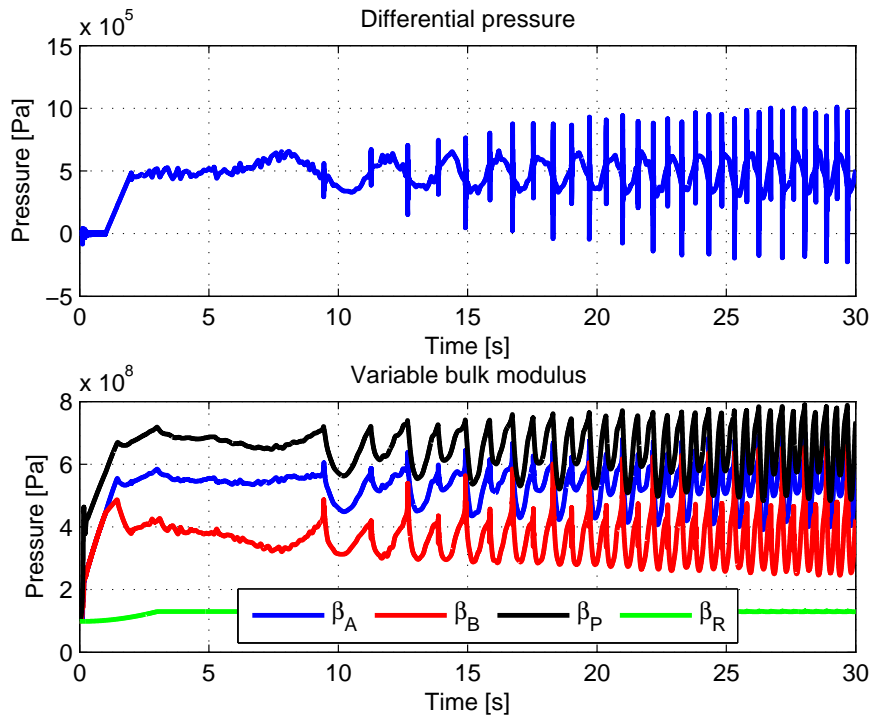


Figure 5.9: Differential pressure across the motor and variable bulk modulus in volume A, B, P and R.

and  $s_1$  is the sliding surface defined as

$$s_1 := e_T + k_1 \int_0^t e_T dt \quad (5.13)$$

$u$  is fed through the dead band compensation given in (5.3) and  $x_H$  is given as the control slide reference to the main valve on the hoisting side of the hydraulic motor and  $x_L = -x_H$  is given to the main valve on the lowering side. The controller ensures GES, Global Exponentially Stability in the controlled system, and is proven by Lyapunov analysis in Skjong and Pedersen (2014a).

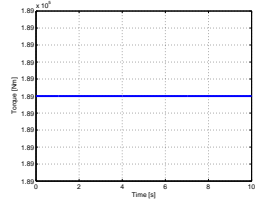
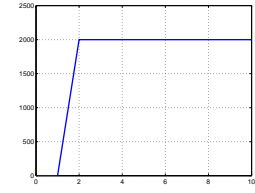
Some expectations and concerns regarding torque control should be given. The differential pressure is expected to change rapidly due to small volumes. This, not only because of the motor load, but also because of the interaction with the pressure compensator, the 3/2-directional valve and the valve flow characteristics. It is expected that in some cases the changes in differential pressure are faster than the main valve dynamics and it will be impossible to track the reference torque with high accuracy, especially when the main valves crosses the dead bands. It is also expected that the reference torque is assumed nearly constant over a short period of time. This is because torque control is often used in heave compensation operations, which is not as precise as AHC-, active heave compensation, operations using the speed controller, in winches on ships where the reference torque is equal to the motor loading. Torque control is also used for safety reasons to avoid loss of load if the load gets stuck or the torque exceeds the torque limit.

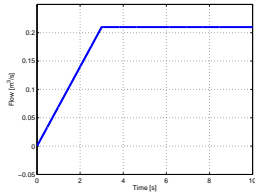
The controller parameters are set to  $k_1 = 5 \text{ 1/s}$ ,  $k_2 = 1000 \text{ Nm/s}$ ,  $D_2 = 8000 \text{ 1/s}$ ,  $\gamma_2 = 1e7$ ,  $\tau = 0.1 \text{ s}$  and the slope in the dead band compensation is set to  $s = 50000$ .  $\gamma_2$  is the gain in the derivative adaptive law and  $\tau$  is the time constant in the low pass filter used to filter the differential pressure. Note that  $s$  is set lower in this controller compared to the speed controller. This is to reduce the large pressure peaks generated when passing the dead bands in the main valves with high speed. The pressure peaks are large and the controller should not be so fast that it tries to control these peaks. If so the controller would become unstable because of all the noise in the differential pressure that have not been filtered out. It is also expected that the tuning of the outer controller is affected by the inner controller.

### 5.3.1 Controller Test using Constant load and Reference

A simple torque controller test is to be initiated. The controller gains and model parameters are as specified and the reference signals are given in table 5.3.

Table 5.3: Reference signals for test of speed controller.

Description	Value
$T_{dm}$ , Reference torque (assumed constant)	
$T_m$ , Hydraulic motor load, assumed constant	

$\dot{Q}_p$ , Pump flow (a ramp starting at $t=0$ s with a slope of $0.07 \text{ m}^3/\text{s}^2$ and stopping at $t=3$ s)	$\dot{Q}_p = 0.07\text{ramp}(0)$ $-0.07\text{ramp}(3)$ 
$r_{3/2}$ , Reference signal for 3/2-directional valve ( $r_{3/2}=2-$ means that the LOGIC-box controls the valve)	$r_{3/2} = 2-$

The values for  $T_{dm}$  and  $T_m$  are set to  $T_{dm} = 30000 \text{ Nm}$  ( $\Delta p = 14.5 \text{ bar}$ ) and  $T_m = 30000 \text{ Nm}$ . The controller is initiated at  $t=2$ s. Figure 5.10 shows the torque compared to the reference.

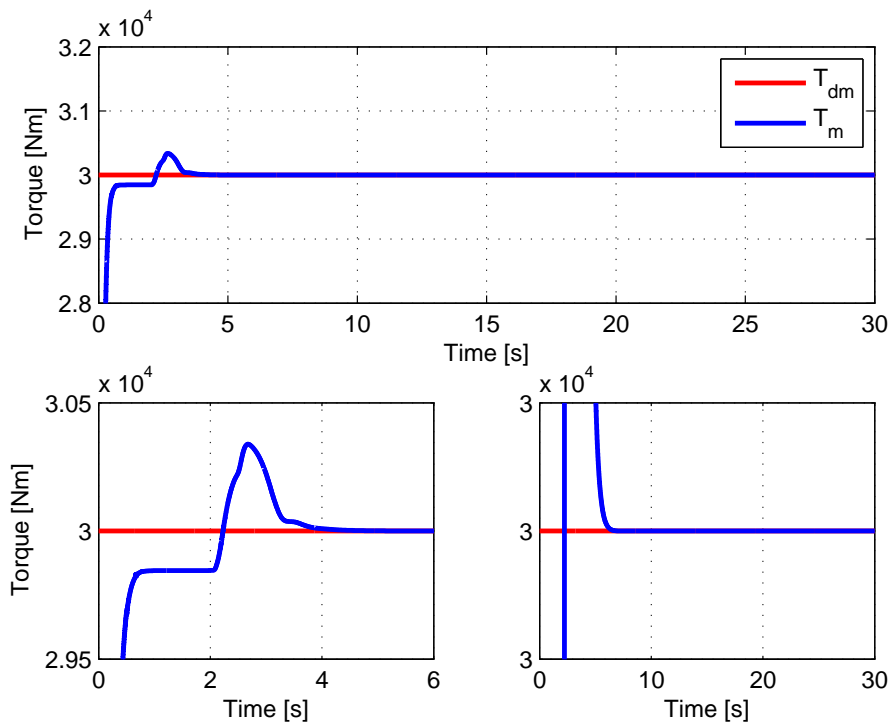


Figure 5.10: Torque and reference.

As seen in the figure the controller seems to control the torque to the desired trajectory with high accuracy. From the initiation of the controller to the desired reference it takes about 3.5s. It also seems like the torque does not converge to the reference before after  $t = 2$ s. This is because the controller is not activated before  $t = 2$ s. If the controller was tuned harder it would have been more sensitive to noise from  $\Delta p$ . Figure 5.11 shows the tracking error given in percentage of the reference torque,

$$e_{T\%} = \frac{T_{dm} - T_m}{T_{dm}} \cdot 100\% \quad (5.14)$$

The error seems to be really small after the initiation phase in the simulation and converges to zero, which it should since both the reference torque and the motor load are constant. Note that the first plot shows the error in the range  $[-100\%,100\%]$  and the second plot shows the error in

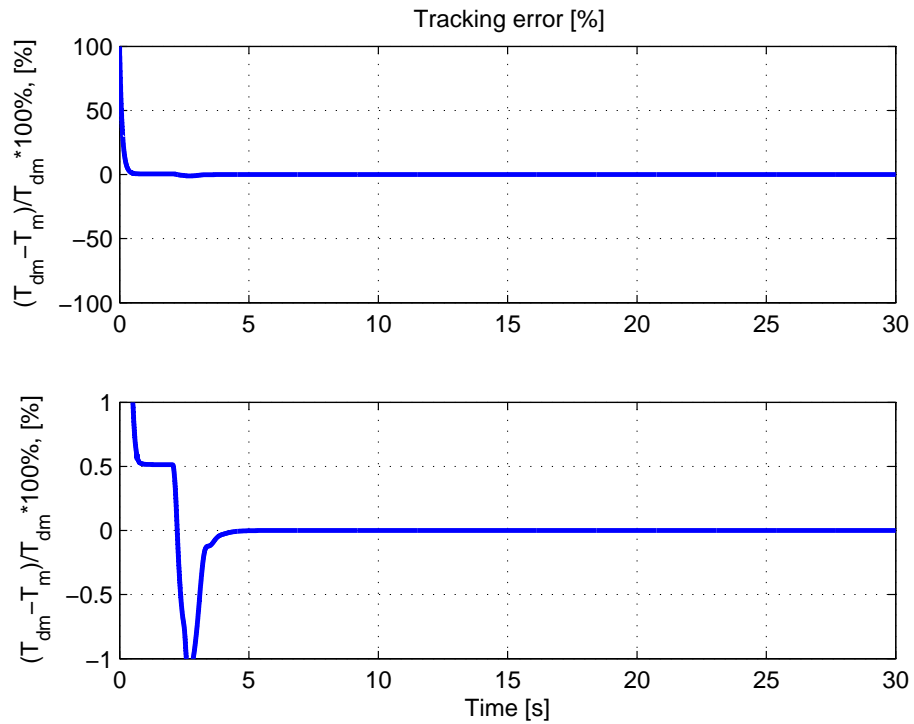


Figure 5.11: Tracking error.

the range  $[-1\%, 1\%]$ . Figure 5.12 shows the control slide positions and the references given by the torque controller.

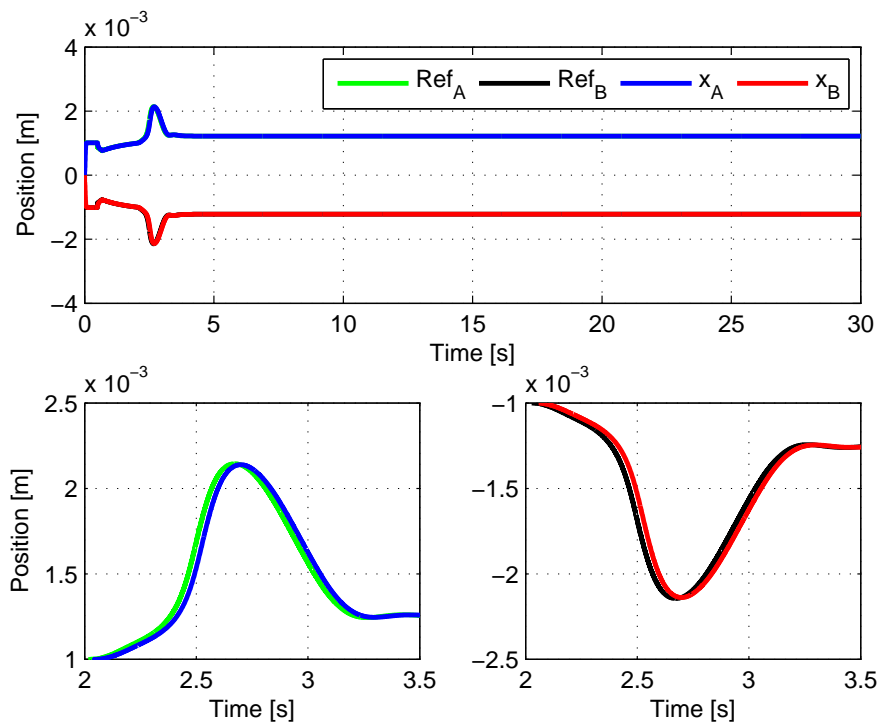


Figure 5.12: Control slide positions and references.

The control slide positions seems to coincide with the references as seen in previous simulations using the adaptive PID controller as inner controller. The derivative gain parameter,  $\gamma_2$ , was increased for the torque controller to give additional damping since small oscillations in the control slide positions would have a huge impact on the differential pressure and thus the torque. Figure 5.13 shows the hydraulic motor velocity.

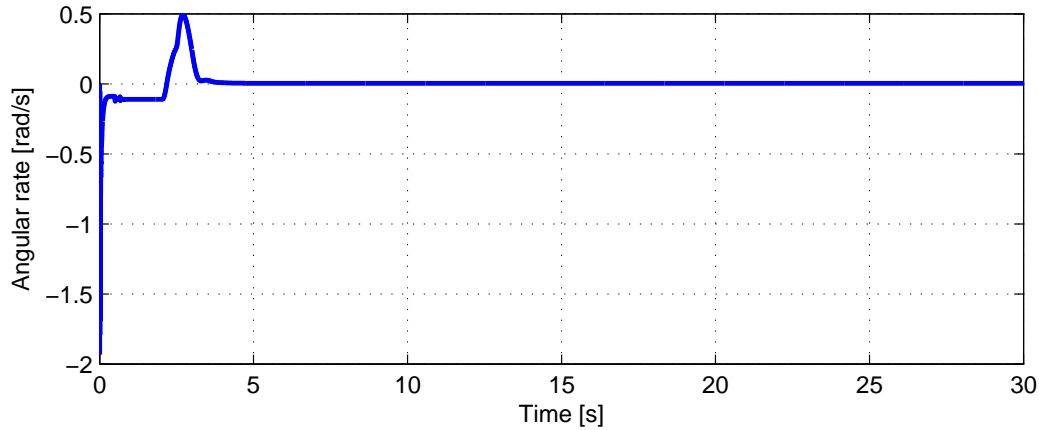


Figure 5.13: Hydraulic motor velocity.

After the initiation phase the motor velocity seems to converge to a constant value. This is because the reference torque,  $T_{dm}$ , was chosen on beforehand so that the motor speed was held as constant as possible in the simulation. The last figure, figure 5.14, shows the differential pressure across the motor and the variable bulk modulus for some interesting fluid volumes in the model.

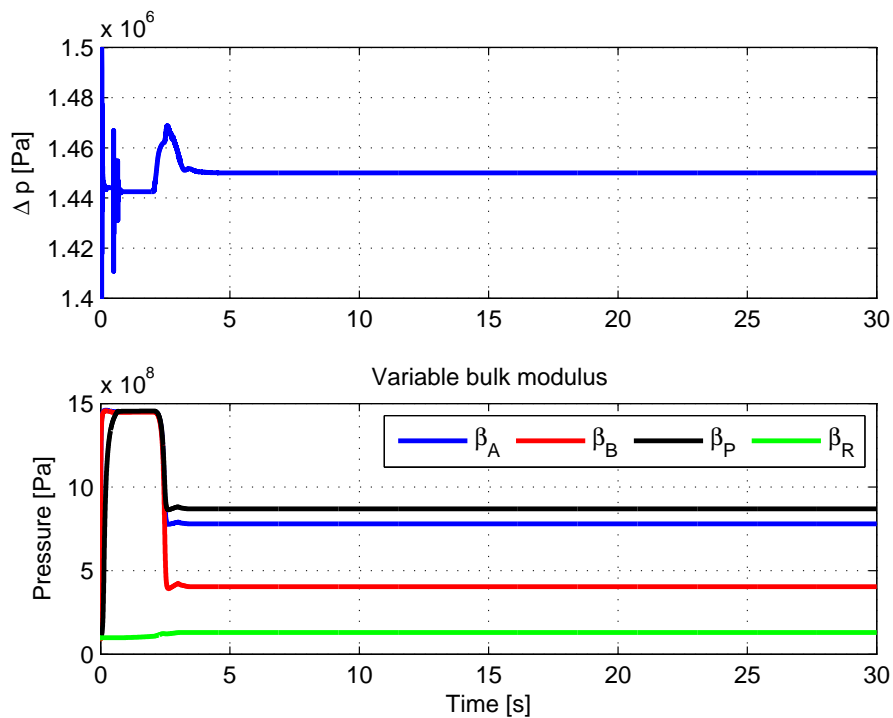


Figure 5.14: Differential pressure across the motor,  $\Delta p$ , and variable bulk modulus.

As the figure shows the differential pressure and the bulk modulus seems to be nearly constant after the initiation phase. This is because the bulk modulus is dependent on the pressure and

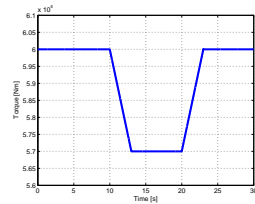
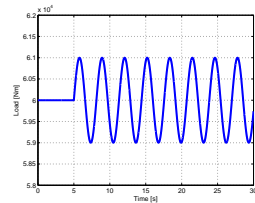
when the pressure is constant then also the bulk modulus.

This controller test was simple and the results shows that it was not very challenging for the torque controller. The next test is harder and gives an idea of the limitations in the controller.

### 5.3.2 Varying Load, Varying Reference

The controller- and model parameters are as before except for the motor load and the reference torque. Also in this case the adaptive PID-controller is used as the inner controller, controlling the main valves. Table 5.4 gives a description of these variables.

Table 5.4: Reference signals for test of speed controller.

Description	Value
$T_{dm}$ , Reference torque (starting at 60000 Nm, decreases to 57000 Nm in 3 s starting at $t = 10$ s and increasing back to 60000 Nm in 3 s starting at $t = 20$ s)	$T_{dm} = 60000 - 1000\text{ramp}(10) + 1000\text{ramp}(13) + 1000\text{ramp}(20) - 1000\text{ramp}(23)$ 
$T_m$ , Hydraulic motor load (a constant load from $t = 0$ s to $t = 5$ s with a magnitude of 60000 Nm and an added $\sin()$ signal at $t = 5$ s, with an amplitude of 1000 Nm and a frequency of $2 \text{ rad/s}$ , $\frac{2}{\pi} \text{ Hz}$ )	$T_m = 60000 + 1000\text{step}(5) \sin(2(t - 5))$ 

The controller is activated at  $t = 1.5$  s. Figure 5.15 shows the torque compared to the reference. As seen in the figure the torque does not coincide with the reference as good as in the previous simulation. This is as expected since this simulation has varying load and varying reference, making it harder for the outer controller. One can also see the small peaks in the first plot generated by crossings of the dead bands in the main valves. These peaks are the main reason for the tracking error and the controller integrates these peaks giving small deflections in the torque compared to the reference. The plot in the lower left corner shows the initiation phase of the controller. It is initiated at  $t = 5$  s and it takes about 1 s to reach the desired torque. The plot in the lower right corner shows the change in reference. As seen the controller follows the changes in the reference but tracking errors are still present. The controller could of course be tuned harder, which should decrease the tracking error, but the inner controller is not fast enough and would begin to oscillate. The inner controller is also in this case the adaptive PID-controller which was designed for manual control of the control slides. By using an ordinary PD-controller as inner controller the outer controller could perhaps be tuned faster. The next figure, figure 5.16, shows the tracking error as defined in (5.14). Note that the first plot shows the error in the range  $[-100\%, 100\%]$  and the second plot  $[-1\%, 1\%]$ .



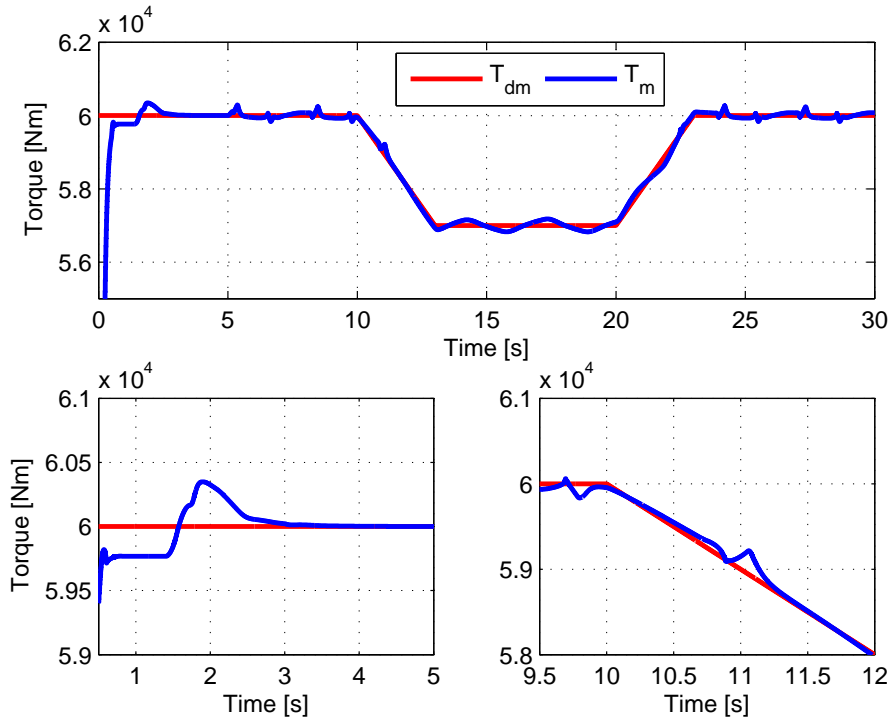


Figure 5.15: Torque and reference.

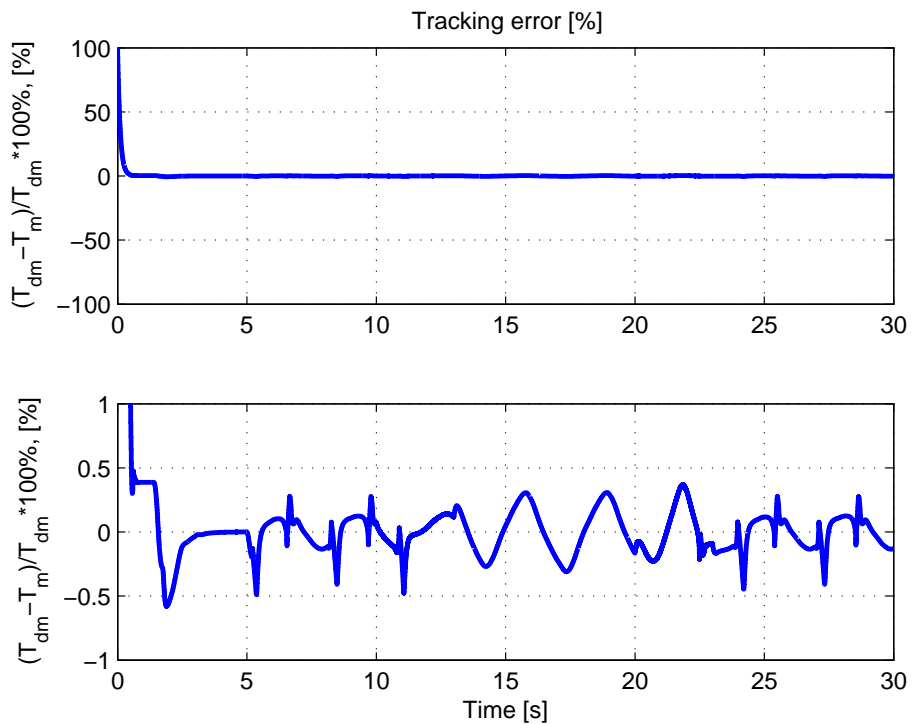


Figure 5.16: Tracking error.

The first plot does not give much information of the tracking error because of the high scale, which indicates low errors, but the second plot reveals more information. As can be seen the absolute value of the error after initiation of the controller does not exceed 0.5%. The largest errors appear as peaks in the plot and is due to the crossings of the dead bands in the main

valves and can not be reduced much. However the oscillations in-between could be decreased by changing the inner controller and tuning the outer controller harder. The maximal absolute error is calculated to be  $\frac{e_T \% T_{dm}}{100\%} = \frac{0.5\% 60000 \text{ Nm}}{100\%} = 300 \text{ Nm}$ . Note that this error is due to a pressure peak from a crossing of the dead bands. Figure 5.17 shows the control slide positions together with the references given by the torque controller.

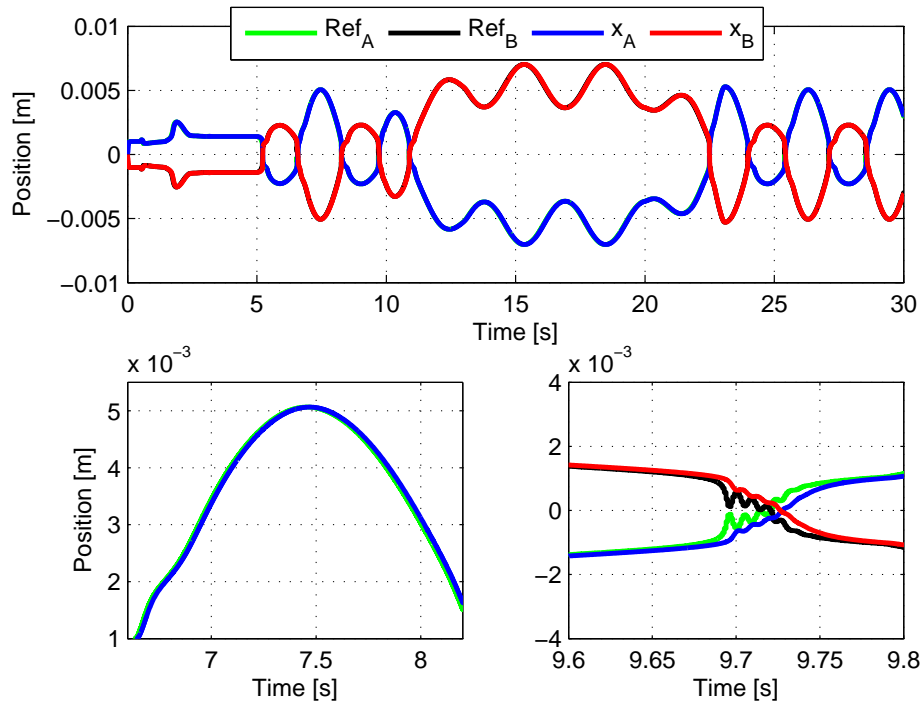


Figure 5.17: Control slide positions and references.

The first plot shows that the control slide positions coincides with the references given by the torque controller as in previous simulations. The plot in the lower left corner shows one of the maximal displacements of the control slide position in main valve A. It is not easy to see but the sampling delay can be seen by noticing that  $\text{Ref}_A$  is a bit faster than  $x_A$ . The plot in the lower right corner shows one of the many crossings of the dead bands in the main valves. Small oscillations can be seen in the dead band crossing and emphasizes for the increase in  $\gamma_2$  in the adaptive control law. Figure 5.18 shows the hydraulic motor velocity.

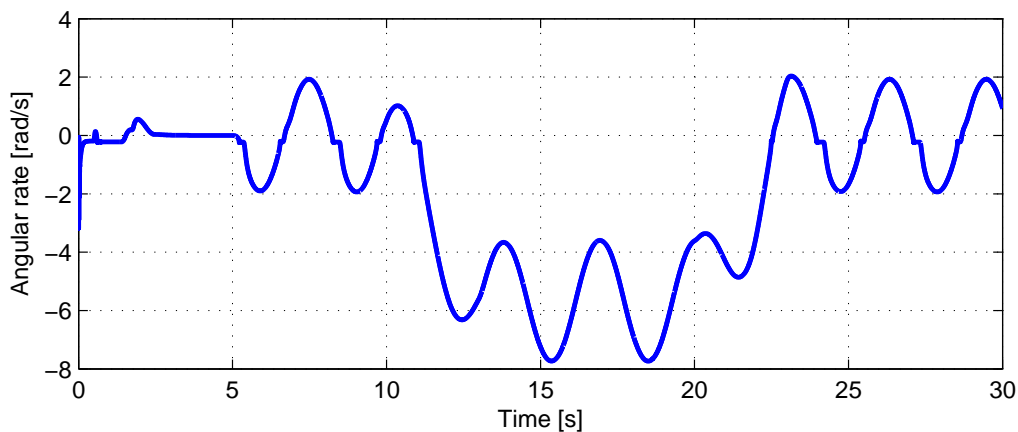


Figure 5.18: Hydraulic motor velocity.

As expected both the changes in motor load and reference torque are reflected in the motor velocity. The "sine-noise" is present and one can see the characteristics of the reference torque, which decreases at  $t = 10$ s and increases again at  $t = 20$ s. Also the small disturbances from when the control slides cross the dead bands can be seen just around zero motor velocity. The last figure, figure 5.19 shows the differential pressure across the motor,  $\Delta p$ , and the variable bulk modulus for some interesting fluid volumes in the system.

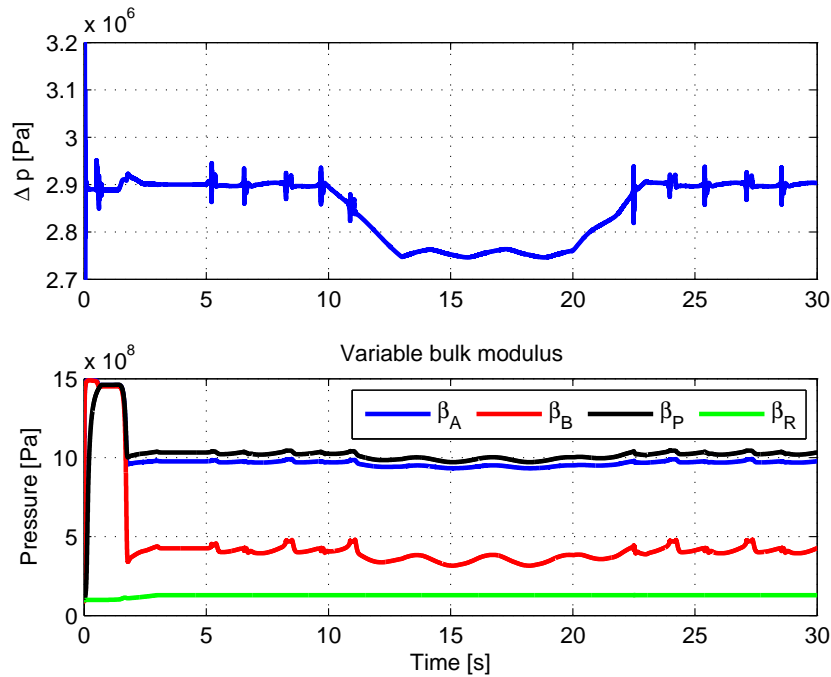


Figure 5.19: Differential pressure across the motor,  $\Delta p$ , and variable bulk modulus.

The figure shows that the peaks in the differential pressure are significant (about 1 bar in average), which is expected since the load is high and due to the crossings of the dead bands as mentioned. The differential pressure shown in the first plot has not been filtered and by multiplying by  $\frac{D_m}{2\pi}$  one can find the unfiltered torque. This indicates that the filtering significantly reduces the large peaks since the peaks in figure 5.15 should have been about 2070 Nm, not 300 Nm as calculated. The second plot shows the variable bulk modulus in volume A, B, P and R, as before. As seen the bulk modulus varies with the pressures in the volumes as expected since the bulk modulus is a function of pressure, see (2.7).

## 5.4 Chapter Summary and Conclusion

In this chapter two controllers have been studied, a speed controller and a torque controller. These controllers are model based and mainly based on sliding mode control theory. The speed controller is also backstepping based since there are two differential equations in the control design enabling feedback of unwanted physical effects. The adaptive PID-controller derived in section 4.1.2 was used as inner controller, controlling the main valves, in all simulations. However this is a slow controller and for future purposes a faster inner controller should be considered. This can also be argued for based on the small oscillations shown in the control slide positions in figure 5.17 and the fact that the controller gains are self deleting due to  $\sigma$  in the adaptive control laws which makes the controller slower, see (4.3).

The results from the test cases that were run to test the two controllers were good even though

the differential equations used in the controller designs were significantly simplified. Also the tuning of these controllers have been done once and it seems like the controllers perform just as well for other test cases with the same tuning. This is one of the strengths by using a model based controller instead of an ordinary PID-controller for a non-linear system. Also if a PID-controller was to be used it may have been necessary to tune the controller between the test cases. As for the inner controller it looks like a PID-controller would work fine.

The speed controller gives the best results compared to the torque controller. This is not surprising since the hydraulic motor has inertia and friction that gives damping to the system. The differential pressure has no damping of importance and varies quite a lot, which sets restrictions to controller tuning in order to assure stability and robustness all over for every load cases using the same controller parameters. Also restrictions to the reference torque should be implemented. A reference that is not physical possible, such as too low or too high values, should be avoided by the use of logics.

It is also of importance to mention that every measurement used, except the differential pressure, have not been filtered. In reality these measurements would be affected by noise and filtering would be necessary. To filter the differential pressure a low pass filter has been used but other filters should be considered such as Kalman based filters. One of the benefits by using such filters is that they do predictions which would be of interest since the sensors have sampling delays.

The next step would be to test the controllers more thoroughly using a more relevant load model. This load model is derived in Skjong and Pedersen (2014c), which is given in Appendix B.3.

# 6 | Controller Testing with Wire Model

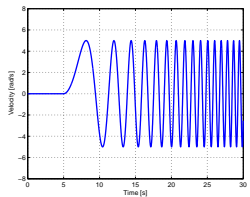
In chapter 5 model based controllers were derived to control the hydraulic motor. The controllers were tested in simulations having predefined load characteristics. In this chapter a lumped load model including hydrodynamics, current, wire dynamics and reel dynamics is added to the hydraulic winch system for a more realistic controller testing. The wire is divided into five equal lengths of submerged wire and each element are assumed to be a mass-spring-damper system. The elements are connected through power bonds and the inertia and diameter of the reel changes with the length of the submerged wire. This load model is elaborated in Skjong and Pedersen (2014c), given in Appendix B.3.

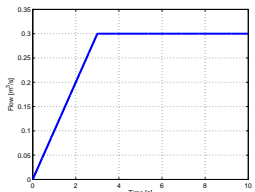
To test the outer speed- and torque controller with the lumped load model an ordinary PD-controller is used as inner controller as suggested in section 5.4. The gains in the controller are set to  $K_p = 6000 \text{ V/m}$  and  $K_d = 20 \text{ Vs/m}$ , proportional- and derivative gain respectively. Different load cases are tested with the two controllers. It is expected that the two controllers work quite well also in these simulation cases. The model parameters used in the tests are as before if not specified. The parameters in the load model are given in B.3, except for the initial length of submerged wire and the load, which are specified in the simulations.

## 6.1 Speed Controller

To test the speed controller two different load cases are to be studied. As previously mentioned the tuning of the controllers are dependent on the inner controllers and since the inner controllers have been changed to faster ones, the outer controllers can be tuned harder. Only one controller parameter is changed,  $D_2 = 800 \text{ 1/s}$ , the rest are as given in section 5.2. These two tests do not include MRU-, Motion Reference Unit, measurements measuring heave motion of the top wire position, but rather just a fast sweep of motor velocity in order to induce variations in the wire tension causing changes in the wire dynamics such as damping and spring stiffness. Later on cases including MRU measurements in AHC operations are to be initiated. In such cases the top wire position is assumed to have a heave motion. The reference signals and load parameters for these two speed controller tests are given in figure 6.1.

Table 6.1: Reference signals for testing of speed controller

Description	Value
$x_{2d}$ , Reference signal for hydraulic motor velocity (a sine()-sweep starting at $t=5\text{s}$ with a magnitude of $5 \text{ rad/s}$ with a frequency of $\omega = 0 \text{ rad/s}$ and ending at $t=30\text{s}$ with a frequency of $\omega = 8 \text{ rad/s}$ , $f = \frac{4}{\pi} \text{ Hz}$ )	

<p style="text-align: center;"><math>\dot{Q}_p</math>, Pump flow (a ramp starting at <math>t=0</math> s with a slope of <math>0.1 \text{ m}^3/\text{s}^2</math> and stopping at <math>t=3</math> s)</p>	<p style="text-align: center;"><math>\dot{Q}_p = 0.1\text{ramp}(0)</math> <math>-0.1\text{ramp}(3)</math></p> 
<p><math>m_{Load}</math>, Weight of mass that is lifted. <math>m_{Load}</math> does not include the mass of the wire.</p>	<p>Specified in simulations</p>
<p><math>r_{3/2}</math>, Reference signal for 3/2-directional valve (<math>r_{3/2} = 2</math> - means that the LOGIC-box controls the valve)</p>	<p><math>r_{3/2} = 2</math> -</p>

In addition to the signals and parameters described in the table low pass filtering of the differential pressure and the motor load measurements are done in the speed controller. This is not just to reduce the peaks in the measurements but also to ensure more stability since the error tolerances in the simulation is set high in order to get a short solving time. The filtering parameters are set equal,  $k = 1$  - and  $\tau = 0.01$  s. It is expected that the speed controller would perform well also with the wire model included. However the tracking error is assumed to be a bit larger since the load the hydraulic motor experiences is varying due to inertial forces and hydrodynamic forces acting on the wire and the load, together with the wire dynamics. The error is also expected to increase with the frequency in the reference signal and load.

### 6.1.1 Load Case 1

The load connected in the end of the wire is set to  $m_{load} = 3000$  kg, the horizontal current  $V_{c,x} = 0$  m/s and the initial length of submerged wire to 100 m. Figure 6.1 shows the motor velocity compared to the reference.

As the figure shows it seems like the motor velocity coincides with the reference. The figure in the lower left corner shows one of the many maximal velocity peaks and it shows that the controller tracks the reference quite well. The crossing of the dead bands in the main valves are shown in the plot in the lower right corner. The deflections from the reference in the crossings are as expected and the tracking error is small when having in mind what actually happens with the pressures in the crossings. By comparing these results with figure 5.1 the results look quite promising for the controller. The oscillations caused by the dead band crossings in figure 5.1 seem to have a higher frequency compared to the results in figure 6.1. This tells that the new load model seems to acts in the favour of the hydraulic motor when dead bands are crossed using the speed controller, causing a higher oscillation period which is easier to control and it seems like more damping is present. Figure 6.2 shows the tracking error.

The figure shows that the error grows with the frequency of the reference signal which is expected due to all inertias and time constants in the model. Also the sampling delay plays a role when the frequency increases. Compared to figure 5.2 the results looks quite good. The largest errors are mostly due to the pressure peaks from the crossings of the dead bands. By taking the highest error, that is not due to a crossing, the error is approximately  $0.2 \text{ rad/s}$ , 1.91 rpm. This gives a maximal error of about 4% relative to the reference signal. Figure 6.3 shows the control slide positions compared to the references given by the outer speed controller.

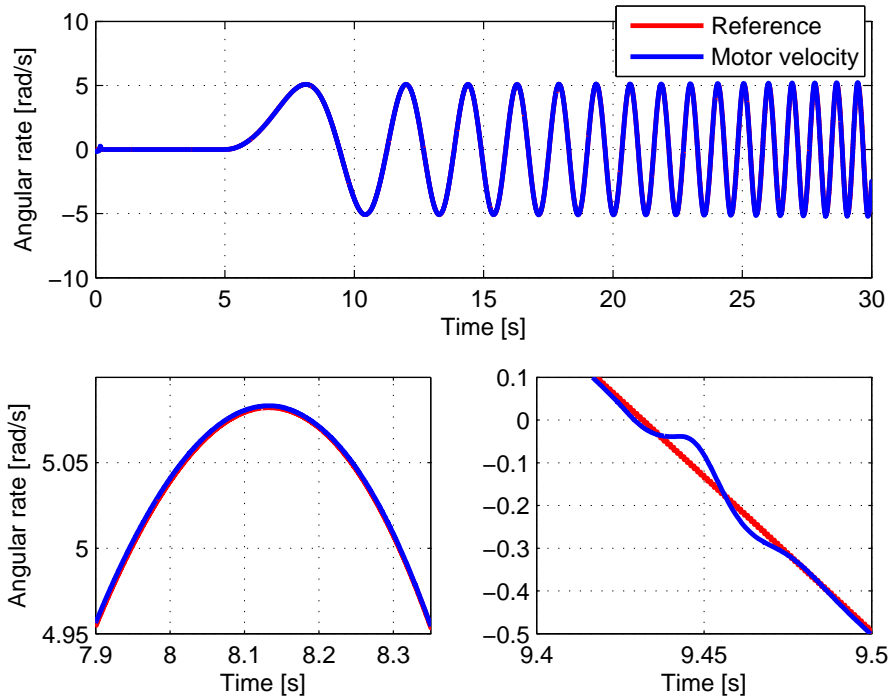


Figure 6.1: Hydraulic motor velocity and reference.

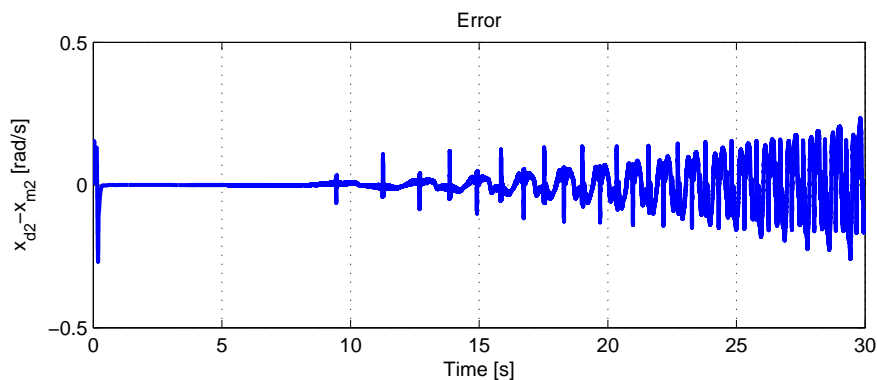


Figure 6.2: Difference between velocity reference and actual motor velocity.

The first plot shows that the control slide positions seems to coincide with the references. This is emphasized in the two plots below in the figure. The plot in the lower left corner shows one of the highest displacements of the control slide in valve A. The plot in the lower right corner shows a magnified area of a crossing of the dead bands. As expected the control slide positions are more difficult to control when passing the dead bands, but as soon as the control slides have passed, the tracking error converges to zero when neglecting the sample delay. Compared to figure 5.3 the control slide positions seems to converge faster to the reference when using the PD-controller. This is expected since the reason for changing the adaptive PID-controller was because it seemed to be a bit slow. Figure 6.4 shows the differential pressure across the motor,  $\Delta p$ , and the variable bulk modulus in volume A, B, P and R.

The first plot shows the differential pressure and it varies quite a lot and increases with the frequency of the motor velocity, as expected. The maximal differential pressure is about 100 bar at the end of the simulation. Since this is a low pressure system the differential pressure is closing in on the maximal design pressure which is assumed to be close to 100 bar. This also

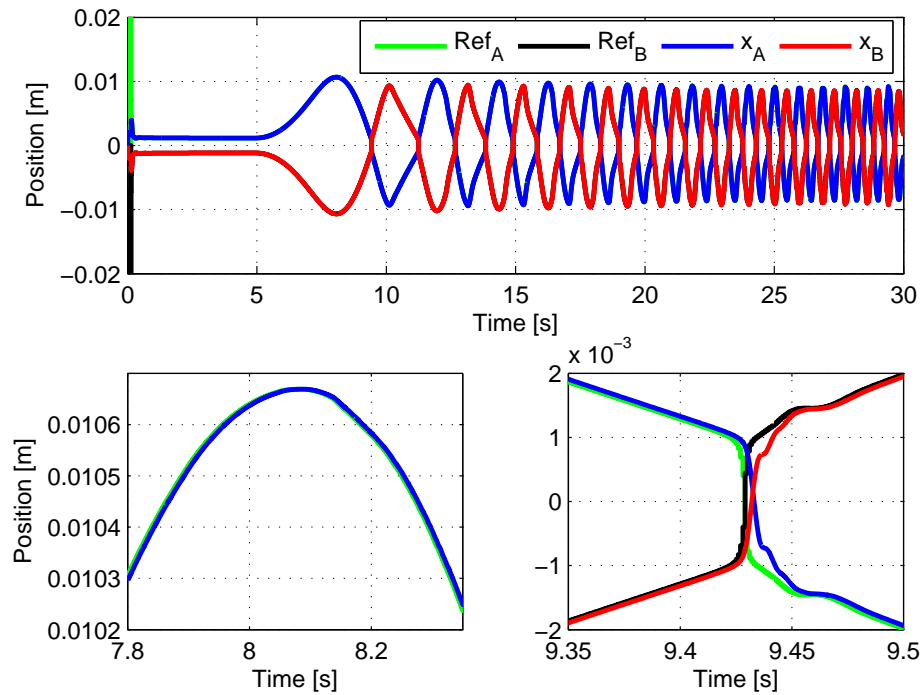


Figure 6.3: Control slide positions and speed controller output.

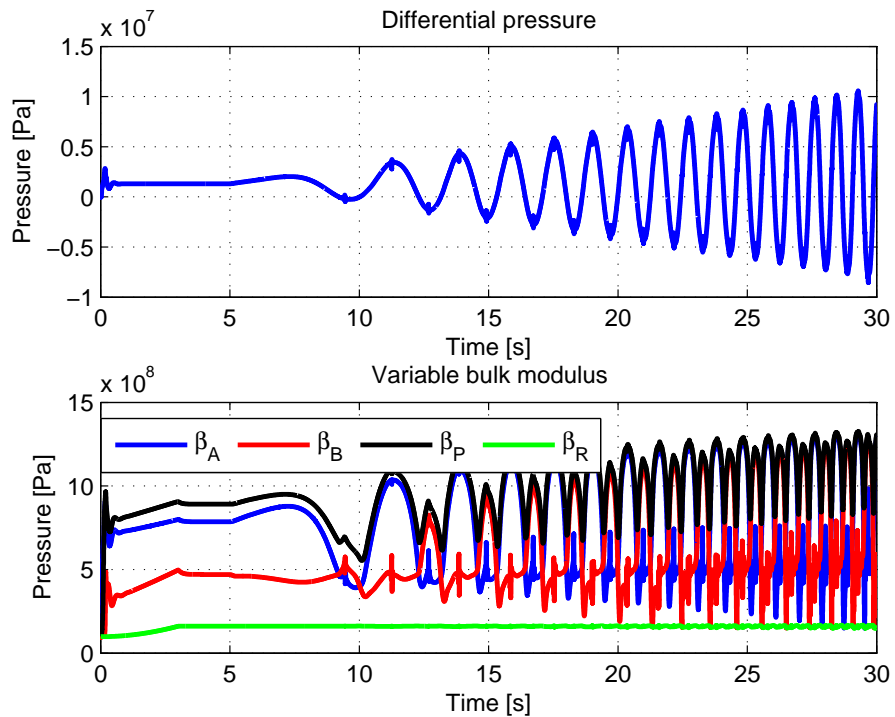


Figure 6.4: Differential pressure across the motor and variable bulk modulus in volume A, B, P and R.

means that when using a heavier load with the same motor velocity reference signal the tracking error of the motor velocity is expected to increase dramatically. The second plot shows the variable bulk modulus in volume A, B, P and R which vary with the same frequencies as the



differential pressure.

### 6.1.2 Load Case 2

The load is now set to  $m_{Load} = 6000$  kg, two times as large as in the previous load case. This will result in a much higher differential pressure which would exceed the maximal design pressure. However this test is only performed to test the speed controller. As a result of the high pressures the tracking error is expected to become larger compared to the previous load case, especially when crossing the dead bands in the main valves. The other model parameters are as in the previous simulations. Figure 6.5 shows the hydraulic motor velocity compared to the reference.

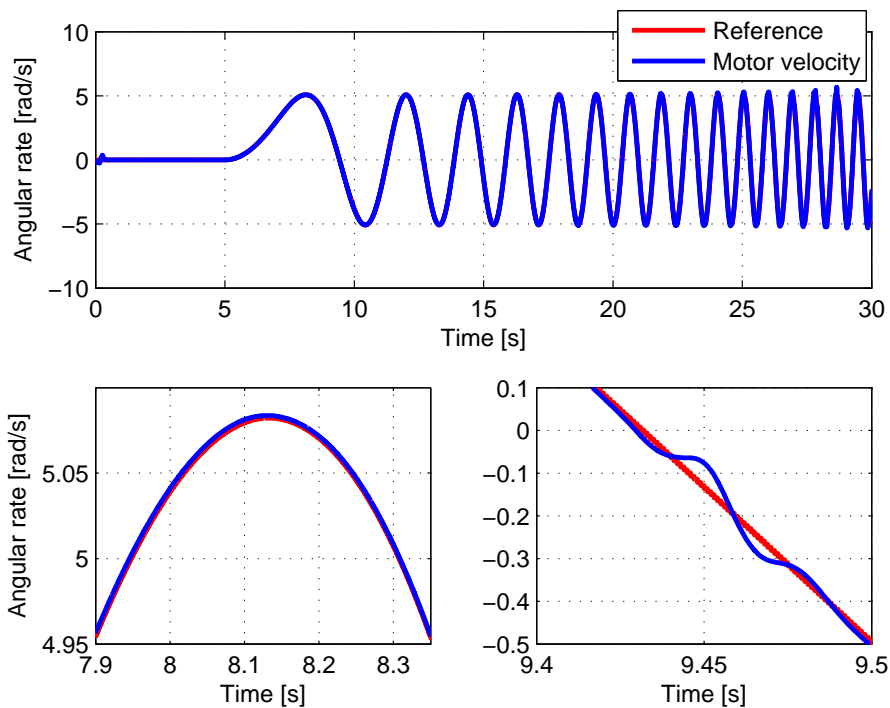


Figure 6.5: Hydraulic motor velocity and reference.

As seen in the figure the motor velocity seems to converge to the reference velocity. When the frequency gets high it is harder to track the desired motor velocity. This is expected since both the differential pressure and the frequency of the reference velocity are high. However the results are still quite good and the speed controller seems to be robust. The plot in the lower left corner shows that the motor velocity coincides with the reference when the frequency of the reference is low. The plot in the lower right corner shows that the crossings of the dead bands affect the motor velocity the same way as before. The next figure, figure 6.6 shows the tracking error.

As expected the tracking error is larger in this load case compared to the first one. However the peaks are the main contributors to the largest errors and when neglecting these the error at the end of the simulation seems to be about  $0.36$  rad/s,  $3.44$  rpm, which is about  $7.2\%$  of the reference velocity at that point. This is also a good result when having in mind that the differential pressure and the frequency in the reference are way too high for the system to handle perfectly. The differential pressure is shown in figure 6.8. Figure 6.7 shows the control slide positions compared to the references given by the outer speed controller.

As before the inner controller works quite good forcing the tracking error to converge to zero. Note that the oscillations in the start of the simulation is due to the initiation phase of the

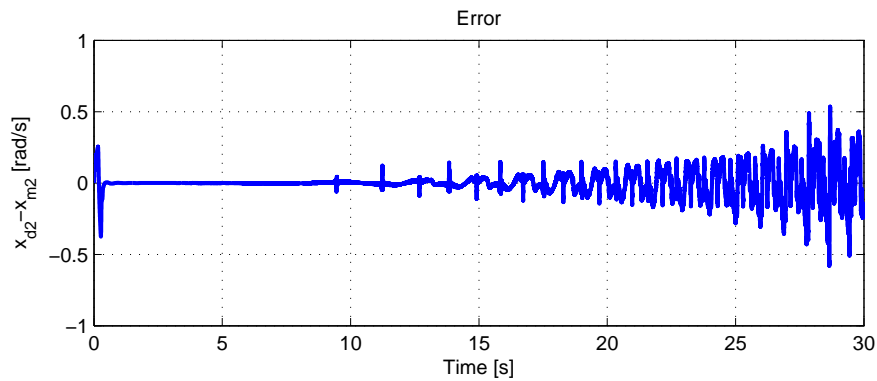


Figure 6.6: Difference between velocity reference and actual motor velocity.

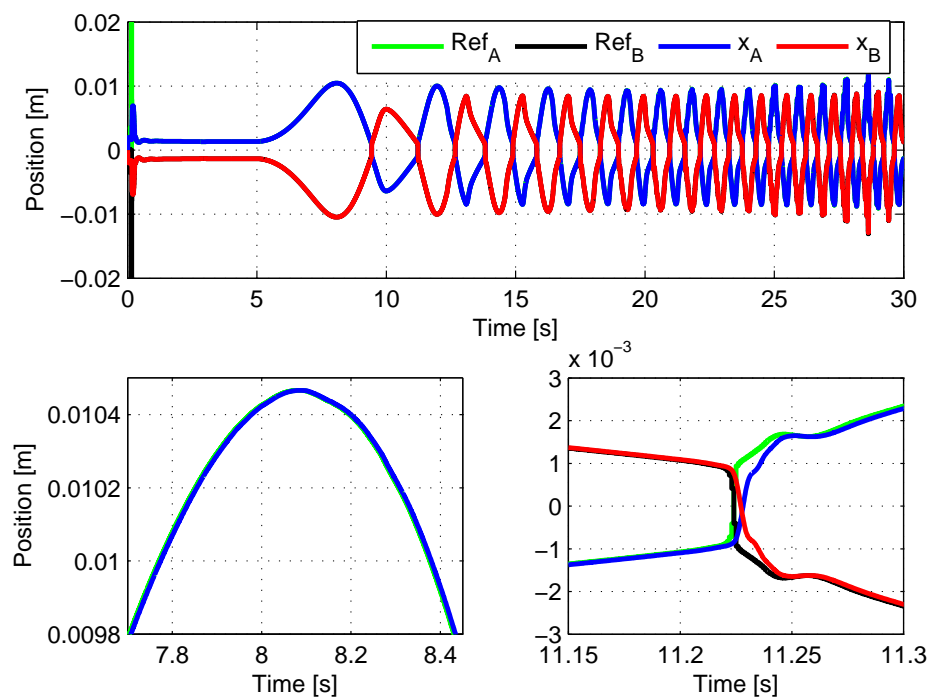


Figure 6.7: Control slide positions and speed controller output.

controller which is initiated at  $t = 0.1$  s. This initiation phase seems to be larger than in the previous load case, which is reasonable since the load is two times as heavy in this case. The plot in the lower left corner emphasize the convergence of the tracking error where only the sampling delay seems to be the difference. The plot in the lower right corner shows one of the crossings of the dead bands and is almost identical to the dead band crossing in the previous simulation, see figure 6.3. Figure 6.8 shows the differential pressure across the motor,  $\Delta p$ , and the variable bulk modulus.

As seen in the figure the differential pressure exceeds 200 bar which is about two times as large as what the hydraulic system is designed for, since it is characterized as a low pressure system. This also means that the load of  $m_{Load} = 6000$  kg is too high with such high frequencies in the motor velocity reference and should be reduced when such high frequencies in the motor velocity reference are to be tested. However waves generating heave motions in ships have a much lower frequency than what is tested here. The second plot shows the variable bulk modulus, having in general higher mean values compared to the results in the previous load case.

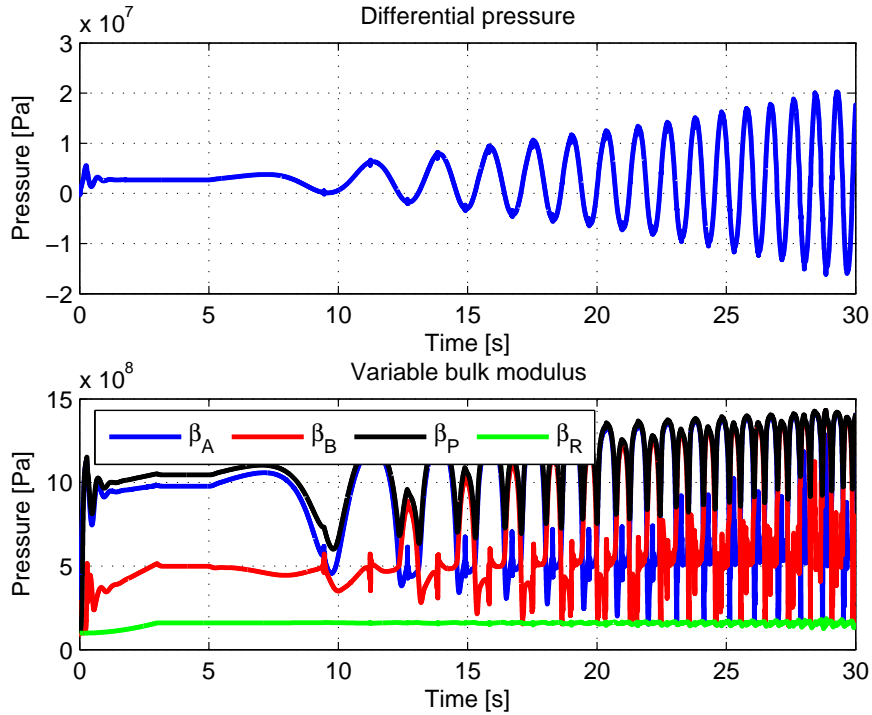


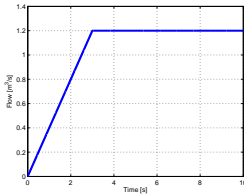
Figure 6.8: Differential pressure across the motor and variable bulk modulus in volume A, B, P and R.

## 6.2 Torque Controller

Also two controller tests are to be initiated for testing the torque controller. Since the inner controller is changed to a PD-controller instead of the adaptive PID-controller the torque controller may be tuned harder to perform better. The new gains are given as  $k_1 = 5 \text{ 1/s}$ ,  $k_2 = 1000 \text{ Nm/s}$  and  $D_2 = 9000 \text{ 1/s}$ . In addition the time constant in the low pass filter is changed to  $\tau = 0.2 \text{ s}$ . In these two tests a heave motion in the top of the wire is set, generating tension in the wire. This heave motion is intended to represent waves acting on a ship making it move up and down, and this movement is set as a  $\sin(\cdot)$ -sweep. The derivative of this movement is fed to the port `boatxy` in the wire model and the torque controller is supposed to feel the changes in the wire tension and try keeping the motor torque converge to its reference. The reference signals are given in table 6.2.

Table 6.2: Reference signals for test of torque controller

Description	Value
$\dot{y}_{heave}$ , Motion of wire at the surface in vertical direction (given as the derivative of a $\sin(\cdot)$ -sweep starting at $t=5 \text{ s}$ with a magnitude of $2 \text{ m}$ with a frequency of $\omega = 0 \text{ rad/s}$ and ending at $t=30 \text{ s}$ with a frequency of $\omega = 8 \text{ rad/s}$ , $f = \frac{4}{\pi} \text{ Hz}$ )	

$\dot{Q}_p$ , Pump flow (a ramp starting at $t=0$ s with a slope of $0.4 \text{ m}^3/\text{s}^2$ and stopping at $t=3$ s)	$\dot{Q}_p = 0.4\text{ramp}(0)$ $-0.4\text{ramp}(3)$ 
$T_{dm}$ , Reference Torque	Specified in simulations
$m_{Load}$ , Weight of mass that is lifted. $m_{Load}$ does not include the mass of the wire	Specified in simulations
$r_{3/2}$ , Reference signal for 3/2-directional valve( $r_{3/2} = 2$ - means that the LOGIC-box controls the valve)	$r_{3/2} = 2$ -

Note that the pump flow is set higher in these tests compared to the speed controller tests. This is because much higher motor velocities are expected which would require a larger flow of hydraulic liquid. The reference torques are chosen so that the motor velocity is as close to zero as possible in the start of the simulations. This will prevent any hoisting or lowering of the load and it is easier to see the influence the torque controller has on the load position. However it is hard to set the reference torque to a value that only holds the load. The horizontal current velocity is also in these tests set to zero.

### 6.2.1 Load Case 1

In this test case  $m_{Load} = 3000$  kg,  $T_{dm} = 26910$  Nm and the initial length of submerged wire is set to 100 m. Note that  $m_{Load}$  does not include the 100 m of wire holding the load. It is expected that the tracking error will grow larger than in the previous simulations because the hydraulic motor velocity becomes large due to the high frequencies in the heave motion of the ship. These frequencies are not realistic in real life scenarios but are used only to test the controller under rough conditions. Figure 6.9 shows the motor torque compared to the reference torque.

As can be seen in the first plot both the peaks, coming from crossings of the dead bands in the main valves, and the torque oscillations at the end of the simulation are larger than before. This is expected since the motor velocity is high in this region. The plot in the lower left corner shows that the controller stabilizes fast in the beginning of the simulation and has a small peak at  $t = 5$  s due to the initiation of the heave motion. The plot in the lower right corner shows the torque oscillation with the maximal amplitude in the end of the simulation. To get a clearer understanding of the difference between the reference torque and the actual motor torque the tracking error is shown as a percentage of the reference torque in figure 6.10.

The figure shows that the tracking error is larger in this simulation compared to the previous simulation, see section 5.3. However when neglecting the error peaks generated by the dead band crossings the maximal error is still below 5%, and that is for a simulation containing heave motion with unrealistic high frequencies. The outer controller is still stable under these conditions which indicates that the torque controller works fine for its purpose.

Figure E.6 in Appendix E.2 shows the results of the inner controller, comparing the reference

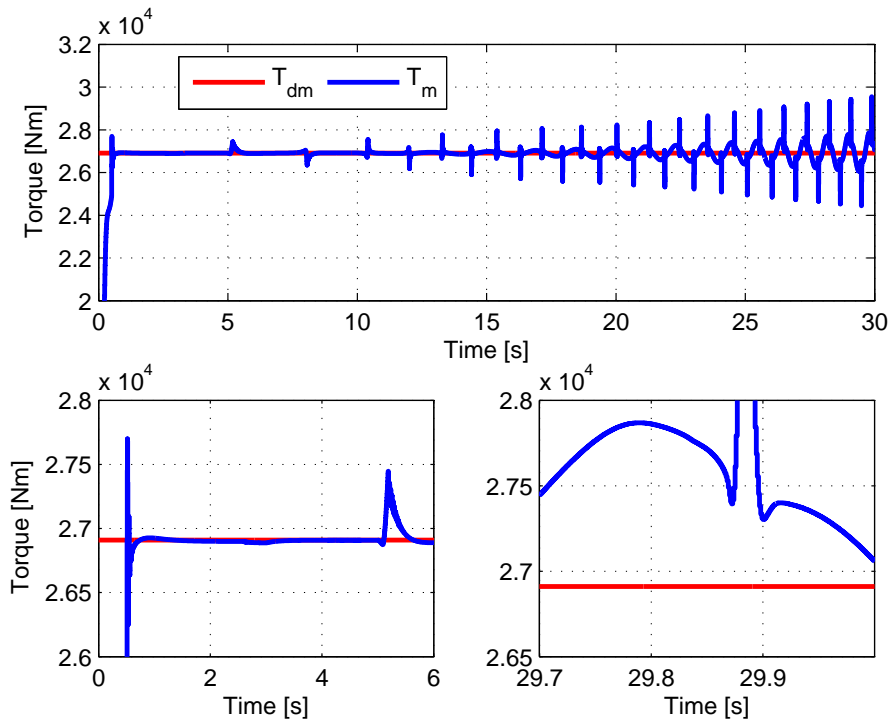


Figure 6.9: Torque and reference.

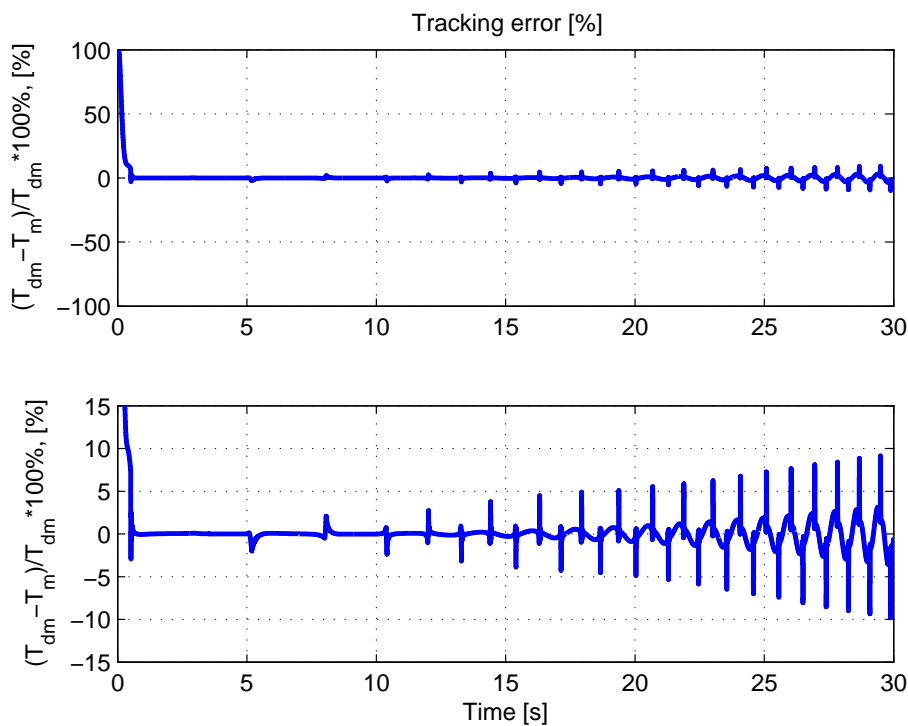


Figure 6.10: Tracking error.

positions given by the outer controller with the actual control slide positions. The results shown in the figure are almost equal to previous results, the inner controller manages to control the control slide positions according to the references. Only small oscillations are present when crossing the dead bands in the main valves. The next figure, figure 6.11 shows the hydraulic

motor velocity.

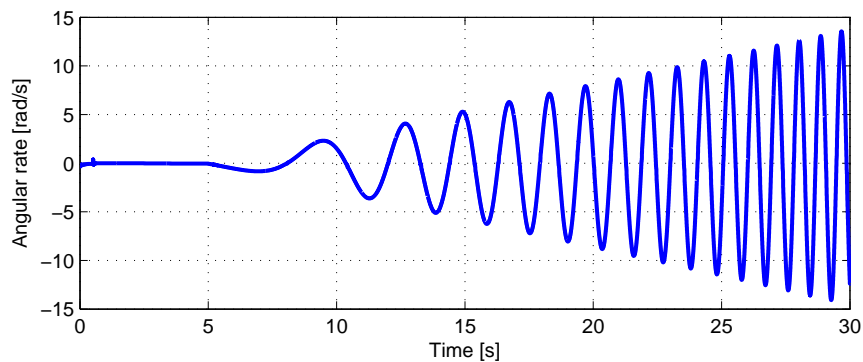


Figure 6.11: Hydraulic motor velocity.

The motor velocity is quite high, about  $15 \text{ rad/s}$ ,  $143.3 \text{ rpm}$ , at the end of the simulation which is higher than what is expected of the hydraulic motor. It can also be seen that the motor velocity has the same form as the derivative of the heave motion that was added to the top of the wire. If the torque controller had zero tracking error then the motor velocity would be proportional to the heave velocity with the inverse of the radius of the reel as parameter. This is however not completely the case. Since there are tracking errors present in the simulation there will be some load motions as well. Figure 6.12 compares the top wire position and the bottom wire position in vertical direction.

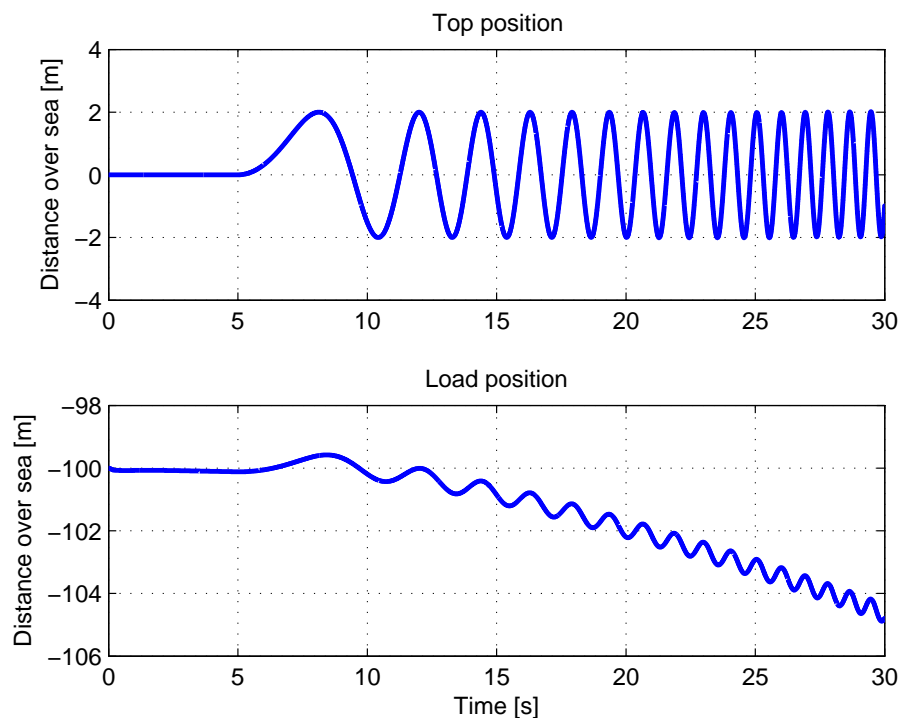


Figure 6.12: Top and bottom vertical wire position.

The first plot shows the heave position in the top position of the wire. As can be seen it is a perfect sine()-sweep as it was supposed to be. The second plot shows the bottom vertical position of the wire, the vertical load position. If the torque controller had no tracking error there would be no oscillations present. However these oscillations are small, about  $0.25 \text{ m}$  in amplitude at most. It can also be seen that the load is lowered. This is due to  $T_{dm}$  which was

set a bit to low to hold the load.

Figure E.7 in Appendix E.2 shows the differential pressure across the motor and the variable bulk modulus. The peaks shown in the measured torque are also present in the differential pressure as expected and both the differential pressure and the bulk modulus oscillate with the frequency of the heave motion.

### 6.2.2 Load Case 2

In this test case  $m_{Load} = 9000$  kg and the reference torque is set to

$$T_{md} = 84600 + 5000\text{ramp}(t = 8) - 5000\text{ramp}(t = 10) - 5000\text{ramp}(t = 14) + 5000\text{ramp}(t = 18) + 5000\text{ramp}(t = 22) - 5000\text{ramp}(t = 24) \quad (6.1)$$

The initial length of submerged wire is still 100 m and the horizontal current is assumed to be zero. Figure 6.13 shows the motor torque compared to the reference.

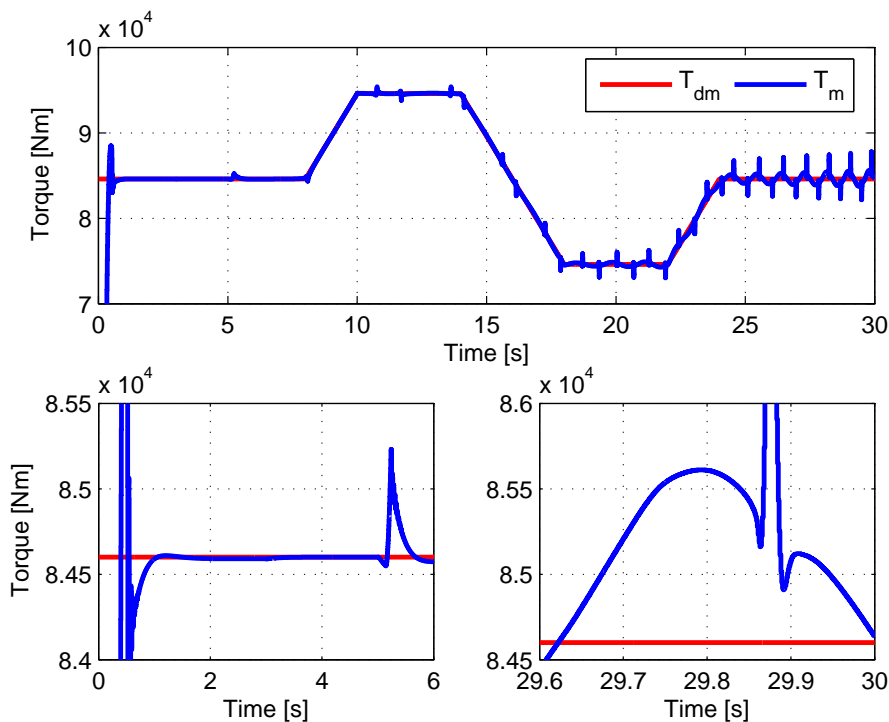


Figure 6.13: Torque and reference.

As the figure shows the torque peaks are still present in the first plot but the controller seems to follow the reference torque with good precision. It also seems like the maximal tracking error is lower in this case since the oscillations look smaller compared to the previous case. This is as expected since the load is three times as large as in the previous case which will generate more tension in the wire that the torque controller experiences. The plot in the lower left corner shows that the controller stabilizes as before and the characteristic torque peak when the heave motion is initiated is present. The plot in the lower right corner shows the maximal torque oscillation in the end of the simulation, when neglecting the torque peaks, indicating that the tracking error is lower in this case. The tracking error is shown in the next figure, figure 6.14.

The figure confirms the suspecting. When neglecting the torque peaks the error seems to be below 2%, which is a good result. This also indicates that the motion of the load should be

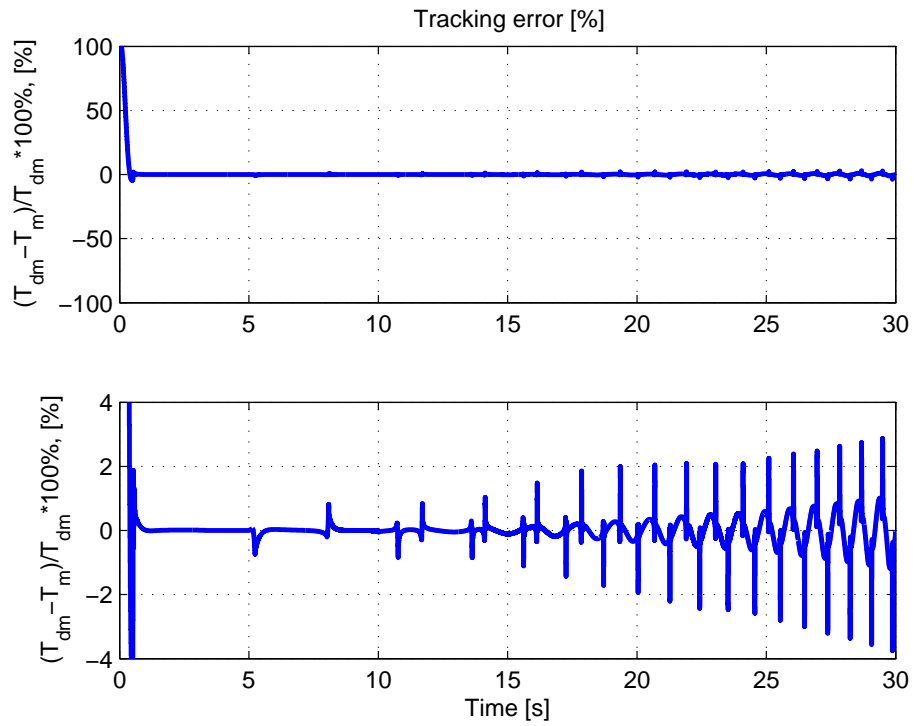


Figure 6.14: Tracking error.

lower than in the previous case. Figure 6.15 shows the top vertical wire position compared to the vertical load position.

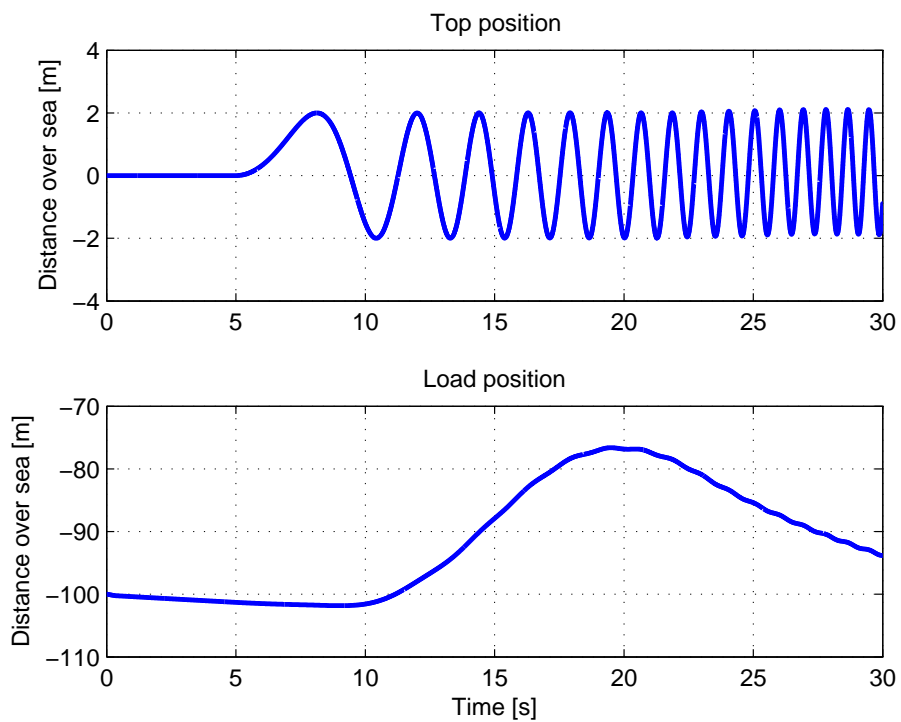


Figure 6.15: Top and bottom vertical wire position.

As can be seen in the figure the oscillations from the heave motion seems to be almost gone and



the amplitude of the oscillations in the end of the simulation is approximately 0.03 m, 3 cm. The small changes in the reference torque lifts the load about 5 m in the end of the simulation. This may be little strange since the reference torque was both increased and decreased and the sum of these changes should be zero. This has to do with the complexity of the model, taking the inertia of the load, the wire and the hydrodynamics into account. If the changes in the reference torque were shifted, first decreased and then increased, the load would be lowered below the start position. Also the mean reference torque was set so that the motor velocity was as close to zero as possible, but as in the previous case this is difficult to do by hand. Also hydrodynamic loads affects the load and the wire and tries to prevent any movement. This means that the load position is affected by many factors giving a complex picture of the quantities that affect the load position.

The motor velocity is comparable to the velocity in the previous case and is given in figure E.8 in Appendix E.2. The control slide positions, the differential pressure across the motor and variable bulk modulus are shown in figure E.9 and E.10, respectively, in Appendix E.2. The results are similar to the cases already discussed.

For the test cases presented in this chapter the horizontal current was set to zero. Therefore two extra cases are studied to also include current acting on the wire and the load.

### 6.3 Additional Controller Tests

Two more controller tests are given in Skjong and Pedersen (2014a), see Appendix B.1, which test the two controllers in AHC operations.

The first simulation tests the speed controller in an AHC case where the MRU gives the reference velocity to the speed controller. The heave position of the vessel is assumed to be a sine wave with an amplitude of 2 m and with an increasing frequency, starting at  $\omega = 0 \text{ rad/s}$  and ending with  $8 \text{ rad/s}$ . The initial length of the submerged wire is set to 100 m, the load is set to 3000 kg and the horizontal current is set to  $2 \text{ m/s}$ . The results from the simulation show that the speed controller gets a maximal tracking error in the end of the simulation of about  $0.2 \text{ rad/s}$  when neglecting the error peaks generated by crossings of the dead bands in the main valves. The heave induced changes in the vertical load position are  $\pm 2 \text{ cm}$  in the end of the simulation, showing that the speed controller works well in AHC operations.

The second simulation tests the torque controller in AHC operation with the same simulation settings as in the previous test. The torque controller has a constant torque reference of  $T_{dm} = 26910 \text{ Nm}$ . The maximal tracking error given in % compared to the reference is about 5% in the end of the simulation, when neglecting the peaks generated by crossings of the dead bands in the main valves. The heave induced changes in the vertical load position are in this case about 25 cm, which shows that the torque controller is not as good as the speed controller in AHC operations, as expected.

### 6.4 Chapter Summary and Conclusion

In this chapter the two controllers derived in chapter 5 have been tested more thoroughly by using the lumped loading model derived in Skjong and Pedersen (2014c), see Appendix B.3. The inner controllers were changed from adaptive PID-controllers to constant gained PD-controllers. This was done in order to improve the speed of the inner controllers, controlling the control slides to the desired positions. The adaptive controller had a "self-deleting" term  $\sigma$  in the control laws which is shown in (4.3). This term made the controller stable but also slow. When changing the

inner controllers the outer controllers could be tuned harder which reduced the tracking errors giving better results.

The speed controller was first tested using a  $\sin(\cdot)$ -sweep reference, having an amplitude of 5 rad/s with increasing frequencies starting at  $f = 0$  Hz and ending in  $f = \frac{4}{\pi}$  Hz, and with two different load cases,  $m_{Load} = 3000$  kg and  $m_{Load} = 6000$  kg. It was also assumed no current and no heave motions in the simulations and the purpose was to induce oscillations in the wire model trying to make the speed controller unstable. The results from both tests indicated that the speed controller seemed to be robust having a low tracking error in the highlight of the two load cases. The frequency at the end of the simulations was set larger than what would be expected for such a hydraulic system to experience in reality. It would never be desired to generate such oscillations when doing a winch operation. The high frequencies generated high differential pressures and the load case  $m_{Load} = 6000$  kg exceeded the maximal design pressure of the hydraulic system. However the speed controller performed well also in this case.

The torque controller was also devoted two controller tests. The reference torque was set constant to a value as close to the torque necessary for holding the load in the first case and a heave motion at the top of the wire was added. The heave motion gave a  $\sin(\cdot)$ -sweep of the vertical top wire position with an amplitude of 2 m with the same range of frequency as for the speed controller tests. The load was set to  $m_{Load} = 3000$  kg and the results showed that also the torque controller performed well emphasized by a global tracking error below 5 % when neglecting the peaks due to crossings of the dead bands in the main valves. Also the torque controller was tested with unrealistic frequencies. For waves generating a heave motion of  $\pm 2$  m would normally have a wave period of at least a few seconds, giving a wave frequency lower than 1 Hz. For heave motions with amplitudes of about 2 m and frequencies larger than 1 Hz a precise winch operation would never be initiated in the first place due to safety issues.

The same test was initiated for a load  $m_{Load} = 9000$  kg and a change of reference torque were added between  $t = 8$  s and  $t = 24$  s, as specified in (6.1). Also in this test the torque controller performed well, giving a maximal global tracking error below 2 %. The results showed that the torque controller perform better when the load is large and also when the hydrodynamics have large influence. This generates larger tensions in the wire and thereby larger changes in the motor torque. Since the torque controller is assumed slower and less precise compared to the speed controller it is less sensitive and hence larger variations and higher values of the torque will result in better performance for the torque controller.

In addition to these tests two more tests were initiated in Skjong and Pedersen (2014a), see Appendix B.1. Both tests were AHC tests, including horizontal current and heave motions of the vessel. The results from these tests were also good showing that the speed controller minimized the effect the heave motion had on the load, giving a change in vertical load position of about 2 cm in amplitude. In this case the load was also lifted about 5 cm because of the horizontal current. The test for the torque controller showed that the controller started lowering the load because the current acting on the wire and the load generated higher tensions in the wire. This resulted in higher horizontal displacement of the load but with the right torque reference the torque controller should be able to keep the load at the same depth.

Now when the two controllers have been tuned and tested thoroughly it would be of interest to see how they act together, performing in situations where anti-spin and torque limitations are desirable.

# 7 | Hybrid Control

As seen in chapter 6 the two controllers that were derived in Skjong and Pedersen (2014a), see Appendix B.1, worked well also when a more realistic hydraulic motor loading model was included in the simulations. In this chapter a combination of these two controllers in a hybrid control system is to be studied. The motivation for this is to be able to give the hydraulic winch functionalities such as anti-spin, load landing, loss of load detection or generally detection of load variations and to detect when the load gets stuck and be able to control the winch in such cases without danger.

## 7.1 Hybrid Control Design

The hybrid controller design is elaborated in Skjong and Pedersen (2014b), see Appendix , and will only be briefly presented here.

The speed controller and the torque controller, that have been derived previously, are connected to the hybrid controller output through a switching algorithm, which in general is what a hybrid controller consists of except controllers. The switching algorithm, or the switching logics, bases its choices on measurements from the hydraulic system, switching restrictions and conditions, as well as operator choices. The most important property in the hybrid controller design is to ensure stability in the controlled system when controllers are interchanged. In this hybrid controller design *dwelt time* switching is chosen as a switching restriction in addition to controller tracking error limits and system restrictions.

Dwell time switching ensures that the switching algorithm does not change controller whenever it wants, which can lead to a phenomenon called *chattering*. When a controller switching has been initiated the hybrid controller must wait a given period of time before allowed to switch controller again. Chattering is when the switching algorithm changes controller with a high frequency which leads to instability in the controlled system. Together with dwell time restriction the tracking error must be within a given region before the switching algorithm is allowed to change controller. These two restrictions ensures that the active controller is stable, and thus the controlled system is stabilized, before a controller switching is initiated.

In addition to the mentioned restrictions, the controlled system also sets restrictions to the hybrid controller, ranging from maximal torque and speed to situations that make the system unstable if not observed and handled right. One such situation is whenever the torque controller is active, the torque limit is reached and the load is too heavy for the winch to hold. Then the load is lowered and if the speed in the lowering exceeds the speed limit the hybrid controller should not be able to switch controller. If it does, the speed controller is activated and tries to force the winch to give a higher torque than allowed. This will either initiate a new controller switching, reactivating the torque controller and the hybrid controller is back to where it started, or the winch generates a higher torque than allowed causing wire rupture or damages in the hydraulic system. This situation, among others, shows that the hybrid controller design with its restrictions also is dependent on system properties and must be included in order to obtain a safe hybrid controller design.

In general the speed- and torque limits are seldom reached in normal winch operations and is often triggered by special cases such as landing a load on the sea floor, wire snapping and stuck

load. These cases are taken into account when designing the hybrid controller and are also studied carefully in Skjong and Pedersen (2014b).

Together with the switching algorithm a torque reference estimator are included. This estimator is a second order Bessel filter, a notch filter, that tries to filter out the heave generated torque variations from the calculated motor torque whenever the operator allows it and when the speed controller is active doing an AHC operation where the load is kept at a constant depth. When the estimate satisfies the restrictions that are set, the torque controller is reactivated and fed the torque estimate as a new reference.

All measurements are filtered which is important for the performance of the hybrid controller. If too much is filtered out the performance would be poor and if too little is filtered out the hybrid controller may try to switch controller when a peak in the measurements appear. As seen previously pressure peaks appear when the control slides in the main valves cross the dead bands, and the hybrid controller should not initiate a controller switching each time this happens.

## 7.2 Hybrid Controller Testing

The hybrid controller derived in Skjong and Pedersen (2014b) should be tested in various simulation cases to ensure stability of the hybrid controller numerically. The first test is an AHC-operation, using the speed controller as the main active controller, where the load changes rapidly generating a torque that exceeds the torque limit. The three next simulations, that are given in Skjong and Pedersen (2014b), tests the hybrid controller in load landing-, loss of load- and stuck load situations.

### 7.2.1 AHC with Changing Load

To test the hybrid control system a simple AHC test is considered. The operator has set the speed controller to be the main active controller, the controller the operator wants to use, trying to keep the load at a constant depth using MRU measurements as reference to the speed controller. The speed limits are set to  $\pm 6 \text{ rad/s}$ , the torque limit is set to  $50 \text{ kNm}$  and the load is set to  $3000 \text{ kg}$ . At  $t = 10 \text{ s}$  the load is doubled in a step and the torque controller should be activated by the switching algorithm since the torque will exceed the torque limit. At  $t = 20 \text{ s}$  the load is changed back to its initial value and the switching algorithm should observe this and reactivate the speed controller. The heave position of the vessel is assumed to be a sum of six sine waves with frequencies  $\omega \in [0.5 \text{ rad/s}, 2 \text{ rad/s}]$  and with amplitudes  $A \in [0.2 \text{ m}, 2 \text{ m}]$ .

Figure 7.1 shows the motor velocity compared to the reference velocity, magnified areas around the controller switching areas and which controller is active.

The first plot shows the hydraulic motor velocity compared to the reference and shows that the motor velocity coincides with the reference when the speed controller is active. In the range  $t \in [10.7 \text{ s}, 20.5 \text{ s}]$  the torque controller is active and the motor velocity decreases. This is because the torque is too low to hold the load and when it got doubled the load is lowered. The two plots on the second row in the figure show a closer view of the motor velocity and the reference when a controller switching is initiated. When the speed controller is reactivated it uses about  $0.4 \text{ s}$  to stabilize fixed at the reference. The last plot shows which controller is active during the simulation. Figure 7.2 shows the torque compared to the torque limit, magnified areas around the controller switching and which controller is active during the simulation.

The first plot shows the torque compared to the torque limit, and shows that the torque converges to the torque limit when the torque controller is active. The torque controller is activated at

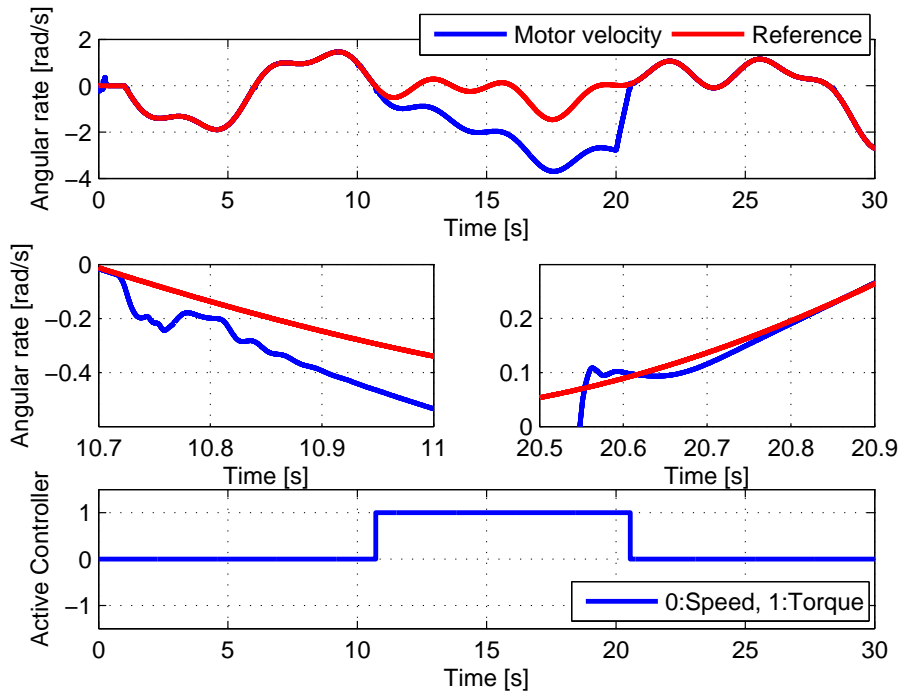


Figure 7.1: Hydraulic motor velocity, reference, magnified areas around controller switching and active controller.

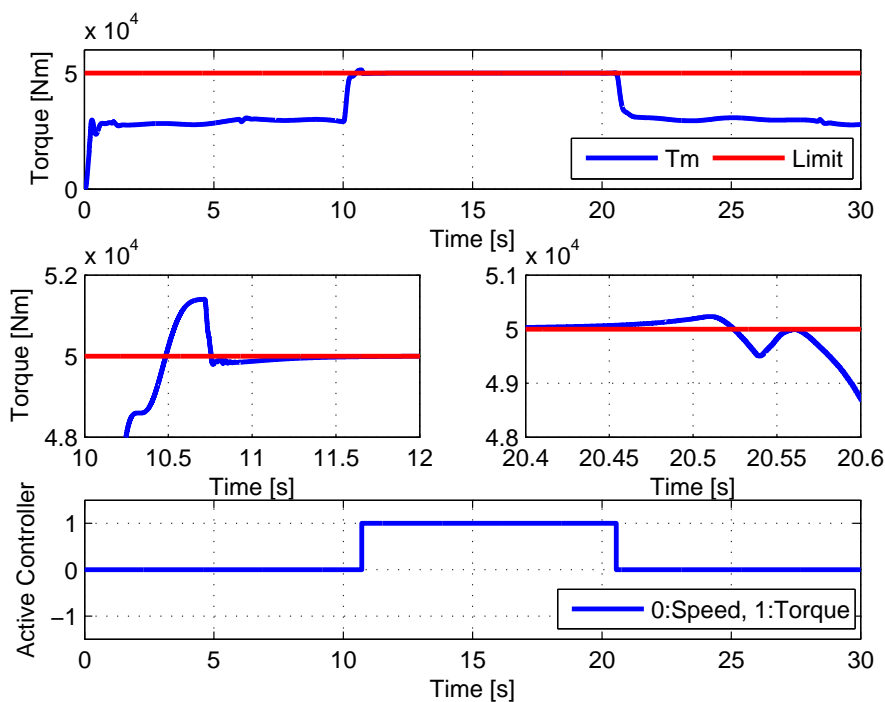


Figure 7.2: Torque, reference, magnified areas around controller switching and active controller.

$t = 10.7$ s and uses about 0.6s to stabilize fixed at the torque limit. This can be seen in the first plot on the second row in the figure. The last plot on the second row shows a magnified area around the torque when the speed controller is reactivated. The last plot shows witch controller

is active during the simulation.

This test shows that when the speed controller is chosen to be the main active controller, the hybrid controller activates the torque controller when the torque exceeds the torque limit and the torque controller keeps the torque at this limit. When the load decreases the hybrid controller observes this and reactivates the speed controller.

## 7.2.2 Controller Tests given in Skjong and Pedersen (2014b)

Additional three hybrid controller tests are given in Skjong and Pedersen (2014b), see Appendix B.2. These tests are briefly explained below.

### Landing of Load using Torque Controller

The first simulation presented tests the hybrid controller in an operation where a landing of the load at the sea floor is to be initiated. The torque controller is chosen to be the main active controller by the operator and the torque reference is set lower than the torque required to hold the load in order to lower the load. The upper speed limit is set to zero in order to observe when the load makes contact with the sea floor. The simulation results show that when the load touches the sea floor the speed controller is activated, having only MRU-measurements as reference in order to perform AHC. After a while both the upper speed limit and the reference torque is increased and the torque controller is reactivated and starts hoisting the load. In the end of the simulation the operator manually activates the speed controller in order to perform AHC, keeping the load at a nearly constant depth.

The controller test shows that the hybrid controller is able to land a load at the sea floor with a tensioned wire, having about constant submerged length, by having the torque controller active performing the lowering and by setting the upper speed limit to zero.

### Loss of Load and Variations using Torque Controller

In this test the torque controller is chosen to be the main active controller, having a constant reference that is about the required torque for holding the load. The load is changed four times during the simulation; the load is lost, regained, doubled and set to its initial value at the end. The operator has chosen that the hybrid controller may try to estimate a new torque reference when the speed controller is active performing AHC keeping the load at a nearly constant depth.

The simulation results show that when the load changes the speed controller is activated and the hybrid controller starts to estimate a new torque reference. The estimated torque references have varying accuracy and the results shows that it is hard to find the right torque reference to just hold the load. This problem is related to the control problem of the inverted pendulum, where the equilibrium point is a saddle point and only a small disturbance is enough to push the system out of its equilibrium point. However the estimated torque reference is only meant as a guide for the winch operator, and the lack of accuracy is therefore relaxed. The results also show that the switching algorithm in the hybrid controller works fine and the controllers stabilize fast when activated.

### Stuck Load using Speed Controller

In this simulation the speed controller is chosen as the main active controller, having only the MRU-measurements as reference performing an AHC that keeps the load at a nearly constant

depth. In the region  $t \in [10\text{s}, 30\text{s}]$  the load is stuck and at  $t = 15\text{s}$  the load is to be hoisted.

The simulation results shows that the speed controller is active until the load is to be hoisted. Then the torque controller is activated due to exceedance of the torque limit. This means that the speed controller performs so good that the hybrid controller does not observe that the load is stuck until the load is to be hoisted. The torque controller is active in the rest of the time region the load is stuck and the speed controller is reactivated when the load is released.

This shows that the hybrid controller works good in cases where the speed controller is active and the load gets stuck. This is an important functionality in the hybrid controller and would lead to damages in the hydraulic system or loss of load if not included in the hybrid control design.

All tests presented show that the hybrid controller works good, and emphasizes that the wanted functionalities in the hybrid controller must be studied and included in the switching algorithm. In Skjong and Pedersen (2014b)  $T_{load}$  was set to zero because it was assumed not measurable. In reality  $T_{load}$  is hard to measure and must be estimated or observed through other measurements. It would also be favourable to have estimates of the motor velocity if the decoder that measures the velocity fails. The differential pressure is always assumed measured and if the velocity and  $T_{load}$  could be observed through the differential pressure measurements, it would be of great interests to design an observer.

### 7.3 Observer Design

By using the simplified differential equations for the motor velocity and the differential pressure, the motor velocity can be related to the differential pressure. However there is no equation describing  $T_{load}$ . By simply assuming that  $T_{load}$  can be modelled a function of itself, the three differential equations that lies the groundwork for the observer can be expressed as

$$\dot{x}_{m2} = \frac{1}{I_m} \left[ \frac{D_m}{2\pi} \Delta p - F_s \mu_v x_{m2} - T_{load} \right] \quad (7.1a)$$

$$\dot{\Delta p} = \frac{\beta \alpha \pi D_s}{V \sqrt{\rho}} x_H \sqrt{\Delta_{pump} - \text{sign}(x_H) \Delta p} - \frac{\beta D_m}{2\pi V} x_{m2} - \frac{\beta G}{V} \Delta p \quad (7.1b)$$

$$\dot{T}_{load} = -\frac{1}{\tau} T_{load} \quad (7.1c)$$

where  $\tau$  is a time constant. The three differential equations can be set in a system and by assuming that a high gain state observer, a Luenberger observer design (Chen, 1998), is a sufficient observer for this purpose, the observer can be given as

$$\dot{\hat{\mathbf{x}}} = \mathbf{A} \hat{\mathbf{x}} + \mathbf{B}(\tilde{y}, u)u + \mathbf{K}(\tilde{y} - \mathbf{C} \hat{\mathbf{x}}) \quad (7.2)$$

where  $\tilde{y} := \Delta p$  is the measured differential pressure across the hydraulic motor,  $\hat{\mathbf{x}} = [\hat{x}_1, \hat{x}_2, \hat{x}_3]^T$  are the states where  $\hat{x}_1$  is the hydraulic motor velocity,  $\hat{x}_2$  is the differential pressure and  $\hat{x}_3$  is the load generated torque acting on the hydraulic motor,  $\mathbf{C} = [0, 1, 0]$ ,  $\mathbf{K} = [k_1, k_2, k_3]^T$  is the observer gain vector,

$$\mathbf{A} = \begin{bmatrix} -\frac{F_s \mu_v}{I_m} & \frac{D_m}{2\pi I_m} & -\frac{1}{I_m} \\ -\frac{\beta D_m}{2\pi V} & -\frac{\beta G}{V} & 0 \\ 0 & 0 & -\frac{1}{\tau} \end{bmatrix} \quad \text{and} \quad \mathbf{B}(\tilde{y}, u) = \begin{bmatrix} 0 \\ \frac{\alpha \beta \pi D_s}{V \sqrt{\rho}} \sqrt{\Delta_{pump} - \text{sign}(u) \tilde{y}} \\ 0 \end{bmatrix} \quad (7.3)$$

To be able to observe the motor velocity and  $T_{load}$  through the differential pressure measurements,  $\Delta p$ , then

$$\mathcal{O} = \begin{bmatrix} C \\ CA \\ CA^2 \end{bmatrix} \quad (7.4)$$

must have full rank. In this case  $\text{rank}(\mathcal{O}) = 3$  and the motor velocity and  $T_{load}$  are therefore observable. To be able to choose  $\mathbf{K}$  to stabilize the observer, the error dynamics in the observer must be studied. The error dynamics are given as

$$\dot{e} = (\mathbf{A} - \mathbf{K}\mathbf{C})e + \mathbf{B}(\tilde{y}, u)u + \mathbf{K}\tilde{y} \quad (7.5)$$

$\mathbf{K}$  must be chosen such that

$$\mathbf{A}_e = \mathbf{A} - \mathbf{K}\mathbf{C} \quad (7.6)$$

is Hurwitz. It is also important that the error dynamics are faster than the dynamics in the system that is to be observed. In this observer, the gains are tuned through simulations and set to  $\mathbf{K} = [-0.001, 2400, 15]^T$ . The time constant in the differential equation giving  $T_{load}$  is set to  $\tau = 4000$  s.

Now, when the observer is derived, it should be tested through simulations. It is expected that the performance of the speed controller decreases when using the observed motor velocity in the control law. Also it is expected that including the observed  $T_{load}$  in the speed controller would give negligible changes in performance for the speed controller, which emphasizes the robustness of the controller.

## 7.4 Simulations using Observer

The observer is to be tested with the same simulation settings as used in section 7.2.1. This gives the opportunity to compare different cases and see the effects from using the observed motor velocity and the observed motor load in the speed controller. Each case study is compared to the simulation done in 7.2.1.

### 7.4.1 Observer out of the Loop

In this case the observer is connected out of the loop, meaning that the speed controller gets the measured motor velocity and  $T_{load} = 0$ . This is done in order to see how accurate the observer is before included in the closed loop.

Figure 7.3 shows the estimated motor velocity compared to the measured motor velocity. The figure shows that the difference between the measured motor velocity and the estimated motor velocity is small. There is a small delay separating them, which comes from a combination of sampling delay and filtering of the differential pressure. The largest differences between them are when the controllers are switched, which are seen in the two plots on the second row in the figure. However the differences decrease after about 0.6 s after the controller switchings. Even though the estimate is good, the estimation error could be large enough to generate a significant decrease in performance in AHC operations.

Figure 7.4 shows the estimated motor load,  $T_{load}$ , compared to the actual motor load. As can be seen in the figure, the motor load oscillates a bit in the start of the simulation. This is due to the initiation phase in the simulation. In the time region after initiation and to  $t = 10.7$  s, the estimated  $T_{load}$  seems to coincide with the measured motor load except for a delay as already



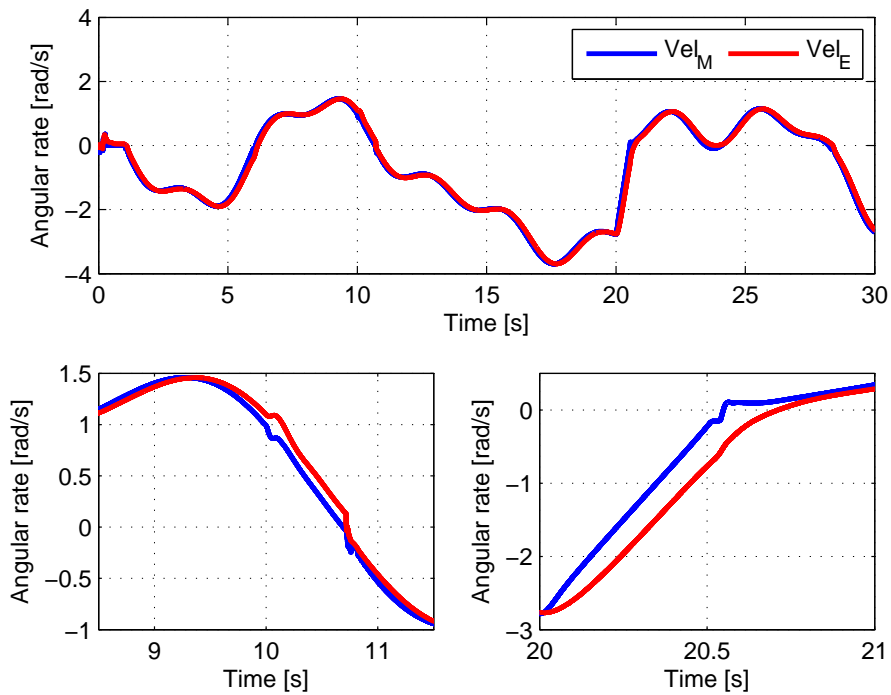


Figure 7.3: Observed motor velocity compared to the measured motor velocity.

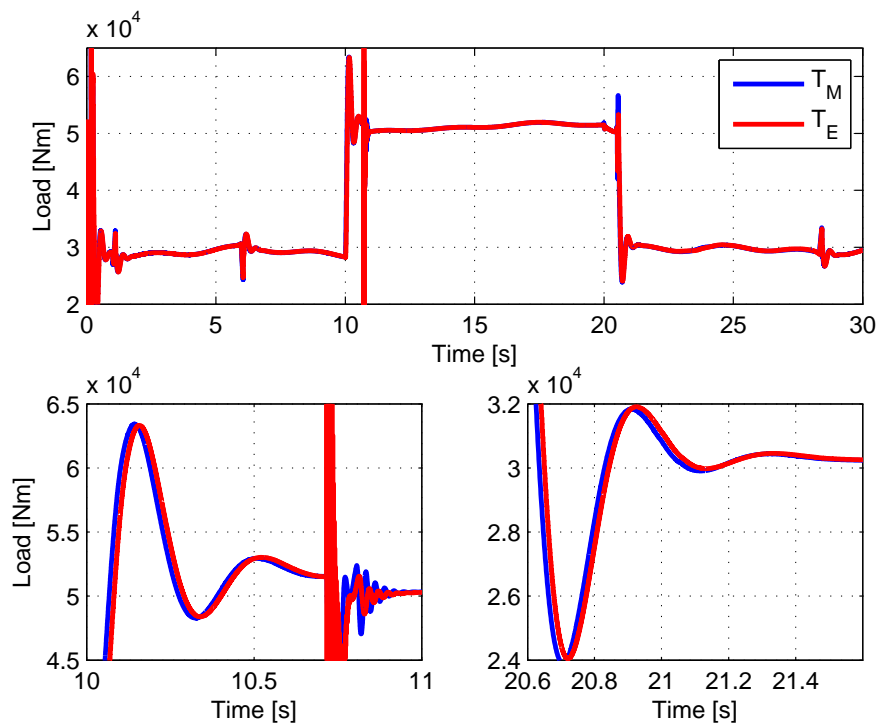


Figure 7.4: Observed motor velocity compared to the measured motor velocity.

mentioned. At  $t = 10.7$ s the estimate starts to oscillate, but stabilizes after a short period of time. This has to do with the change of active controller, and since the observer is out of the loop such oscillations are to expect.

The results from this simulation shows that the observer works quite well when having in mind that the differential equations used are simplified and that the motor load is assumed to be a Markov process with no noise. This also emphasizes the assumptions done when deriving the simplified state equations.

### 7.4.2 $T_{load}$ in Feed Forward

The objective in this simulation is to verify the assumption of setting  $T_{load} = 0$  in the speed controller. The hydraulic motor velocity is measured and  $T_{load}$  is estimated and given in feed forward in the control law in the speed controller. Figure 7.5 shows the tracking error in the speed controller in the simulation done in 7.2.1 compared to the simulation with estimated  $T_{load}$  given in feed forward. The plots given on the first row in the figure are the tracking error with

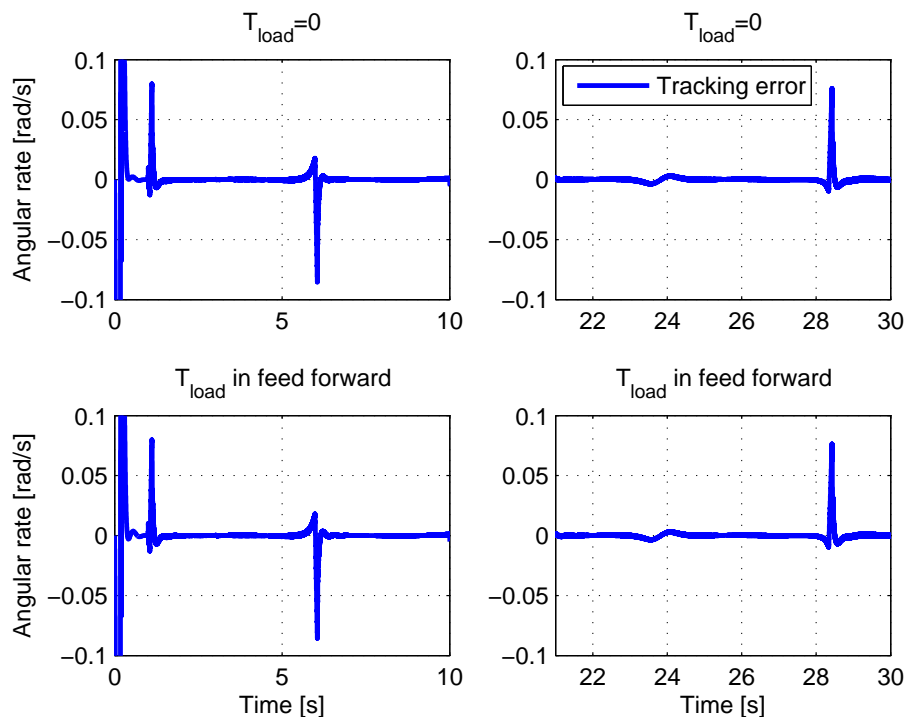


Figure 7.5: Comparison of simulations with and without  $T_{load}$  in feed forward.

$T_{load} = 0$  for the two time regions where the speed controller is active. The plots in the second row shows the tracking error in the simulation with estimated  $T_{load}$  given in feed forward in the control law for the same two time regions. As the figure shows the difference between them are negligible, which emphasizes the assumption about setting  $T_{load} = 0$ . It also emphasizes the robustness of the speed controller, which was based on simplified state equations.

### 7.4.3 Closed Loop with Observed Motor Velocity in Feedback

In this case study the speed controller is fed to the estimated motor velocity as feedback, meaning that the observer is part of the closed loop. Since the controller worked fine with  $T_{load} = 0$ , as shown in section 7.4.2, it is also used in this simulation. It is expected that the speed controller doing an AHC operation with the estimated motor velocity in feedback performs poorer than compared to the simulation done in section 7.2.1. To compare the two simulations the vertical load position is used. Figure 7.6 shows this comparison.

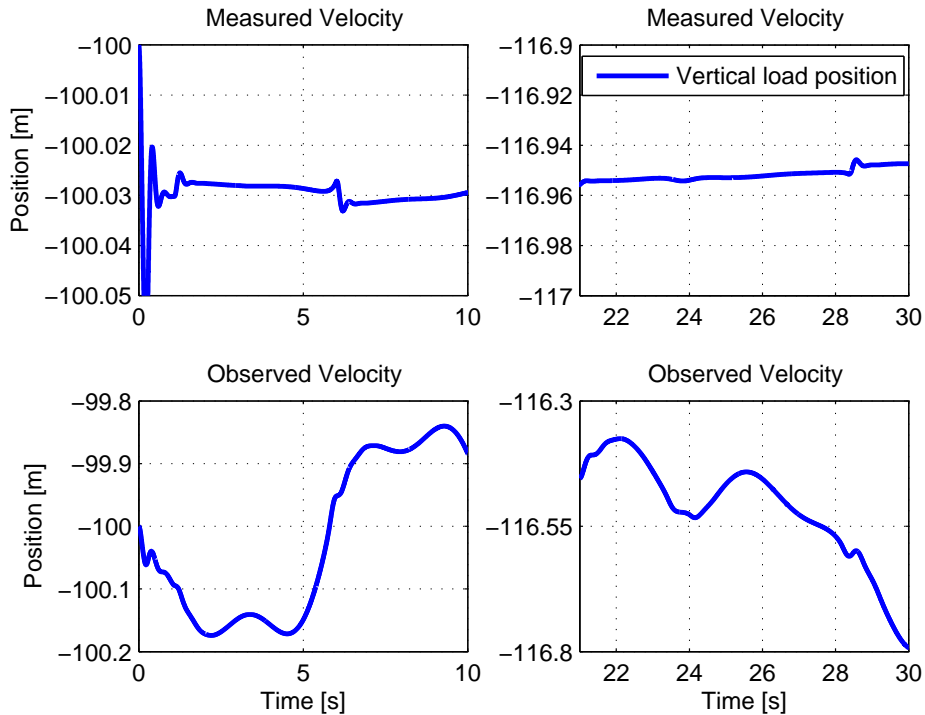


Figure 7.6: Comparison of vertical load positions between simulations with measured velocity and estimated velocity.

As can be seen in the figure the performance of the speed controller in the AHC operation, in the time regions the speed controller is active, has decreased when comparing to the case where the speed controller gets the measured motor velocity in feedback. The two plots in the first row in the figure shows the simulation results with measured motor velocity in feedback, and shows that the maximal changes in the vertical load position is about  $\pm 1$  cm. The plots in the last row in the figure shows the simulation results with estimated motor velocity in feedback and the maximal changes in vertical load position in this case are about  $\pm 20$  cm, 20 times larger. This supports the assumption about poorer speed controller performance, but the results are still good, giving a total error in vertical load position of 3.33 % compared to the maximal heave position of the vessel, which is about 6 m. It also shows that the estimated motor velocity can be implemented in the system for safety purposes so that the winch would still be controllable even when the decoder that measures the motor velocity fails.

## 7.5 Chapter Summary and Conclusion

In this chapter the hybrid control design derived in Skjong and Pedersen (2014b), see Appendix B.2, was presented and tested. The functionalities that were implemented in the hybrid controller showed to be related to the switching stability and the switching algorithm was designed to take care of this and ensure stability in the hybrid controller.

The finished hybrid controller was tested in a simulation where the speed controller was set to be the main active controller performing an AHC operation trying to keep the load at a constant depth. The torque limit was set to a low value and when the load was doubled the torque approached this limit forcing a controller switching in the hybrid controller. The torque controller was activated with the torque limit as reference. When the load decreased back to its initial value the speed controller was reactivated. This simulation showed that the hybrid

controller switched controller when the torque limit was reached which tells that the hybrid controller manages such cases.

In Skjong and Pedersen (2014b) three more test cases were initiated. Landing of load, loss of load and load variation with estimated torque reference, and stuck load. These three tests were initiated to test the functionalities implemented in the hybrid controller and showed that the hybrid controller was stable performing well in all these cases. A Bessel filter was used to estimate the torque reference when the load changed in the "loss of load"- test. The estimates showed varying accuracies and none of the new estimated torque references managed to keep the load perfectly still in AHC using the torque controller. This problem is related to the inverted pendulum control problem, where the torque reference for holding the load must be perfect and no disturbances can be present in order to perform AHC by using the torque controller. This is of course impossible since current effects, wave effects and wire dynamics, that are seen as disturbances in this case, are present in the simulation. If the length of submerged wire, tension or the load changes slightly the load would either be hoisted or lowered, which by itself would change the torque reference. This emphasizes the fact that the torque controller is not ideal in AHC operations, but has its strengths in other operations such as towing.

Also an observer was designed in order to estimate  $T_{load}$  and the motor velocity. A Luenberger observer, a high gain state observer, was chosen and tuned.  $T_{load}$  was in this chapter assumed not measurable and therefore it was set to zero in the speed controller law. Simulations done with this assumption showed that the speed controller performed well also in this case and the differences were negligible. This also emphasizes the robustness of the speed controller. The observer has the differential pressure,  $\Delta p$ , as measurement,  $\tilde{y}$ , and uses this to estimate  $T_{load}$  and the motor velocity based upon the simplified state equations derived in Skjong and Pedersen (2014a) and a Markov process representing  $T_{load}$ . It was assumed that the observer would give some errors, and this was confirmed in simulations. However the observer in the closed loop, feeding the speed controller with the estimated motor velocity, showed that the performance decreased a bit, but the system were still stable and controllable. This gives redundancy in the controller design, and the winch would still be operable if the decoder measuring the motor velocity fails.

## 8 | Conclusion and Further Work

In this thesis a hydraulic winch system has been modeled using bond graph theory and controlled using sliding mode-, backstepping- and hybrid control theory. The total bond graph model consists mainly of clean power bonds and well known bond graph building blocks such as **C**-, **R**- and **I**-elements, with a few exceptions. Some transfer functions are used to model the velocity limitation function and the fast dynamics in the pilot valve and the 3/2-directional valve. Also signal bonds are used in the main valves to connect the hydraulic flow with the valve dynamics. The same can be seen in the lumped wire-load model where the reel is connected to the wire elements through signal bonds. This is not the desirable way of modeling using bond graph theory where clean power bonds connecting submodels are preferable. However in these two cases clean power bond connections can not be used. In general in every modeling cases where the flow and the effort are interchanged asymmetrically, meaning the effort has to be handled different than the flow between submodels, clean power bonds can not be used. Then a hybrid modeling approach, including both bond graph theory and block theory, must be used.

The derived bond graph model for the hydraulic winch system shows reasonable responses in the simulations performed, which is expected since the main dynamics describing the system are present. Fluid inertia and variable bulk modulus in the main valves were removed to cut down the simulation time and by comparing simulations these simplifications were argued for since the differences were negligible. To verify the total model full scale tests should be performed. As a guide to tune the model against benchmark tests, model parameter sensitivity analysis have been initiated. This also gives a deeper understanding of how the model parameters affect the model response.

A thorough relation study, relating the control slide positions in the main valves to the motor velocity and the torque, was performed for control purposes. A clear relation between the main valve on the load side of the motor and the motor velocity and the torque was found and it showed to be possible to calculate the control slide positions from a desired velocity or torque in order to reproduce it in simulations. The results were not accurate but emphasized that the winch operator could act as an outer controller by observing the motor velocity and the torque and manually set the references for the control slides in the main valves. An adaptive PID-controller was used as inner controller and seemed to work good except for being a bit slow. However the adaptive controller is faster than the operator and is therefore argued for in such operations. Moreover the results showed that the relations were dependent on other quantities as well, such as pump flow and motor loading. This gives rise to believe an ordinary PID-controller would not work as an outer controller since the system is highly nonlinear, and stability of the system using the PID-controller can not be guaranteed except for a small region around the point the controller is tuned. That is why model based nonlinear controllers were derived.

The derivation of the speed controller and the torque controller were given in Skjong and Pedersen (2014a), see Appendix B.1. The two control laws are based on simplified state equations describing the controlled states in the hydraulic system. The state equations extracted from the bond graph model showed to be difficult to use in the control designs since they included lots of logic. Even though the control laws were based on simplified state equations they worked well which the controller tests and the simulations have shown. The controllers showed to be easy to tune and not very sensitive for small changes in the controller parameters and model parameters. This is expected since the control theory used to derive the two controllers tend

to give controllers with such preferences. In general the speed controller showed better performance than the torque controller, which is favourable since the speed controller is expected to be more in used compared to the torque controller. In simulations where the torque controller was used in AHC operations it was seen that the load was either lowered or hoisted. This was not unexpected since a small shortening or elongation of the submerged wire would change the torque reference needed to hold the load. Disturbances like current and vessel motions contribute to the tracking error in the torque controller and the load is automatically lowered or hoisted. This problem was said to be related to the inverted pendulum control problem, where the equilibrium point is a saddle point and only a small disturbance would cause the pendulum to change equilibrium point. However it is not an impossible task to control such systems, and should be studied more thoroughly in order to design a suitable control algorithm for using the torque controller in AHC operations where the load is kept at a constant depth.

The two controllers were put together to form a hybrid controller and a switching algorithm was designed to ensure stability in both the hybrid controller and the controlled system. The stability showed to be dependent on different functionalities and load cases, which was not unexpected. That is why operations such as landing a load on the sea floor and cases where the load gets stuck were studied for switching algorithm design purposes. More cases and operations should be investigated and included in the switching algorithm to ensure stability in every offshore operations. However in the studied operations the hybrid controller showed to be stable, robust and well suited for its purpose. To ensure redundancy in the control system an Luenberger observer was designed based on the simplified state equations, giving estimates of the motor velocity and the motor loading based on differential pressure measurements. Simulations where the estimates were included in the closed loop showed to be poorer than the results from simulations where measurements were used. This was expected but the winch would still be operational if the decoder measuring the motor velocity fails. For further work more advanced estimators should be investigated such as an Extended Kalman Filter, EKF. The beauty of this filter is that it does predicting of the estimates and would be a huge help for minimizing the effects from the time delays in the sensors. An estimator for estimating the reel diameter should also be included. Also measurement noise should be studied and more advanced filters should be investigated than the first order low pass filters used to filter the measurements in the control laws.

# Bibliography

- Borutzky, W., Barnard, B., and Thoma, J. (2002). An orifice flow model for laminar and turbulent conditions. *Simulation Modelling Practice and Theory*, 10(3–4):141 – 152.
- Chen, C.-T. (1998). *Linear System Theory and Design*. Oxford University Press, Inc., New York, NY, USA, 3rd edition.
- Controllab (2014). *20Sim, Simulation software*.
- Çetin, S. and Akkaya, A. V. (2010). Simulation and hybrid fuzzy-pid control for positioning of a hydraulic system. *Nonlinear Dynamics*, 61(3):465–476. Cited By (since 1996):19.
- Hespanha, J. P. (2002). Tutorial on supervisory control.
- Iwai, Z., Mizumoto, I., and Lin, L. (2006). Adaptive stable pid controller with parallel feedforward compensator. In *2006 SICE-ICASE International Joint Conference*, pages 3264–3269. Cited By (since 1996):1.
- Karnopp, D. C., Margolis, D. L., and Rosenberg, R. C. (2006). *System Dynamics: Modeling and Simulation of Mechatronic Systems*. John Wiley & Sons, Inc., New York, NY, USA.
- Küchler, S., Mahl, T., Neupert, J., Schneider, K., and Sawodny, O. (2011). Active control for an offshore crane using prediction of the vessels motion. *IEEE/ASME Transactions on Mechatronics*, 16(2):297–309. cited By (since 1996)22.
- Küchler, S. and Sawodny, O. (2010). Nonlinear control of an active heave compensation system with time-delay. pages 1313–1318. cited By (since 1996)1.
- Kim, W., Won, D., and Chung, C. C. (2010). High gain observer based nonlinear position control for electro-hydraulic servo systems. In *American Control Conference (ACC), 2010*, pages 1440–1446.
- Lei, J., Wang, X., and Pi, Y. (2013). Sliding mode control in position control for asymmetrical hydraulic cylinder with chambers connected.
- McCloy, D. and Martin, H. R. (1980). *Control of fluid power, analysis and design*. John Wiley & Sons, Inc., New York, NY, USA.
- Pedersen, E. and Engja, H. (2010). Mathematical Modelling and Simulation of Physical Systems; Lecture Notes in TMR4275 - Modelling, Simulation and Analysis of Dynamic Systems.
- Skjong, S. (2013). Modeling and Simulation of Directional Valve System, Specialization Project in TMR4510.
- Skjong, S. and Pedersen, E. (2014a). Control of Hydraulic Winch System (1/2), Model Based Control Designs.
- Skjong, S. and Pedersen, E. (2014b). Control of Hydraulic Winch System (2/2), Hybrid Control Design.
- Skjong, S. and Pedersen, E. (2014c). Modeling Hydraulic Winch System.
- Yang, K. U., Hur, J. G., Kim, G. J., and Kim, D. H. (2012). Non-linear modeling and dynamic analysis of hydraulic control valve; effect of a decision factor between experiment and numerical simulation. *Nonlinear Dynamics*, 69(4):2135–2146. Cited By (since 1996):1.





# *Appendices*



# A | Work Description



## **THESIS IN MARINE CYBERNETICS**

**SPRING 2014**

**FOR**

**STUD. TECH. Stian Skjong**

### **Modeling, Simulation and Control of Hydraulic Winch System**

#### **Work Description**

A proportional valve configuration for low pressure hydraulic winch systems, that is suspected to give a faster response than existing valve configurations in low pressure hydraulic winch systems, is to be studied. This valve configuration may give winch customers an alternative system to high pressure winch system that already exist in the market without losing functionalities. The main focus in this thesis is to design suitable control laws and algorithms which provides the desired functionality for the hydraulic winch system. This thesis is meant to be a continuation of the specialization project in TMR4510 where most of the process model for the hydraulic winch system was developed using bond graph theory.

#### **Scope of Work**

- Build a control model of the process model developed in the specialization project including relevant dynamics.
- Initiate a sensitivity study of interesting model parameters and look into the effect of variable bulk modulus and fluid inertia in the proportional valve configuration.
- Design suitable control laws for inner and outer control where inner control is the control of control slides in the main valves and outer control generates the reference positions for the control slides in the main valves from speed or torque control of the hydraulic motor.
  - Look into both first hand control laws/algorithms and advanced control laws/algorithms.
  - Design observers and/or estimators where needed.
  - Ensure robustness and stability.
  - Look into adaptive or at least easy tuned control laws and algorithms if possible.
  - Design an antispin algorithm for the hydraulic motor controlled by the valve.
  - Add controller functionalities for handling extreme cases without damaging the hydraulic system or the load.
- Conduct simulation for controller tuning and testing .

- Build control model for the whole system including the chosen control laws/algorithms.
- Document each step in the process

The report shall be written in English and edited as a research report including literature survey, description of mathematical models, description of control algorithms, simulation results, model test results, discussion and a conclusion including a proposal for further work. It is supposed that Department of Marine Technology, NTNU, can use the results freely in its research work, unless otherwise agreed upon, by referring to the student's work. The thesis should be submitted in two copies within 10<sup>th</sup> of June.

Advisers: Jo-Einar Emblemsvåg, Asgeir Sørensen

Eilif Pedersen  
Supervisor



# B | Papers

## B.1 Control of Hydraulic Winch System (1/2) Model Based Control Designs

Submitted for publication.

# Control of Hydraulic Winch System (1/2)

## Model Based Control Designs <sup>\*</sup>

Stian Skjong, <sup>\*</sup> Eilif Pedersen <sup>\*\*</sup>

<sup>\*</sup> *Department of Marine Technology, Norwegian University of Science and Technology (NTNU), 7491 Trondheim, Norway*  
(e-mail: stiansk@stud.ntnu.no)

<sup>\*\*</sup> *Associate Professor*  
*Department of Marine Technology, Norwegian University of Science and Technology (NTNU), 7491 Trondheim, Norway*  
(e-mail: eilif.pedersen@ntnu.no)

---

**Abstract:** A speed controller and a torque controller are derived to control a hydraulic power system via proportional valves using backstepping and sliding mode control theory. The hydraulic motor is driving a winch designed for heavy lift operations on sub-sea installations in rough environments. A lumped wire-load model is used to generate a realistic load case for the hydraulic system including hydrodynamic forces acting on the wire and the load, horizontal current and heave motions of the vessel. The hydraulic system includes many different components and they are only briefly elaborated in this paper. The control system consists of several inner control loops to control the valves, and an outer system control loop controlling the overall system. For inner controller, controlling the 3/3-directional valves, a simple PD controller is used. The speed controller and torque controller, characterised as outer controllers, feed the inner controllers with control slide reference positions. Both controllers are tested in simulations with realistic load characteristics.

*Keywords:* Hydraulic offshore winch control systems · Sliding mode · Backstepping · Bond graph theory · Lyapunov stability · Simplified state equations · Tracking error · Lumped wire-load model

---

### 1. INTRODUCTION

In this paper the objective is to derive suitable control laws for controlling the hydraulic motor velocity and the hydraulic motor torque for the hydraulic winch system shown in figure 1 by controlling the two proportional valves in a 4/3-valve configuration. The hydraulic winch is assumed to be designed for winch operations from an offshore vessel and the test cases presented in this paper will be characterized thereby. As seen in the figure the hydraulic system consists of a hydraulic motor driven by two servo operated proportional valves, pilot operated by two 4/3-directional valves, a pressure relief valve, pilot operated by a 3/2-directional valve feeding the pressure relief valve with the highest hydraulic motor pressure. The pressure relief valve ensures that the highest pressure in the system is a few bars higher than the loading pressure across the hydraulic motor. In addition there is a HPU, hydraulic power unit, that drives the 3/3-directional valves, a fixed flow main pump system that generates pressure to control the hydraulic motor and some check-valves that set restrictions to the flow directions through the valves and avoid vacuum pressure at each sides of the hydraulic motor. As for motor loading the lumped wire-load model derived in Skjong and Pedersen (2014a) is used. This model includes wire dynamics, reel dynamics, hydrodynamic forces acting on the wire and the load as

well as the ability to include heave motions, drifting and horizontal current. In this wire-load model the wire is divided into five equal wire lengths and modeled as mass-damper-spring systems in series.

The 4/3-directional valves, which hereafter are referred to as pilot valves, are assumed to be solenoid operated valves that are controlled with a voltage limited in the range  $[-10\text{ V}, 10\text{ V}]$ , generating electromagnetic forces that moves the slides in the valves. This voltage source is fed to the solenoid from a PD-controller which hereafter is referred to as a inner controller. The gains in these inner controllers are set to  $K_p = 6000\text{ V/m}$  and  $K_d = 20\text{ Vs/m}$ . Both the pilot valve dynamics and the 3/2-directional valve dynamics are assumed represented by a second order transfer function.

The 3/3-directional valves, which hereafter are referred to as main valves, are assumed to have varying flow characteristics which are dependent on the displacements of the control slides in the valves. These flow characteristics are modelled but assumed to be unknown from a control point of view. The main valves are self centred by a pre-tensioned centring spring and are allowed to have a maximal displacement of  $\pm 0.05\text{ m}$ . The HPU driving the main valves is assumed to be a pressure compensated pump that keeps a nearly constant HPU pressure of 200 bar. The main valves are also assumed to have dead

<sup>\*</sup> Based on the master thesis by Stian Skjong (Skjong, 2014).



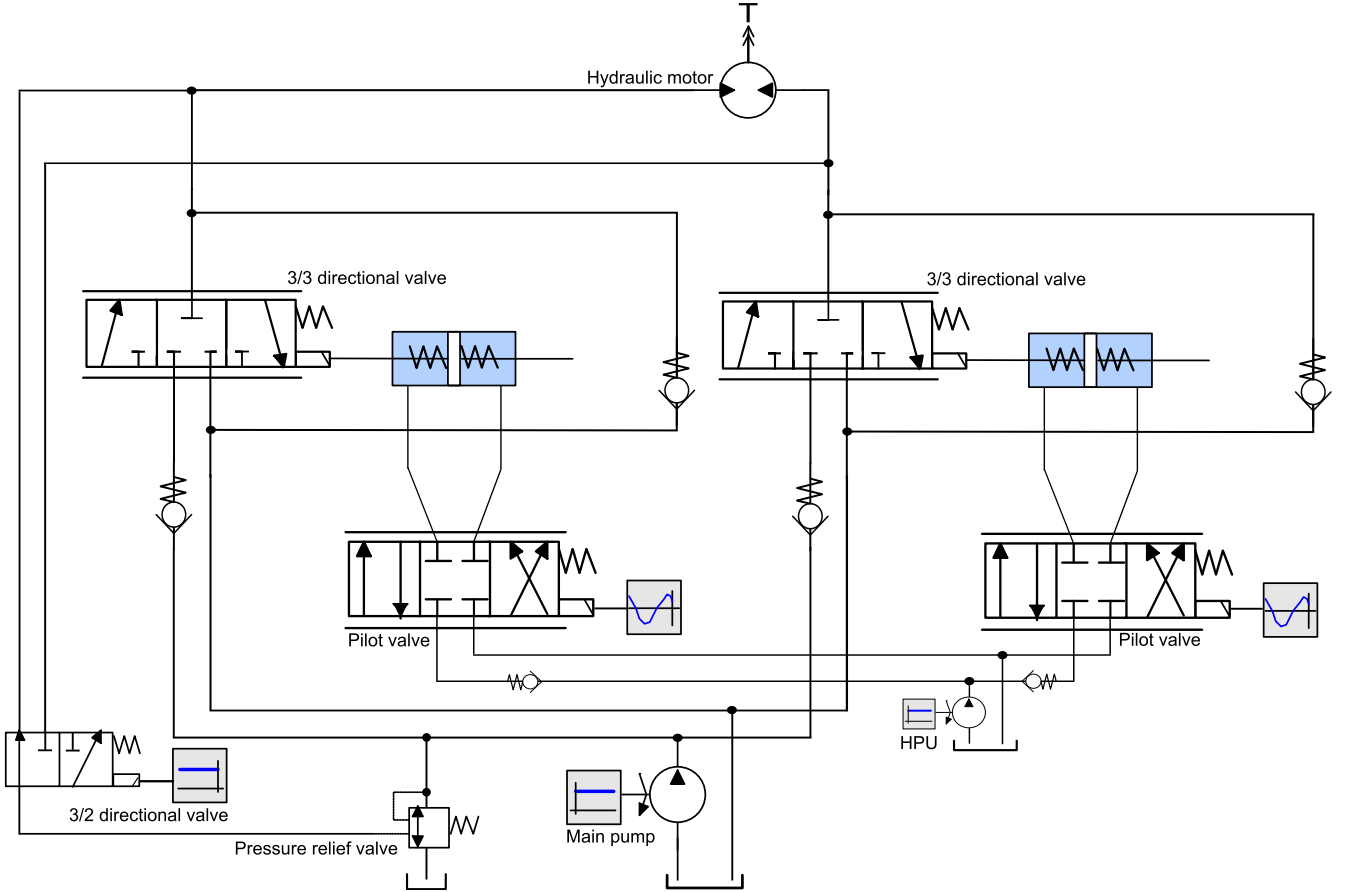


Fig. 1. Sketch of hydraulic system.

bands in the range  $[-x_{olap}, x_{olap}]$  of the control slide displacements.

The pressure relief valve is assumed to have a nozzle with a variable opening area, dependent on the displacement of the valve, connecting the valve to the 3/2 directional valve. Like the main valves the pressure relief valve is assumed to experience characteristic flow forces acting on the moving control slide in addition to flow characteristics. The pressure relief valve has also a spring that forces the maximal pressure in the pressurised main pipelines to be about 3 bar higher than pressure generated by the motor loading. The frictions in the main valves, caused by the moving slides, are assumed to consist of static friction, coulomb friction and linear friction.

The hydraulic motor is assumed to be a one chambered motor that experiences both friction and internal leakages. The friction is as for the pressure relief valve assumed to contain static friction, coulomb friction and linear friction. The internal leakages are assumed proportional to the differential pressure over the hydraulic motor with  $G$ , conductance of laminar resistance, as proportionality parameter. The motor can also experience vapour pressures that gives cavitation. This is modeled as a coefficient multiplied with the gear ratio  $n$  and is in the range,  $0 \leq n \leq 1$ . The coefficient is zero whenever the pressure is below the vapour pressure of the hydraulic fluid. The equation for determining the magnitude of the coefficient is a second order polynomial which is a function of pressure ratios.

Volumes on each side of the hydraulic motor, in the 3/2-directional valves, the pressure relief valve, the main pressure line and the main return line are assumed to have variable bulk modulus, or *equivalent bulk modulus*, that is pressure dependent, given in McCloy and Martin (1980) as

$$\frac{1}{\beta(p)} = \frac{1}{\beta_h} + \frac{1}{\beta_f} + \frac{n}{1.4p} \quad (1)$$

where  $\beta_h$  is the constant bulk modulus for the pipeline or the valve housing,  $\beta_f$  is the constant bulk modulus for the hydraulic fluid and  $n = \frac{V_g}{V_l}$  is the volume ratio of gas and liquid in the hydraulic fluid.

The total model shown in figure 1 has been modeled using bond graph theory and is thoroughly described in Skjong (2014), with the same model parameters as used here. Because of all the check-valves, the friction in the hydraulic motor and the variable bulk modulus, the state equations derived from the bond graph model are way to advanced for control design purposes, containing too much logics. Therefore simplified state equations must be derived containing only the essential dynamics in order to proceed with controller designs.

## 2. SIMPLIFIED STATE EQUATIONS

Starting with the hydraulic motor dynamics the differential equation can be by using Newton's 2nd law for rotations be expressed as

$$\ddot{x}_m = \frac{1}{I_m} \left[ \frac{D_m}{2\pi} \Delta p - F_f(\dot{x}_m) - T_{load} \right] \quad (2)$$

where  $x_m$  is the hydraulic motor angle,  $I_m$  is the inertia of rotation,  $D_m$  is the motor displacement,  $\beta$  is the bulk modulus which is assumed constant,  $\Delta p$  is the differential pressure across the motor,  $F_f(\dot{x}_m)$  is the motor friction and  $T_{load}$  is the motor loading, assumed measurable. This is not completely true because the motor loading is hard to measure and must be estimated, but as for now it is assumed measurable. The motor friction containing static friction, coulomb friction and linear friction is hard to express accurately in reality and feedback of uncertain values are never recommended.

*Proposition 1.* Since the coulomb friction for the hydraulic motor is hard to quantify in reality, assumed small and since feedback of uncertain values are not recommended, the coulomb friction is neglected, accepting the errors this leads to, and the total motor friction is assumed to consist of only linear friction.

*Hypothesis 2.* The contributions from the coulomb friction are assumed small and last only for a short period of time. Thus the coulomb friction can be neglected in the control state equations causing negligible errors.

By using Proposition 1 and Hypothesis 2 the motor friction can be expressed as

$$F_f(\dot{x}_m) = F_s \mu_v \dot{x}_m \quad (3)$$

where  $F_s$  is the static friction and  $\mu_v$  is a linear friction coefficient. In reality the friction would be dependent on the load of the motor, causing the surfaces in the hydraulic motor to be pushed closer to each other giving a higher friction. However this effect are assumed small and neglected. By defining

$$\begin{aligned} \dot{x}_{m1} &:= x_{m2} \\ \dot{x}_{m2} &:= \ddot{x}_m \end{aligned} \quad (4)$$

the second order differential equation describing the hydraulic motor dynamics can be equated as

$$\begin{aligned} \dot{x}_{m1} &= x_{m2} \\ \dot{x}_{m2} &= \frac{1}{I_m} \left[ \frac{D_m}{2\pi} \Delta p - F_s \mu_v x_{m2} - T_{load} \right] \end{aligned} \quad (5)$$

In (5)  $\Delta p$  is treated as the control input to the differential equation and has its own dynamics described by the flow characteristics through the main valves, the hydraulic motor velocity, the internal motor leakages, the volumes on each side of the motor and the control slide positions in the main valves.

*Hypothesis 3.* Since the two main valves are controlled in 4/3-mode, having the opposite displacement of each other, the flow through the two valves are assumed to be equal. From a control design point of view the pressure losses through the valves are also assumed equal.

Starting with the volumes on each side of the hydraulic motor and Bernoulli's equation the accumulated volume can be expressed as

$$\dot{x}_a = \begin{cases} \alpha \pi D_s u \sqrt{\frac{2p_L}{\rho}} & \text{for } p_L \geq 0 \\ 0 & \text{else} \end{cases} \quad (6)$$

where  $\alpha$  is a flow coefficient describing the flow through the valve opening,  $u$  is the ideal control input to the inner

controller giving the reference position to an ideal main valve without dead band on the hoisting side of the motor,  $D_s$  is the hydraulic diameter in the main valves,  $A = \pi D_s u$  is the approximated opening area in the control slide,  $p_L$  is the pressure losses due to flow through the main valve and  $\rho$  is the density of the hydraulic fluid. Note that  $\dot{x}_a = 0$  when  $p_L < 0$ . This is only true for  $u \geq 0$  because of the check-valves between the pressure line and the main valves. However this is relaxed by adjusting the expression for  $p_L$  to also be valid in this case. Also note that the motor velocity and the internal leakages have not yet been included.

By using Hypothesis 3 the pressure losses through the two main valves may be expressed as

$$2p_L = P_{pump} - T_{pump} - \text{sign}(u) \Delta p \quad (7)$$

where  $P_{pump}$  is the main pump system pressure and  $T_{pump}$  is the return pressure in the main return pipeline. By rearranging (7) and defining  $\Delta_{pump} := P_{pump} - T_{pump}$  the pressure losses through one of the main valves can be expressed as

$$p_L = \frac{1}{2} (\Delta_{pump} - \text{sign}(u) \Delta p) \quad (8)$$

By inserting (8) in (6) the accumulated volume can be expressed as

$$\dot{x}_a = \begin{cases} \alpha \pi D_s u \sqrt{\frac{\Delta_{pump} - \text{sign}(u) \Delta p}{\rho}} & \text{for } p_L \geq 0 \\ 0 & \text{else} \end{cases} \quad (9)$$

*Hypothesis 4.* The pressure relief valve is fast and the flow from the main pump system is high, ensuring that  $\Delta_{pump} > \Delta p$ .

By using Hypothesis 4, (9) can be reduced to

$$\dot{x}_a = \alpha \pi D_s u \sqrt{\frac{\Delta_{pump} - \text{sign}(u) \Delta p}{\rho}} \quad (10)$$

The pressure in the volume is defined as

$$p_a := \frac{\beta x_a}{V_a} \quad (11)$$

where  $\beta$  is the bulk modulus which is assumed constant and  $V_a$  is the initial volume.

*Hypothesis 5.* The differential pressure,  $\Delta p$ , can be approximated as the mean value of the accumulated volumes on each side of the hydraulic motor.

By defining the positive hydraulic motor velocity as clockwise in figure 1, main valve A as the main valve on the left side of the motor and main valve B as the main valve on the right side of the motor, the derivative of the differential pressure,  $\Delta \dot{p}$ , can be approximated by using Hypothesis 5 and (11),

$$x_M = \frac{x_A + x_B}{2} \quad (12)$$

which gives

$$\begin{aligned} \Delta \dot{p} &= \frac{\beta \dot{x}_M}{V_M} \\ &= \frac{\alpha \beta \pi D_s u}{V_M \sqrt{\rho}} \sqrt{\Delta_{pump} - \text{sign}(u) \Delta p} - H(x_{m2}, \Delta p) \end{aligned} \quad (13)$$

where  $H(x_{m2}, \Delta p)$  includes the effect of motor pumping when the motor rotates and the internal leakages in the motor,

$$H(x_{m2}, \Delta p) = \frac{\beta D_m}{2\pi V_M} x_{m2} + \frac{\beta G}{V_M} \Delta p \quad (14)$$

By setting  $V_M = V$  and inserting (14) into (13) the differential equation describing the differential pressure can be expressed as

$$\Delta \dot{p} = \frac{\alpha \beta \pi D_s u}{V \sqrt{\rho}} \sqrt{\Delta_{pump} - \text{sign}(u) \Delta p} - \frac{\beta D_m}{2\pi V} x_{m2} - \frac{\beta G}{V} \Delta p \quad (15)$$

The simplified state equations describing the hydraulic motor dynamics and the differential pressure across the motor have now been derived. The hypotheses used must be verified in the end by simulations using the derived control laws.

### 3. SPEED CONTROLLER

To design a suitable speed control law, controlling the hydraulic motor velocity, a sliding mode controller with backstepping is to be derived. Sliding mode controller designs are robust controller designs that forces trajectories to reach a sliding manifold in finite time and stay on the manifold for all future time according to Khalil (2002). A sliding mode controller is also designed to achieve the control objective even though a lower order control model is used to describe the process. Backstepping is added to the controller design because more than one state equation is used to describe the motor velocity. Backstepping also gives the ability to give undesired dynamics in feedback and cancel them out.

First, (5) must be rewritten to describe the error defined as the difference between the motor velocity and the reference velocity. By defining

$$e_2 := x_{m2} - x_{d2} \quad (16)$$

the error dynamics can be written as

$$\begin{aligned} \dot{e}_1 &= e_2 \\ \dot{e}_2 &= \frac{1}{I_m} \left[ \frac{D_m}{2\pi} \Delta p - F_s \mu_v x_{m2} - T_{load} \right] - \dot{x}_{d2} \end{aligned} \quad (17)$$

Defining

$$z_{s1} := e_2 \quad (18)$$

as virtual control in the first differential equation and

$$s_1 := z_{s1} + k_1 \int_0^t z_{s1} dt \quad (19)$$

as the first sliding surface where  $k_1$  is a gain and a tuning parameter. The derivative of the first sliding surface is

$$\begin{aligned} \dot{s}_1 &= \dot{z}_{s1} + k_1 z_{s1} \\ &= \frac{D_m}{2\pi} \Delta p - \frac{F_s \mu_v}{I_m} x_{m2} - \frac{T_{load}}{I_m} - \dot{x}_{d2} + k_1 z_{s1} \end{aligned} \quad (20)$$

Using the lyapunov function

$$V_{s1} = \frac{1}{2} s_1^2 \quad (21)$$

gives

$$\begin{aligned} \dot{V}_{s1} &= s_1 \dot{s}_1 \\ &= s_1 \left( \frac{D_m}{2\pi I_m} \Delta p - \frac{F_s \mu_v}{I_m} x_{m2} - \frac{T_{load}}{I_m} - \dot{x}_{d2} + k_1 z_{s1} \right) \end{aligned} \quad (22)$$

The next step is to define

$$\begin{aligned} \Delta p &:= v_1 \\ &= \frac{2\pi I_m}{D_m} \left( \frac{F_s \mu_v}{I_m} x_{m2} + \frac{T_{load}}{I_m} + \dot{x}_{d2} \right) \\ &\quad - \frac{2\pi I_m}{D_m} (D_2 s_1 + k_2 \text{sign}(s_1)) \end{aligned} \quad (23)$$

where  $D_2$  and  $k_2$  are tuning parameters and  $v_1$  is a virtual control variable. This gives

$$\begin{aligned} \dot{V}_{s1} &= s_1 (k_1 z_{s1} - D_2 s_1 - k_2 \text{sign}(s_1)) \\ &\leq -D_2 (1 - \theta) \|s_1\|_2^2 - D_2 \theta \|s_1\|_2^2 \\ &\quad - k_2 s_1 \text{sign}(s_1) + k_1 \|z_{s1}\|_2 \|s_1\|_2 \\ &\leq -D_2 (1 - \theta) \|s_1\|_2^2 - k_2 s_1 \text{sign}(s_1) \end{aligned} \quad (24)$$

for  $\|s_1\|_2 \geq \frac{k_1 \|z_{s1}\|_2}{D_2 \theta}$ , which means that the solutions are globally uniformly ultimately bounded according to Theorem 4.18 in Khalil (2002) (given in Theorem 6 in Appendix), under the assumption that  $z_{s1}$  is bounded.  $\theta$  is a parameter chosen to be  $0 < \theta < 1$ . Next, the second sliding surface is defined as

$$s_2 := s_1 + z_{s2} \quad (25)$$

where

$$z_{s2} := \Delta p - v_1 = s_2 - s_1 \quad (26)$$

This changes (24) to

$$\begin{aligned} \dot{V}_{s1} &= -D_2 s_1^2 - k_2 s_1 \text{sign}(s_1) + k_1 z_{s1} s_1 \\ &\quad - \frac{D_m}{2\pi} s_1^2 + \frac{D_m}{2\pi} s_1 s_2 \\ &\leq -D_2 (1 - \theta) \|s_1\|_2^2 - k_2 s_1 \text{sign}(s_1) \\ &\quad - \frac{D_m}{2\pi} \|s_1\|_2^2 + \frac{D_m}{2\pi} s_1 s_2 \end{aligned} \quad (27)$$

for  $\|s_1\|_2 \geq \frac{k_1 \|z_{s1}\|_2}{D_2 \theta}$ .

The last term in (27) must be included in the derivative of the second sliding surface which is given as

$$\begin{aligned} \dot{s}_2 &= \dot{s}_1 + \dot{z}_{s2} \\ &= k_1 z_{s1} - D_2 s_1 - k_2 \text{sign}(s_1) + \frac{D_m}{2\pi I_m} s_1 - \dot{v}_1 \\ &\quad + \frac{\beta \alpha \pi D_s}{V \sqrt{\rho}} u \sqrt{\Delta_{pump} - \text{sign}(u) \Delta p} \\ &\quad - \frac{\beta D_m}{2\pi V} x_{m2} - \frac{\beta G}{V} \Delta p \end{aligned} \quad (28)$$

Note that  $s_1 s_2$  is replaced with  $s_1$  because of the lyapunov function ( $s_2 \dot{s}_2$ ). The second lyapunov function is given as

$$V_{s2} = \frac{1}{2} s_2^2 \quad (29)$$

Differentiating gives

$$\begin{aligned}\dot{V}_{s_2} &= s_2 \dot{s}_2 \\ &= s_2 \left( k_1 z_{s1} - D_2 s_1 - k_2 \text{sign}(s_1) + \frac{D_m}{2\pi I_m} s_1 \right. \\ &\quad \left. - \dot{v}_1 + \frac{\beta \alpha \pi D_s}{V \sqrt{\rho}} u H \sqrt{\Delta p_{pump} - \text{sign}(u) \Delta p} \right. \\ &\quad \left. - \frac{\beta D_m}{2\pi V} x_{m2} - \frac{\beta G}{V} \Delta p \right)\end{aligned}\quad (30)$$

By choosing

$$\begin{aligned}u &= \frac{V \sqrt{\rho}}{\beta \alpha \pi D_s \sqrt{p_L(u_{pre})}} \left( -k_1 z_{s1} + D_2 s_1 + k_2 \text{sign}(s_1) \right. \\ &\quad \left. - \frac{D_m}{2\pi I_m} s_1 + \dot{v}_1 + \frac{\beta D_m}{2\pi V} x_{m2} \right. \\ &\quad \left. - D_3 s_2 - k_3 \text{sign}(s_2) + \frac{\beta G}{V} \Delta p \right)\end{aligned}\quad (31)$$

where

$$p_L(u_{pre}) = \Delta p_{pump} - \text{sign}(u_{pre}) \Delta p \quad (32)$$

the derivative of the second lyapunov function is reduced to

$$\begin{aligned}\dot{V}_{s_2} &= -D_3 s_2^2 - k_3 s_2 \text{sign}(s_2) \\ &< 0\end{aligned}\quad (33)$$

where  $D_3$  and  $k_3$  are controller gains and tuning parameters. Note that  $u_{pre}$ , which is the previous controller output, is used in the square root in the control law instead of  $u$ .

Since the last sliding surface includes the first sliding surface, stability of the given control law is guaranteed by  $V_{s_2}$ . By using LaSalle's Theorem (given in Theorem 7 in Appendix), globally asymptotically stability, GAS, can be concluded for the system using  $V_{s_2}$  because

$$s_2 = 0 \implies s_1 + z_{s2} = 0 \quad (34)$$

which means that the solution is on the second sliding surface and will converge to  $(s_1, z_{s2}) = (0, 0)$  in finite time. This is shown graphically in figure 2.

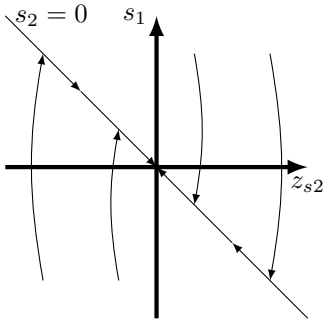


Fig. 2. Graphically representation of the second sliding surface.

In addition to the control law (31), some logics preventing division by zero in the control law must be included in the controller design. Also numerically derivation of  $v_1$  should be considered. To overcome the dead bands in the main valves a step over the dead bands is added using an  $\arctan(\cdot)$  function, and to prevent too high controller outputs the controller output is saturated. The controller output is now given as

$$x_H = \text{limit} \left( u + \frac{2x_{olap}}{\pi} \arctan(s \cdot u), -x_{max}, x_{max} \right) \quad (35)$$

where  $x_{max}$  is the maximal displacement of the control slide and  $s$  is a design parameter describing the slope of the  $\arctan(\cdot)$ -function. Note that  $x_H$  is fed to main valve A and  $x_L = -x_H$  is fed to main valve B.

The controller parameters are set to  $k_1 = 900 \text{ 1/s}$ ,  $D_2 = 800 \text{ 1/s}$ ,  $k_2 = 0.01 \text{ rad/s}^2$ ,  $D_3 = 20 \text{ Pa/rad}$ ,  $k_3 = 1000 \text{ Pa/s}$ ,  $s = 200000$ -,  $\tau_1 = 0.01 \text{ s}$  and  $\tau_2 = 0.01 \text{ s}$ .  $\tau_1$  and  $\tau_2$  are time constants in the low pass filters, filtering the differential pressure and the measured motor torque respectively.

#### 4. TORQUE CONTROLLER

Also to design a suitable torque control law, controlling the hydraulic motor torque, a sliding mode controller is to be derived. Now backstepping is not included since only one state equation is used in the controller design. As for the speed controller the tracking error in the torque controller is defined as

$$e_T = T_m - T_{dm} \quad (36)$$

where  $T_m$  is the measured torque and  $T_{dm}$  is the desired torque. By using the fact that

$$T_m := \frac{D_m}{2\pi} \Delta p \quad (37)$$

and (15) the error dynamics may be expressed as

$$\begin{aligned}\dot{e}_T &= \frac{\beta \alpha \pi D_s D_m}{2\pi V \sqrt{\rho}} u \sqrt{\Delta p_{pump} - \text{sign}(u) \Delta p} \\ &\quad - \frac{\beta D_m^2}{4\pi^2 V} x_{m2} - \frac{\beta G D_m}{2\pi V} \Delta p - \dot{T}_{dm}\end{aligned}\quad (38)$$

The sliding surface is defined as

$$s := e_T + k_1 \int_0^t e_T dt \quad (39)$$

Differentiating gives

$$\begin{aligned}\dot{s} &= \dot{e}_T + k_1 e_T \\ &= \frac{\beta \alpha \pi D_s D_m}{2\pi V \sqrt{\rho}} u \sqrt{\Delta p_{pump} - \text{sign}(u) \Delta p} \\ &\quad - \frac{\beta D_m^2}{4\pi^2 V} x_{m2} - \frac{\beta G D_m}{2\pi V} \Delta p - \dot{T}_{dm} + k_1 e_T\end{aligned}\quad (40)$$

and by using

$$V_s = \frac{1}{2} s^2 \quad (41)$$

as lyapunov function the derivative of the lyapunov function is given as

$$\begin{aligned}\dot{V}_s &= s \dot{s} \\ &= s \left( \frac{\beta \alpha \pi D_s D_m}{2\pi V \sqrt{\rho}} u \sqrt{\Delta p_{pump} - \text{sign}(u) \Delta p} \right. \\ &\quad \left. - \frac{\beta D_m^2}{4\pi^2 V} x_{m2} - \frac{\beta G D_m}{2\pi V} \Delta p - \dot{T}_{dm} + k_1 e_T \right)\end{aligned}\quad (42)$$

By choosing

$$\begin{aligned}u &= \frac{2V \sqrt{\rho}}{\beta \alpha \pi D_s D_m \sqrt{p_L(u_{pre})}} \left( \frac{\beta D_m^2}{4\pi^2 V} x_{m2} + \frac{\beta G D_m}{2\pi V} \Delta p + \dot{T}_{dm} \right. \\ &\quad \left. - k_1 e_T - D_2 s - k_2 \text{sign}(s) \right)\end{aligned}\quad (43)$$

where  $k_2$  and  $D_2$  are controller gains, the derivative of the lyapunov function is reduced to

$$\dot{V}_s = -Ds^2 - k_2 \text{sign}(s)s \quad (44)$$

which means that globally exponential stability, GES, is achieved according to Theorem 4.10 in Khalil (2002) (given in Theorem 8 in Appendix). The same logics as for the speed control must be implemented in the torque controller to avoid dividing by zero or taking the square root of a negative number. The controller outputs are given as before,

$$\begin{aligned} x_H &= \text{limit} \left( u + \frac{2x_{olap}}{\pi} \arctan(s \cdot u), -x_{max}, x_{max} \right) \\ x_L &= -x_H \end{aligned} \quad (45)$$

The controller parameters are set to  $k_1 = 5 \text{ }^1/\text{s}$ ,  $k_2 = 1000 \text{ Nm}/\text{s}$ ,  $D_2 = 9000 \text{ }^1/\text{s}$ ,  $\tau = 0.2 \text{ s}$  and  $s = 50000$ .  $\tau$  is the time constant in a low pass filter used to filter the differential pressure across the hydraulic motor. Note that  $s$  is set lower in this controller compared to the speed controller. This is to reduce the large pressure peaks generated when passing the dead bands in the main valves. The pressure peaks are high and the controller should not be so fast that it tries to control these peaks. If so the controller would become unstable because of all the peaks and variations in the differential pressure that has not been filtered out. It is also expected that the tuning of the outer controller is affected by the inner controller.

## 5. IMPLEMENTATION AND TESTING

As mentioned before, there must be some logics implemented to ensure that dividing by zero and squaring negative numbers in the control laws does not happen. This is avoided by implementing an IF-ELSE logic, given by Algorithm 1,

**Algorithm 1.** Algorithm for avoiding dividing by zero and squaring negative values.

```

 $p_L(u_{pre}) = \Delta_{pump} - \text{sign}(u_{pre})\Delta p$ 
if  $p_L(u_{pre}) \leq 0$  then
   $\hat{u} = 0$ 
else
   $\hat{u} = u$ 
end if

```

where  $\hat{u}$  is the controller output and used instead of  $u$  in (35) and (45), and  $u$  is given by (31) and (43). The differentiations in the controllers are calculated numerically,

$$\dot{x} = \frac{x - x_{pre}}{T_s} \quad (46)$$

where  $x_{pre}$  is the value of the variable in the previous step and  $T_s$  is the sample time. Also integrations are done numerically,

$$\int_0^t x dt = \int_0^t x_{pre} dt + T_s x \quad (47)$$

This is the simplest way of differentiating and integrating a variable and would bring errors into the control laws.

Both controllers are tested in a rough environment. It is assumed that all variables needed in the control laws are available and measurable. All measurements are assumed to be influenced by a sampling delay of  $T_{delay} = 0.002 \text{ s}$ .

### 5.1 Simulation with Speed Controller

The speed controller is tested in an AHC-, Active Heave Compensation, case where a MRU, Motion Reference Unit, gives the reference velocity to the speed controller. It is assumed that data from the MRU gives the heave velocity of the vessel and the hydraulic motor velocity reference is then calculated as

$$x_{d2} = -\frac{2\dot{\eta}n}{D_r(L_w)} \quad (48)$$

where  $\dot{\eta}$  is the heave velocity,  $n$  is the gear ratio between the hydraulic motor and the reel and  $D_r(L_w)$  is the diameter of the reel. This diameter is varying with the length of wire stored,  $L_w$ , and must be estimated or measured.

The heave motion is assumed to be equal to a  $\sin(\cdot)$ -wave,

$$\eta = -\text{step}(\psi)\eta_A \sin(\omega t - \epsilon) \quad (49)$$

propagating with an amplitude of  $\eta_A = 2 \text{ m}$  and a variable frequency, starting with  $\omega = 0 \text{ rad}/\text{s}$  and ending with  $\omega = 8 \text{ rad}/\text{s}$ . Note that these frequencies are not expected to appear in reality, but are only used here to test the controller. This heave motion is initiated at  $t = \epsilon = 5 \text{ s}$  in the simulation. The heave velocity is then given as

$$\dot{\eta} = -\omega \text{step}(\psi)\eta_A \cos(\omega t - \epsilon) \quad (50)$$

The horizontal top wire position is assumed to be zero. The initial length of submerged wire is set to  $L_{ws} = 100 \text{ m}$ , the load in the end of the wire is set to  $m_{Load} = 3000 \text{ kg}$ , assumed having a spherical volume with a diameter of  $1 \text{ m}$  and the horizontal current velocity is set to  $V_{x,c} = 2 \text{ m}/\text{s}$ . The speed controller is initiated at  $t = 0.1 \text{ s}$  and the total simulation time is set to  $30 \text{ s}$ .

Figure 3 shows the hydraulic motor velocity compared to the reference.

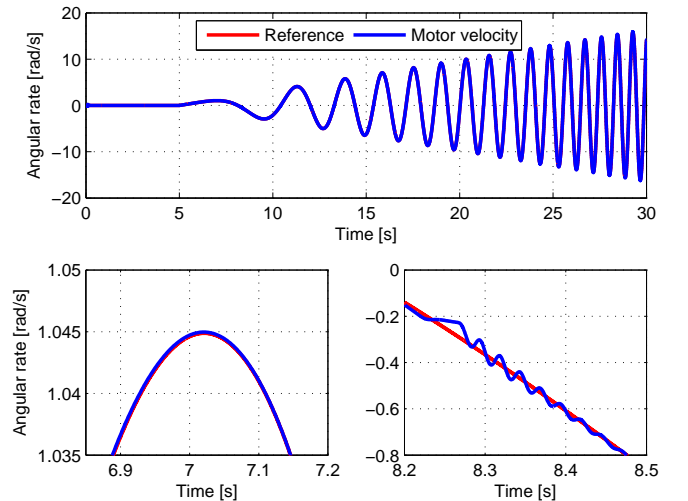


Fig. 3. Hydraulic motor velocity.

As can be seen in the figure the hydraulic motor velocity coincides with the reference velocity, even when the frequency and the amplitude are high at the end of the simulation. It may look like the motor velocity is unstable, but since the frequency of the heave motion of the vessel increases, so does the amplitude and the frequency in the

heave velocity. The maximal motor velocity at the end of the simulation is about  $16 \text{ rad/s}$ ,  $\approx 153 \text{ rpm}$  and may be higher than what is expected for such a motor. The plot in the lower right corner in the figure shows a magnified area of the motor velocity compared to the reference when the control slides in the main valves cross the dead bands. The motor velocity oscillates a bit before stabilized fixed at the reference. These oscillations can not be compensated for since they appear when the main valves are closed. However the oscillations are small showing that the arctan( $\cdot$ )-function given in (35), that was added to the controller output, helps the control slides in the main valves to cross the dead bands as fast as possible to minimize the crossing effects. The figure in the lower left corner shows a magnified area of the maximal motor velocity compared to the reference in the first oscillation in order to show the tracking performance of the controller. The plot shows that the tracking error is small and except for some inertia effects and sampling delays the motor velocity seems to coincide with the reference. This is emphasized in figure 4.

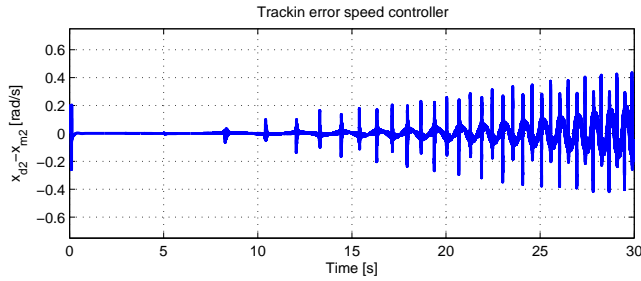


Fig. 4. Tracking error in speed controller.

As expected the tracking error increases during the simulation with the increase of  $\omega$ . The plot also shows some peaks of tracking error that have a magnitude of about  $0.4 \text{ rad/s}$  in the end of the simulation. These peaks are generated when the control slides cross the dead bands in the main valves and can not be compensated for except for what is already done. When neglecting these peaks the tracking error at the end of the simulation has a maximal absolute value of about  $0.2 \text{ rad/s}$ ,  $\approx 1.91 \text{ rpm}$ . This is low compared to the rough test the speed controller experiences.

Figure 5 shows the positions of the control slides in the main valves compared to the references given by the speed controller.

The first plot compares the two control slide positions with the reference positions and shows that the positions seem to coincide with the references. This suggests that the inner PD-controllers used to control the control slide positions seem to be stable, robust and fast enough follow the references given by the outer speed controller. This is emphasized in the plot in the lower left corner in the figure which shows that the control slide position for main valve A coincides with the reference when neglecting the sample delays. The plot in the lower right corner shows a crossing of the dead bands in the main valves. Also the crossings seem to be stable and done in about  $0.03 \text{ s}$ . The control slide positions compared to the references seem to deviate a bit but follow through and are stabilized after the crossing.

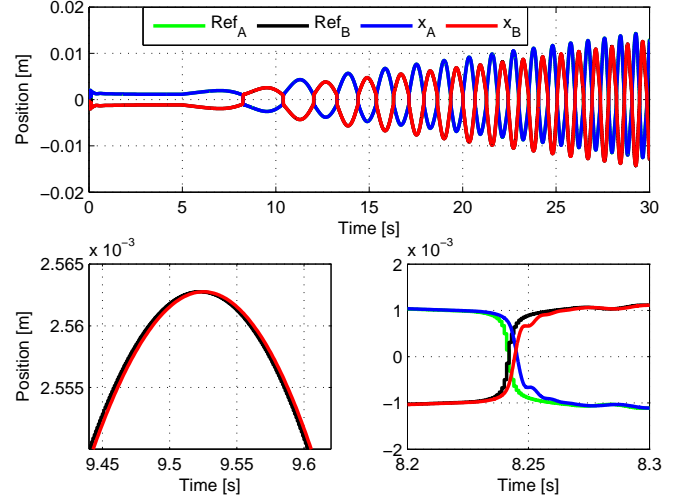


Fig. 5. Control slide positions in main valves and references.

The top vertical wire position and the load position are shown in figure 6.

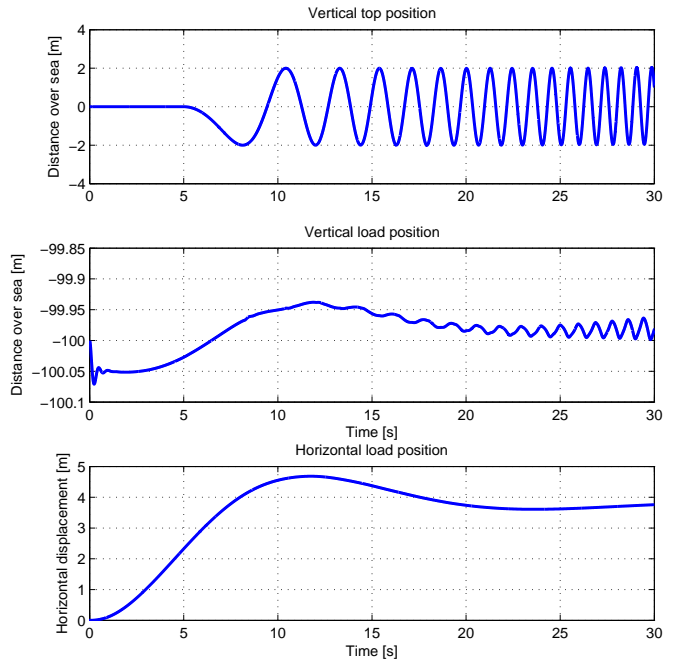


Fig. 6. Top vertical wire position and load position.

The first plot in the figure shows the heave position at the top end of the wire. It has the same form as the heave position given in (49) with increasing  $\omega$ . The second plot shows the horizontal load position, starting at a submerged position of  $100 \text{ m}$  below the sea surface. The load is stabilized at  $100.05 \text{ m}$  below the surface, because the load stretches the wire a bit, before it is lifted about  $10 \text{ cm}$  due to the horizontal current forces. After a while some oscillations with a maximal amplitude of about  $2 \text{ cm}$  can be seen at the end of the simulation. This comes as a result of the tracking error in the controller caused by the

high frequencies in the reference velocity. The last plot in the figure shows the horizontal load displacement of the load which is induced by the current. The displacement seems to stabilize around 4m and causes the lift of the load which seems to have the same characteristics as the horizontal displacement. To get a better understanding of the submerged wire displacement the wire is plotted through the simulation for time steps with an increment of 0.5s in figure 7. Darker color shows the wire displacement with increasing simulation time.

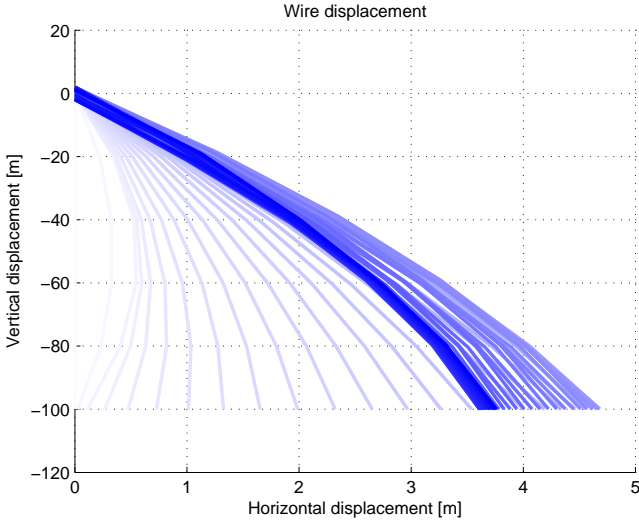


Fig. 7. Submerged wire displacement at time steps of  $t=0.5s$  where darker color denotes higher simulation time.

The influence of the high current velocity on the wire and the load is significant and the speed controller does not have the ability to keep the load at the initial depth since no measurements of this are available. One can also see an overshoot of the horizontal displacement of the wire. This is due to high current forces and inertia of the load. The hydrodynamic damping is small since the load geometry is assumed spherical and the horizontal wire displacement gets an overshoot before stabilized.

### 5.2 Simulation with Torque Controller

The same controller test as described in section 5.1 is used to test the torque controller, but no MRU measurements are used. The reference torque is set to a constant value,  $T_{dm} = 26910 Nm$ , close to the torque that is required to hold the load. The torque controller is initiated at 0.5s. Figure 8 compares the motor torque and the reference torque. Note that the motor torque is calculated from the differential pressure across the motor,  $\Delta p$ .

The first plot shows the motor torque compared to the reference torque. As for the speed controller simulation the error seems to grow through the simulation with the increase of  $\omega$ . The torque controller is not tuned as hard as the speed controller due to stability reasons. The differential pressure varies much more than the motor velocity and is filtered more to avoid compensating too much for the pressure peaks generated when crossing the dead bands in the main valves. The largest deviations

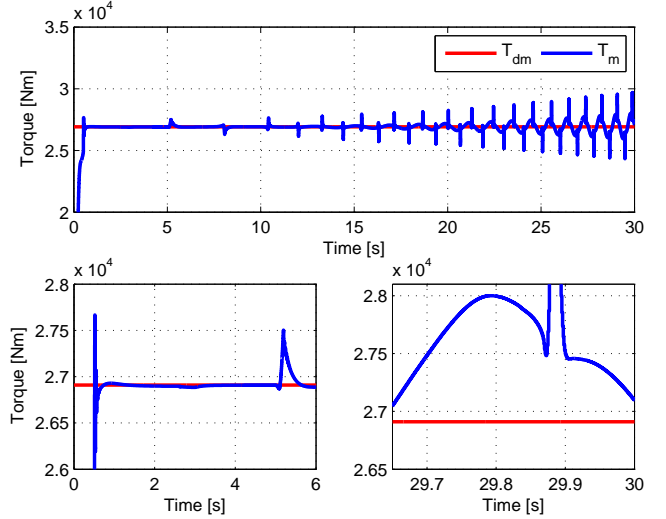


Fig. 8. Hydraulic motor torque and reference torque.

from the reference torque seem to be generated by such peaks and when neglecting these the difference between the motor torque and the reference torque is not that large when having in mind the rough test the torque controller experiences. The plot in the lower left corner shows the stabilization of the controller after initiation and it takes about 0.5s to reach the reference torque. There is also a torque peak at  $t=5s$  that comes from the initiation of the heave motion. The plot in the lower right corner shows the maximal deviation between the motor torque and the reference torque when neglecting the pressure peaks.

Figure 9 shows the tracking error, given as a percentage of the reference torque, and the hydraulic motor velocity.

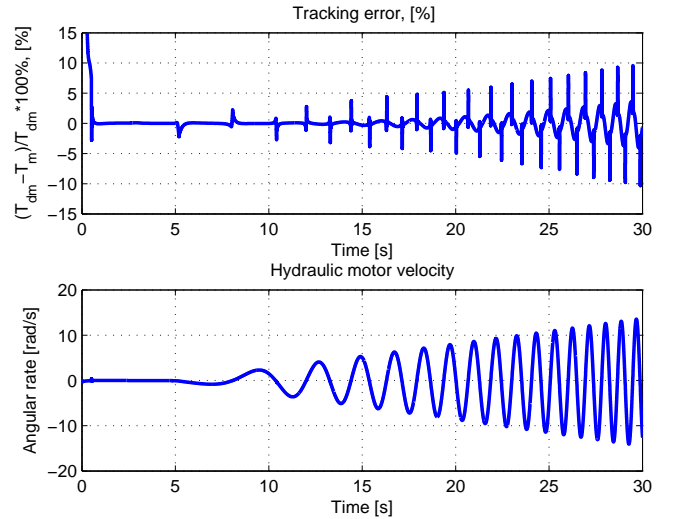


Fig. 9. Tracking error in torque controller and hydraulic motor velocity.

The first plot shows that the tracking error is below 5% when neglecting the peaks. Since the differential pressure is filtered more for the torque controller than for the speed controller, less is compensated for when a pressure peak appears. The motor torque used to calculate the tracking

error is not filtered and is not the same tracking error as the torque controller uses. The second plot shows the hydraulic motor velocity which compared to figure 3 seems to be equal. However the maximal motor velocity at the end of the simulation is a bit lower in this case, about  $14 \text{ rad/s}$ ,  $\approx 133.8 \text{ rpm}$ , which is about 12.5 % lower than for the simulation testing the speed controller, see figure 3.

Figure 10 shows the control slide positions in the main valves compared to the references given by the outer torque controller. For reference the valve dynamics are elaborated in Skjong (2014).

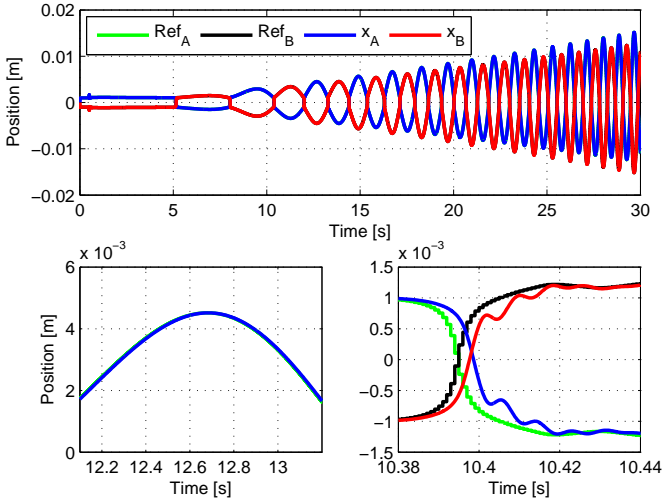


Fig. 10. Control slide positions in main valves and references.

The first plot shows that the control slide positions seem to coincide with the references, which is emphasized in the two next plots. This suggest that the inner PD-controller works good for its purpose. One can also see that the valve dynamics are really fast. This is due to high pressures and high capacity in the pump system. The plot in the lower left corner shows a magnified area around the control slide position in main valve A and its reference. The position seems to coincide with the reference also in this simulation. The last plot given in the lower right corner shows a crossing of the dead bands in the main valves. Compared to figure 5 the control slide positions seem to contain more oscillations in the crossing. These come from the pressures in the fluid volume on the load side of the hydraulic motor that increases because the motor also rotates a bit when the main valves are closed. This is felt in the differential pressure measurements that are fed to the torque controller. Figure 11 shows the top end vertical wire position and the load position.

The first plot shows the heave position of the top end of the wire which is equal to (49). The second plot shows the vertical load position and shows that the load is lowered. This can be explained by the fact that the reference torque was set a bit too low to hold the load by itself and when the current forces are added the load is lowered. The velocity of the lowering increases as the length of the submerged wire grows larger due to increased load. Also in this simulation small oscillations with a maximal

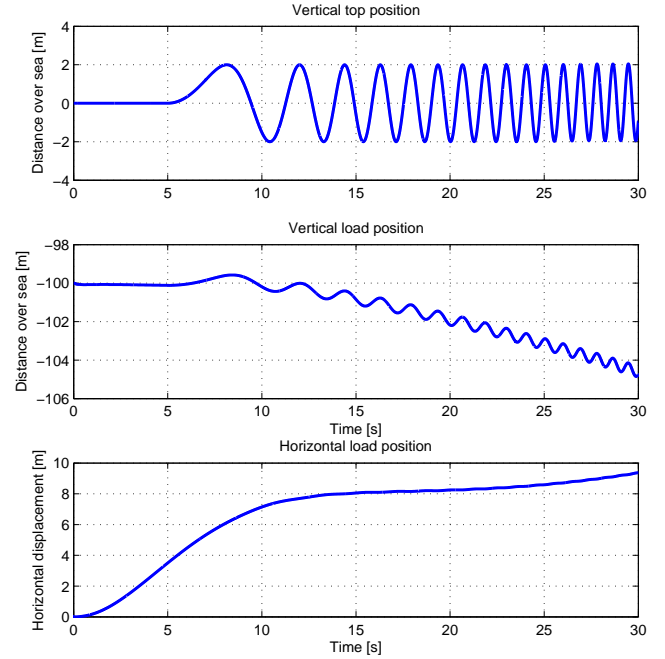


Fig. 11. Top vertical wire position and load position.

amplitude of about 0.25 m can be seen due to the tracking error. The last plot shows the horizontal load position that seems to increase without stabilizing through the simulation. This is as expected since the load is lowered and the total current forces grow with increasing length of submerged wire. To get a better understanding of the submerged wire displacement the wire is plotted through the simulation for time steps with an increment of 0.5 s in figure 12. Also in this case darker color shows the wire displacement with increasing simulation time.

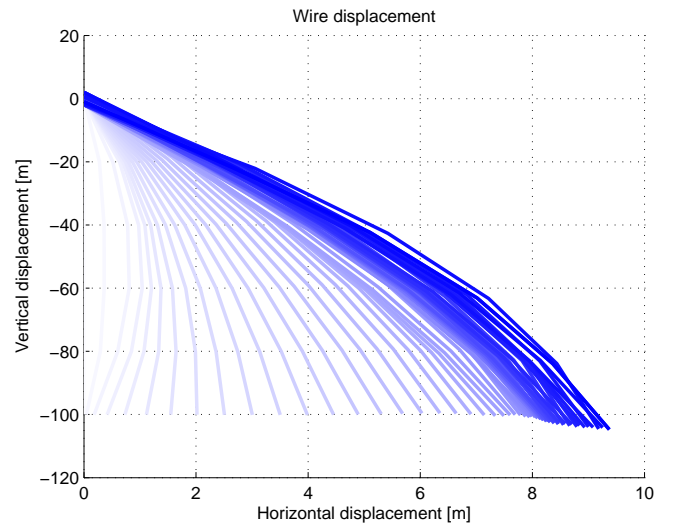


Fig. 12. Submerged wire displacement at time steps of  $t=0.5 \text{ s}$  where darker color denotes higher simulation time.

The horizontal wire displacement has not an overshoot like in figure 7 but keeps growing due to the increase of



submerged wire length. By assuming that the reference torque could be set accurately to hold the load and updated due to the increase in length of submerged wire it would be reasonable to assume that the horizontal wire displacement would stabilize and the vertical load position would be almost constant except for the oscillations.

## 6. CONCLUSION

A speed controller and a torque controller have been derived using sliding mode control theory, backstepping control theory and simplified state equations for the hydraulic system presented in figure 1. The controllers have been tested using the lumped wire-load model derived in Skjong and Pedersen (2014a), enabling heave motions, hydrodynamic loads and horizontal current acting on the wire and the load. The heave position in the top end of the wire was set as a  $\sin(\cdot)$ -sweep starting at  $t = 5$  s with an amplitude of 2 m and an increasing frequency  $\omega$ , starting at  $0 \text{ rad/s}$  and ending in  $8 \text{ rad/s}$ . As inner controller, controlling the control slide positions in the main valves, PD-controllers were used.

The speed controller got the top end vertical wire velocity, only affected by sampling delays, transformed to angular rate as control input to perform AHC. Both the inner and outer controller showed good responses, minimizing their respective tracking errors. They were both stable and seemed to be robust. The current lifted the load about 10 cm due to a horizontal load displacement of about 4 m. The tracking error in the speed controller was about  $0.2 \text{ rad/s}$  at the end of the simulation, giving an error of approximately 1.25% compared to the reference velocity. Some oscillations were spotted at the vertical load position having a maximal amplitude of about 2 cm, about 0.02% of the total length of the submerged wire. These results show that the speed controller is well suited for AHC, even in harsh environment including high current velocities and large heave motions having high frequencies.

The torque controller had a constant torque reference which was set a bit too low to hold the load and as a result the load was slowly lowered. However the motor velocity induced through torque control is comparable to the motor velocity in the speed control test. The torque controller was tuned to be slower compared to the speed controller due to large variations in the differential pressure but managed to force the tracking error below 5% compared to the reference torque. The current forces forced the torque controller to lower the load even more but the heave induced vertical load position oscillations had only a maximal amplitude of about 0.25 m, about 0.25% of the total length of the submerged wire. The torque controller may not be as good in AHC operations as the speed controller, but the results show that the torque controller together with the inner PD-controllers were stable and seemed robust. The torque controller has its strengths in feeling the transient loads acting on the wire and the load, and when the load has a large volume the hydrodynamic forces will be larger making it possible for the torque controller to perform even better.

Both controllers were influenced by sampling delays and low pass filtering generating tracking errors. When the frequency of the heave motion was increased these effects

had larger influence and played a significant role in the controller tracking errors together with the dead band crossings in the main valves. As seen in figure 7 and figure 12 the load is lifted in the speed controller simulation but lowered in the torque controller simulation. A mean of these results would be desired, but the two controllers can not be initiated at the same time. However by choosing the right references for the two controllers the heave motion of the load can be minimized, giving good results.

In an offshore winch operation a hybrid control system containing both controllers would be preferred. Controller functionalities like anti-spin, load loss control and torque limitations should be considered. This gives new challenges in assuring stability in control switching. In Hespanha (2002) such topics are discussed and methods for assuring stability are presented. In Skjong and Pedersen (2014b) the two controllers derived in this paper are put together in a hybrid controller and tested.

## ACKNOWLEDGEMENTS

Thanks to Eilif Pedersen at MTC, NTNU, for good discussions around the topics this paper deals with. His vast modeling skills and experiences have given me help many times.

It is also highly appropriate to thank Roger Skjetne and Asgeir Sørensen at MTC, NTNU, for good conversations about the control issues this paper presents.

## REFERENCES

- S. Skjong and E. Pedersen. *Modeling Hydraulic Winch System*, 2014a.
- S. Skjong. *Master Thesis - Modeling, Simulation and Control of Directional Valve System*, 2014.
- D. McCloy and H. R. Martin. *Control of Fluid Power, Analysis and Design*, 1980.
- H. K. Khalil. *Nonlinear Systems*, 2002.
- J. P. Hespanha. *Tutorial on Supervisory Control*, 2002.
- S. Skjong and E. Pedersen. *Control of Hydraulic Winch System (2/2), Hybrid Control Design 2014b*.
- J. Choi. *Robust Control of Hydraulic Actuator using Back-Stepping Sliding Mode Controller*, 2011.
- D. C. Karnopp. *System Dynamics: Modeling and Simulation of Mechatronic Systems*, 2006.
- O. Faltinsen. *Sea Loads on Ships and Offshore Structures*, 1993.

## APPENDIX

The control theorems used when deriving the control laws are presented below.

*Theorem 6.* Theorem 4.18, p.172 in Khalil (2002):

$$\dot{x} = f(x) \quad (51)$$

Let  $D \subset R^n$  be a domain that contains the origin and  $V : [0, \infty] \times D \rightarrow R$  be a continuously differentiable function such that

$$\alpha_1(\|x\|) \leq V(t, x) \leq \alpha_2(\|x\|) \quad (52)$$

$$\frac{\partial V}{\partial t} + \frac{\partial V}{\partial x} f(t, x) \leq -W_3(x), \forall \|x\| \geq \mu > 0 \quad (53)$$

$\forall t \geq 0$  and  $\forall x \in D$ , where  $\alpha_1$  and  $\alpha_2$  are class  $\mathcal{K}$  functions and  $W_3(x)$  is a continuous positive definite function. Take  $r > 0$  such that  $B_r \subset D$  and suppose that

$$\mu < \alpha_2^{-1}(\alpha_1(r)) \quad (54)$$

Then, there exists a class  $\mathcal{KL}$  function  $\beta$  and for every initial state  $x(t_0)$ , satisfying  $\|x(t_0)\| \leq \alpha_2^{-1}(\alpha_1(r))$ , there is  $T \geq 0$  (dependent on  $x(t_0)$  and  $\mu$ ) such that the solution of (51) satisfies

$$\|x(t)\| \leq \beta(\|x(t_0)\|, t - t_0), \forall t_0 \leq t \leq t_0 + T \quad (55)$$

$$\|x(t_0)\| \leq \alpha_1^{-1}(\alpha_2(\mu)), \forall t \geq t_0 + T \quad (56)$$

Moreover, if  $D = R^n$  and  $\alpha_1$  belongs to class  $\mathcal{K}_\infty$ , then (55) and (56) holds for any initial state  $x(t_0)$ , with no restriction on how large  $\mu$  is.

*Theorem 7.* LaSalle's Theorem, p. 128 in Khalil (2002):

Let  $\Omega \subset D$  be a compact set that is positively invariant with respect to (51). Let  $V : D \rightarrow R$  be a continuously differentiable function such that  $\dot{V}(x) \leq 0$  in  $\Omega$ . Let  $E$  be the set of all points in  $\Omega$  where  $\dot{V}(x) = 0$ . Let  $M$  be the largest invariant set in  $E$ . Then every solution starting in  $\Omega$  approaches  $M$  as  $t \rightarrow \infty$ .

*Theorem 8.* Theorem 4.10, p. 154 in Khalil (2002):

$$\dot{x} = f(t, x) \quad (57)$$

Let  $x = 0$  be an equilibrium point for (57) and  $D \subset R^n$  be a domain containing  $x = 0$ . Let  $V : [0, \infty) \times D \rightarrow R$  be a continuously differentiable function such that

$$k_1\|x\|^a \leq V(t, x) \leq k_2\|x\|^a \quad (58)$$

$$\frac{\partial V}{\partial t} + \frac{\partial V}{\partial x} f(t, x) \leq -k_3\|x\|^a \quad (59)$$

$\forall t \geq 0$  and  $\forall x \in D$ , where  $k_1, k_2, k_3$  and  $a$  are positive constants. Then,  $x = 0$  is exponentially stable. If the assumptions hold globally, then  $x = 0$  is globally exponentially stable.

## **B.2 Control of Hydraulic Winch System (2/2)**

### **Hybrid Control Design**

Submitted for publication.

# Control of Hydraulic Winch System (2/2)

## Hybrid Control Design<sup>\*</sup>

Stian Skjong,<sup>\*</sup> Eilif Pedersen<sup>\*\*</sup>

<sup>\*</sup> Department of Marine Technology, Norwegian University of Science and Technology (NTNU), 7491 Trondheim, Norway  
(e-mail: stiansk@stud.ntnu.no)

<sup>\*\*</sup> Associate Professor

Department of Marine Technology, Norwegian University of Science and Technology (NTNU), 7491 Trondheim, Norway  
(e-mail: eilif.pedersen@ntnu.no)

---

**Abstract:** A hybrid control system containing a speed controller and a torque controller, that were derived in Skjong and Pedersen (2014a), is designed for the hydraulic winch system elaborated in Skjong (2014). The backstepping based sliding mode speed controller and the sliding mode torque controller are implemented in a hybrid control system, containing switching restrictions and conditions. Stability and switching logics in the hybrid controller are studied with focus on hybrid control theory used in practice. Dwell-time switching and error restriction based switching are used to obtain switching stability and for avoiding chattering. Different functionalities for the hybrid controller are looked into, giving both the winch operator opportunities to configure the hybrid controller and functionalities to the hydraulic winch system. The hybrid controller is tested in case studies such as load landing on the sea floor, loss of load and stuck load.

*Keywords:* Hydraulic offshore winch control systems · Load landing · Stuck load · Loss of load · Bond graph theory · Dwell time · Switching logics · Operator configurations · AHC · Hybrid control design

---

### 1. INTRODUCTION

In this paper the objective is to combine the speed controller and the torque controller, the outer controllers, derived and tested in Skjong and Pedersen (2014a), in a hybrid control system to control a hydraulic motor driving a winch installed on an offshore vessel. The hydraulic winch system is elaborated in Skjong (2014) and is not described further here other than mentioning that the hydraulic motor is controlled through two 3/3-directional pilot operated valves, the main valves, affected by dead bands, in a 4/3-valve configuration driven by 4/3-directional solenoid valves that are controlled by PD-controllers, the inner controllers. Bond graph theory is used to model a control plant model of the total hydraulic system for controller testing. This model is thoroughly elaborated in Skjong (2014). The speed- and torque controller are model based controllers derived using sliding mode and backstepping control theory and lyapunov stability analysis. Simplified state equations were used in the controller designs because the actual state equations extracted from the bond graph model contained much logics which would have increased the complexity of the controller designs. The simplified state equations are given as

$$\dot{x}_{m1} = x_{m2} \quad (1a)$$

$$\dot{x}_{m2} = \frac{1}{I_m} \left[ \frac{D_m}{2\pi} \Delta p - F_s \mu_v x_{m2} - T_{load} \right] \quad (1b)$$

$$\Delta \dot{p} = \frac{\alpha \beta \pi D_s u}{V \sqrt{\rho}} \sqrt{\Delta p_{pump} - \text{sign}(u) \Delta p} - \frac{\beta D_m}{2\pi V} x_{m2} - \frac{\beta G}{V} \Delta p \quad (1c)$$

where  $x_{m2}$  is the hydraulic motor velocity,  $I_m$  is the rotational inertia,  $D_m$  is the motor displacement per revolution,  $\Delta p$  is the differential pressure across the hydraulic motor,  $F_s$  and  $\mu_v$  are friction parameters,  $T_{load}$  is the loading of the hydraulic motor,  $\alpha$  is a flow coefficient for the 3/3-directional valves that may vary,  $\beta$  is the bulk modulus that is assumed constant,  $D_s$  is the diameter of the control slides (pistons) in the 3/3-directional valves,  $V$  is the fluid volume between the valves and the motor,  $\rho$  is the fluid density,  $\Delta p_{pump}$  is the pressure difference between the pump pressure and the pressure in the return pipeline,  $u$  is the control output before dead band compensation and  $G$  is the conductance of laminar resistance, describing the internal leakages in the hydraulic motor.  $T_{load}$  is seldom measured in such systems and should be estimated or simply neglected. The controllers have been tested without including  $T_{load}$  with equally results in simulations. As for now  $T_{load} = 0$ ,  $\Delta p$  and  $x_{m2}$  are assumed measured. The controller outputs are given as

$$x_H = \text{limit} \left( u + \frac{2x_{olap}}{\pi} \arctan(s \cdot u), -x_{max}, x_{max} \right) \quad (2)$$

where  $x_H$  is the control slide position reference given as input to the inner controller for the main valve on the hoisting side of the motor,  $x_L = -x_H$  is the control slide

---

<sup>\*</sup> Based on the master thesis by Stian Skjong (Skjong, 2014).

position reference given as input to the inner controller for the main valve on the lowering side of the motor.

The speed controller is a backstepping based sliding mode controller. (2) is the equation for the dead band compensation, where  $x_{olap}$  is half the dead band in the main valves,  $s$  is a slope parameter that gives the speed of the jump over the dead bands,  $x_{max}$  is the maximal displacement in the main valves and  $u$  is the control output for the main valve on the hoisting side of the motor for an ideal main valve without dead band and is given as

$$u = \frac{V\sqrt{\rho}}{\beta\alpha\pi D_s\sqrt{p_L(u_{pre})}} \left( -k_1 z_{s1} + D_2 s_1 + k_2 \text{sign}(s_1) - \frac{D_m}{2\pi I_m} s_1 + \dot{v}_1 + \frac{\beta D_m}{2\pi V} x_{m2} - D_3 s_2 - k_3 \text{sign}(s_2) + \frac{\beta G}{V} \Delta p \right) \quad (3)$$

where

$$p_L(u_{pre}) := \Delta_{pump} - \text{sign}(u_{pre})\Delta p \quad (4)$$

and  $u_{pre}$  is the previous value for  $u$ .  $k_1$ ,  $k_2$ ,  $k_3$ ,  $D_2$  and  $D_3$  are controller gains,  $z_{s1}$  is the tracking error defined as

$$z_{s1} := x_{m2} - x_{d2} \quad (5)$$

where  $x_{d2}$  is the reference motor velocity,  $s_1$  is the first sliding surface defined as

$$s_1 := z_{s1} + k_1 \int_0^t z_{s1} dt \quad (6)$$

$v_1$  is a virtual control variable given as

$$v_1 = \frac{2\pi I_m}{D_m} \left( \frac{F_s \mu_v}{I_m} x_{m2} + \frac{T_{load}}{I_m} + \dot{x}_{d2} - D_2 s_1 - k_2 \text{sign}(s_2) \right) \quad (7)$$

and  $s_2$  is the second sliding surface defined as

$$s_2 := s_1 + z_{s2} \quad (8)$$

where

$$z_{s2} := \Delta p - v_1 \quad (9)$$

The controller was tuned hard and tested in rough environments in AHC-, Active Heave Compensation, mode in Skjong and Pedersen (2014a) giving good results.

The torque controller is a sliding mode controller where  $x_H$  is given as in (2),  $x_L = -x_H$  and

$$u := \frac{2V\sqrt{\rho}}{\beta\alpha D_s D_m \sqrt{p_L(u_{pre})}} \left( \frac{\beta D_m^2}{4\pi^2 V} x_{m2} + \frac{\beta G D_m}{2\pi V} \Delta p + \dot{T}_{dm} - k_1 e_T - D_2 s - k_2 \text{sign}(s) \right) \quad (10)$$

where  $T_{dm}$  is the reference torque,  $k_1$ ,  $k_2$  and  $D_2$  are controller gains and  $e_T$  is the tracking error defined as

$$e_T := \frac{D_m}{2\pi} \Delta p - T_{dm} \quad (11)$$

and  $s$  is the sliding surface defined as

$$s := e_T + k_1 \int_0^t e_T dt \quad (12)$$

The torque controller was tuned softer than the speed controller, giving larger tracking error, but through simulations the controller performance showed good results. The torque controller used a little longer time to stabilize after

initiation which means that the torque controller would set most of the restrictions related to dwell time switching stability in the hybrid controller that is to be designed. For reference, both the speed controller and the torque controller are elaborated in Skjong and Pedersen (2014a).

In addition to the switching algorithm and the switching restrictions, different functionalities are to be included. This is because some of the functionalities themselves set restrictions to the switching logics and should be included in the switching framework. An example of such a functionality is the switching to the torque controller if the upper torque limit is reached when the torque controller is set as the main active controller. Then an emergency program should be initiated to prevent, by all means, an increase in the torque to avoid loss of load due to wire rupture.

## 2. SWITCHING THEORY

Switching stability is a huge issue in hybrid control and may be one of the main reasons for failure or success. The controllers included in a hybrid control system should be fast and as accurate as possible but it would not help if the switching stability in the hybrid control system fails. One of the most common switching stability failure is that the switching algorithm has the opportunity to switch controller whenever it wants and as often it wants. In other words the hybrid controller switching algorithm has low restrictions and may switch controllers in such high frequencies that the controllers have no time to stabilize. This phenomenon is called *chattering* and is avoided by designing the restrictions so that high controller switching frequencies are avoided.

Two well known switching restrictions are hysteresis switching and dwell time switching. Hysteresis switching can be scale dependent or scale independent and moves the switching point up and down generating a switching point region. If the switching variable increases up to the switching point the switching variable must pass the upper switching region to switch controllers. If the switching variable decreases down to the switching point the switching variable must pass the lower switching region to switch controllers. A graphical representation of the hysteresis switching is shown in figure 1. When the lower

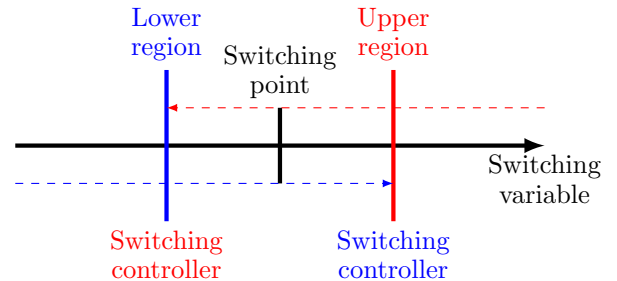


Fig. 1. Hysteresis switching.

and upper regions in the hysteresis switching are hard to determine or should be scale dependent and changes in a nonlinear way, dwell time switching is often used instead. Dwell time switching sets an upper limit for the switching frequency and keeps the active controller active until the

dwelt time is reached. If the switching algorithm still wants to switch controller the switching is initiated. Both dwell time switching and hysteresis switching are elaborated in Hespanha (2002).

In this hybrid controller dwell time switching is used. The reason for choosing dwell time switching over hysteresis switching is because the switching points in the hydraulic system are crucial for the performance of the winch. If a torque limit is set and the speed controller is active it is important that the hybrid controller switches to the torque controller when reaching the torque limit, not exceeding the limit to an upper region as in the hysteresis switching. The torque limit may be equal to the maximal tension the wire can withstand before snapping. Another example is if the torque controller is active trying to do AHC. If the speed limit is reached the hybrid controller should switch to speed controller at that point, not waiting to reach an upper region. If so the AHC performance would be bad and unnecessary movements of the load generates unwanted pressure peaks in the hydraulic system. Of course a small region could be chosen in a hysteresis switching logic, but then chattering would become a larger concern.

Together with switching restrictions a smooth switching between controllers are necessary to maintain stability in the system. If the switching is done in a step, oscillations will be generated and may destabilize the controlled system. To make a smooth switching a smooth continuous function must be used. By naming the output of the active controller that is to be deactivated as  $u_{A \rightarrow D}$ , and the output of the inactive controller that is to be activated as  $u_{D \rightarrow A}$  the total output of the hybrid controller,  $u_H$ , at the switching time  $t_0$  can be defined as

$$u_H := Du_{A \rightarrow D} + Au_{D \rightarrow A} \quad (13)$$

where

$$\begin{aligned} A &:= 1 - e^{-\gamma(t-t_0)} \\ D &:= e^{-\gamma(t-t_0)} \end{aligned} \quad (14)$$

where  $t$  is the time and  $\gamma$  is a tuning parameter,  $\gamma > 0$ . Note that  $u_H$  is the output given to the ideal main valve without dead band on the hoisting side and  $u_L = -u_H$  is the output given to the ideal main valve on the lowering side. It is often common to filter the hybrid controller output when controller switching is initiated. This is not done here because the measured differential pressure is filtered and because a filtering presents a phase lag and poorer control of the hydraulic system in the transition phase. The hybrid controller and the controlled process are sketched in figure 2.

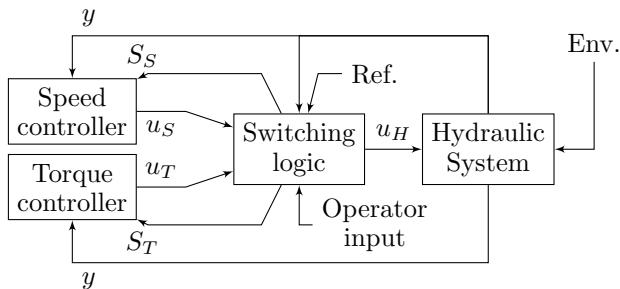


Fig. 2. Sketch of hybrid controller.

In the figure "Ref." is the abbreviation for Reference and "Env." for Environmental disturbances such as current. Starting in the left in the figure the measured states are given in feedback to the two controllers in addition to other needed measurements in the control laws. The controller references are fed to the controllers through  $S_S$  and  $S_T$ . The references goes through the switching logic box before fed to the controllers because the reference for the inactive controller may be set as a limit by the switching logic, not the reference set by the user. Moving on, the outputs from the two controllers,  $u_S$  and  $u_T$  are fed to the switching logic box and the output  $u_H$  is equal to the active controller if no controller switching is initiated. If controller switching is initiated the output is given as in (13). The switching logic box also has an operator input, giving the operator the opportunity to choose which controller to use as the main active controller, the active controller within the limits of the inactive controller. The output from the switching logic box  $u_H$  goes through the dead band compensation and is fed to the inner controller for the main valve on the hoisting side of the motor. Since 4/3 valve configuration are studied  $x_L = -x_H$  is fed to the inner controller for the main valve on the lowering side of the motor.

The switching logic box in figure 2 has also measurements from the hydraulic system as input. These measurements are used to determine when to switch between the controllers. The switching logics used are not general and are often customized for every hybrid controller.

Stability of the hybrid controller is proven numerically through case studies presented later in this paper.

### 3. SWITCHING LOGICS

The logics used to switch between the speed controller and the torque controller are dependent on many different things such as control slide positions, which controller is chosen as the main active controller by the operator, which controller is active and which is inactive, controller limits and hybrid controller settings. Before even checking the measurements to determine about switching, the control slide positions are checked. As an addition to the switching restrictions already presented the hybrid controller can not switch between controllers when the control slides in the main valves are within the region of the dead bands. A switching when the control slides are in the dead band zones is not appropriate since the main valves are closed.

To present the different switching logics the hybrid controller with its settings are divided into cases and presented. For convenience some abbreviations are used. The speed controller is given as controller 0 and the torque controller is given as controller 1. The operator chosen main active controller are given as O:"controller" and the active controller is given as A:"controller", where "controller" is either 0 or 1.

#### 3.1 O:1 and A:1

The operator has chosen the torque controller as the main active controller and the active controller "now running" is the torque controller. The following inequalities must be satisfied to switch from the torque controller to the speed controller:

$$|x_{m2} - x_{d2}| \geq x_{m2,lim} \quad (15a)$$

$$(x_{m2} \geq x_{m2,UL} \text{ or } x_{m2} \leq x_{m2,LL}) \quad (15b)$$

$$|T_m - T_{dm}| < T_{dm}T\% \quad (15c)$$

$$Em = 0 \quad (15d)$$

(15a) tells something about the the hydraulic motor velocity and if it would be safe to switch to the speed controller. For conventional torque control  $x_{d2} = 0$  and the speed controller is activated if  $x_{m2} \geq x_{m2,UL}$  or  $x_{m2} \leq x_{m2,LL}$  where  $x_{m2,LL}$  is the lower velocity limit and  $x_{m2,UL}$  is the upper velocity limit. Note that when the upper velocity limit and the lower velocity limit is equal in absolute value the second inequality is equal to the first one for conventional torque control. For convenience the MRU-measurements are used as  $x_{d2}$  in the simulations when the torque controller is set by the operator to be the main active controller in an AHC operation mode and then the first inequality in (15a) is used. This is because when the torque controller is deactivated, the speed controller is activated and has  $x_{m2,lim}$  as reference, a lowering or hoisting of the load is initiated. This will change the torque reference required to hold the load and since the simulations are not solved in real time it is difficult to change the torque reference by hand, without an estimator estimating the new torque reference. When the speed controller reference is set to be the MRU-measurements the length of the wire would be almost the same as before the controller switching and when switching back to the torque controller the torque reference would still be usable. In real life situations the operator changes the reference torque in real time and this problem would not be an issue. When other operations than AHC is initiated  $x_{d2}$  is set to zero when the torque controller is chosen to be the main active controller. Note that this restriction is related to the tracking error of the speed controller. The reference for the speed controller when the torque controller is the main active controller can be the speed limit or the MRU-measurements. This choice is implemented to be an operator input.

Also a second order Bessel filter is implemented trying to extract the torque required to hold the load by filtering out the heave induced torque variations. This is implemented as a controller setting, giving the operator the opportunity to choose whether to estimate a new torque reference or not. This is elaborated in the next subsection. Note that the speed reference must be chosen to be the MRU-measurements in order to estimate a new torque reference.

The second restriction is the dwell time restriction presented in section 2.  $N$  is the minimum number of simulation steps required before switching controller. The third switching criteria is the tracking error in the torque controller. The speed controller is not activated before the tracking error is below a percentage,  $T\%$ , of the torque reference. This restriction ensures that the torque controller is stable, and thereby the hydraulic system is stabilized, before switching to the speed controller.

The last restriction, where  $Em$  is an abbreviation for "Emergency", tells if an emergency program is initiated.  $Em = 0$  means that the emergency program is inactive.

This program is initiated when the speed controller is active and the torque reaches the maximal torque limit the system can handle. Then the emergency program is activated ensuring that the torque does not increase any further. When this program is active no controller switching is initiated before the motor velocity increases which tells that the torque can be decreased.

When the torque controller is deactivated and the speed controller activated the motor velocity is checked and if it is below the negative limit,  $T_{2low} = 1$ , then the torque reference is too low to hold the load and the torque controller is not activated again before the torque reference is high enough to hold the load.

### 3.2 O:1 and A:0

The operator has chosen the torque controller as the main active controller and the active controller "now running" is the speed controller. The following inequalities must be satisfied to switch from the speed controller to the torque controller:

$$|x_{m2} - x_{d2}| < |x_{d2}|x\% \quad (16a)$$

$$|\dot{T}_{dm}| < \dot{T}_{max} \text{ or } T_{mF} \geq T_{dm} \quad (16b)$$

$$n \geq N \quad (16c)$$

$$T_{2low} = 0 \quad (16d)$$

The first inequality ensures that the speed controller is stable, and thereby the hydraulic system is stabilized, before switching to the torque controller.  $x\%$  is a percentage and multiplied with the absolute value of the reference speed it creates a region which must include the tracking error in order to switch controller.

(16b) is dependent on the operator choice, and if the operator wants the hybrid controller to estimate a new reference for the torque controller in AHC mode, the torque required to hold the load, then the first inequality yields. Then the slope of the estimated reference must be below a given value in order to switch back to the torque controller. If the operator does not want a new estimated reference torque the second inequality yields. This inequality tells that if the filtered torque is higher than the reference torque then the torque controller should be activated.

The third inequality is the dwell time restriction, forcing the hybrid controller to wait  $N$  simulation steps before a controller switching can be initiated.

The last inequality ensures that the torque controller is not activated before the reference torque is high enough to hold the load. This is not the same as the last inequality in (16b) because when the speed controller is activated the torque oscillates a bit in AHC mode and the reference torque must at some point be higher than the torque in the system before even checking the other conditions to switch back to the torque controller.

If a controller switching is initiated the torque is compared to the maximal allowed torque in the system in order to determine whether to initiate the emergency program or not. If the program is initiated the torque controller is activated and  $Em = 1$ .

When the speed controller is activated, the operator has chosen the torque controller to be the main active controller and the hybrid controller is permitted to try to estimate a new reference torque, some other restrictions for estimating a new reference is required. First, a new torque reference is not estimated if the torque is close to the maximal allowed torque. This has to do with safety issues and a slight oscillation in the estimated reference torque may give a reference that is higher than the maximal allowed torque. If this condition is satisfied the new reference torque is estimated through a small control law given as

$$T_{dm} = T_{dm} + \text{limit}((T_{Bes} - T_{dm})K_p, -T_{max,h}, T_{max,h}) \quad (17)$$

$T_{Bes}$  is the torque given as output from the Bessel filter, which tries to neglect the heave induced torque changes in the system,  $K_p$  is a small proportional gain and  $T_{max,h}$  is the maximal allowed change in the reference update in each simulation step. In addition to this update law the dwell time variable,  $n$ , is reset if the difference between the torque given by the Bessel filter and the updated reference torque is larger than a given value,

$$|T_{bes} - T_{dm}| > T_{B\%}|T_{Bes}| \quad (18)$$

where  $T_{B\%}$  is a percentage creating a region around the filtered torque for the reference torque to be inside.

### 3.3 O:0 and A:1

The operator has chosen the speed controller as the main active controller and the active controller "now running" is the torque controller. The following inequalities must be satisfied to switch from the torque controller to the speed controller:

$$|x_{m2}| \geq |x_{d2}| \quad \text{or} \quad (19a)$$

$$[(x_{m2} \geq x_{m2,lim}) \text{ or } (x_{m2} \geq x_{m2,UL} \text{ or } x_{m2} \leq x_{m2,LL})] \quad (19b)$$

$$|T_{mF} - T_{dm}| < |T_{dm}|T\% \quad (19b)$$

$$n \geq N \quad (19c)$$

In (19a) one of the two condition sets inside [ ] is active at once and together with the first condition (above) it forms the first two sets of inequality conditions where at least one of them must be satisfied in order to switch controller. The first inequality says something about the torque in the system. Since the torque controller is active the torque would accelerate the hydraulic motor if it is too high or too low and a controller switching is initiated due to the velocity limit.

In the inequality set below, the first inequality tells that if the hydraulic motor velocity is equal to or higher than the maximal allowed motor velocity then the speed controller should be activated. This condition is chosen when the operator wants the MRU-data to set the speed limit. The second condition in the inequality set is when the operator wants specific limits for the motor velocity. Note that the motor velocity may decrease dramatically if the load increases significantly, but if the maximal limit for the torque is reached the speed controller should not be activated because the motor starts lowering the load with a high speed. This has to do with the hydraulic system. It is better to drop the load than destroying the

hydraulic system or waiting for the wire to snap. This condition is also related to the emergency program that is present when the torque controller is chosen as the main active controller. Often brakes on the reel is a part of the hydraulic system and in that case this condition is not necessary. Then the controller output should be zero driving the control slides to closing positions in the main valves. However in this system no brakes are present.

The second condition ensures that the torque controller is stable and thereby the hydraulic system is stabilized, as before, and the third condition is the dwell time condition.

### 3.4 O:0 and A:0

The operator has chosen the speed controller as the main active controller and the active controller "now running" is the speed controller. The following inequality must be satisfied to switch from the speed controller to the torque controller:

$$T_{mF} \geq T_{lim} \quad (20)$$

As can be seen there is only one condition in this case. Even the dwell time restriction is removed. This is because when the torque is equal to or higher than the maximal allowed torque then the torque controller must be initiated to avoid loss of load caused by wire snapping or destroying the hydraulic system.

## 4. IMPLEMENTATION AND REFERENCES

First of, the torque measurements used in the switching logics are filtered more than the torque used in the control laws in the two controllers. This is because the controllers should have the opportunity to try compensate for some of the pressure peaks in the hydraulic system, except the pressure peaks generated by dead band crossings in the main valves. The filters used to filter the differential pressure and the torque measurements are low pass filters,

$$H_F(s) = \frac{x(s)}{y(s)} = \frac{k}{Ts + 1} \quad (21)$$

and the second order Bessel filter, which acts as a notch filter, is given as a fourth order transfer function,

$$H_B(s) = \frac{x(s)}{y(s)} = \frac{as^4 + bs^2 + c}{ds^4 + es^3 + fs^2 + gs + h} \quad (22)$$

where  $a, b, c, d, e, f, g$  and  $h$  are filter constants. This filter filters out frequencies in the range of the heave motions, the wave frequency region, in order to determine the torque that is required to hold the load. When estimating this torque the speed controller must be active in an AHC operation. This is because the vertical load position is almost constant in this case and held in place by the speed controller. The torque used in this operation is related to the torque needed to hold the load. Instead of using a filter, an estimator based on the model equations may be used.

As mentioned before, the controller references set by the operator is fed through the switching logic box in figure 2 before entering the controllers. If the speed controller is chosen as the main active controller the reference to the torque controller should be the torque limit and controller switching is initiated if the torque increases to this limit. However torque peaks generated by dead band crossings in the main valves may exceed this torque limit because they



are filtered out in the torque used to determine controller switching.

Starting with the torque controller, if the emergency program is initiated the torque reference should be set to the torque limit. This happens when the speed controller is active and the torque exceeds the torque limitation. If the torque controller is active and the torque reference exceeds the torque limit the reference signal is limited to the torque limit and fed to the torque controller. When the torque controller is the active controller and the hydraulic motor velocity exceeds the speed limit a controller switching is initiated and the speed reference is set as speed limit. In other words, the main active controller chosen by the operator has the limited reference set by the operator as input and the inactive controller gets the limit the system approaches to as reference.

The last implementation issue is the hybrid controller output. The output of the controller, the reference positions for the control slides in the main valves, are limited between  $-0.05$  m and  $0.05$  m. When this happens the integrators in the control laws must be reset. The integrators must also be reset for every controller switching.

## 5. CASE STUDIES

Under normal circumstances controller switching is not initiated as often. This is because the load that is lifted would be lower than the maximal allowed torque in the system and the operator will not allow high hydraulic motor velocities in an operation. This will prevent controller switching in normal operations and switching would only be an issue in special cases such as landing the load at the sea floor and losing the load. Both these cases will cause an acceleration of the hydraulic motor if the torque controller is active. Cases where the load gets stuck in the sea bottom will increase the torque significantly when the speed controller is active. If the torque limit is reached a controller switching should be initiated.

For every simulation in this section the heave position of the ship is assumed to be a sum of six sine waves with frequencies  $\omega \in [0.5 \text{ rad/s}, 2 \text{ rad/s}]$  and with amplitudes  $A \in [0.2 \text{ m}, 2 \text{ m}]$ . The current is set to  $0.5 \text{ m/s}$  and the horizontal ship movement is assumed to be zero, perfect dynamic positioning. The load, excluding the weight of the wire, is set to  $3000 \text{ kg}$ . The initial length of the submerged wire is assumed to be  $100 \text{ m}$ .

### 5.1 Landing of Load using Torque Controller

The torque required to hold the load is approximately  $27000 \text{ Nm}$  and to lower the load the torque reference is set to  $25000 \text{ Nm}$  in the start of the simulation. The upper speed limit is set to  $0 \text{ rad/s}$  and the lower speed limit is set to  $-5 \text{ rad/s}$ . To simulate the sea floor a spring-damper system is initiated when the load reaches a depth of  $150 \text{ m}$ , which is the depth of the assumed sea floor. After a while a hoist is initiated, the upper speed limit is changed to  $5 \text{ rad/s}$  in  $1 \text{ s}$ , starting at  $t = 35 \text{ s}$ , forcing a hoist of the load and the reference torque is changed to  $30000 \text{ Nm}$  in a step at  $t = 35 \text{ s}$ . When the torque starts increasing the torque controller is then reactivated due to the switching condition presented earlier. At  $t = 50 \text{ s}$

the speed controller starts holding the load at a constant depth in an AHC operation, assumed to be initiated by the operator. Note that when the load reaches the sea floor the speed controller is supposed to be activated, keeping the load at the sea floor in an AHC operation, by the switching logics.

Figure 3 shows the hydraulic motor velocity compared to the reference, magnified areas in motor velocity around controller switching regions and which controller is active. Note that the speed reference is the speed needed in reference to keep the vertical load position nearly constant in an AHC operation.

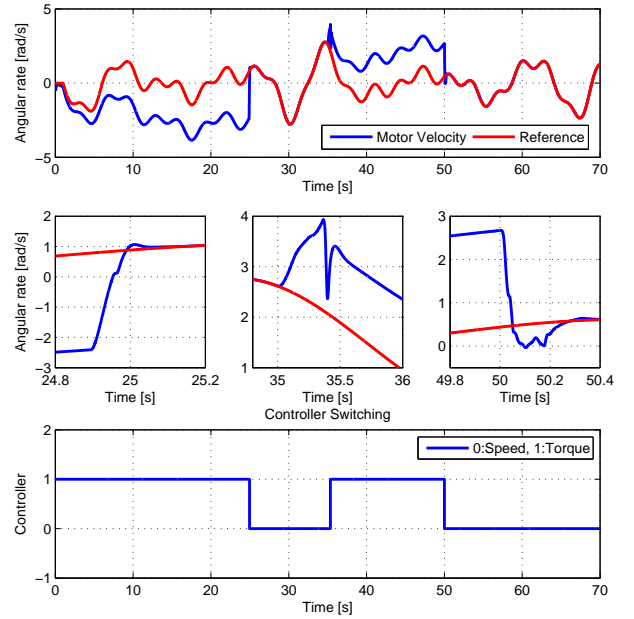


Fig. 3. Hydraulic motor velocity, magnified areas and active controller.

The first plot shows the hydraulic motor velocity compared to the reference velocity. The torque controller is chosen to be the main active controller by the operator and is the active one in the start of the simulation initiating a lowering of the load. It can be seen in the first plot that the motor velocity has the same form as the reference in the start of the simulation but is lower due to lowering of the load. This is one of the strengths of the torque controller, keeping a smooth lowering of the load by holding a constant torque. At approximately  $t = 24.9 \text{ s}$  the switching algorithm switches to the speed controller, because the motor velocity gets positive, and the hydraulic motor velocity coincides with the reference velocity. A magnified area of the motor velocity when the first controller switching is initiated can be seen in the first plot in the second row in the figure. The motor velocity in the switching seems to be smooth and the speed controller uses about  $0.2 \text{ s}$  to reach the reference velocity.

At  $t = 35 \text{ s}$  the upper speed limit and the reference torque are changed and a new controller switching is initiated, setting the torque controller as the active controller. Now the torque is higher than what is needed to hold the load

and initiates a hoist of the load. The second plot in the second row in the figure shows a magnified area around the controller switching. The motor velocity oscillates a bit before stabilized due to an overshoot in the torque controller. The torque controller takes about 0.4 s to stabilize and the motor velocity is comparable to the reference velocity, only higher due to the hoist.

The last controller switching is manually activated by the operator at  $t = 50$  s which initiates an AHC operation at the depth the load is hoisted to. The motor velocity around the last controller switching is shown in the last plot on the second row in the figure. The speed controller uses about 0.4 s to stabilize at the reference velocity and from this point on the motor velocity coincides with the reference velocity for the rest of the simulation. The last plot in the figure shows which controller is active during the simulation.

Figure 4 shows the torque, the reference fed to the torque controller and which controller is active.

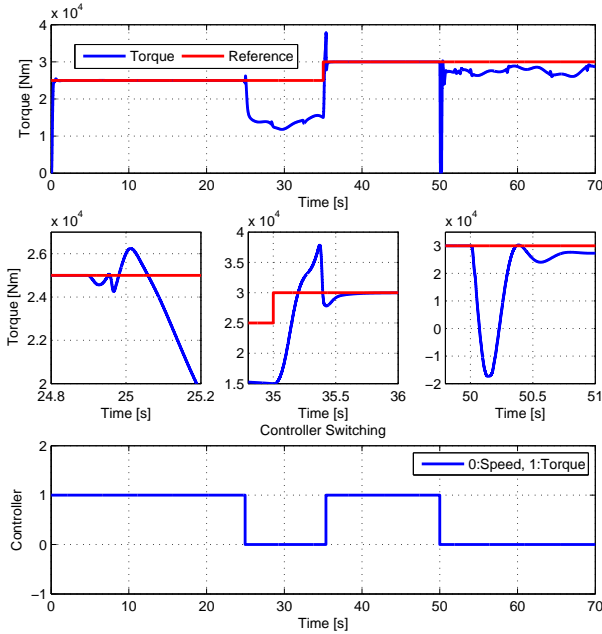


Fig. 4. Torque, reference and active controller.

The first plot in the figure shows the torque compared to the torque reference and from the start of the simulation to the first controller switching the torque seems to coincide with the reference. The first plot on the second row in the figure shows the torque in a magnified area around the controller switching. The torque drops to about 14000 Nm due to landing of the load and the speed controller initiates an AHC operation to keep the length of the submerged wire as constant as possible. Due to current, hydrodynamic effects, the weight of the wire and the tension in the wire before controller switching, the torque is still relatively high.

At  $t = 35$  s the torque controller is reactivated and the torque reference is changed to 30000 Nm. The torque controller has an overshoot causing a small oscillation and the controller uses approximately 0.5 s to coincide with the

new reference. The load is now hoisted and the hydraulic motor has a small acceleration since the weight of the submerged wire decreases with its length.

The last controller switching, which is initiated at  $t = 50$  s by the operator, is shown in the last plot in the second row in the figure. The torque decreases rapidly below zero due to inertia effects and the speed controller but increases and stabilizes in about 1 s. The load is in motion when the speed controller is activated and the speed controller has an overshoot of the reference causing the rapid drop in torque. For the rest of the simulation the torque varies a bit due to the heave motion of the ship.

The next figure, figure 5, shows the vertical position of the ship, caused by waves, and the vertical and horizontal position of the load.

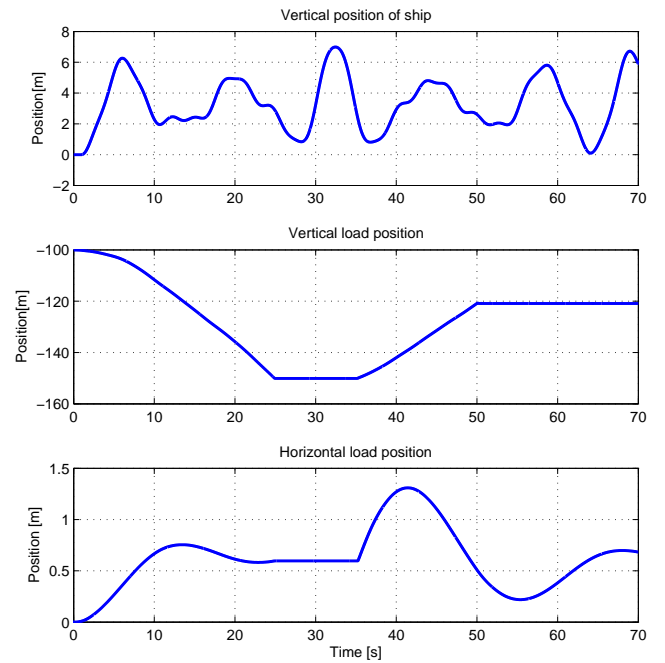


Fig. 5. Vertical ship position and load position.

The first plot in the figure shows the vertical ship position over the sea surface. Note that the heave motion seems to oscillate about 3 m above the surface. This is due to the choice of the vertical ship velocity that was set and the vertical ship position, that is the integral of this velocity, gets a bias of about 3 m due to a not so well defined vertical ship velocity. However the velocity was set only to test the controllers and is therefore justified.

The second plot in the figure shows the vertical position of the load. Note that negative values for the vertical position means below the sea surface due to the sign convention used when modeling the lumped wire-load model. In the start of the simulation the load is lowered until it reaches a depth of 150 m, which was assumed to be the sea floor. The vertical load position is kept constant by the spring-damper system that was added to simulate the sea floor. At  $t = 35$  s the load is hoisted and is stabilized around 120 m below the sea surface at  $t = 50$  s when the AHC operation is initiated by the speed controller that is manually activated

by the operator. For the rest of the simulation the vertical load position seems to be constant which tells that the speed controller works fine in AHC operations.

The last plot in the figure shows the horizontal load position which seems to always be above 0m. This is due to the positive current that was set to 0.5 m/s. At  $t = 24.9$  s the horizontal load position is kept constant due to the assumption that the static friction between the load and the sea floor is high enough to overcome the current forces acting on the load and the wire. At  $t = 35$  s the load is hoisted and the horizontal load position starts to increase. This is due to the fact that the wire gets a characteristic displacement due to the current before the hoist is initiated which causes the load to swing out in horizontal direction when leaving the sea floor. The load oscillates in horizontal direction but seems to stabilize after a while when reactivating the speed controller at  $t = 50$  s.

The last figure, figure 6 shows the wire displacement at time steps of 0.5 s. Note that the figure is divided into three plots showing different situations in the simulation. Darker color of the graphs shows increased time in the simulation.

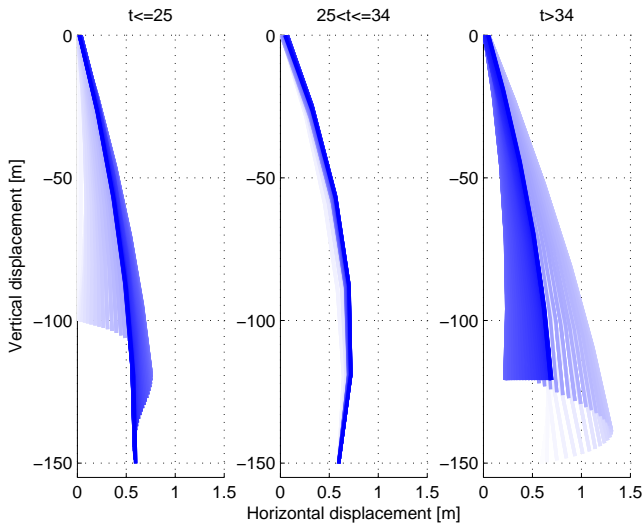


Fig. 6. Wire displacement in time steps of 0.5 s.

The first plot shows the lowering of the load until it reaches the sea floor. As the plot shows the horizontal wire displacement increases in the start of the simulation due to the current and gets an overshoot in horizontal direction before stabilizing. The second plot shows the wire displacement when the load is in contact with the sea floor. As can be seen the wire displacement is largest at the middle of the wire when drawing a straight line between the two ends of the wire. This is as expected due to the horizontal current. The last plot shows the hoisting of the load and the AHC operation in the end of the simulation. The horizontal load position oscillates, as was seen in figure 5 and the wire displacement seems to stabilize a while after the initiation of the AHC operation.

## 5.2 Loss of Load and Variations using Torque Controller

In this simulation the hybrid controller is tested when the torque controller is set by the operator to be the main

active controller with a constant reference and varying loading. The load is first set to 3000 kg but is changed to 0 kg at  $t = 10$  s in a step to simulate a load loss. At  $t = 40$  s the load is regained, 3000 kg, before changed to 6000 kg at  $t = 70$  s. At last the load is changed back to 3000 kg at  $t = 100$  s.

The operator has given permission for the hybrid controller to try to estimate a new torque reference using the Bessel filter and to change back to the main active controller with the new reference. It is expected that the new reference torque would either lower or hoist the load because it is nearly impossible to find the right torque reference to keep the torque at a constant depth using the torque controller. Also, the tracking error in the torque controller is larger than in the speed controller and with a small hoisting or lowering the load would change the weight of the submerged wire and load, and thereby the torque reference. However an estimate of the new torque reference would be of help for the operator, who sets the torque reference manually. The initial torque reference is set to 27000 Nm which is about the torque needed to hold the load. Note that this test is not intended for testing the torque controller in AHC operations but to test the sensitivity of the hybrid controller in cases where the load is varying.

The speed limits are set to be a region of  $\pm 1.5$  rad/s around the speed reference which is set to be the feedback from the MRU, the reference needed in AHC operations when using the speed controller. This means that the speed controller is activated if the hydraulic motor velocity deflects more than 1.5 rad/s, 14.3 rpm, from the speed reference.

Figure 7 shows the hydraulic motor velocity compared to the MRU feedback, magnified areas of the motor velocity around the controller switching regions and the active controller.

The first plot in the figure compares the motor velocity to the speed reference. In the time range  $[0\text{s}, 10\text{s})$  the torque controller is active. The load is constant in this area and the torque reference is good enough to keep the motor velocity within the tolerance which was set to 1.5 rad/s. However it can be seen that the motor speed is in general higher than the reference which means that the torque reference is set littlebit high causing a hoist of the load. This is one of the main problems with using the torque controller in AHC operations. The torque must be well defined in order to just hold the load, and a constant torque would never do the job. This has to do with tracking errors, changes in torque due to changing reel diameter and change in weight of submerged wire, among other contributions.

At  $t = 10$  s the load is changed to 0 kg in a step simulating a loss of load due to wire rupture. The first plot on the second row in the figure shows a magnified area of the motor velocity when this happens. The motor velocity starts increasing due to high torque reference compared to the new motor loading. The motor velocity reaches about 2 rad/s at  $t = 10.3$  s before a change of controller is initiated. It takes about 0.5 s before the speed controller stabilizes and the controller seems to force the tracking error to zero making the motor velocity coincide with the reference. While the speed controller is active a new torque reference

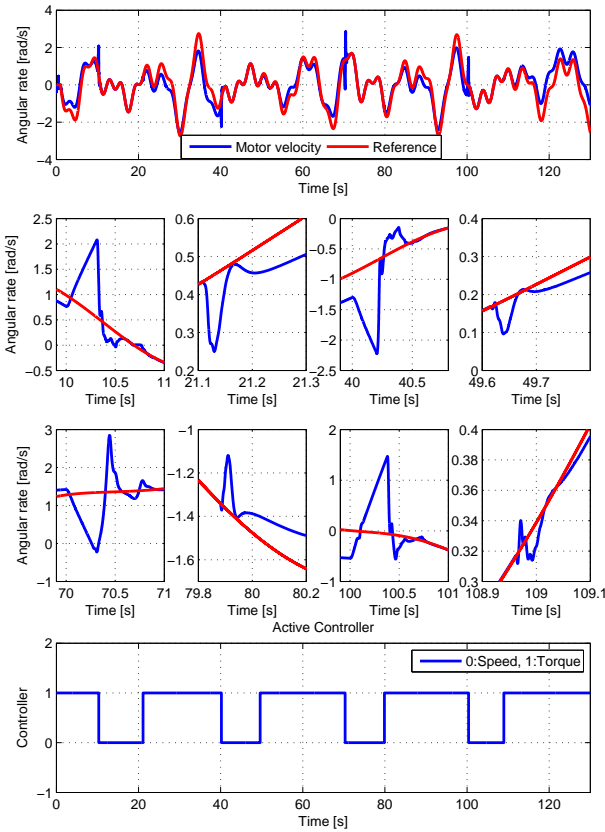


Fig. 7. Hydraulic motor velocity compared to reference and active controller.

is estimated and the torque controller is reactivated at approximately  $t = 21.1$  s. As can be seen in the figure the new torque reference is littlebit too low to hold the load and the load is therefore lowered. However the lowering is within the tolerances and is accepted. A magnified area of the motor velocity around reactivation of the torque controller is shown in the second plot on the second row in the figure. The torque controller uses about 0.5 s to stabilize the system around the new torque reference.

The load is regained, 3000 kg, at  $t = 40$  s and the torque reference is now too low to hold the load resulting in a lowering of the load. At  $t = 40.2$  s the motor speed is about  $-2.25$  rad/s and the speed controller is activated due to the speed tolerance in the switching logics. Again, the speed controller forces the tracking error to zero in about 0.3 s making the motor velocity converge to the reference. A magnified area of the motor velocity around the activation of the speed controller is shown in the third plot in the second row in the figure. A new estimate of the reference torque starts being calculated and the torque controller is again reactivated at  $t = 49.65$  s. The torque controller uses about 0.4 s to stabilize and the new estimated reference torque seems to be much better than the previous estimate since the motor velocity is closer to the reference velocity than compared to the previous estimate.

At  $t = 70$  s the load is doubled, 6000 kg, in a step and the motor velocity starts to drop to about  $-0.2$  rad/s before the speed controller is activated by the switching algorithm. A closer view of the motor velocity around the controller switching is shown in the first plot in the third row in the figure. The speed controller is stabilized in about 0.7 s and the motor velocity converges to the reference velocity. A new torque reference starts being estimated and the torque controller is reactivated at  $t = 79.9$  s. The magnified area of the motor velocity around the controller switching is shown in the second plot on the third row in the figure. The torque converges to the torque reference in about 0.3 s and as for the previous torque reference estimate, the estimate seems to be good forcing the motor velocity to be close to the reference velocity as shown in the first plot.

The load is changed back to its initial value, 3000 kg at  $t = 100$  s causing an increase in the motor velocity. The speed controller is activated at  $t = 100.35$  s caused by an exceedance of the velocity tolerance. The motor velocity converges to the reference velocity in about 0.4 s which the third plot on the third row in the figure shows. After about 8.2 s a new estimate of the reference torque is ready and the torque controller is reactivated. The torque converges to the reference torque in about 0.4 s. However this new torque estimate is not as good as the previous estimates, being too high causing a hoist of the load, but since the velocity tolerance is high the estimate is accepted.

Figure 8 shows the torque compared to the reference and the estimate, magnified areas of the torque for every controller switching and which controller is active.

In the first plot, showing the torque compared to the reference and the estimate, it is easy to see when the load is changed. One can also see the high torque peaks when the speed controller is activated. In general the Bessel filter uses about 10 s to estimate a new torque reference for each change in load during this simulation. This is because each load step is equal in absolute value. The plots in row two and three show the magnified area of torque for every controller switching. It can also be seen that the torque reference starts being estimated whenever the speed controller is activated. The last plot in the figure shows which controller is active. By comparing the last plot on row two with the last plot on row three in the figure one can see that the estimated torque references are not equal. About 500 Nm separates them from each other. Of course the length of the submerged wire in the two cases are not equal since the torque controller has changed the depth of the load, but the changes in the length of the submerged wire is not more than about 2 m. The wire used is assumed to have a diameter of 0.025 m and by using a density of steel of  $7800$  kg/m<sup>3</sup> gives a total weight of about 7.65 kg for two meters of wire. The reel diameter is assumed to be about 1 m giving a torque increase of about 75 Nm for an increase in submerged wire length of 2 m. This is also the torque generated by the weight of the wire in air, not in water where buoyancy also is presents. This tells that the estimation of the new torque reference is not perfect. However by having in mind that the torque reference is estimated based upon filtering out the torque variations generated by the heave motion the results are quite good. The wire has its own dynamics that is not included in

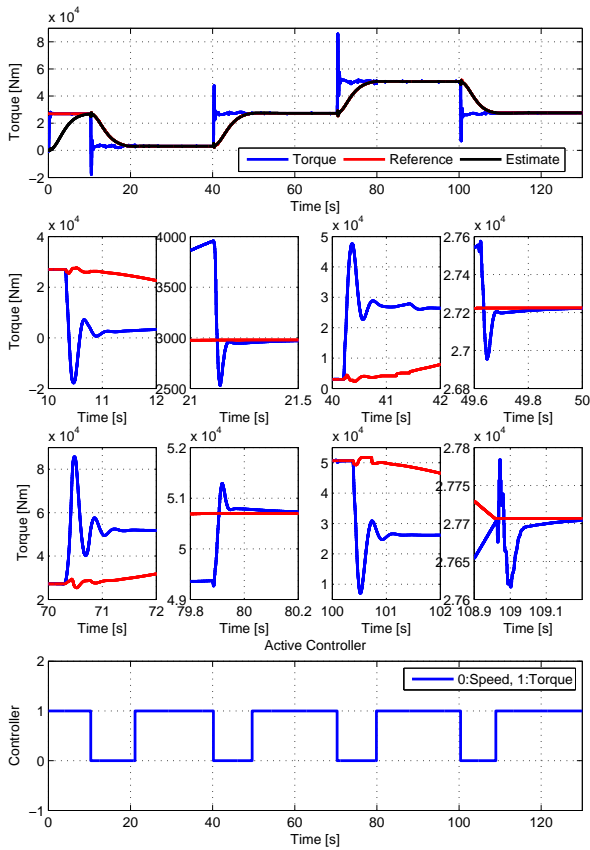


Fig. 8. Torque, reference, estimate and active controller.

this estimation process. Nor is the hydrodynamics and the current forces.

Figure 9 shows the vertical position of the ship and the load positions during the simulation.

The first plot is the same vertical heave position as used in the first case study and the second plot shows the vertical load position. As can be seen every straight horizontal position in the plot is when the speed controller is active. It is easier to see in this plot how good the torque estimate is. The initial torque reference causes a small hoisting of the load, the first estimate causes a lowering of the load, the second causes a slight hoisting, the third a slight lowering and the last estimate hoists the load. It is also easy to see that the last estimate is the poorest one. However through the simulation the vertical load position is within  $\pm 7$  m of the initial vertical load position.

The last plot in the figure shows the horizontal load position. When  $t \in [0s, 40s]$  the horizontal load position increases to the largest fluctuation in the simulation. for  $t < 10s$  this swing out is due to the current. After  $t = 10s$  the load is lost and the current forces becomes more significant and forces the horizontal wire displacement to increase. The horizontal wire displacement does not reach equilibrium before the load is regained and the horizontal load displacement decreases rapidly. For  $t \in [40s, 70s]$  the horizontal load position oscillates around the equilibrium

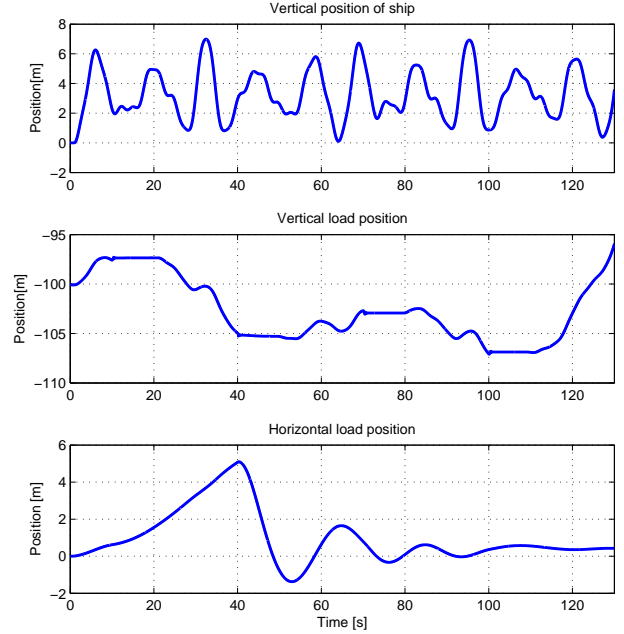


Fig. 9. Vertical ship position and load position.

point and when the load is doubled the oscillations does not increase in magnitude, but the average horizontal position seems to decrease a bit, which is expected since the load is heavier. The oscillations also seems to be damped out and when the load decreases to its initial value at  $t = 100s$  and the horizontal position seems to increase again but without new oscillations.

To get a clearer understanding of the total wire- and load displacement the wire is plotted for time increments of 0.5 s in figure 10. Note that darker color gives higher simulation time.

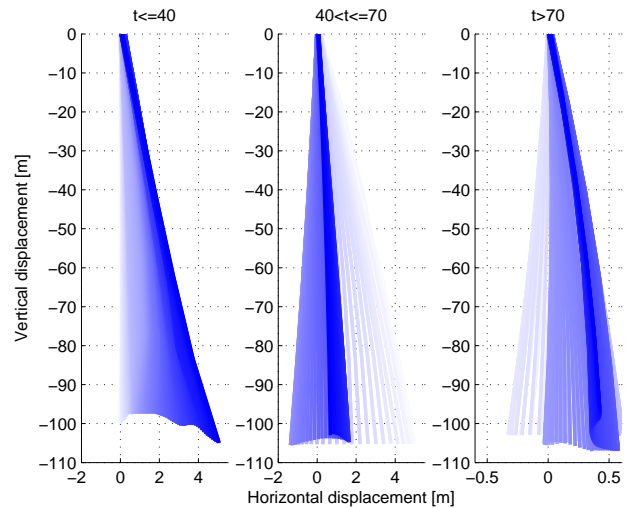


Fig. 10. Wire displacement in time steps of 0.5 s.

As the figure shows the simulation is divided into three cases,  $t \in [0s, 40s]$ ,  $t \in (40s, 70s]$  and  $t \in (70s, 130s]$ . The first plot shows the largest fluctuation of the wire displacement and it is easy to recognize the vertical and

horizontal load positions shown in figure 9 in the plot. The same yields for the second plot, showing the wire displacement when the load increases back to 3000 kg. The last plot shows the doubling and halving of the load, showing that the horizontal displacement oscillates a bit but seems to converge to an equilibrium point in the end of the simulation.

### 5.3 Stuck Load using Speed Controller

In this simulation the hybrid controller is tested when the speed controller is set by the operator to be the main active controller with MRU- and operator defined reference. The torque limit is set to 80000 Nm and the load is stuck when  $t \in [10\text{s}, 30\text{s}]$ . To simulate this a stiff and powerful spring-damper system is added to the load model and is activated in this time period. At  $t = 15\text{s}$  a hoist of the load is initiated,

$$r_s = MRU + 0.5\text{ramp}(15) - 0.5\text{ramp}(20) - 0.5\text{ramp}(40) + 0.5\text{ramp}(45) \quad (23)$$

and the load is supposed to come to rest after  $t = 45\text{s}$ . The lower speed limit is set to  $-6\text{ rad/s}$  and the upper speed limit to  $6\text{ rad/s}$ , about  $\pm 57.3\text{ rpm}$ .

Figure 11 shows the motor velocity compared to the reference, magnified areas of the motor velocity when changing controllers and which controller is active during the simulation.

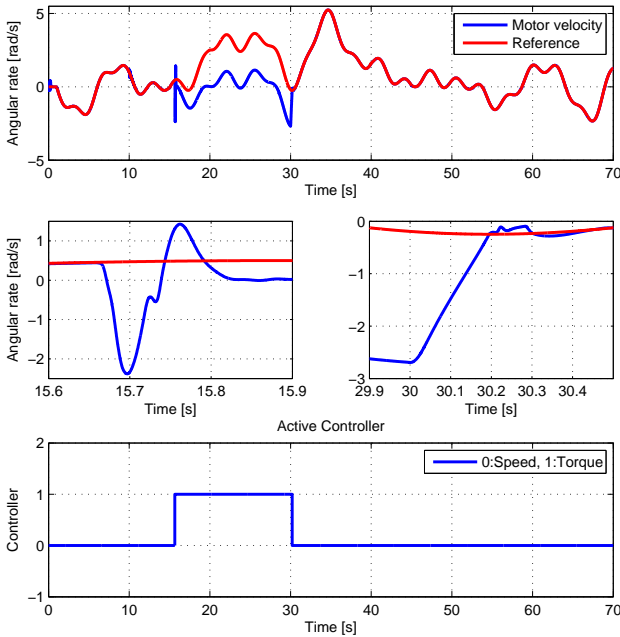


Fig. 11. Hydraulic motor velocity compared to reference and active controller.

The first plot in the figure shows the motor velocity compared to the velocity reference. At  $t = 10\text{s}$  the load gets stuck but switching of controller is not initiated before the hoisting of the load is started at  $t = 15\text{s}$ . This is due to the performance of the speed controller which manages to keep the load at a constant depth and is therefore almost not

affected by the fact that the load is jammed. For reference Skjong and Pedersen (2014a) gives a more elaborated study of the performances of the two controllers. When the hoist is initiated it takes about 0.6 s before a controller switching is initiated due to the significant increase of torque that in the end overshoots the torque limit. A closer view of the motor velocity when the switching is initiated is shown in the first plot on the second row in the figure. The torque converges to the torque limit in about 0.3 s and the motor velocity coincides with the MRU reference when the torque controller is active. This can be seen in the first plot where the motor velocity is equal to the velocity reference, except for the fact that the motor velocity is  $2.5\text{ rad/s}$  lower than the reference after  $t = 20\text{s}$ .

At  $t = 30\text{s}$  the load is released and the speed controller is reactivated by the switching logics. The motor velocity converges to the reference in about 0.4 s and the load is hoisted. The second plot on the second row in the figure shows a magnified area of the motor velocity around the controller switching. The hoisting stops when  $t = 45\text{s}$  and the vertical load position is kept as constant as possible through AHC using the speed controller.

Figure 12 shows the torque compared to the torque limit, magnified areas of the torque for the two controller switchings and which controller is active.

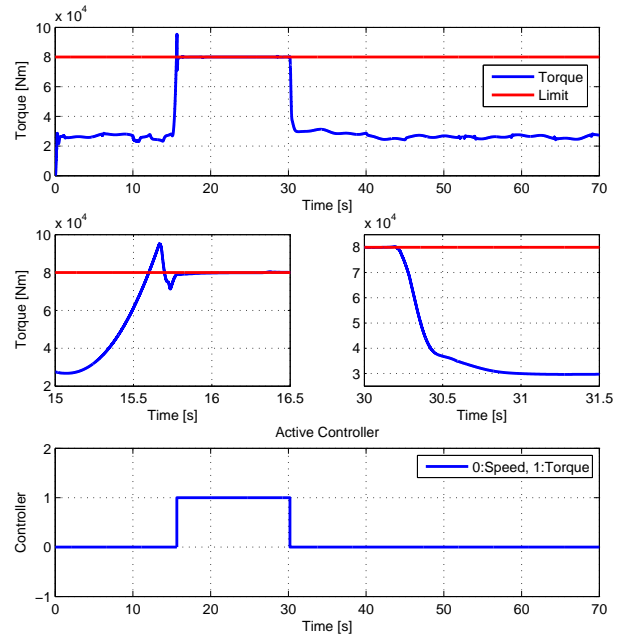


Fig. 12. Torque, reference, estimate and active controller.

In the first plot it can be seen that when the speed controller is active the torque varies a bit even though the vertical load position is kept nearly constant. This emphasizes the discussion about the reference torque estimates. It is hard to find one constant torque reference for a constant load case that keeps the vertical load position as constant as the speed controller in AHC operations. When the torque varies that much, as the figure shows, the torque controller will hoist or lower the load at some point which decreases or increases the motor loading respectively due

to the length of the submerged wire. If the load is lowered the torque reference needed for holding the load increases, and opposite if the load is hoisted the torque needed to hold the load decreases.

At  $t = 15$  s the torque increases significantly and overshoots the torque limit before converging to it. This is shown in the first plot on the second row in the figure. When  $t = 30$  s the speed controller is reactivated and the torque decreases significantly back to the initial torque region, which is shown in the second plot on the second row in the figure. The last plot shows which controller is active throughout the simulation.

Figure 13 shows the vertical heave position of the ship and the load positions.

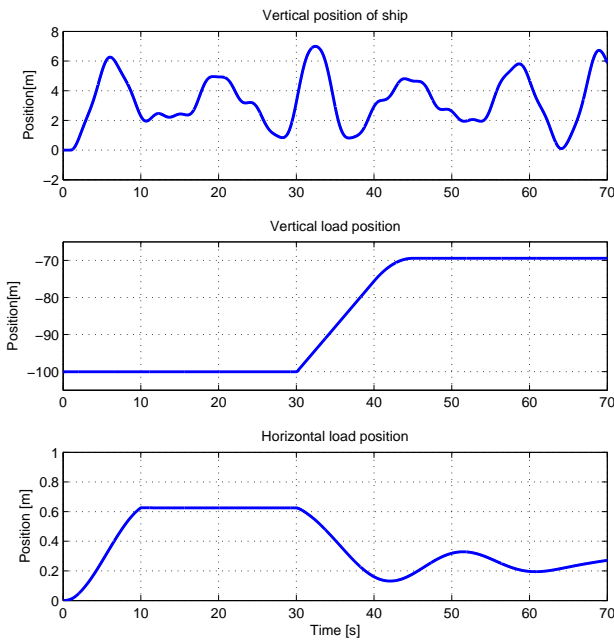


Fig. 13. Vertical ship position and load position.

The first plot, showing the vertical ship position, is as in the two previous simulation cases. The second plot shows the vertical load position. As can be seen the depth of the load seems to be constant when  $t \in [0, 30]$  s. In Skjong and Pedersen (2014a) the deflections between the initial depth and the load depth in such AHC operations were about  $\pm 2$  cm. The jamming of the load at  $t = 10$  s can not be seen in the plot. When the load is released the length of the submerged wire decreases and at  $t = 45$  s the vertical load position comes to rest at an approximate depth of 70 m. The vertical load position is smooth and shows that the speed controller does a good job in AHC operations, as is expected.

The last plot shows the horizontal load position and as in the previous simulation cases the horizontal load position increases when  $t \in [0, 10]$  s). The slope of the horizontal load position in this time region shows that the vertical load displacement does not reach any equilibrium before the load gets stuck. The horizontal load position is kept constant, like the vertical load position, when  $t \in [10, 30]$  s]

by the stiff and powerful spring-damper system that holds the load position constant.

When the load is released the horizontal load displacement decreases and starts oscillating around the equilibrium. Note that the horizontal load displacement is in general larger, with current present, when the load is hoisted compared to lowering or constant depth AHC operations. Also note that the weight of the load and the hydrodynamics acting on the load are related to the damping of the horizontal load oscillations.

To get a clearer understanding of the complex wire displacement the wire is plotted through the simulations with time increments of  $t = 0.5$  s. As before, darker color means increase in simulation time.

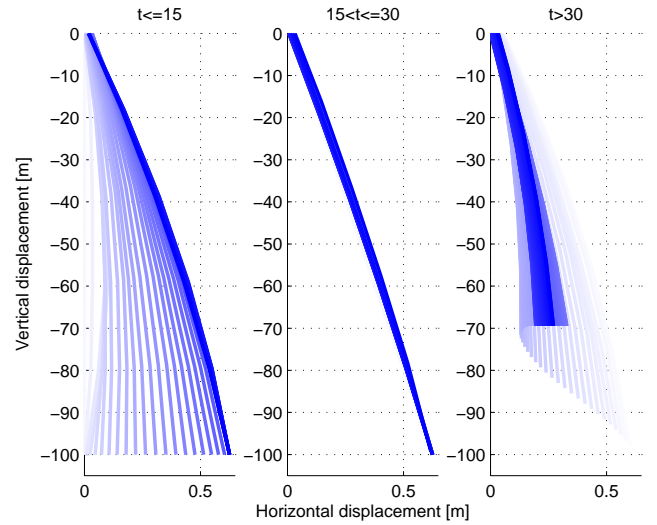


Fig. 14. Wire displacement in time steps of 0.5 s.

The first plot in the figure shows the wire displacement for  $t \in [0, 15]$  s). This is the first region the speed controller is active. The initial wire displacement is a straight vertical displacement and when the current forces starts acting on the wire and the load the horizontal wire displacement increases. The wire displacement converges to an equilibrium when the load is jammed, which can be seen by the graphs with the darker color.

The second plot shows the wire displacement when the load is stuck. The displacement is nearly constant, only small changes in the wire displacement are present due to the heave motion of the ship.

The last plot shows that the load is hoisted and the horizontal wire displacement decreases. In the end of the simulation the wire displacement seems to converge to an equilibrium since the horizontal load position and the vertical load position seem to converge.

## 6. SUMMARY AND CONCLUSION

Hybrid switching logics, determining when the hybrid control system should switch controller, based on measurements and operator choices, were proposed in the start of this paper. The switching restrictions and conditions showed to be system- and functionality dependent and

simple functionalities such as torque reference estimation, loss of load and stuck load contributed to the final hybrid controller design.

The first case study, landing of load using the torque controller as the main active controller, showed how to combine the torque controller and the speed controller with references and limits to perform such an operation. The torque controller was chosen as the main active controller with a constant reference torque lower than the torque necessary to hold the load, initiating a lowering of the load. When the load reached the sea floor the motor velocity changed sign and the speed controller was activated with MRU reference initiating an AHC operation of the load at the sea floor. The upper speed limit and the torque reference were increased and the torque controller was reactivated, starting to hoist the load. After a while the speed controller was manually activated by the operator to perform an AHC operation, keeping the load at a constant depth. The results from this test showed that landing a load on the sea floor by combining the two controllers as specified gave good results.

The second case study, loss of load and load variations using the torque controller as the main active controller, was initiated to test the response of the hybrid controller in cases with varying load. The operator allowed the hybrid controller to try to estimate a new torque reference in order to reactivate the torque controller when the speed controller was active. This case, except for the torque reference estimation, is similar to the load landing case. It was expected that the torque reference estimate would not be perfect because cases doing nearly perfect AHC operations keeping the load at a constant depth using the speed controller show that the torque varies significantly. This torque variation is a sum of many contributors such as hydrodynamics, time constants in the system, wire dynamics and tracking errors. By assuming the torque reference can be chosen perfect and set constant it would only take a small tracking error in the torque controller to change the torque reference for keeping the load at a constant depth. This is similar to the inverted pendulum problem, where only a small disturbance would change the equilibrium point. In control theory such an equilibrium point is called a saddle point and is not characterized as a stable equilibria. However, the velocity error tolerance was set high in the simulation resulting in only one torque reference estimate for each change in load. The velocity error tolerance, giving switching restrictions to the hybrid controller, is closely related to the chattering phenomenon in the hybrid controller. If the tolerance is low the hybrid controller would switch between the two controllers as often as possible in order to try finding a better torque reference estimate. Since the reference torque is comparable to a saddle point it would be nearly impossible to estimate the right reference.

In the simulation two of the torque reference estimates gave good results, keeping a lowering or hoisting at a minimum. To estimate the torque reference only a second order Bessel filter was used, filtering out the torque variations from torque measurements when the speed controller was active in an AHC operation keeping the load at a constant depth. To make a better estimate a model based

filter or estimator should be studied, but the inverted pendulum problem would never disappear. However the torque reference estimate would be a good aid for the operator that is to set the torque reference manually. It can also be used in safety systems, setting restrictions for the upper and lower limit for the torque reference that is set by the operator.

The last case study, stuck load using the speed controller as the main active controller, was initiated to test the reaction of the hybrid controller when the load got stuck. Functionalities for handling such cases are crucial for saving both the load and the hydraulic winch system. An upper limit for the torque was set in the hybrid controller and the simulation started with the speed controller active performing an AHC operation keeping the load at a constant depth. Even though the load got stuck the performance of the AHC operation was good enough to keep the pressure in the system in the same region as before the load got stuck. When the hoist of the load was initiated the torque increased quickly and when the torque reached the torque limit the torque controller was activated. A small overshoot of the torque limit before the activation of the torque controller was allowed telling that a safety factor in the torque limit should be present, if the torque limit is the highest torque the system can handle, in order to prevent damages on the system. After a while the load was released and after a short period with hoisting the load came to rest due to initiation of AHC, keeping the load at a constant depth. This simulation showed that the hybrid controller works good also in such cases.

## ACKNOWLEDGEMENTS

Thanks to Eilif Pedersen at MTC, NTNU, for good discussions around the topics this paper deals with. His vast modeling skills and experiences have given me help many times.

It is also highly appropriate to thank Roger Skjetne and Asgeir Sørensen at MTC, NTNU, for good conversations about the control issues this paper presents.

## REFERENCES

- S. Skjong and E. Pedersen. *Control of Hydraulic Winch System (1/2), Model Based Control Designs, 2014a.*
- S. Skjong. *Master Thesis - Modeling, Simulation and Control of Directional Valve System, 2014.*
- J. P. Hespanha. *Tutorial on Supervisory Control, 2002.*
- S. Skjong and E. Pedersen. *Modeling Hydraulic Winch System, 2014b.*
- J. Choi. *Robust Control of Hydraulic Actuator using Back-Stepping Sliding Mode Controller, 2011*
- H. K. Khalil. *Nonlinear Systems, 2002.*
- D. C. Karnopp. *System Dynamics: Modeling and Simulation of Mechatronic Systems, 2006.*



## **B.3 Modeling Hydraulic Winch System**

Submitted to International Conference on Bond Graph Modeling and Simulation 2014, ICBGM'2014.

# Modeling Hydraulic Winch System<sup>1</sup>

Stian Skjong  
Graduate Student  
stiansk@stud.ntnu.no

Eilif Pedersen  
Associate Professor  
eilif.pedersen@ntnu.no

Norwegian University of Technology and Science  
Department of Marine Technology

**Keywords:** Hydraulic modeling · Lumped wire modeling · Varying inertia of rotation · Bond graph · Hydraulic winch system · Morrison's equation · Wire storing · Reel dynamics

## Abstract

In sub-sea operations winches and cranes are used in almost every task performed from a surface vessel. Heavy payloads are lifted and installed at the sea floor such as "christmas trees", anchors, pipelines and various constructions with high precision in rough environments. These operations set criterions to the vessel's equipment.

Winches used in such operations are multidisciplinary systems including mechanical, electrical, hydraulic and cybernetic systems that act together in a well defined way so that the performance comply with the criterions. To verify the systems HIL-, Hardware In the Loop, tests or sea-tries are necessary. In this paper a lumped wire-load model affected by environmental forces are derived with the purpose of testing winching systems. The wire is divided into five equal wire elements and are modeled as series of mass-damper-spring systems connected to the payload. Both the elasticity of the wire and the damping characteristics are dependent of the wire length and modeled using bond graph theory. This gives variable natural frequencies which is desirable for testing winch control systems. The model also includes current, vessel motions and hydrodynamics acting on both the wire and the payload. The wire is packed on a reel giving variable inertia and reel diameter that also affect the powering system of the winch.

The lumped wire model are tested in both a hoist and a lowering operation of the payload with horizontal current present using a hydraulic powering system that includes two directional valves in a 4/3 valve configuration connected to a hydraulic motor. The powering system also includes safety valves to ensure that vapour pressures do not appear in the system. The simulation results shows that the powering system are highly affected by the wire-load model, giving a variable loading of the hydraulic motor, and winch control systems, such as speed and torque controllers, must be designed in such a way the natural frequencies are not amplified giving resonance.

## 1. INTRODUCTION

In this study the objective is to derive a reasonable winch model for a winch operating in a marine environment with realistic load characteristics. A sketch of the winch with wire and payload is given in figure 1.

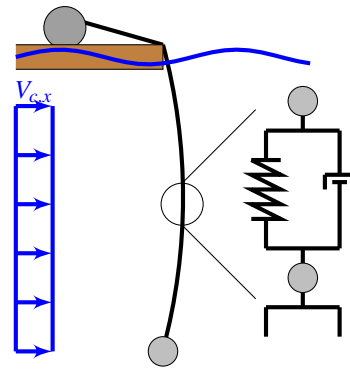


Figure 1. Sketch of winch in operation.

As the figure shows the wire is connected to the reel on the vessel and the submerged wire is suspected to get a horizontal displacement due to current effects. The figure also shows a closer view of the wire represented as mass-spring-damper systems in series. This is how the wire is to be modeled.

The hydraulic powering system for the winch is not in the scope of this paper, but is modeled as a hydraulic motor controlled by two servo operated proportional valves in a 4/3 valve configuration in addition to filters, pipelines, volumes, a pressure relief valve and a HPU, Hydraulic Power Unit, for pilot control of the proportional valves. Figure 2 shows a general schematic of the valve system connected to the hydraulic motor.

Here  $p_p$  is the pump pressure,  $p_T$  is the return pressure,  $u_H$  and  $u_L$  are the control references for the inner controllers controlling the valve displacements for the valve on the hoisting side and lowering side respectively. This hydraulic powering system is more elaborated in Skjong (2013), but detailed info can't be given because of confidentiality. It is important to note that there is a check valve at each side of the hydraulic motor to prevent vacuum. The pilot pressure is set to 200 bar and the main flow in the system is given from two pumps,

<sup>1</sup>Based on the specialization project by Stian Skjong (Skjong, 2013).

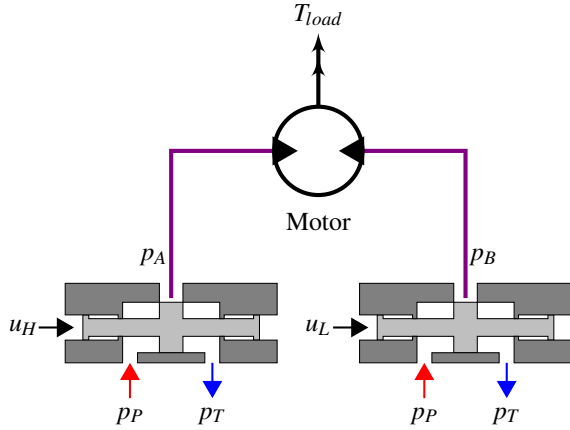


**Figure 2.** Sketch of hydraulic motor and valve configuration.

giving a total flow of  $7000 \text{ l/min}$ . The pressure relief valve is set to open when the pump pressure is a bit higher than the largest pressure in the motor. The motor is also affected by internal leakage.

## 2. WINCH MODEL

The winch model consists of a flexible coupling, reel, wire and a payload. The reel is connected to the hydraulic motor via the flexible coupling and the wire is rolled onto the reel causing a varying rotational inertia. The wire is modeled as a lumped mass-damper-spring system in series as figure 1 shows. In this paper  $y$  is the distance in vertical direction, positive above surface, and  $x$  is the distance in horizontal direction.

### 2.1. Wire

The wire affected by current should be modeled as series of elements in order to get a realistic deflection form and FEM, Finite Element Methods, are often used in such problems. Another way of modeling the wire is to approximate it as mass-damper-spring systems in series. This was done in T. Pedersen and E. Pedersen (2007) where marine seismic cables were modeled as lumped mass-damper-spring systems in series and compared to FEM. The same idea of a lumped system is used here to model the wire. In this case it is sufficient with a 2D model of the wire<sup>2</sup>. Figure 3 shows a sketch of one wire element. In the figure  $L_{we}$  is the length of one wire element,  $r_{we}$  is the elongation of one wire element,  $\theta_{we}$  is the angle between the vertical axis and the wire element,  $m_{we}$  is the mass of the wire element,  $y_0$  and  $x_0$  are the coordinates

<sup>2</sup>By assuming only horizontal current, as the only environmental disturbance, the coordinate system can be located in such a way that the forces and displacements of the wire only forms a 2D system.

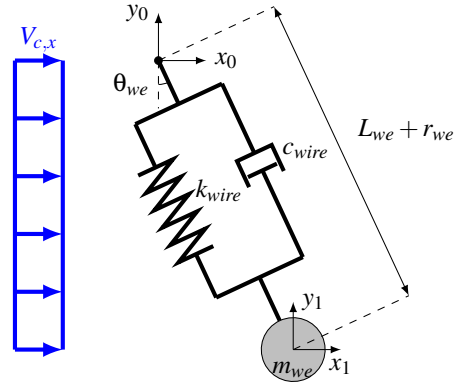


**Figure 3.** Sketch of a wire element.

for the top position of the element,  $x_1$  and  $y_1$  are the coordinates for the bottom position of the wire element,  $k_{wire}$  is the spring stiffness,  $c_{wire}$  is the damping coefficient and  $V_{c,x}$  is the current velocity in horizontal direction.

#### 2.1.1. Wire Dynamics

The spring stiffness is given as

$$k_{wire} = \frac{EA_w}{L_{we}} = \frac{ED_w^2\pi}{4L_{we}} \quad (1)$$

where  $E = 200 \text{ GPa}$  is the Elasticity modulus for steel,  $A_w$  is the area of the wire cross section and  $D_w$  is the diameter of the wire. The spring force is then given as

$$F_{ws} = k_{wire}r_{we} \quad (2)$$

The damping is given from a constant damping ratio assumed to be  $5^{-3}$ ,

$$\zeta = \frac{c_{wire}}{c_{cr}} = 5 \quad (3)$$

where

$$c_{cr} = 2m_{we}\sqrt{\frac{k_{wire}}{m_{we}}} = 2\sqrt{k_{wire}m_{we}} \quad (4)$$

This gives

$$c_{wire} = 2\zeta\sqrt{k_{wire}m_{we}} \quad (5)$$

The damping force is then given as

$$F_{wd} = c_{wire}\dot{r}_{we} \quad (6)$$

The elongation of the wire element is expressed as

$$r_{we} = \sqrt{(x_1 - x_0)^2 + (y_1 - y_0)^2} - L_{we} \quad (7)$$

<sup>3</sup>Assuming the damping ratio to be 5 - gives a over-damped system which is true for a wire.

and the derivative is

$$\begin{aligned} \dot{r}_{we} &= \frac{(x_1 - x_0)\dot{x}_1 + (y_1 - y_0)\dot{y}_1}{\sqrt{(x_1 - x_0)^2 + (y_1 - y_0)^2}} \\ &\quad - \frac{(x_1 - x_0)\dot{x}_0 + (y_1 - y_0)\dot{y}_0}{\sqrt{(x_1 - x_0)^2 + (y_1 - y_0)^2}} - \dot{L}_{we} \\ &= r_{i1}(\dot{x}_1 - \dot{x}_0) + r_{i2}(\dot{y}_1 - \dot{y}_0) - \dot{L}_{we} \end{aligned} \quad (8)$$

where

$$\begin{aligned} r_{i1} &= \frac{(x_1 - x_0)}{\sqrt{(x_1 - x_0)^2 + (y_1 - y_0)^2}} \\ r_{i2} &= \frac{(y_1 - y_0)}{\sqrt{(x_1 - x_0)^2 + (y_1 - y_0)^2}} \end{aligned} \quad (9)$$

The mass of the wire in air is given as

$$m_{we,Air} = A_w L_{we} \rho_{steel} = \rho_{wire} L_{we} \quad (10)$$

where  $\rho_{wire} = \rho_{steel} A_w = \rho_{steel} \frac{D_w^2 \pi}{4}$  kg/m and  $\rho_{steel} = 7800$  kg/m<sup>3</sup>. By including added mass from Morrison's equation a mass matrix is obtained. Morrison's equation is given by

$$\begin{aligned} F_M &= \\ \begin{bmatrix} F_{M,x} \\ F_{M,y} \end{bmatrix} &= \rho_{water} A_w L_{we} \begin{bmatrix} C_{I,x} \ddot{x} \\ C_{I,y} \ddot{y} \end{bmatrix} \\ &+ \frac{1}{2} \rho_{water} D_w L_{we} \begin{bmatrix} C_{d,x} \cos \theta_{we} (\dot{x} - V_{c,x}) |\dot{x} - V_{c,x}| \\ C_{d,y} \sin \theta_{we} (\dot{y} - V_{c,y}) |\dot{y} - V_{c,y}| \end{bmatrix} \end{aligned} \quad (11)$$

By including the first part of Morrison's equation in the mass matrix, it can be written as

$$\begin{aligned} M &= \begin{bmatrix} \rho_{wire} L_{we} & 0 \\ 0 & \rho_{wire} L_{we} \end{bmatrix} \\ &+ \begin{bmatrix} C_{a,x} \frac{\rho_{water}}{2} A_w L_{we} & 0 \\ 0 & C_{a,y} \frac{\rho_{water}}{2} A_w L_{we} \end{bmatrix}, \end{aligned} \quad (12)$$

where  $C_{a,x}$  and  $C_{a,y}$  are the added mass coefficients. By assuming the mass as a sphere, one may set  $C_{a,x} = C_{a,y} = 1$ . Note that  $C_I = 1 + C_a$ , see Faltinsen (1993). The assumption about the mass is not completely true, but for this purpose it is a sufficient assumption. In (5)  $m_{we}$  is set to  $\rho_{wire} L_{we} + c_{a,x} \frac{\rho_{water}}{2} A_w L_{we}$ .

The last part of Morrison's equation is the drag force<sup>4</sup>. For now  $C_{d,x} = C_{d,y} = 0.45$ ,  $V_{c,y} = 0$  m/s and  $V_{c,x} = 5$  m/s. A horizontal current of 5 m/s is perhaps too high, but is used only to verify the model. One can also use a time and depth dependant current later on. The gravity and buoyancy forces are given as

$$F_{BG} = [0, (\rho_{wire} L_{we} - \rho_{water} A_w L_w) g]^T \quad (13)$$

Note that the last wire element also should include the load.

<sup>4</sup>See T. Pedersen and E. Pedersen (2007) and (Faltinsen, 1993). In (Faltinsen, 1993) the drag coefficients for a sphere is said to lie between 0.23 and 0.5, depending on the Reynold's number. In T. Pedersen and E. Pedersen (2007) 0.45 was suggested.

## 2.1.2. Implementation

By implementing this in 20Sim a bond graph model for a wire element as shown in figure 4 can be obtained. The MTF-elements shown in the figure use  $r_{i1}$  and  $r_{i2}$  as transformer modulus and the MSf-element is the change of the length of the wire element, given by the winch speed. For a reel with diameter  $D$  and a wire with  $n$  elements,  $\dot{L} = \frac{D\omega}{n}$  where  $\omega$  is the winch speed. Inside the box Pos\_angle\_deltapos

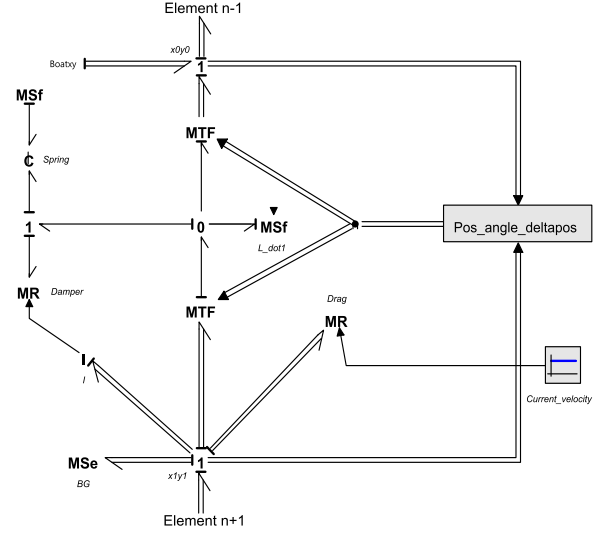


Figure 4. Bond-graph model of a wire element.

the length of the wire element, the angle and the transformer variables are calculated. The angle is given as

$$\theta_{we} = -\arctan\left(\frac{x_1 - x_0}{y_1 - y_0}\right) \quad (14)$$

and the length of the wire element is calculated from the positions. This is not completely true since that gives  $L_{we} + r_{we}$ , but since  $r \ll L_{we}$  and  $r_{we} \approx 0$  when  $L_{we}$  is small it is a reasonable assumption. Because most of the elements have variables as parameters, connections need to take place in the model as shown in the figure. Note that for the first element the position of the boat in xy-direction is added to the top position of the model through the Boatxy port. This is done only in the first wire element, giving the motion of the boat to the lumped system. Also an effort sensor is added only in the first wire element to connect the tension of the wire with the reel. The total wire model contains five wire elements, and in the last element the payload effects are added to the I-element, MSe-element and the MR-element (drag). The payload is assumed to be a sphere with diameter of 1 m and a mass of 6000 kg. This gives the same added mass coefficients and drag force coefficients as the wire. The elements are connected to each other in the top and bottom 1-junctions as seen in the figure.

## 2.2. Reel

The wire is connected to the reel, and the reel is influenced by the wire and its dynamics.

### 2.2.1. Reel Dynamics

The reel dynamics are dependent on the amount of wire stored onto it and the amount of wire in the water. Figure 5 shows the geometry of the reel. A full reel has a storage

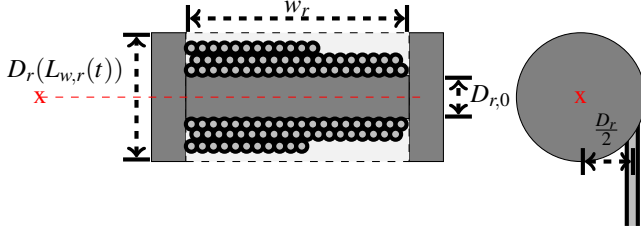


Figure 5. Reel sketch.

volume given by

$$V_{r,full} = \frac{D_{r,full}^2 - D_{r,0}^2}{4} w_r \pi \quad (15)$$

where  $V_{r,full}$  is the maximal storage volume on the reel,  $D_{r,full}$  is the diameter of a full reel,  $D_{r,0}$  is the diameter of an empty reel and  $w_r$  is the width of the reel. The volume of the wire is given by

$$V_w = \frac{D_w^2}{4} \pi L_w \quad (16)$$

By setting  $V_w = V_{r,full}$  we obtain the maximal length of wire stored on a full reel,

$$L_{w,r,full,ideal} = \frac{D_{r,full}^2 - D_{r,0}^2}{D_w^2} w_r \quad (17)$$

This is only an ideal length of wire, since no air is trapped in between. Therefore a correction factor,  $f_w$ ,  $0 < f_w < 1$ , should be included.

Then the actual maximal length of wire stored on the reel is given by

$$L_{w,r,full} = \frac{D_{r,full}^2 - D_{r,0}^2}{D_w^2} w_r f_w \quad (18)$$

The value of  $f_w$  is found by looking at how the wire can be stored. There are at least two ways the wire could be stored and one is given in figure 6. From the geometry in the figure  $f_w$  is given as

$$f_w = \frac{\frac{D_w^2}{4} \pi}{D_w^2} = \frac{\pi}{4} \approx 0.7854 \quad (19)$$

This is not the most effective way of storing the wire. Figure 7 shows a more compact packing of the wire and is the most

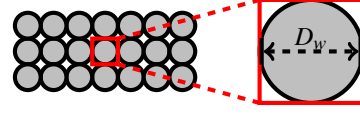


Figure 6. Wire packing on reel.

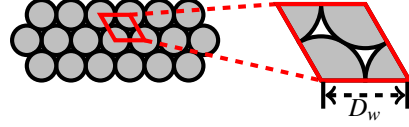


Figure 7. Compact wire packing on reel.

effective storing when the wire has a circular cross-section. Since the parallelogram has a sum of the angles equal to  $360^\circ$  and there is a circle center in each corner, there is in total one wire cross-section inside it.  $f_w$  is now given as

$$f_w = \frac{D_w^2 \pi}{4} \frac{1}{D_w^2 \sqrt{1 - \frac{1}{4}}} = \frac{\pi}{2\sqrt{3}} \approx 0.9069 \quad (20)$$

By solving for  $D_{r,full}$  in (18) the diameter of the reel with a given length of wire stored onto it is given as

$$D(L_{w,r}(t)) = \sqrt{\frac{L_{w,r}(t) D_w^2}{w_r f_w} + D_{r,0}^2} \quad (21)$$

Then the inertia of the reel can be calculated as

$$\begin{aligned} J(L_{w,r}(t)) &= J_{reel} + 2J_{flange} + J_{wire}(t) \\ &= \frac{1}{2} m_{reel} \frac{D_{r,0}^2}{4} \\ &\quad + 2 \frac{1}{2} m_{flange} \frac{D_{r,full}^2}{4} \\ &\quad + \frac{1}{2} \rho_{wire} L_{w,r}(t) \left( \frac{D(L_{w,r}(t))^2 - D_{r,0}^2}{4} \right) \\ &= \frac{1}{8} m_{reel} D_{r,0}^2 + \frac{1}{4} m_{flange} D_{r,full}^2 \\ &\quad + \frac{1}{8} \rho_{wire} L_{w,r}(t) \left( D_w^2 \frac{L_{w,r}(t)}{w_r f_w} + 2D_{r,0} D_w \sqrt{\frac{L_{w,r}(t)}{w_r f_w} + D_0^2} \right) \end{aligned} \quad (22)$$

### 2.2.2. Implementation

By implementing the reel in 20Sim a bond-graph model as shown in figure 8 can be retrieved. The IC-element calculates the total length of the wire with given  $D_{r,full}$  and  $D_{r,0}$  and from an initial length submerged wire it calculates the wire left on the reel. From this and a flow measurement  $L_{w,r}(t)$ ,  $D(L_{w,r}(t))$  and  $J(L_{w,r}(t))$  are calculated. For now  $D_{r,full} = 1$  m,  $D_{r,0} = 0.5$  m,  $m_{reel} = 200$  kg,  $m_{flange} = 50$  kg

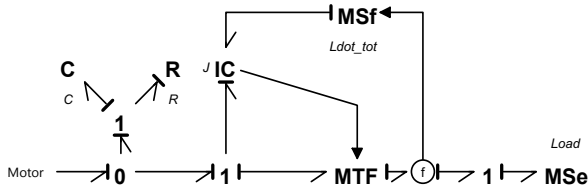


Figure 8. Bond-graph model of the reel.

and  $D_w = 0.025$  m. The transformer modulus for the MTF-element is  $\frac{D(L_{w,r}(t))n}{2}$ , where  $n = 2$  - is a gear ratio between the hydraulic motor and the reel, the spring and damping coefficient in the flexible coupling are set to  $k_{flex} = 1e7$  Nm/rad and  $c_{flex} = 1e5$  Nms/rad respectively. The MSe-element gets the tension from the wire.

By connecting the reel model to one wire element we get the total bond graph model shown in figure 9.

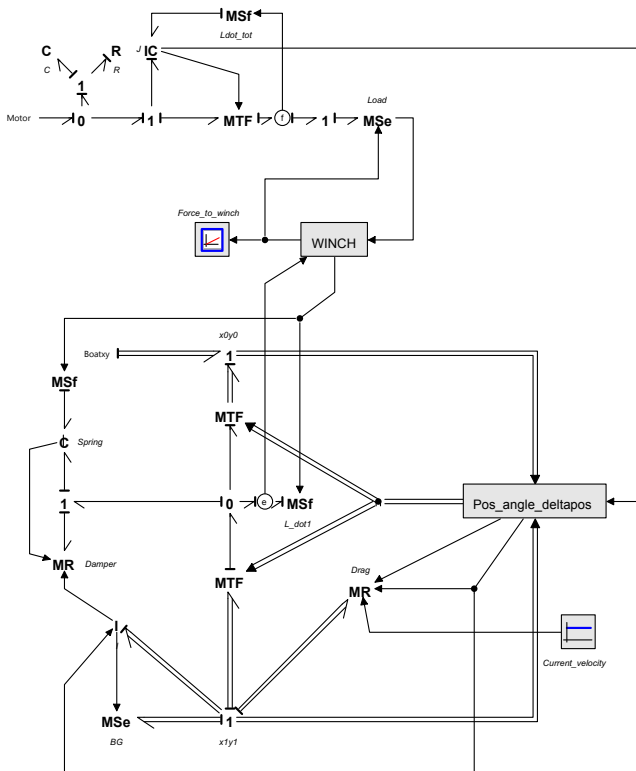


Figure 9. Total model of one wire element connected to the reel.

### 3. RESULTS AND DISCUSSION

The input signals used in the simulations are given in figure 10. The first two plots show the reference signals that are fed to the two inner controllers controlling the proportional valves. The last plot shows the flow delivered from the pump.

In these simulations simple P-controllers are used as inner controllers controlling the proportional valves.

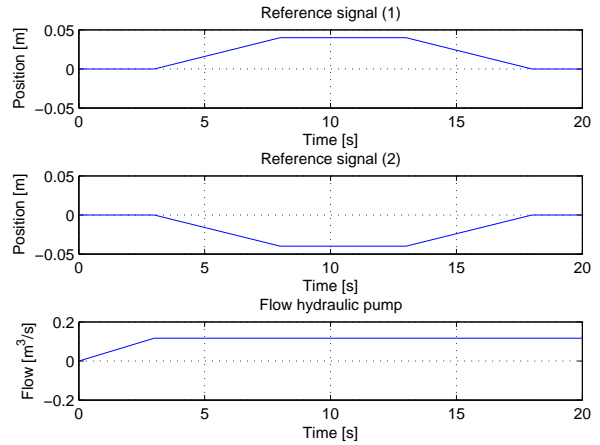


Figure 10. Reference signals for valve and flow delivered from the pump.

#### 3.1. Hoisting

The initial length of submerged wire is set to  $L_w = 100$  m. Reference signal (1) is fed to the proportional valve on the hoisting side of the motor, and reference signal (2) to the proportional valve on the lowering side. It can be seen from figure

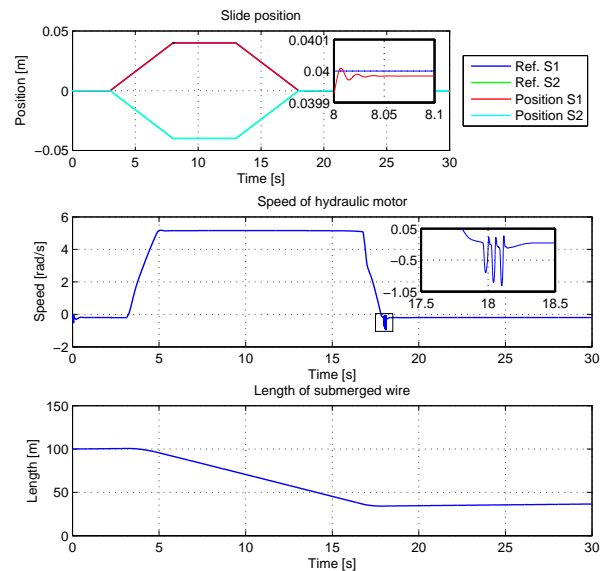
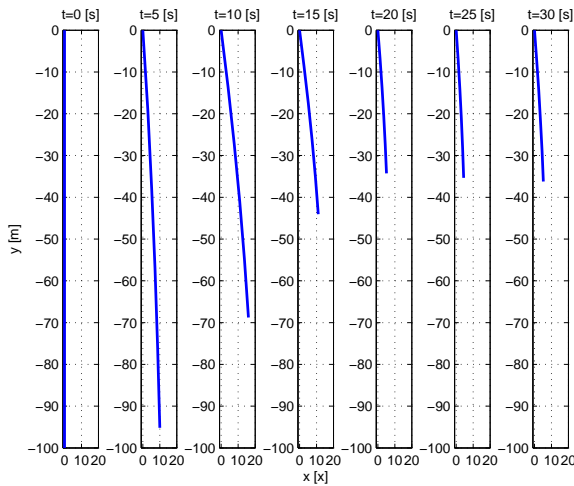


Figure 11. Reference signal, valve position, hydraulic motor velocity and length of submerged wire during hoisting operation.

11 that the position of the proportional valve and the motor velocity are reasonable. It looks like the actual position of the valves coincide with the references, but by looking at the magnified area in the plot it can be seen that there are small oscillations and a small bias present. This is because the reference signal is filtered through a first order transfer function acting as a velocity limitation function. A PI-controller should be implemented inside the velocity limiting transfer function to avoid bias on the reference signal. In addition there is also delay on the valve position sensors in the hydraulic model. It can also be seen that the maximal motor velocity is reached before maximal valve displacement. This means that the flow from the pump system sets the motor velocity. In the last plot, showing the length of submerged wire, it is illustrated the effect of internal leakage inside the motor. When the reference signal is zero it is possible to see that the wire slowly gets lowered. This can also be seen in the second plot where the motor velocity is slightly below zero when the reference signal is zero.



**Figure 12.** Wire displacement in water.

In figure 12 it is possible to see the wire in water in different time frames. Note that negative values mean below the surface. At  $t=0$  s the wire is 100 m long in a completely vertical displacement. At  $t=5$  s the hoist has started and the current displaces the wire horizontally. When the wire has a horizontal displacement the hoist operation gives an added horizontal displacement to the wire as it is possible to see in  $t=10$  s and  $t=15$  s. When the motor stops the horizontal displacement becomes smaller and an equilibrium between the forces acting on the wire is obtained. The equilibrium displacement after hoist is shown in  $t=30$  s.

### 3.2. Lowering

The initial length of submerged wire is set to  $L_w = 10$  m. Reference signal (2) is fed to the proportional valve on the hoisting side of the motor and reference signal (1) to proportional valve on the lowering side. It can be seen in figure

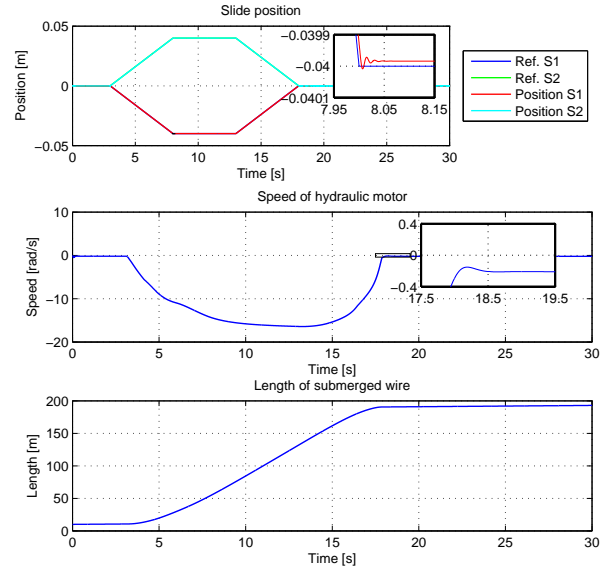


**Figure 13.** Reference signal, valve position, hydraulic motor velocity and length of submerged wire during lowering operation.

13 that the position of the proportional valve is as good controlled as in the hoisting simulation, but the motor velocity is relatively high. This is because a check valve opens to return pressure on the unloaded side of the motor, to prevent cavitation in the motor, which results in high motor velocities. When outer controllers, such as a speed controller, are to be designed, restrictions should be implemented to avoid such high motor velocities. In the last plot it is possible to see the length of submerged wire, which is approximately 193 m at the end of the simulation.

Figure 14 shows the displacement of the wire in sea in different time frames. As can be seen the horizontal displacement is largest when the motor velocity is zero. This has to do with the velocity of the wire with respect to the current is largest when the motor speed is zero, or positive as in the hoisting operation. This gives larger drag forces and hence the displacement in x-direction is larger.

## 4. CONCLUSION

It has been shown that even a simplified lumped wire model has a huge impact on the winch powering system. Without the winch model, simple P-controllers were enough to control the

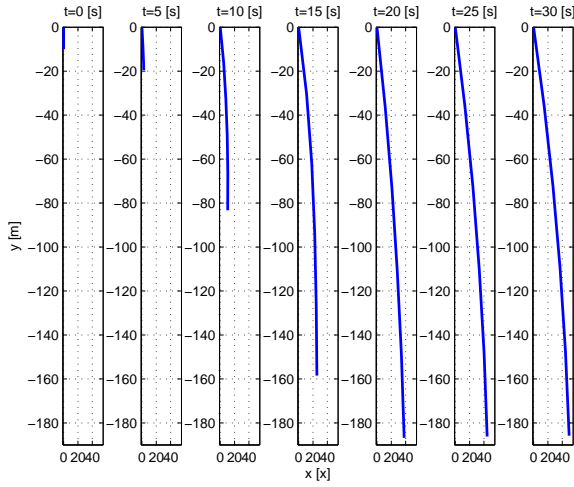


**Figure 14.** Wire displacement in water.

valve positions, but, with the wire model included an integral effect should also be included. In the hoisting case, the horizontal displacement of the wire was increased by the operation. This is because the sum of the current velocity and the horizontal wire velocity gets higher and therefore larger drag forces are acting on the wire. In the lowering case the opposite effect was seen. This is because the sum of the velocities gets lower in this case.

Since the length of the wire changes, the natural frequencies in the winch system also change. The undamped natural frequency of a wire element is given as

$$f_n = \frac{1}{2\pi} \sqrt{\frac{k}{m}} = \frac{1}{2\pi} \sqrt{\frac{EA_w}{L_{we}m}}. \quad (23)$$

These natural frequencies are important in the winch model, also for control design purposes. The responses from the winch model are also important if active heave compensation is to be designed. Then a MRU, Motion Reference Unit, should be used to measure the heave motion and give the measurements as input to outer controllers.

Figure 15 shows the loading of the hydraulic motor for the two simulations. It is possible to see that there are large forces

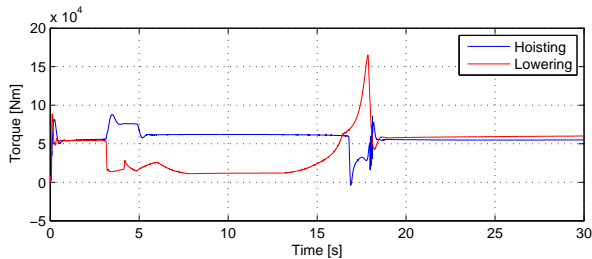


**Figure 15.** Loading of hydraulic motor.

in the beginning of the hoisting simulation but small in the end. This is because it requires more power to start hoisting than to stop hoisting. In the lowering simulation it is the opposite. The large forces are due to stopping the lowering operation, which requires more power than starting it. More discussions and results regarding forces, pressures, check valves and fluid flows are elaborated in Skjong (2013).

In general the major results and findings can be summarized as

- Even a model with few wire elements modeled as lumped mass-damper-spring systems in series tend to describe more accurately the main dynamics of a submerged wire influenced by environmental forces and by the operation performed.
- Using position control of the directional valve system in lowering operations give large forces on the winch powering system when a stop is performed. This would result in wear and tear of the system and should be avoided by using a speed controller to control the hydraulic motor.
- P-controllers were sufficient to control the valve displacements when neglecting the bias caused by the velocity limitation function. Controller including integral effects should be implemented in the velocity limitation functions to deal with the bias caused by it. Also derivative effect should be included in the valve controllers to damp out oscillations.

In the simulations performed the current was set as a constant, independent of time and depth. This is not the case in reality where the current slowly changes both direction and magnitude. This effect is easy to implement in the model and should be considered. Also a study of how many wire elements are necessary to include in the model to obtain good results compared to other modeling methods could be of interest. This is elaborated in T. Pedersen and E. Pedersen (2007).

## ACKNOWLEDGEMENTS

Thanks to Eilif Pedersen for the fruitful discussions regarding drag coefficients and damping ratio and for providing me additional data.

## REFERENCES

- Stian Skjong. *Specialization Project - Modeling and Control of Directional Valve System*, 2013. Confidential report.
- Tom A. Pedersen and Eilif Pedersen. *Bond Graph Modeling of Seismic Cables*, 2007.
- O. Faltinsen, 1993. *Sea Loads on Ships and Offshore Structures*



# C | Parameters

Table C.1: Parameters and coefficients used in the bond graph model.

Part	Description	Value
Global	$\rho$ , Fluid density	889 kg/m <sup>3</sup>
	$\beta_f$ , Bulk modulus, hydraulic fluid	1.6e9 Pa
	$\beta_h$ , Bulk modulus, pipes	60e9 Pa
	$s$ , Gas-fluid ratio in bulk modulus equation (2.7)	0.002-
	$T_s$ , Sampling time	0.001 s
	$T_d$ , Sampling delay	0.002 s
	$p_{vap}$ , Vapour pressure for hydraulic fluid	-99900 Pa
Pilot valve	$f$ , Natural frequency in valve dynamics	120 Hz
	$K$ , Gain in valve dynamics	1 m/N
	$\zeta$ , Relative damping in valve dynamics	0.9-
	$C_d$ , Flow coefficient in pilot valve given by third order polynomial, if $p \cdot f > 7$ , $C_d = p_1 p \cdot f^3 + \dots + p_4$ else $C_d = 0.92$	$p_1 = 0.001979 \text{ s}^3/\text{m}^9$ $p_2 = -0.060833 \text{ s}^2/\text{m}^6$ $p_3 = 0.560729 \text{ s}/\text{m}^3$ $p_4 = -0.703125-$
	$A_{max}$ , Maximal opening area	6.6406e-6 m <sup>2</sup>
3/3-Directional valve (with fluid inertia and cylinder accumulation)	$V_0$ , Initial volume in Vol1, see figure 2.3	0.01 m <sup>3</sup>
	$V_0$ , Initial volume in Vol2, see figure 2.3	1e-5 m <sup>3</sup>
	$V_0$ , Initial volume in Vol3, see figure 2.3	1e-5 m <sup>3</sup>
	$p_0$ , Initial pressure	1.5e5 Pa
	$k_c$ , Design parameter in check-valve located between HPU and pilot valve	4e11 m <sup>6</sup> /Pas <sup>2</sup>
	$\tau$ , Time constant in check-valve, loacted between HPU and pilot valve	0.005 s
	$f_{pl}$ , Loss factor in pipe A	2-
	$D_{pi}$ , Internal diameter in pipe A	0.008 m
	$L_p$ , Length of pipe A	0.16 m
	$f_{pl}$ , Loss factor in pipe ,	2-
	$D_{pi}$ , Internal diameter in pipe B,	0.008 m
	$L_p$ , Length of pipe B	0.1 m
	$A_s$ , Area of control slide	0.001583 m <sup>2</sup>
	$V_0$ , Initial volume in cylinder accumulation (A and B)	1e-4 m <sup>3</sup>
	$k_s$ , Spring stiffness in centring spring	11700 N/m
	$x_{s0}$ , Pre-compression of centring spring	0.03 m
	$s$ , Slope in arctan( $\cdot$ )-function, centring spring	10000-
$p_{L1}$ , Parameter in loss function	32389 Ns <sup>2</sup> /m <sup>2</sup>	
$p_{L2}$ , Parameter in loss function	37333 Ns/m	

	$m_s$ , Weight of control slide	35 kg
	$V_{max}$ , Maximal velocity in velocity limitation function	0.315 m/s
	$K_p$ , Proportional controller gain in velocity limitation function	5000 -
	$K_i$ , Integral controller gain in velocity limitation function	15 -
	$K_p$ , Proportional controller gain in control slide position controller	6000 -
	$k_c$ , Design parameter in check-valve located between delivering and return line in main valve	$40 \text{ m}^6/\text{Pas}^2$
	$\tau$ , Time constant in check-valve, loacted between delivering and return line in main valve	0.05 s
	$k_f$ , Flow force parameter for the bond graph element MR, PA and AT	0.5 -
	$\alpha_{x_s}$ , Flow parameter for the bond graph element MR, PA and AT, assumed constant	$0.7 \frac{\text{m}}{\text{s}} \sqrt{\frac{\text{kg}}{\text{Nm}}}$
	$D_s$ , Diameter of control slide	0.14 m
Hydraulic motor	$G$ , Conductance of laminar resistance	$4.8\text{e-}9 \text{ m}^3/\text{Pas}$
	$D_m$ , Motor displacement	$0.13 \text{ m}^3/\text{rev}$
	$F_s$ , Static friction in (2.22)	105 Nm
	$s$ , Coefficient in (2.22)	10 -
	$c$ , Coefficient in (2.22)	5 -
	$\mu_s$ , Coefficient in (2.22)	1 -
	$\mu_c$ , Coefficient in (2.22)	0.2 -
	$\mu_v$ , Coefficient in (2.22)	2 -
	$J$ , Rotational inertia	$50 \text{ kgm}^2$
	$V_0$ , Initial volume, VolumeA and VolumeB	$0.04 \text{ m}^3$
Pressure compensator	$C_d$ , Flow coefficient in nozzle	0.3 -
	$A_n(x_c)$ , Area in nozzle, assumed to be given as $A_n(x_c) = p_1 x_c + p_2$	$p_1 = 6\text{e-}4 \text{ m}$ $p_2 = 1\text{e-}4 \text{ m}^2$
	$V_0$ , Initial volume, Vol	$0.001 \text{ m}^3$
	$A_{cp}$ , Piston area in pressure compensator	$0.01131 \text{ m}^2$
	$m$ , Weight of moving parts in pressure compensator	20 kg
	$x_{clim}$ , Maximal stroke of piston in pressure compensator	0.04 m
	$k_{cstop}$ , Spring stiffness in stopping element	$1\text{e}8 \text{ N/m}$
	$b_{cstop}$ , Damping parameter in stopping element	$1\text{e}6 \text{ Ns/m}$
	$k_{cs}$ , Spring stiffness in plunger spring	$16250 \text{ N/m}$
	$x_{c0}$ , Pre-compression in plunger spring	0.21 m
	$F_s$ , Static friction in (2.22)	1000 N
	$s$ , Coefficient in (2.22)	100 -
	$c$ , Coefficient in (2.22)	5 -
	$\mu_s$ , Coefficient in (2.22)	1 -
	$\mu_c$ , Coefficient in (2.22)	0.1 -

	$\mu_v$ , Coefficient in (2.22)	3 -
	$D_h$ , Hydraulic diameter	0.1 m
	$A_{co}(x_c)$ , Opening area in pressure compensator, assumed to be given as $A_{co}(x_c) = \pi D_h x_c$	-
	$k_{cf}$ , Flow force coefficient	0.6 -
	$\alpha_{x_c}$ , Flow parameter assumed constant	$0.7 \frac{m}{s} \sqrt{\frac{kg}{Nm}}$
3/2-directional valve	$f$ , Natural frequency in valve dynamics	120 Hz
	$\zeta$ , Damping ratio in valve dynamics	0.9 -
	$K$ , Gain in transfer function, valve dynamics	1 m/N
	$V_0$ , Initial volume	$0.001 m^3$
	$A_{max}$ , Maximal opening area	$1.9643e-4 m^2$
	$C_d$ , Flow coefficient	0.8 -
HPU	$p_P$ , Pilot pressure	193e5 Pa
	$p_T$ , Tank pressure	1.5e5 Pa
Total model	$D_i$ , Internal diameter in pressure line	$0.25 m^2$
	$f_{pl}$ , Loss factor in pressure line	16 -
	$L_p$ , Length of pressure line	40 m
	$D_i$ , Internal diameter in return line	$0.20 m^2$
	$f_{pl}$ , Loss factor in return line	10 -
	$L_p$ , Length of return line	40 m
	$V_0$ , Initial volume, VolumeP	$0.343 m^3$
	$V_0$ , Initial volume, VolumeR	$1.037 m^3$
	$p_T$ , Tank pressure	1.5e5 Pa
	$G$ , Conductance of laminar resistance	$1.04166e-9 m^3/Pas$
	$D_h$ , Hydraulic diameter in loss function	0.15 m
	$C_d$ , Flow coefficient in loss function	0.2218 -



# D | Additional Sensitivity Studies

This chapter includes additional parameter sensitivity studies to those given in section 3.2.

## D.1 Volume Ratio in Bulk Modulus

The volume ratio between the air and the fluid in the bulk modulus is set to 0.002- in tabel C.1. It is changed with  $\pm 50\%$  and the results are given in figure D.1.

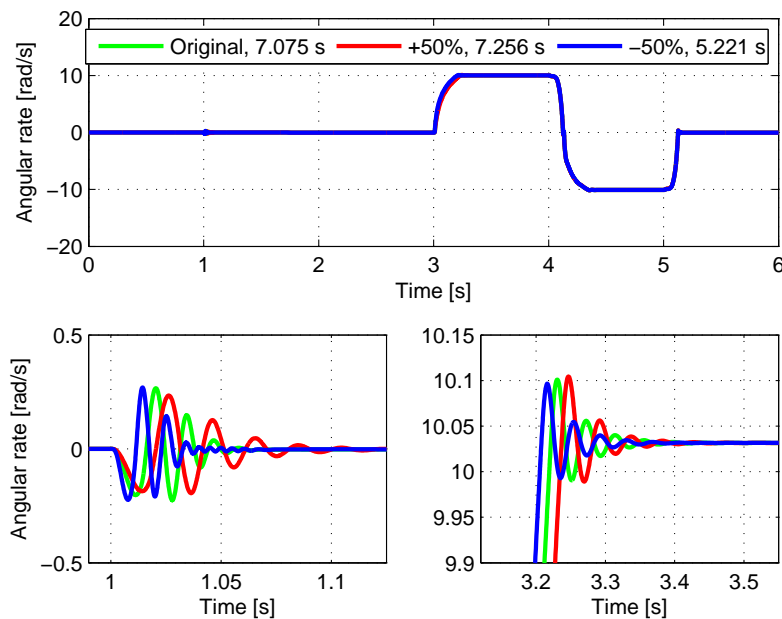


Figure D.1: Sensitivity of volume rate in bulk modulus.

As the results show an increase in the volume rate gives a slower response for the hydraulic motor and an increase gives a faster response. Also the decrease of the volume rate gives more damping than an increase. The solving time for the simulation is reduced by about 1.8 s, which is significant.

## D.2 Pressure Compensator

### D.2.1 Nozzle Area in Pressure Compensator

The opening area in the nozzle in the pressure compensator is given in table C.1 as  $A_n(x_c) = p_2 x_c + p_1 = 1e-4 + 6e-4 x_c \text{ m}^2$ . This means that the nozzle always is littlebit open. The parameter  $p_1$  is changed with  $\pm 50\%$ . The results are shown in figure D.2.

By reducing the nozzle area more oscillations occur at  $t = 1 \text{ s}$ , but the amplitude of these oscillations are lower. By making the area larger, fewer oscillations occur but the amplitudes of these are higher. Looking at the plot in the lower right corner of the figure it can be seen that

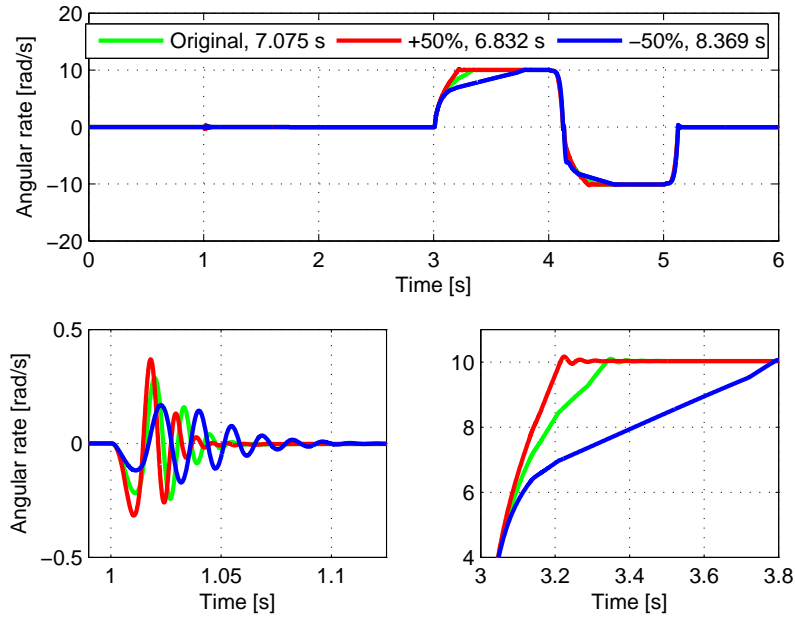


Figure D.2: Sensitivity of nozzle area in pressure compensator.

the motor gets slower with a reduced area than with an increased. This is because the reduced area gives more damping than an increased nozzle area, but the solving time gets higher. The nozzle area should be treated carefully and not changed too much in order to retain the same motor dynamics. If to be changed it should be increased.

## D.2.2 Nozzle Flow Coefficient

The flow coefficient for the nozzle in the pressure compensator is given as  $C_d = 0.3$  in table C.1. The flow coefficient is changed with  $\pm 50\%$  and the result is shown in figure D.3.

The figure shows that a reduction in flow coefficient gives a higher solving time and slower motor dynamics than an increase.

## D.2.3 Plunger Diameter

The diameter of the plunger, the moving piston in the pressure compensator, is given as 0.1 m in table C.1. The diameter is changed with  $\pm 50\%$  and the results are shown in figure D.4.

The results given in the figure are almost identical to the results in D.2.1 except that reduced diameter gives larger oscillation amplitudes and increased diameter gives lower oscillation amplitudes. The duration of the oscillations are the same and the solving time is almost the same for the three simulations.

## D.2.4 Flow Coefficient

The flow coefficient in the pressure compensator determines the flow through the valve and is in table C.1 given as 0.7-. The coefficient is changed with  $\pm 50\%$  and the results are given in figure D.5.

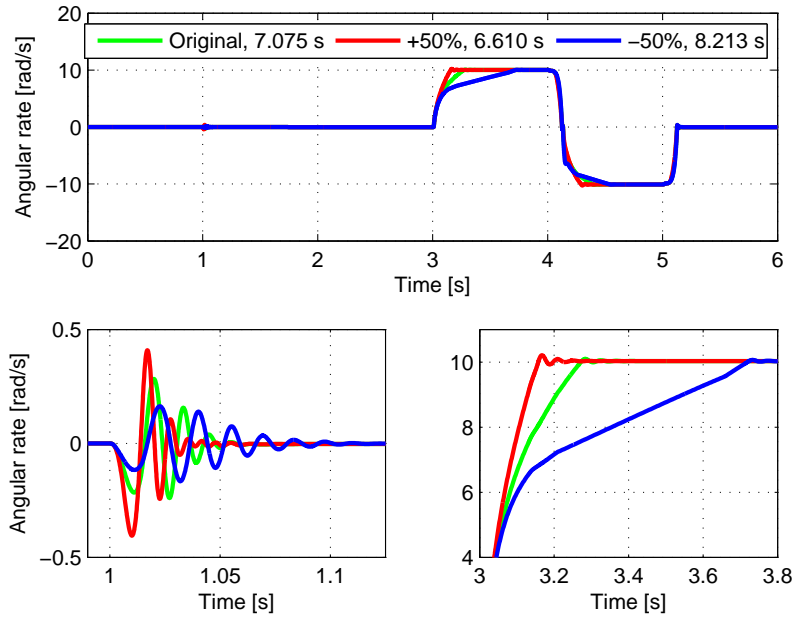


Figure D.3: Sensitivity of nozzle flow coefficient in pressure compensator.

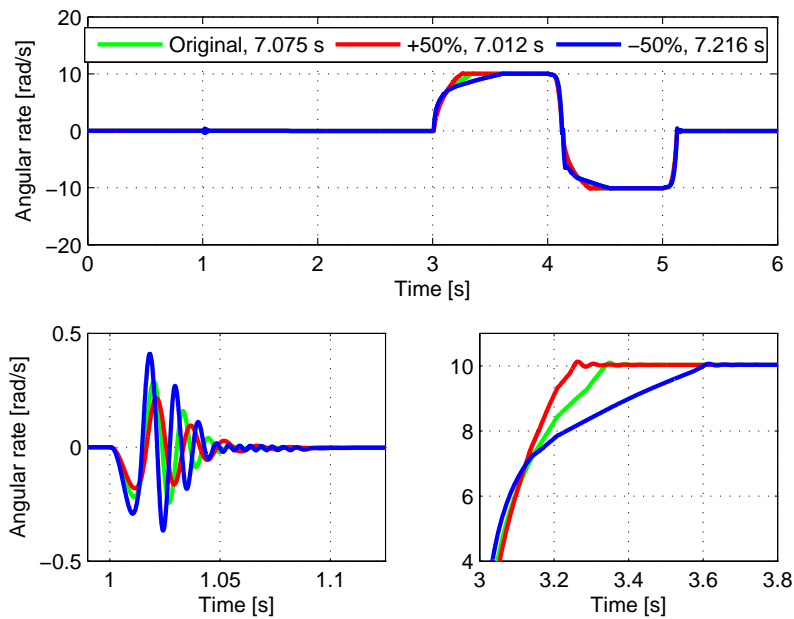


Figure D.4: Sensitivity of plunger diameter in pressure compensator.

As can be seen from the figure the results are almost the same as in D.2.3.

### D.2.5 Inertia

The weight of the moving parts in the pressure compensator is set to 20 kg. The inertia is changed with  $\pm 50\%$  and the results are shown in figure D.6. The change in the inertia for the moving parts in the pressure compensator has less implications for the total model than the other parameters studied before, both in motor velocity and solving time.

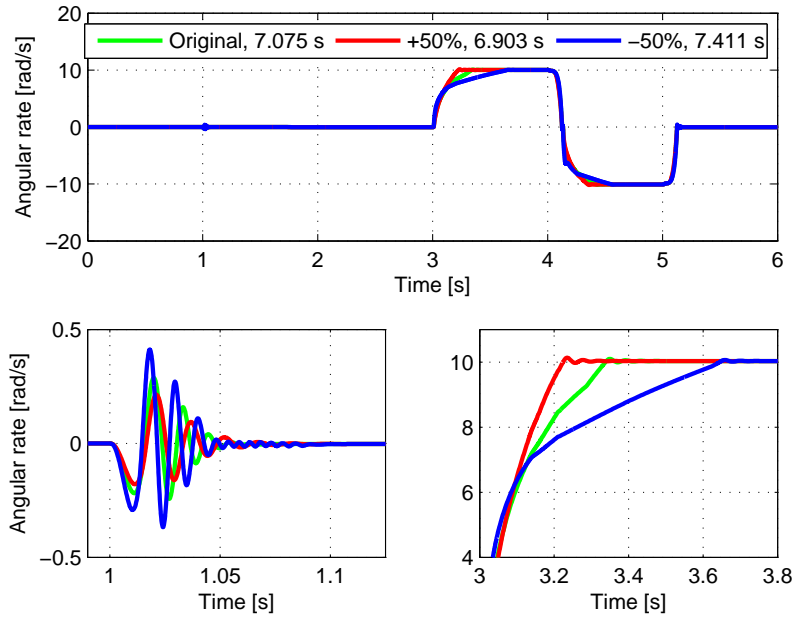


Figure D.5: Sensitivity of flow coefficient,  $\alpha$  in pressure compensator.

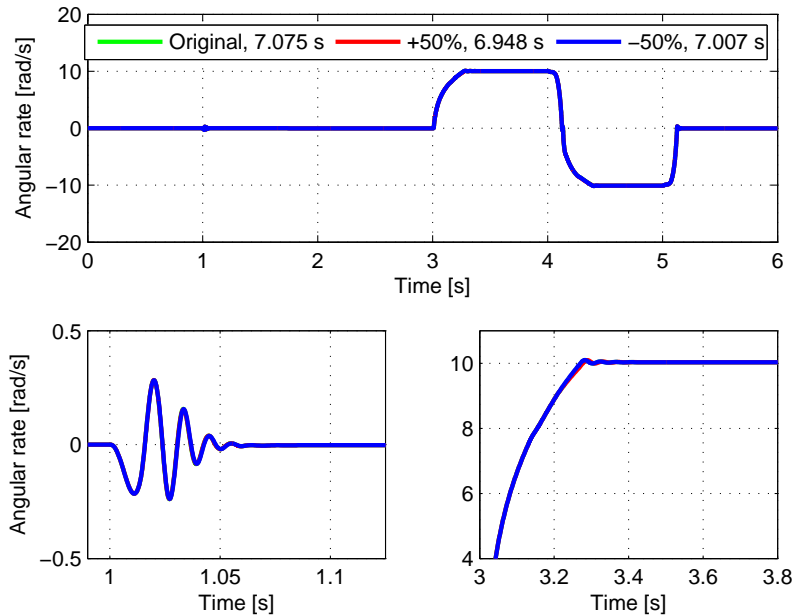


Figure D.6: Sensitivity of inertia in pressure compensator.

### D.2.6 Spring Stiffness

The spring stiffness in the pressure compensator is in table C.1 given as  $16250 \text{ N/m}$ . The spring stiffness is changed with  $\pm 50\%$  and the pre-compression is also changed so that the difference between the pump pressure and the highest pressure of the sides of the hydraulic motor is retained. The results are shown in figure D.7.

Also for this parameter the changes have less implications on the hydraulic motor response, both for the angular rate and for the solving time.



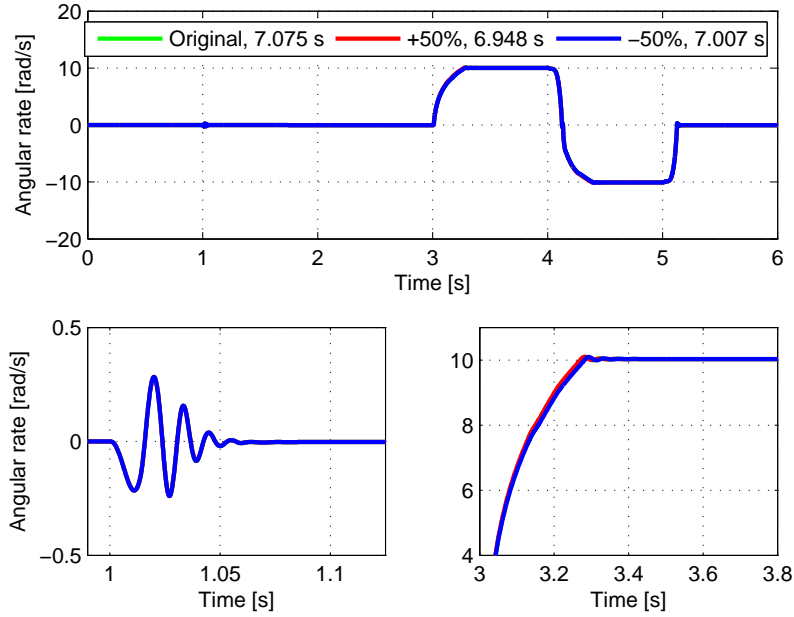


Figure D.7: Sensitivity of spring stiffness in pressure compensator.

### D.2.7 Slope in Friction Function

The slope in the friction function in the pressure compensator is given as 100- in table C.1. The slope is changed with  $\pm 50\%$  and the results are given in figure D.8.

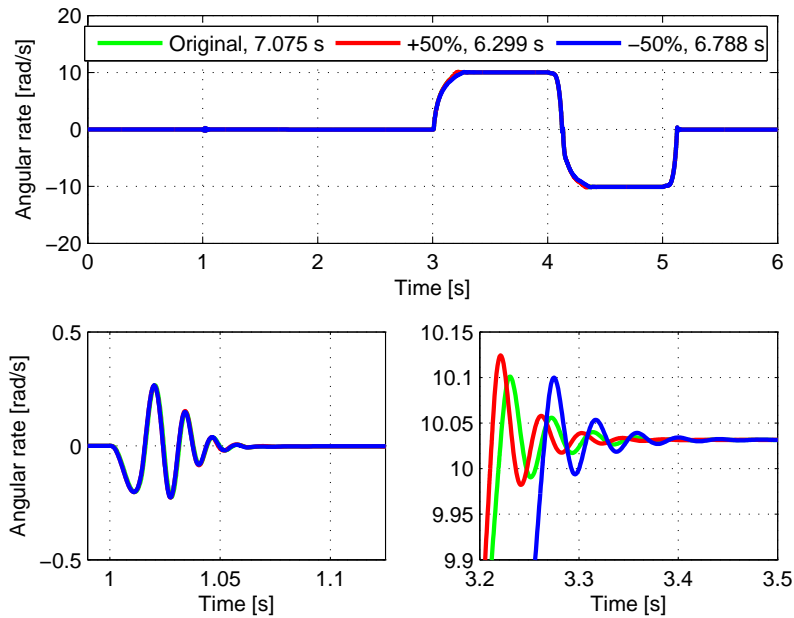


Figure D.8: Sensitivity of slope in friction function in pressure compensator.

As can be seen in the figure the changes in the slope do not affect the oscillations in the start of the simulation but the response of the hydraulic motor. A decreased slope gives both decreased solving time and faster motor response. An increased slope gives a slower motor response.

### D.2.8 Static Friction

The static friction in the pressure compensator is given as 1000 N in table C.1. The static friction is changed with  $\pm 50\%$  and the results are given in figure D.9.

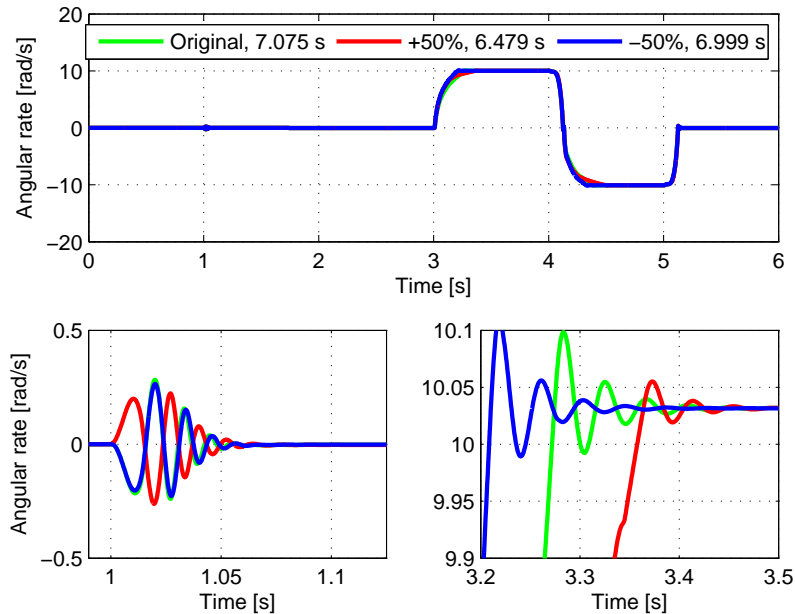


Figure D.9: Sensitivity of static friction in pressure compensator.

The results show that an increase in the static friction both gives more damping to the system and slows the hydraulic motor response down as well as reducing the solving time. A decrease in the static friction gives less damping to the system, increases the response time of the hydraulic motor as well as reducing the solving time. However reducing the damping and increasing the static friction is not ideal, since decreased damping gives more oscillations and increased static friction gives more wear and tear of the pressure compensator.

### D.2.9 Volume in Pressure Compensator

The oil volume in the pressure compensator is small and acts as a non-linear spring due to the variable bulk modulus. The initial volume is in table C.1 given as  $V_0 = 0.001 \text{ m}^3/\text{s}$ . The initial volume is changed with  $\pm 50\%$ . The results are shown in figure D.10.

As can be seen in the figure at  $t = 1 \text{ s}$ , when the load is initiated, the changes in the volume gives a change of phase for the motor velocity oscillations. Also the results show that the motor acceleration is lower for a higher volume. The change in solving time is not large, but if a more complex simulation was to be studied the change in volume could make the solving time lower without changing the results too much.

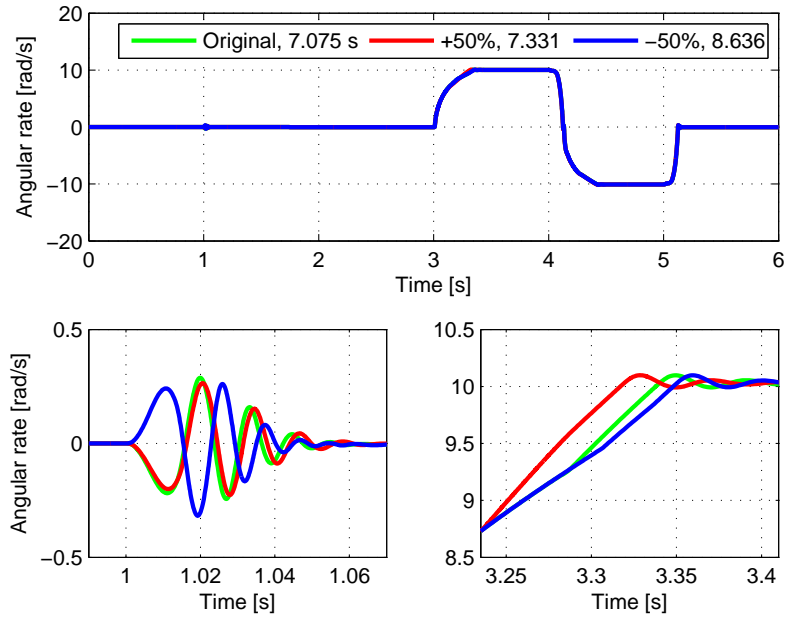


Figure D.10: Sensitivity of initial volume in pressure compensator.

### D.3 3/2-Directional Valve

#### D.3.1 Gain in 3/2-Directional Valve Dynamics

The gain in the 3/2-directional valve dynamics is given in table C.1 as 1 m/N. The gain is changed with  $\pm 50\%$  and the results are given in figure D.11.

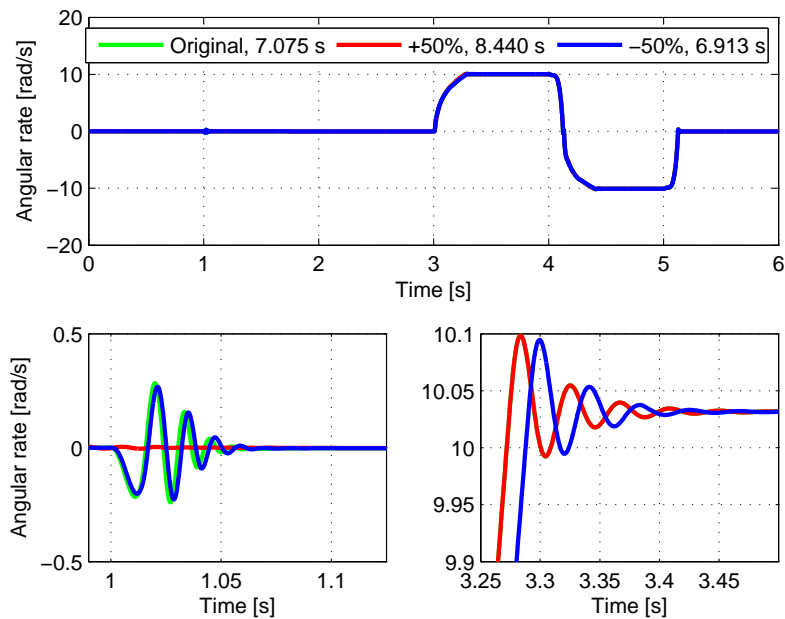


Figure D.11: Sensitivity of gain in the 3/2-directional valve dynamics.

As can be seen in the figure a decrease in the gain gives not large changes in the motor ve-

locity response and solving time. However an increase gives less oscillation in the start of the simulation, a faster response of the hydraulic motor and an increase in solving time.

### D.3.2 Natural Frequency

The natural frequency in the 3/2-directional valve is set to 120 Hz. The natural frequency is changed with  $\pm 50\%$  and the results are given in figure D.12.

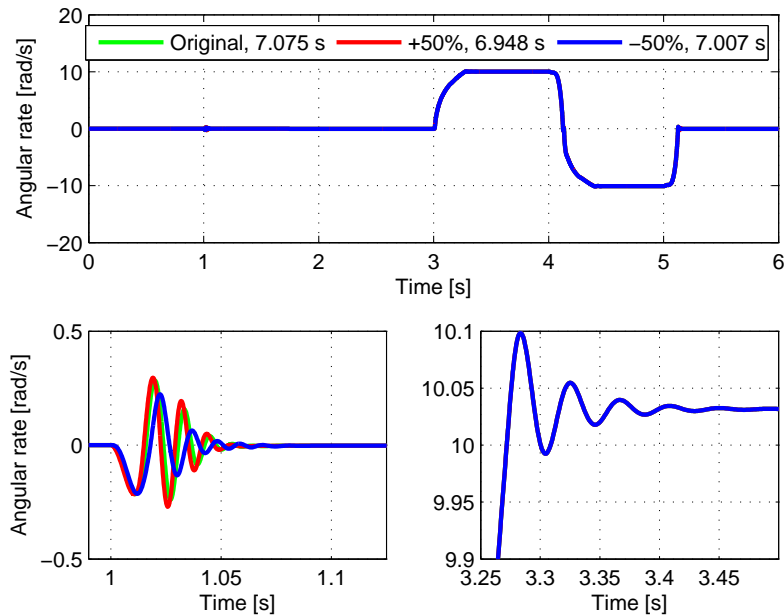


Figure D.12: Sensitivity of natural frequency in the 3/2-directional valve dynamics.

As can be seen in the figure the difference in both motor velocity response and solving time is not large.

### D.3.3 Damping Ratio

The damping ratio,  $\zeta$ , is in table C.1 given as 0.9-. The damping ratio is changed with  $\pm 50\%$  and the results are given in figure D.13.

As can be seen from the figure the changes in the damping ratio do not affect the motor velocity or the solving time of the simulation that much.

### D.3.4 Flow Coefficient

The flow coefficient for the 3/2-directional valve is set to 0.8- in table C.1. The flow coefficient is changed with  $\pm 50\%$  and the results are given in figure D.14.

A decrease in the flow coefficient seems to give a faster motor response and an increase seems to have no effect. Also a decrease in the flow coefficient gives additional damping, but the effect is moderate.

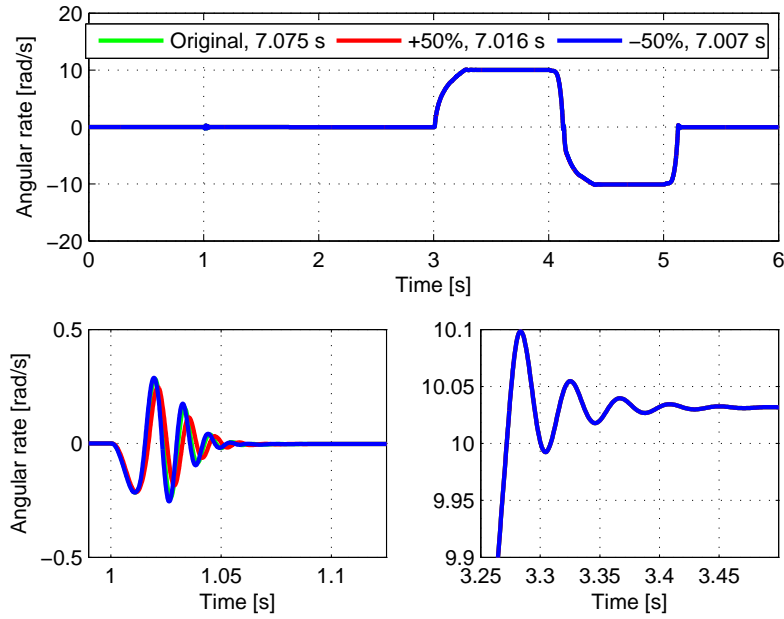


Figure D.13: Sensitivity of damping ratio,  $\zeta$ , in the 3/2-directional valve dynamics.

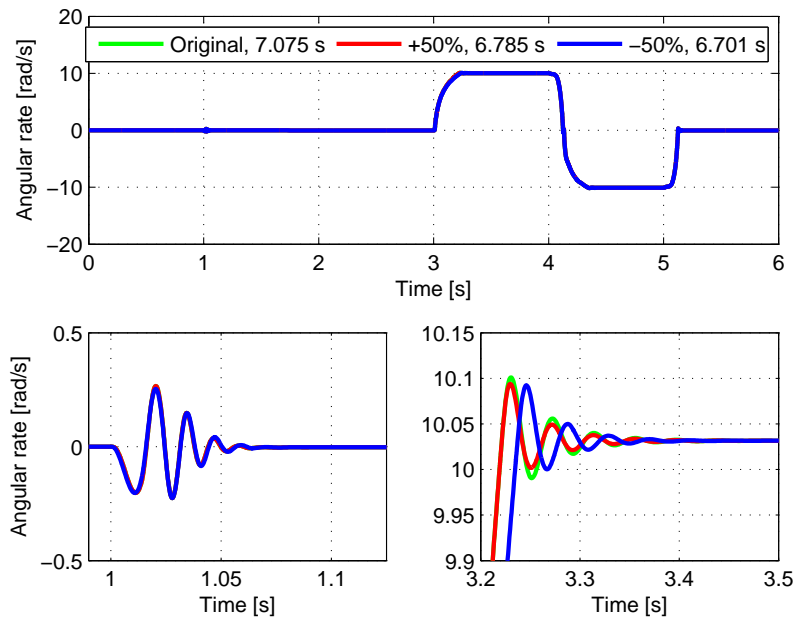


Figure D.14: Sensitivity of the flow coefficient in the 3/2-directional valve.

### D.3.5 Initial Volume in 3/2-Directional Valve

The initial volume in the 3/2-directional valve is in table C.1 given as  $0.001 \text{ m}^3$ . The initial volume is changed with  $\pm 50\%$  and the results are given in figure D.15.

As shown in the figure the changes in the hydraulic motor response are moderate but a decrease in initial volume gives an increase in solving time in the simulation. This means that the initial volume should not be decreased.

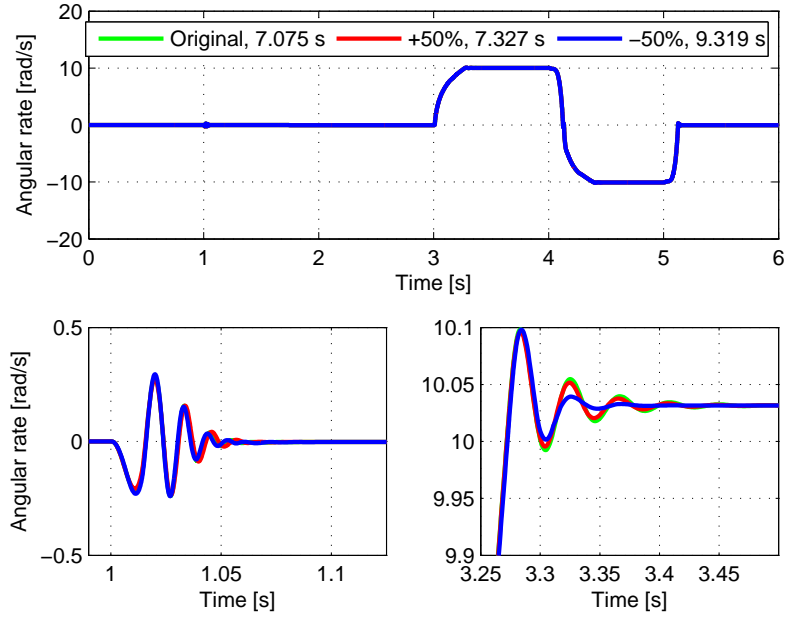


Figure D.15: Sensitivity of initial volume in the 3/2-directional valve dynamics.

## D.4 Hydraulic Motor

### D.4.1 Internal Leakage in Hydraulic Motor

The conductance of linear resistance is given as  $4.8e-9 m^3/Pas$  in table C.1. The conductance is changed with  $\pm 50\%$  and the results are given in figure D.16.

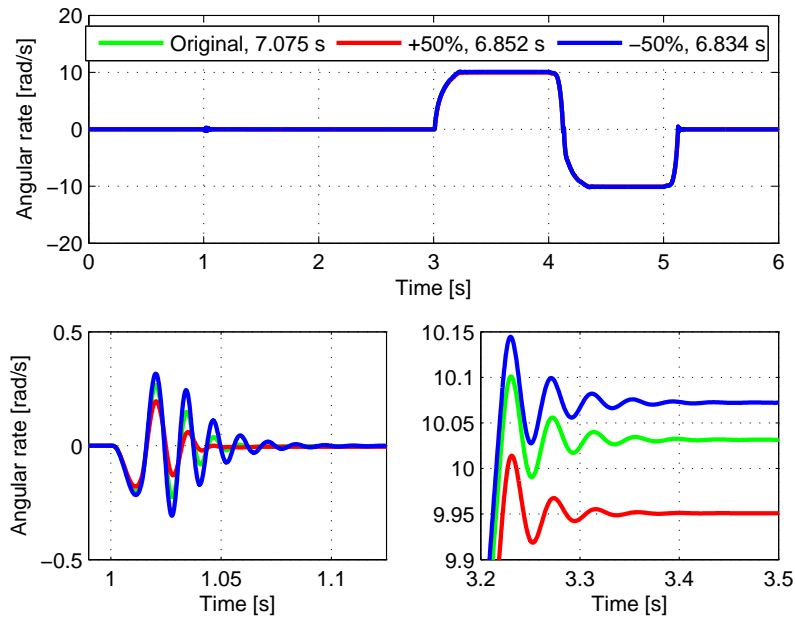


Figure D.16: Sensitivity of internal leakage in the hydraulic motor.

The results show that increased conductance gives more damping, but the maximal motor

velocity is lowered. A decrease in conductance gives an increase in maximal motor velocity but also more oscillations. The figure also shows that the increase or decrease in maximal motor velocity is not linear with the conductance.

#### D.4.2 Static Friction in Hydraulic Motor

The static friction in the hydraulic motor is given as  $105 \text{ Nms/rad}$  in table C.1. The static friction is changed with  $\pm 50\%$  and the results are given in figure D.17.

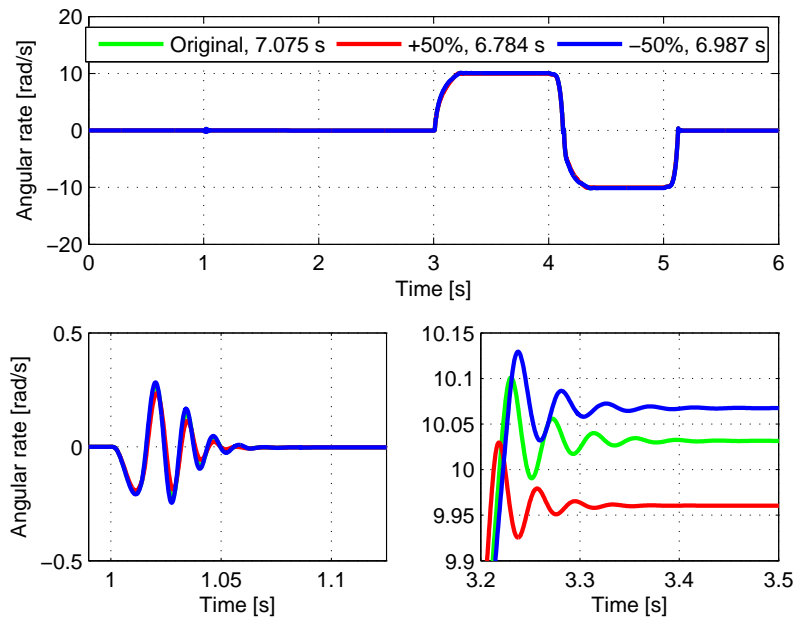


Figure D.17: Sensitivity of static friction for the hydraulic motor.

As expected the maximal motor velocity goes down by increasing the static friction, but the motor response seems to be littlebit faster. By decreasing the static friction the maximal motor velocity goes up, but the motor response seems to be slower. The difference between the increase and decrease shows that linear changes in the static friction gives non-linear changes in the maximal motor velocity, as it was for the internal motor leakage in the hydraulic motor, see figure D.16.

#### D.4.3 Friction Slope in Hydraulic Motor

The slope in the friction function for the hydraulic motor is set to 10- in table C.1. The slope is changed with  $\pm 50\%$  and the results are given in figure D.18.

Both a decrease and an increase in the slope in the friction function for the hydraulic motor do not affect the motor response. It also reduces the solving time for the simulation. However it does not give any additional damping and the solving time is only reduced by almost 0.25 s. The solving time in the simulations vary even though all parameters are the same, so it is not certain that there is a reduction in solving time at all.

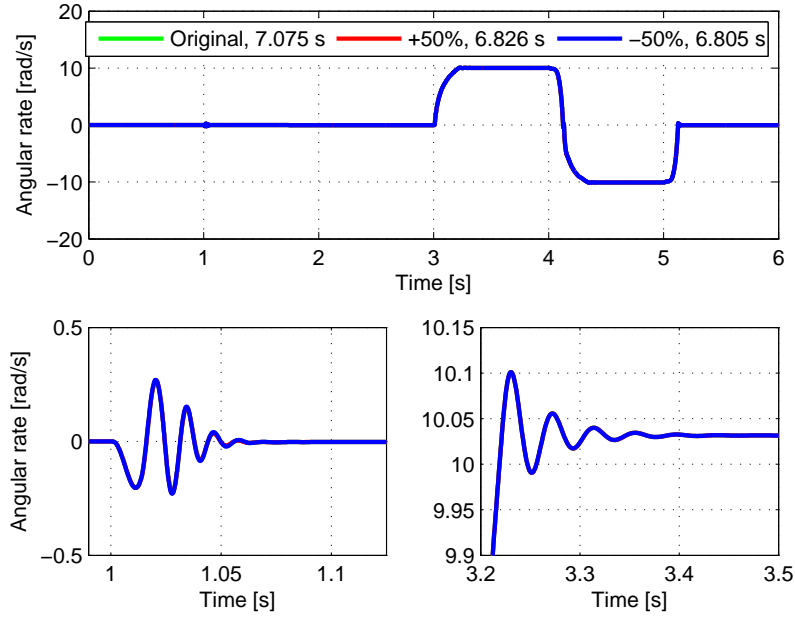


Figure D.18: Sensitivity of slope in friction function for the hydraulic motor.

## D.5 Outer System

### D.5.1 Loss Factor in Pressure Line

The loss factor in the pressure line connecting the pump to the two main valves has a loss factor given as 8- in table C.1. The loss factor is changed with  $\pm 50\%$  and the results are given in figure D.19.

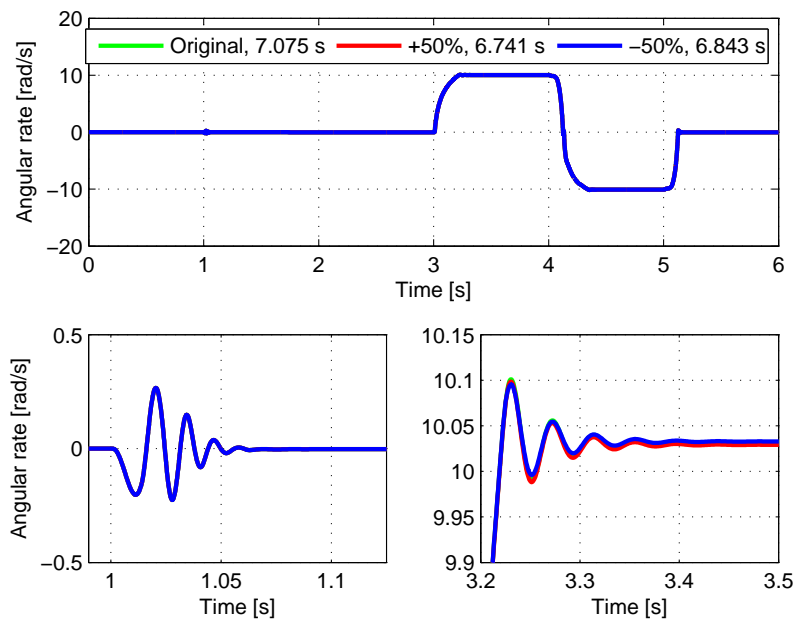


Figure D.19: Sensitivity of loss factor in pressure line.



The results show the changes in the loss factor do not affect the motor response significantly and can be neglected.

## D.5.2 Initial Volume in Volume P

The initial volume in volume P is given as  $0.343 m^3$  in table C.1. The initial volume is changed with  $\pm 50\%$  and the results are given in figure D.20.

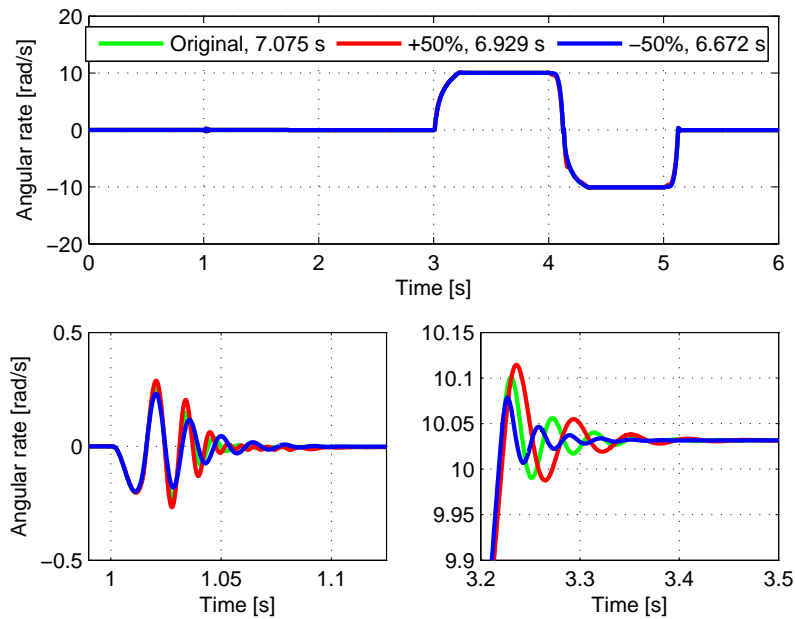


Figure D.20: Sensitivity of initial volume in volume P.

As the figure shows an increase in the initial volume gives less damping and a decrease in the initial volume gives more damping to the motor velocity.

## D.6 3/3-Directional Valve

### D.6.1 Control Slide Inertia

The control slide inertia is given as 35 kg in table C.1. The inertia is changed with  $\pm 50\%$  and the results are given in figure D.21.

The results show that the motor response is not significantly affected by the changes in the inertia. This is due to the position controller that manages to track the reference signal even though the inertia is changed.

### D.6.2 Initial Volume, Volume 1 and 2

The volumes 1 and 2 in the main valves have initial volumes of  $1e-5 m^3$ . The initial volumes are changed with  $\pm 50\%$  and the results are given in figure D.22.

As the results show the changes in the initial volumes 1 and 2 do not affect the motor response significantly.

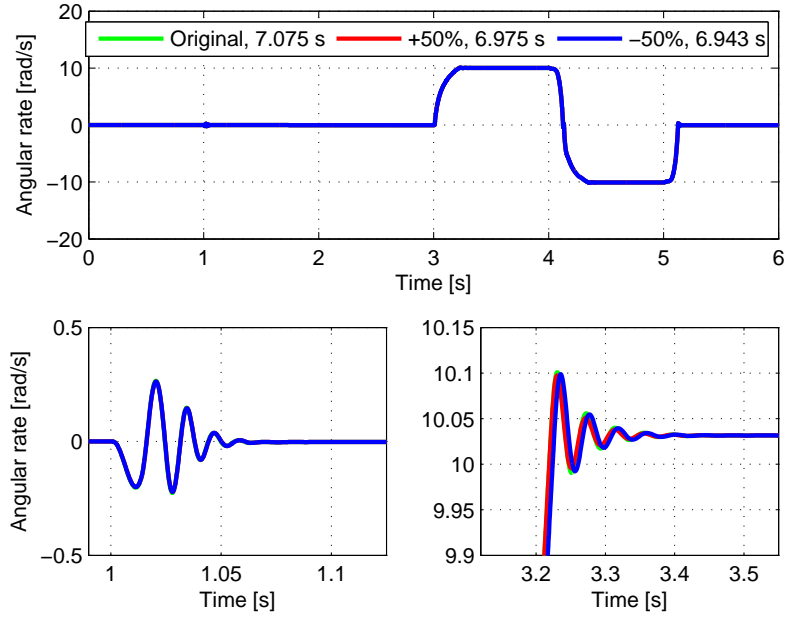


Figure D.21: Sensitivity of inertia in control slide, main valves.

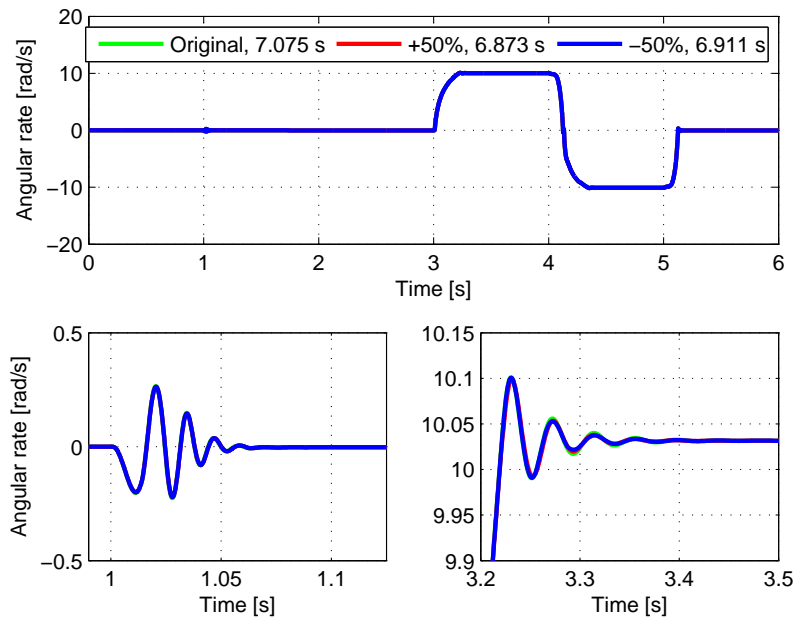


Figure D.22: Sensitivity of initial volumes 1 and 2 in control slide, main valves.

### D.6.3 Natural Frequency in 4/3-Directional Valve Dynamics

The natural frequency in the pilot valve is set to 120 Hz in table C.1. The natural frequency is changed with  $\pm 50\%$  and the results are given in figure D.23.

As the figure shows the motor response is not affected by the changes in natural frequency for the pilot valve dynamics. However the solving time seems to increase when decreasing the natural frequency.

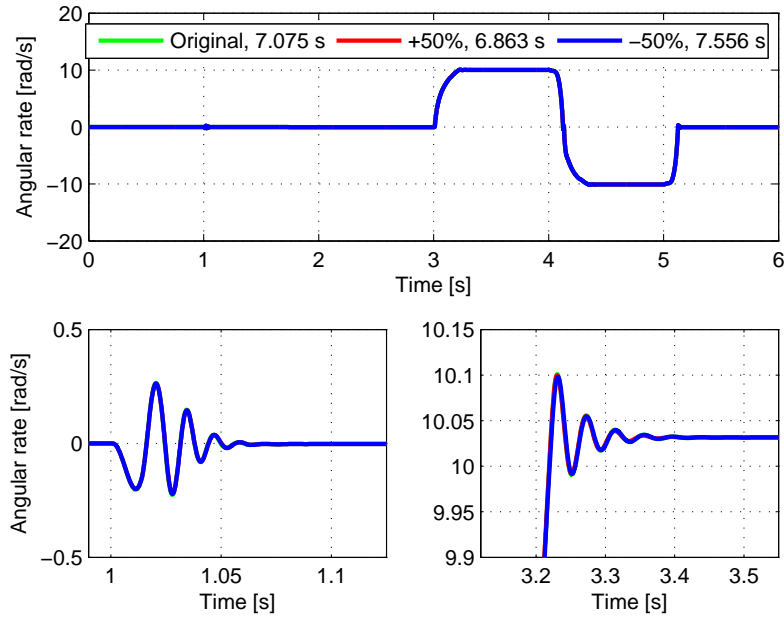


Figure D.23: Sensitivity of natural frequency in pilot valve dynamics.

#### D.6.4 Gain in 4/3-Directional Valve Dynamics

The gain in pilot valve dynamics is given in table C.1 as  $1 \text{ m/N}$ . The gain is changed with  $\pm 50\%$  and the results are given in figure D.24.

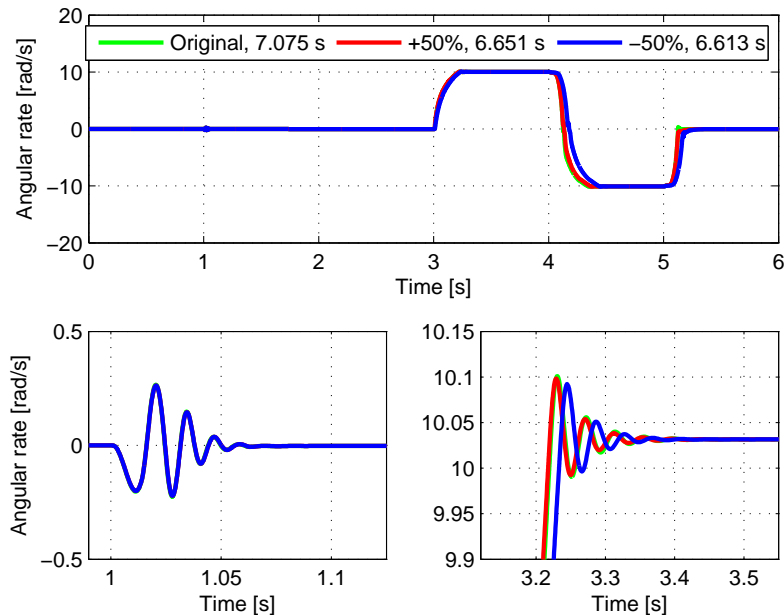


Figure D.24: Sensitivity of gain in the pilot valve dynamics.

As can be seen in the figure a decrease in the gain gives not large changes in the motor velocity response and solving time. However an increase gives a faster response of the hydraulic motor, especially when the motor speed is decreasing and negative.

### D.6.5 Damping Ratio in 4/3-Directional Valve Dynamics

The damping ratio,  $\zeta$ , is in table C.1 given as 0.9-. The damping ratio is changed with  $\pm 50\%$  and the results are given in figure D.25.

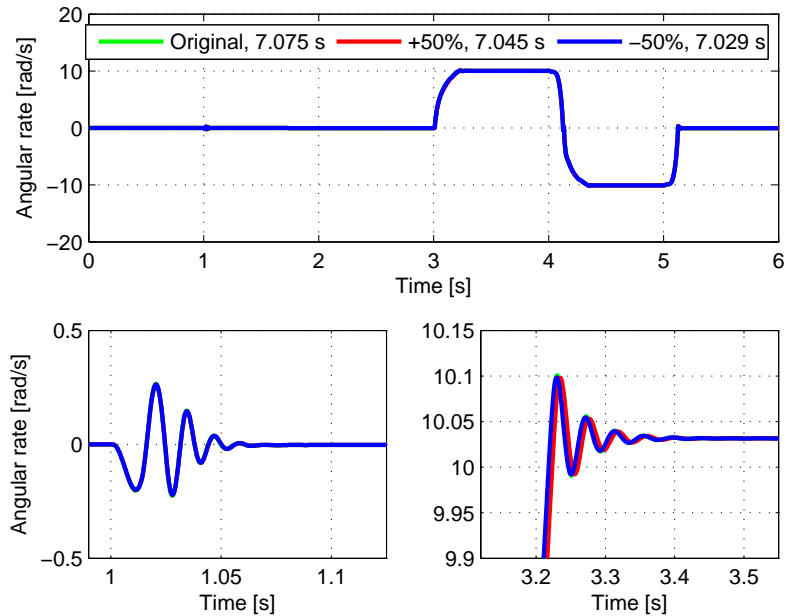


Figure D.25: Sensitivity of damping ratio,  $\zeta$ , in the pilot valve dynamics.

As can be seen from the figure the changes in the damping ratio do not affect the motor response or the solving time in the simulation significantly, but more than the changes in natural frequency, see figure D.23.

# E | Additional Plots and Case Studies

## E.1 Adaptive Controller

### E.1.1 Adaptive Controller Gains

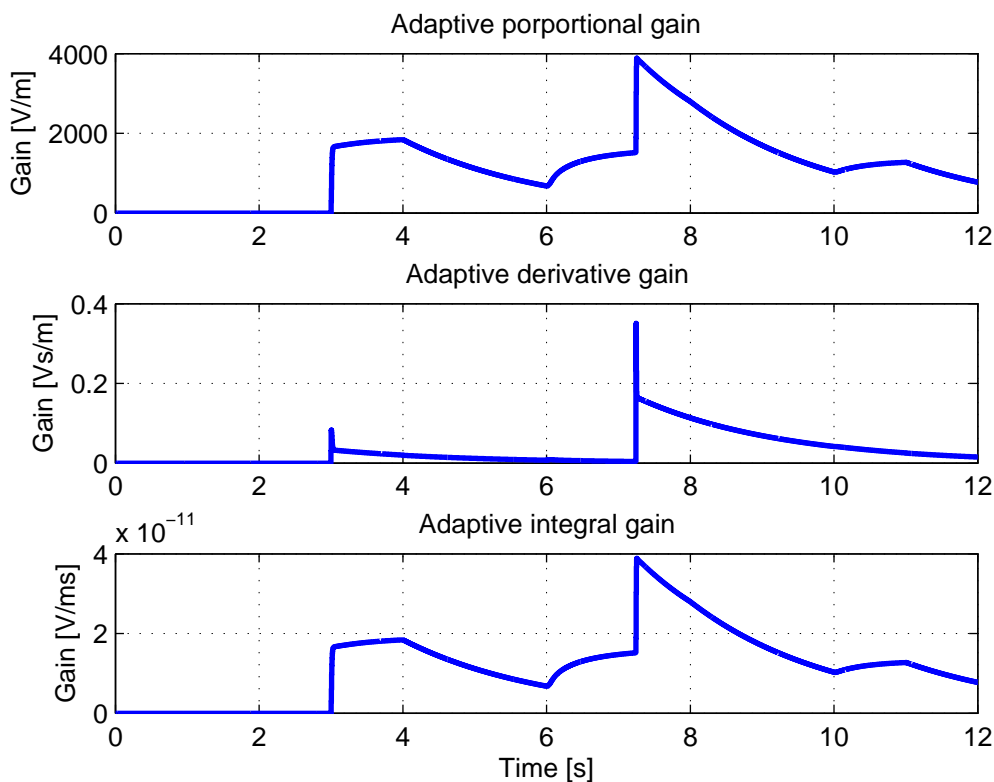


Figure E.1: Adaptive gains for controller given in section 4.1.2.  $T_{ms} = 20000$  Nm, control slide references as given in figure 4.7.

### E.1.2 Random Reference Response

In this simulation a random reference signal with a maximal frequency of  $f = 5$  Hz and an amplitude of 0.04 is applied to test the adaptive controller. Only one main valve is used in this simulation, connected to constant pressures. Figure E.2 shows the slide position, the reference signal and the output from the velocity limitation.

As can be seen in the figure the slide position follows the reference signal with high accuracy, except when the absolute value of the slope of the reference signal gets too large. Then the velocity limitation generates a new reference which is fed to the controller. This is shown in the two last magnified subplots. The adaptive gains are shown in figure E.3, the controller output

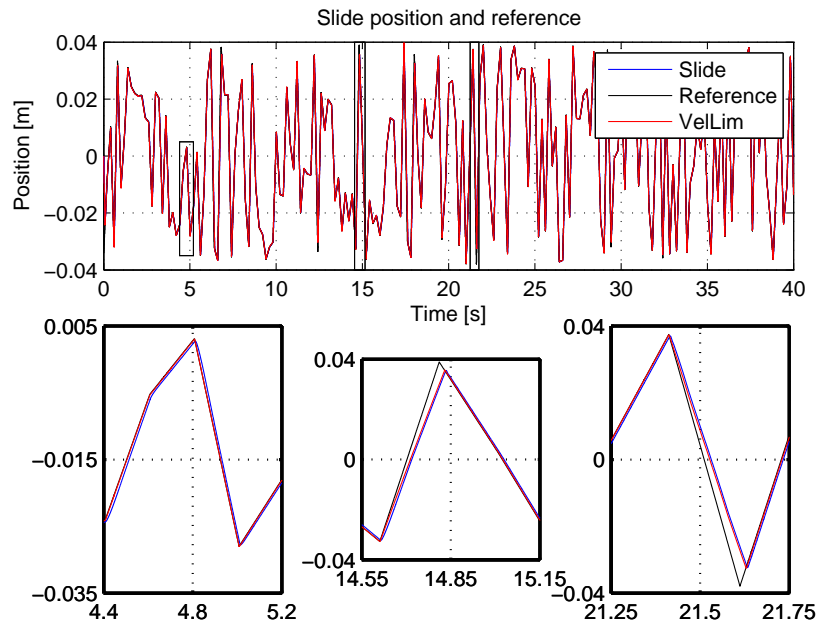


Figure E.2: Slide position, reference signal and velocity limitation.

before saturation and its components are shown in figure E.4 and the volume states are shown in figure E.5.

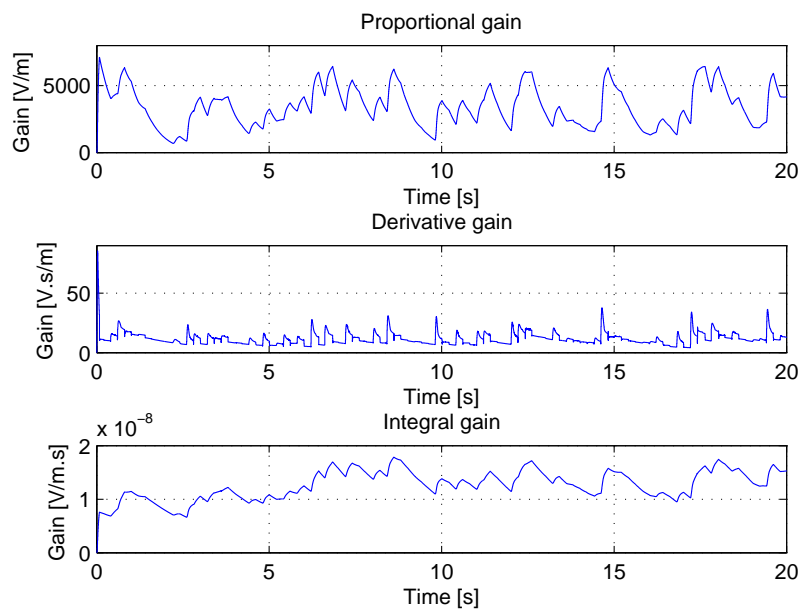


Figure E.3: Adaptive gains.

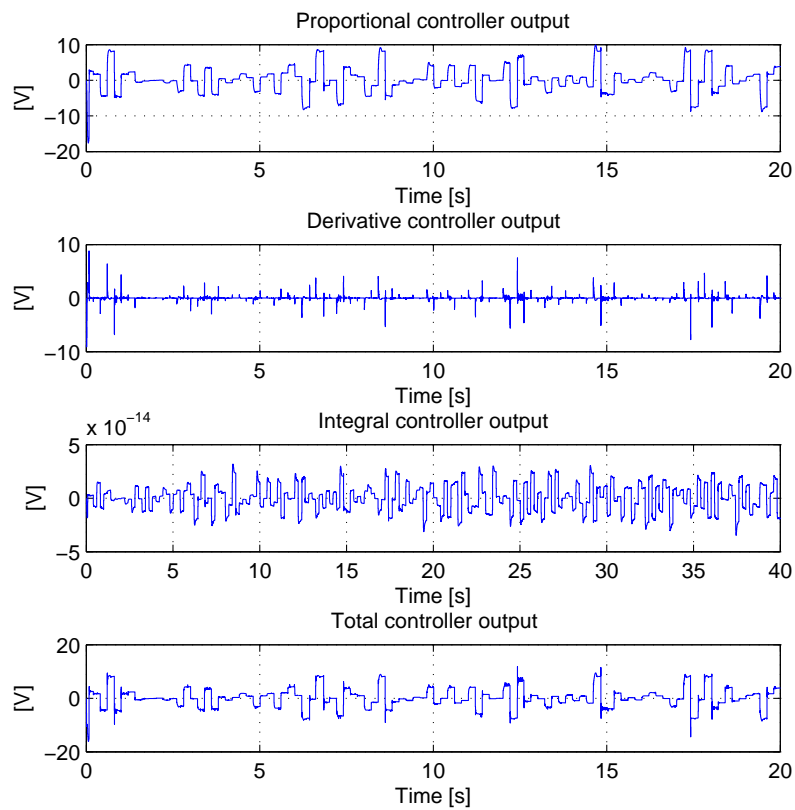


Figure E.4: Controller output and its components before saturation.

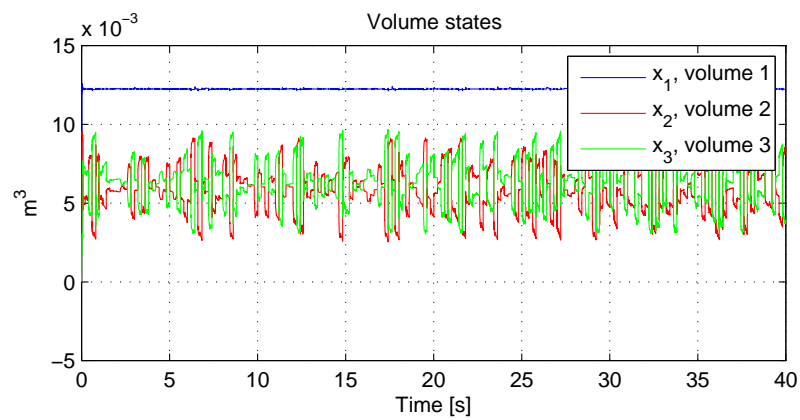


Figure E.5: Volume states.

## E.2 Additional Plots from 6.2

In this section some additional plots from section 6.2 are given.

### E.2.1 Control Slide Positions and References, 6.2.1

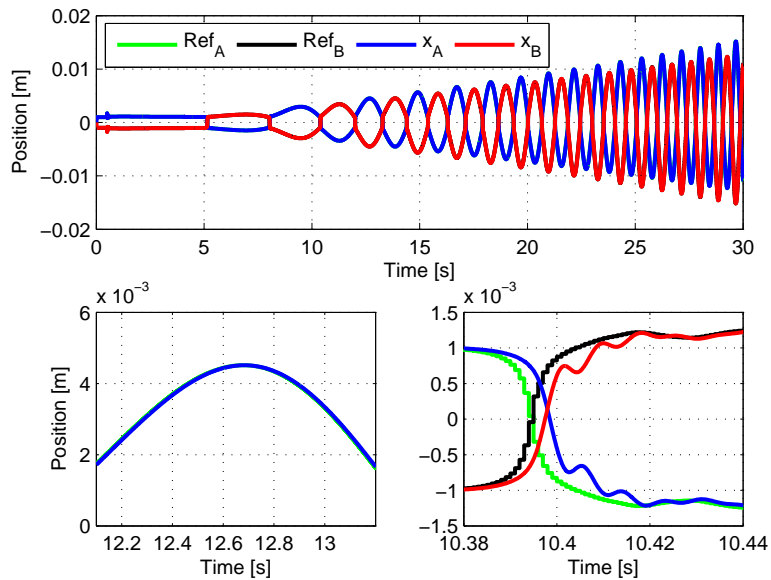


Figure E.6: Control slide positions and references.

### E.2.2 Differential Pressure and Variable Bulk Modulus, 6.2.1

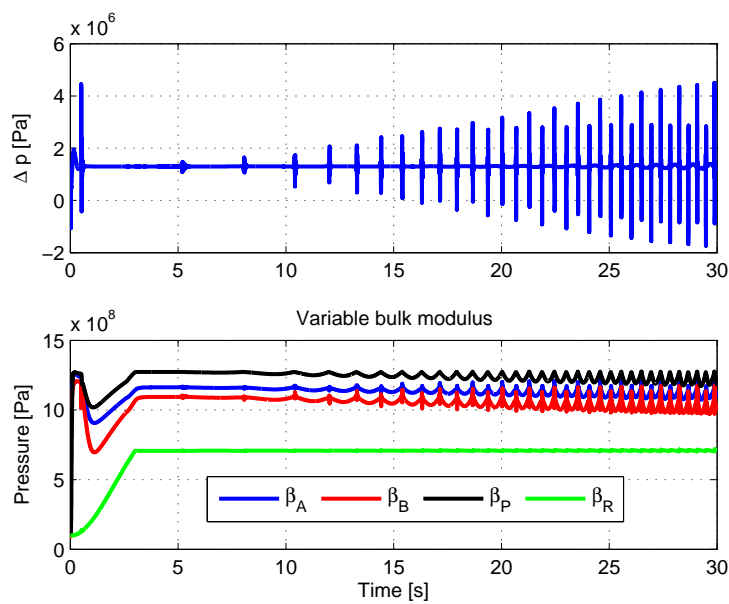


Figure E.7: Differential pressure across the motor,  $\Delta p$ , and variable bulk modulus.



### E.2.3 Hydraulic Motor Velocity, 6.2.2

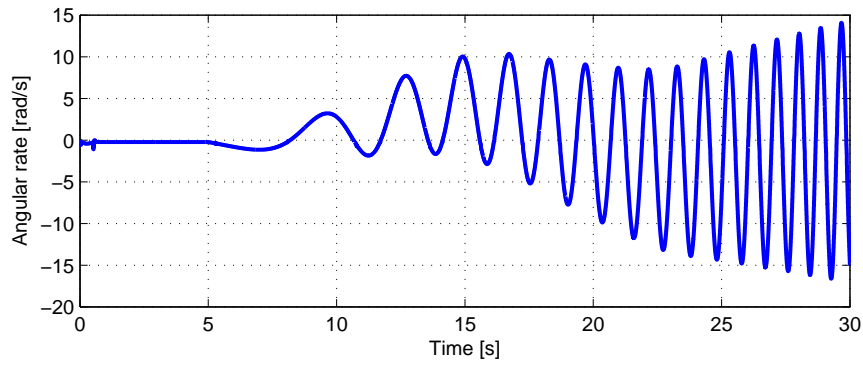


Figure E.8: Hydraulic Motor Velocity.

### E.2.4 Control Slide Positions and References, 6.2.2

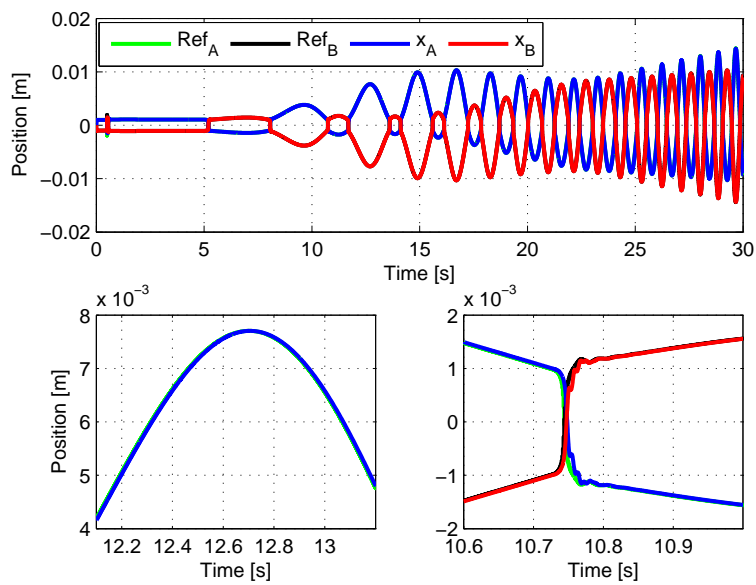


Figure E.9: Control slide positions and references.

### E.2.5 Differential Pressure and Variable Bulk Modulus, 6.2.2

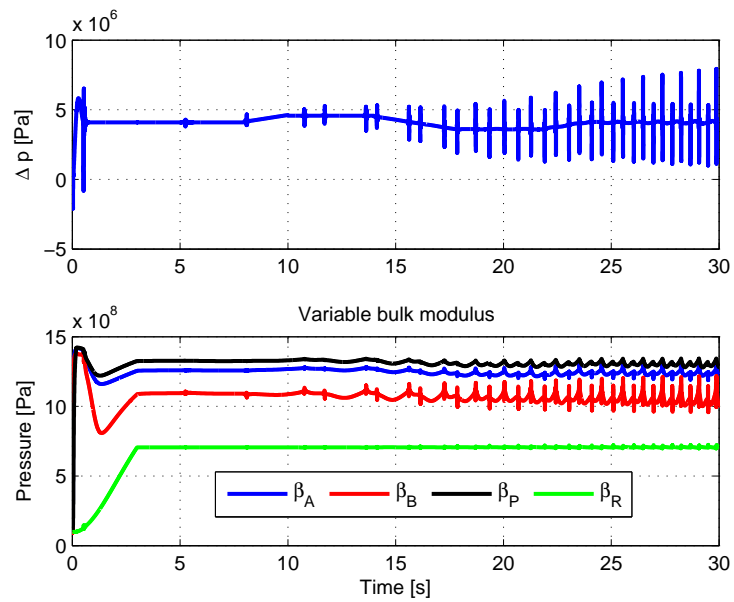


Figure E.10: Differential pressure across the motor,  $\Delta p$ , and variable bulk modulus.